ANTIMICROBIAL AND WOUND HEALING PROPERTIES OF NITRIC OXIDE-RELEASING XEROGELS AND SILICA NANOPARTICLES

by
Evan M. Hetrick

A dissertation submitted to the faculty of the University of North Carolina at Chapel Hill in partial fulfillment of the requirements for the degree of Doctor of Philosophy in the Department of Chemistry (Analytical Chemistry).

Chapel Hill
2008

Approved by:

Professor Mark H. Schoenfisch

Professor Royce W. Murray

Professor R. Mark Wightman

Professor Bruce M. Klitzman

Professor Matthew R. Redinbo

ABSTRACT

Evan M. Hetrick: Antimicrobial and Wound Healing Properties of Nitric Oxide-Releasing Xerogels and Silica Nanoparticles
(Under the direction of Professor Mark H. Schoenfisch)

Indwelling medical devices continue to be plagued by the body's response to foreign materials and the ever-present threat of microbial infection. Endogenously-produced nitric oxide (NO) has been shown to play beneficial roles in both wound healing and the body's defense against infection. To exploit NO's favorable properties for biomaterials applications, previous studies have detailed the synthesis of xerogel polymers and silica nanoparticles capable of storing and releasing NO via diazeniumdiolate NO-donors. Here, the ability of NO-releasing materials to reduce bacterial adhesion under flow conditions, modulate the foreign body response, and kill microbial pathogens is described.

To more thoroughly characterize the antibacterial properties of NO-releasing xerogels, studies were conducted with *Pseudomonas aeruginosa* in a parallel plate flow cell. Xerogels modified to release NO reduced bacterial adhesion in a flux-dependent manner, with a NO flux of ~21 pmol·cm^{-2}·s^{-1} inhibiting *P. aeruginosa* adhesion by 65% compared to controls. Fluorescent viability probes indicated that bacteria adhered to NO-releasing xerogels were killed within 7 h of adhesion. In terms of tissue biocompatibility, the foreign body response was studied in an animal model at the site of subcutaneous implants coated with NO-releasing xerogels. Implant-derived NO reduced capsule thickness and the chronic inflammatory response by 50 and 30%, respectively, compared to controls. Additionally,

77% more blood vessels were observed in proximity to NO-releasing implants after 1 week compared to controls.

Along with their ability to reduce bacterial adhesion and mitigate the foreign body response, NO-releasing materials may prove useful for treating infections due to the broad-spectrum antimicrobial properties of NO. Recently, silica nanoparticles have been developed that release micromolar quantities of NO, and here the efficacy of such nanoparticles was examined against both planktonic and biofilm-based pathogens. Comparison of the antibacterial activity of NO-releasing 45 mol% AHAP3/TEOS nanoparticles to the small molecule NO donor PROLI/NO demonstrated greater bactericidal efficacy of nanoparticle-derived NO and reduced cytotoxicity to mammalian fibroblasts. Treatment of gram-negative, gram-positive, and fungal biofilms with 70 mol% MAP3/TEOS silica nanoparticles killed ≥99% of biofilm-based cells for each species tested, with the greatest efficacy (≥99.999% killing) against gram-negative biofilms.

ACKNOWLEDGEMENTS

This work was made possible by the support and contributions of several people. I would like to express thanks to my advisor, Prof. Mark Schoenfisch, for providing an environment conducive for collaboration and exploring new research areas that are not guaranteed to pay off. You get out of graduate school what you put in, and in the end it is good to have been encouraged to constantly keep pushing.

As with all science, the results presented here are the outcome of collaboration with, and assistance from, several people. The foreign body response studies were conducted in collaboration with Dr. Heather Prichard and Prof. Bruce Klitzman at Duke University. Both have been more than generous with their time helping me understand in vivo experiments and tissue histology. The antimicrobial studies were the result of collaboration with Dr. Jae Ho Shin and Dr. Nathan Stasko. I want to express my gratitude to three exceptional undergraduates with whom I had the privilege of working: Daniel Wespe, Bryce Johnson, and Gregory Charville. Both Dan and Bryce were instrumental in collecting data for the antibacterial nanoparticles project, and Greg extended the bacterial adhesion studies to protein-coated substrates. I am very appreciative of the time that Heather Egolf-Fox spent conducting cytotoxicity experiments and helping me interpret the results.

To my colleagues in the Schoenfisch lab, past and present, thank you for your friendship and support. I have always considered myself lucky that my co-workers are also my friends.

TABLE OF CONTENTS

LIST OF TABLES xi

LIST OF SCHEMES xii

LIST OF FIGURES xiii

LIST OF ABBREVIATIONS AND SYMBOLS xx

CHAPTER 1. INTRODUCTION: RECENT ADVANCES IN THE DESIGN OF MORE BIOCOMPATIBLE AND ANTIMICROBIAL BIOMATERIALS 1

1.1 Biomedical implants and associated biocompatibility issues 1

1.1.1 Foreign body response 1

1.1.2 Device-associated infection 4

1.2 Overview of current methods to mitigate the foreign body response 9

1.2.1 Control over implant surface microarchitecture 9

1.2.2 Implants engineered to elute anti-inflammatory and pro-angiogenic compounds 12

1.3 Overview of current methods to prevent device-associated infections 17

1.3.1 Passive strategies for polymeric device coatings 18

1.3.2 Antimicrobial agents covalently anchored to polymers 20

1.3.3 Silver-releasing device coatings 22

1.3.4 Antibiotic-releasing device coatings 26

1.3.5 Antibody-eluting device coatings 27

1.4 Nitric oxide 30

1.4.1 Physiological sources of NO 31

1.4.2 Physiological roles of NO 31

1.4.3 Nitric oxide, infection, and the foreign body response 34

1.5 Nitric oxide-releasing materials for enhanced biocompatibility and antimicrobial applications 36

1.5.1 Nitric oxide-releasing polymers for blood-contacting devices 38

1.5.2 Xerogel films 39

1.5.3 Silica nanoparticles 43

1.6 Summary of dissertation research 45

1.7 References 48

CHAPTER 2. ANTIBACTERIAL NITRIC OXIDE-RELEASING XEROGELS: CELL VIABILITY AND PARALLEL PLATE FLOW CELL ADHESION STUDIES 61

2.1 Introduction 61

2.2 Methods and materials 64

2.2.1 Synthesis of AHAP3/BTMOS xerogel films 64

2.2.2 Diazeniumdiolate formation 65

2.2.3 Poly(vinyl chloride)-coated xerogels 65

2.2.4 Nitric oxide release measurements 65

2.2.5 Bacterial adhesion in a parallel plate flow chamber 65

2.2.6 Bacterial adhesion under static conditions 66

2.2.7 Fluorescent viability staining of adhered bacteria 68

2.2.8 Quantification of viable adhered bacteria 69

2.3 Results and discussion 70

2.3.1 Nitric oxide release 70

2.3.2 Nitric oxide-mediated reduction in bacterial adhesion under flowing conditions 70

2.3.3 Bacterial adhesion under static conditions 75

2.3.4 Adhered bacterial viability 77

2.4 Conclusions 87

2.5 References 88

CHAPTER 3. REDUCED FOREIGN BODY RESPONSE AT NITRIC OXIDE-RELEASING SUBCUTANEOUS IMPLANTS 91

3.1 Introduction 91

3.2 Methods and materials 93

3.2.1 NO-releasing xerogel-coated implants 93

3.2.2 Nitric oxide release measurements 94

3.2.3 In vivo studies to examine the foreign body response 95

3.2.4 Histological evaluation and data analysis 96

3.3 Results and discussion 97

3.3.1 Nitric oxide releasing xerogel coatings 97

3.3.2 Effect of NO release on foreign body capsule formation and collagen deposition 99

3.3.3 Effect of NO release on angiogenesis 105

3.3.4 Effect of NO release on the inflammatory response 109

3.4 Conclusions 113

3.5 References 115

CHAPTER 4. BACTERICIDAL EFFICACY OF NITRIC OXIDE-RELEASING SILICA NANOPARTICLES 119

4.1 Introduction 119

4.2 Methods and materials 121

4.2.1 Synthesis of NO-releasing silica nanoparticles 122

4.2.2 Characterization of diazeniumdiolate-modified silane (AHAP3/NO) 124

4.2.3 Synthesis of fluorescently-labeled NO-releasing silica nanoparticles 124

4.2.4 Size characterization of silica nanoparticles 126

4.2.5 Synthesis of PROLI/NO 126

4.2.6 Nitric oxide release measurements 126

4.2.7 Bactericidal assays under static conditions 127

4.2.8 Time-based bactericidal assays under nutrient growth conditions 127

4.2.9 Interaction between nanoparticles and bacterial cells 127

4.2.10 Confocal fluorescence microscopy for detection of intracellular NO and cell killing 128

4.2.11 Propidium iodide cytotoxicity assay 129

4.2.12 Lactate dehydrogenase cytotoxicity assay 129

4.2.13 Statistics 130

4.3 Results and discussion 130

4.3.1 Characterization of NO-releasing silica nanoparticles and PROLI/NO 130

4.3.2 Bactericidal efficacy under static conditions 134

4.3.3 Time-based bactericidal assays under nutrient growth conditions 137

4.3.4 Confocal microscopy studies 144

4.3.5 Cytotoxicity of AHAP3 nanoparticles and PROLI/NO against L929 mouse fibroblasts 151

4.4 Conclusions 154

4.5 References 157

CHAPTER 5. ANTI-BIOFILM EFFICACY OF NITRIC OXIDE-RELEASING MATERIALS: INHIBITION OF MICROBIAL SURFACE PROLIFERATION AND ACTIVITY AGAINST ESTABLISHED MICROBIAL BIOFILMS 162

5.1 Introduction 162

5.1.1 Device-associated biofilms: formation and prevention 163

5.1.2 Biofilm-based wound infections 163

5.1.3 Antimicrobial properties of nitric oxide 165

5.2 Methods and materials 166

5.2.1 Xerogel synthesis 167

5.2.2 Diazeniumdiolate formation 167

5.2.3 Synthesis of NO-releasing silica nanoparticles 167

5.2.4 Nitric oxide release measurements 168

5.2.5 Bacterial surface proliferation and doubling-time experiments 168

5.2.6 Treatment of mature biofilms with NO-releasing silica nanoparticles 170

5.2.7 In vitro toxicity testing of NO-releasing nanoparticles 171

5.3 Results and discussion 172

5.3.1 NO-release for preventing biofilm formation 172

5.3.2 NO-releasing nanoparticles for treating established biofilms 179

5.3.3 Cytotoxicity of MAP3 nanoparticles to mammalian fibroblasts 188

5.4 Conclusions 190

5.5 References 193

CHAPTER 6. SUMMARY AND FUTURE RESEARCH DIRECTIONS.....200

6.1 Summary.....200

6.2 Future research directions.....203

6.3 Conclusions.....208

6.4 References.....209

LIST OF TABLES

Table 2.1. *P. aeruginosa* adhesion (percent surface coverage) under static conditions 78

Table 2.2. *P. aeruginosa* adhesion (percent surface coverage) in parallel plate flow chamber 79

Table 5.1. Log-based and percent reductions in biofilm viability at the highest dose of NO-releasing MAP3 silica nanoparticles tested (8 mg/mL) compared to controls (0 mg/mL nanoparticles) 186

LIST OF SCHEMES

Scheme 4.1. Synthesis of AHAP3 NO donor and co-condensation with TEOS to form NO-releasing silica nanoparticles. R = $–(CH_2)_3Si≡$ and R' = $H_2N(CH_2)_6–$ 123

Scheme 4.2. Synthesis of FITC-modified NO-releasing 45 mol% AHAP3 silica nanoparticles (balance TEOS). Abbreviations: AHAP3 = *N*-(6-aminohexyl)aminopropyltrimethoxysilane; APTMS = 3-aminopropyltrimethoxysilane; FITC = fluorescein isothiocyanate; TEOS = tetraethoxysilane 125

LIST OF FIGURES

Figure 1.1. The progression of the foreign body response from device implantation to collagen capsule formation. Following protein adsorption to the implant, macrophages interrogate the foreign material, leading to frustrated phagocytosis and foreign body giant cell formation. Finally, fibroblasts form a collagen capsule around the implant, sequestering the foreign material from surrounding tissue. Adapted from Ratner, B.D., *J. Controlled Release*, 2002, *78*, 211-218 3

Figure 1.2. The foreign body response as it relates to the utility of implantable subcutaneous sensors. In the ideal scenario, the sensor heals within healthy vascularized tissue, ensuring sufficient mass transport of analytes from the blood to the sensor surface and adequate sensitivity. The typical foreign body response, however, sequesters the sensor within a dense capsule of avascular collagen, drastically reducing analyte diffusion to the sensor and severely limiting sensor performance 5

Figure 1.3. Representation of bacterial adhesion to a biomaterial substrate. Phase I adhesion involves reversible cellular association with the surface. During Phase II, bacteria undergo irreversible molecular bridging with the substrate through cell surface adhesin compounds. After approximately 1 d, certain bacterial species are capable of secreting a protective exopolysaccharide matrix (biofilm) that protects the adhered bacteria from host defenses and systemically-administered antibiotics 8

Figure 1.4. A) At smooth implant surfaces, macrophage attack is followed by the formation of foreign body giant cells and eventual collagen capsule formation. B) At micropatterned implants, it has been proposed that macrophages become spatially confined within the microstructures and are unable to fuse together to form foreign body giant cells. As a result, foreign body capsule formation at the micropatterned implant is significantly reduced 11

Figure 1.5. Structure of 3-(trimethoxysilyl)-propyldimethyloctadecyl ammonium chloride 21

Figure 1.6. Structure of unmodified chitosan 23

Figure 1.7. A) Opsonization of a bacterial cell via IgG binding to specific cell-surface epitopes, thereby blocking adhesin compounds. B) Opsonized bacteria are targeted to phagocytes for destruction 28

Figure 1.8. Reaction for the nitric oxide synthase-catalyzed conversion of L-arginine to L-hydroxyarginine, which is then oxidized to yield L-citrulline and nitric oxide....32

Figure 1.9. A) Reaction of NO with amines to produce diazeniumdiolate NO-donors; and B) diazeniumdiolate decomposition and NO release in the presence of a proton source such as water or buffer....37

Figure 1.10. A) Hydrolysis of silane precursors; and B) subsequent condensation to form a xerogel polymer where R is typically a methyl or ethyl group and R′ is the amine-containing NO-donor precursor....40

Figure 2.1. Schematic representation of flow cell design used to study *P. aeruginosa* adhesion to xerogel polymer coatings. A peristaltic pump was used to flow a suspension of *P. aeruginosa* (10^8 colony forming units per mL) through custom-machined flow cells that were placed on the stage of an inverted optical microscope. The suspension was exposed to control xerogel films prior to NO-releasing xerogels....67

Figure 2.2. Nitric oxide release in PBS (pH 7.4) at 25 °C from 40 (A), 30 (B), 20 (C) and 10% (D) AHAP3 (v/v) xerogel polymers (balance BTMOS)....71

Figure 2.3. Phase contrast optical micrographs of *P. aeruginosa* adhesion to control (A), and NO-releasing 10 (B), 20 (C), 30 (D), and 40% (E) AHAP3 (v/v) xerogels (balance BTMOS) after 1 h exposure to a flowing suspension of *P. aeruginosa*. Flow rate = 0.2 mL/min. Control is non-NO-releasing 40% AHAP3/BTMOS....72

Figure 2.4. *P. aeruginosa* adhesion under flowing conditions (0.2 mL/min) to xerogel films with average 2 h NO flux values of 0 (■), 0.42 (●), 1.9 (▲), 10.8 (▼), and 21.3 (◆) $pmol \cdot cm^{-2} \cdot s^{-1}$. Nitric oxide release was achieved with 10 (●), 20 (▲), 30 (▼), and 40% (◆) AHAP3 (v/v) xerogel films (balance BTMOS). For clarity, the data presented for controls (■) represent the average of all control samples at each time point (surface coverage values for all controls were identical (within error) at each time point)....74

Figure 2.5. *P. aeruginosa* adhesion to control (■ and ▲) and NO-releasing (▼ and ●) 40% AHAP3 (v/v) xerogel films (balance BTMOS). Adhesion was studied at controlled flow rates of 0.2 mL/min (■ and ●) and 0.6 mL/min (▲ and ▼)....76

Figure 2.6. Bright field (A, D), Syto 9 fluorescent (B, E), and propidium iodide fluorescent (C, F) micrographs (20x magnification) of *P. aeruginosa* adhered to control (non-NO-releasing) 40% AHAP3 (v/v) xerogels (balance BTMOS). Images were acquired immediately (A, B, C) and 7 h after (D, E, F) initial bacterial adhesion....81

Figure 2.7. Bright field (A, D), Syto 9 fluorescent (B, E), and propidium iodide fluorescent (C, F) micrographs (20x magnification) of *P. aeruginosa* adhered to NO-releasing 40% AHAP3 (v/v) xerogels (balance BTMOS). Images were acquired immediately (A, B, C) and 7 h after (D, E, F) initial bacterial adhesion....82

Figure 2.8. Bright field (A, D), Syto 9 fluorescent (B, E), and propidium iodide fluorescent (C, F) images of *P. aeruginosa* adhered to the xerogel-coated side (A, B, C) and the glass side (D, E, F) of a glass microscope slide (20x magnification). Images were acquired after 7 h incubation in PBS. The cells adhered to the glass remain viable, while those adhered to the NO-releasing xerogel were killed after 7 h. Xerogel coating is 40% AHAP3 (v/v, balance BTMOS)....84

Figure 2.9. Viable *P. aeruginosa* adhered to AHAP3 xerogels with varying NO release capabilities removed by sonication after 15 h incubation in sterile PBS. Initial levels of *P. aeruginosa* adhered to each substrate were identical (20% surface coverage). Values represent average ± standard error of the mean....86

Figure 3.1. Nitric oxide release from silicone elastomer implants coated with diazeniumdiolate-modified 40% AHAP3/BTMOS (v/v) xerogels. Inset: Total NO release....98

Figure 3.2. Optical micrographs showing foreign body capsule formation after 6 weeks at (A) bare silicone elastomer; (B) xerogel-coated control; and, (C) NO-releasing xerogel-coated subcutaneous implants. Xerogel polymer coating was 40% AHAP3/BTMOS (v/v). Scale is the same in each image and arrows denote the foreign body capsule. The implant was located in the upper white region of each image....101

Figure 3.3. Foreign body capsule thickness at uncoated blank, xerogel-coated control, and NO-releasing xerogel-coated subcutaneous implants. Xerogel polymer coating was 40% AHAP3/BTMOS (v/v). Significant differences ($p < 0.05$) between NO-release implants and blanks (#), and NO-release and controls (*) are indicated....102

Figure 3.4. Collagen density indexes observed at (A) 1 week; (B) 3 weeks; and, (C) 6 weeks at uncoated blank, xerogel-coated control, and NO-releasing xerogel-coated subcutaneous implants. Xerogel polymer coating was 40% AHAP3/BTMOS (v/v). Significant differences ($p < 0.05$) between NO-release implants and blanks (#), and NO-release and controls (*) are indicated.....104

Figure 3.5. Fluorescence micrographs of CD-31-stained tissue samples adjacent to (A) bare silicone elastomer; (B) xerogel-coated control; and, (C) NO-releasing xerogel-coated subcutaneous implants after 1 week. Xerogel polymer coating was 40% AHAP3/BTMOS (v/v). The green fluorescence represents blood vessel presence via positive labeling of endothelial cells with CD-31 immunohistochemical stain. Scale is the same in each image. Each image shows tissue within approximately 340 μm of the implant, which was located at the bottom of each image 107

Figure 3.6. Blood vessels observed per 20x field at (A) 1 week; (B) 3 weeks; and, (C) 6 weeks at uncoated blank, xerogel-coated control, and NO-releasing xerogel-coated subcutaneous implants. Xerogel polymer coating was 40% AHAP3/BTMOS (v/v). Significant differences ($p < 0.05$) between NO-release implants and controls (*) are indicated.....108

Figure 3.7. Optical micrographs of hematoxylin & eosin (H&E)-stained tissue samples showing the inflammatory response after 3 weeks at (A) bare silicone elastomer; (B) xerogel-coated control; and, (C) NO-releasing xerogel-coated subcutaneous implants. Xerogel polymer coating was 40% AHAP3/BTMOS (v/v). Nuclei stain purple while collagen appears pink with H&E stain. Scale is the same in each image. The implants were located in the white region at the left (A, B) or bottom (C) of each image.....110

Figure 3.8. Inflammatory response factors observed at (A) 1 week; (B) 3 weeks; and, (C) 6 weeks at uncoated blank, xerogel-coated control, and NO-releasing xerogel-coated subcutaneous implants. Xerogel polymer coating was 40% AHAP3/BTMOS (v/v). Significant differences ($p < 0.05$) between NO-release implants and blanks (#) and NO-release implants and controls (*) are indicated.....111

Figure 4.1. UV absorbance of control and diazeniumdiolate-modified (Nanoparticle/NO) 45 mol% AHAP3/TEOS silica nanoparticles (concentration = 160 $\mu g \cdot mL^{-1}$ in phosphate buffered saline).....132

Figure 4.2. Nitric oxide release profiles of (A) 45 mol% AHAP3 silica nanoparticles and (B) PROLI/NO in PBS, pH 7.4, 37 °C. Inset of (A) represents total NO release. $[NO]_m$ = maximum NO flux; t_m = time to reach maximum NO flux; t[NO] = total NO released; $t_{1/2}$ = half life of NO release 133

Figure 4.3. AC mode AFM height image of 45 mol% AHAP3 silica nanoparticles (balance TEOS) on a mica surface 135

Figure 4.4. Bactericidal efficacy of (A) proline and PROLI/NO and (B) control and NO-releasing 45 mol% AHAP3 silica nanoparticles (balance TEOS) against *P. aeruginosa* in phosphate buffered saline 138

Figure 4.5. Time- and concentration-based bactericidal efficacy of (A) proline (control) and PROLI/NO and (B) control (Nanoparticle) and NO-releasing 45 mol% AHAP3 silica nanoparticles (Nanoparticle/NO) 140

Figure 4.6. Real-time NO release of the small molecule diazeniumdiolate NO-donor DETA/NO before, during, and after injection of 1% tryptic soy broth (TSB), as measured using a chemiluminescent nitric oxide analyzer 141

Figure 4.7. Comparison of the NO doses necessary from silica nanoparticles (dark blue) and PROLI/NO (grey) to achieve 100% bactericidal efficacy against *P. aeruginosa* in (A) PBS and (B) TSB 143

Figure 4.8. Scanning confocal microscopy images of FITC-modified NO-releasing silica nanoparticle association with *P. aeruginosa* cells. Images were acquired in bright-field mode (A-E) and on the FITC fluorescence channel (A′-E′) before injection (A, A′) of 100 $\mu g \cdot mL^{-1}$ NO-releasing FITC-modified AHAP3 silica nanoparticles, and 10 (B, B′), 20 (C, C′), 30 (D, D′) and 60 (E, E′) minutes post-injection 145

Figure 4.9. Intracellular DAF-2 (green) and propidium iodide (red) fluorescence from *P. aeruginosa* bacterial cells incubated with 100 $\mu g \cdot mL^{-1}$ 45 mol% AHAP3/TEOS NO-releasing silica nanoparticles. DAF-2 fluorescence indicates the presence of NO and reactive nitrogen species, while propidium iodide fluorescence indicates membrane destruction and cell death. Images were acquired (A) 30 min, (B) 83 min, (C) 113 min, (D) 124 min, (E) 132 min, and (F) 140 min after nanoparticle addition 147

Figure 4.10. Bright field and fluorescence images of *P. aeruginosa* cells treated with 5 $mg \cdot mL^{-1}$ PROLI/NO. Propidium iodide (PI) fluorescence indicates cell death. Images were acquired (A) 0 min, (B) 10.5 min, (C) 21min, and (D) 31 min after addition of 5 $mg \cdot mL^{-1}$ PROLI/NO 149

Figure 4.11. Proposed mechanisms by which NO acts as an antibacterial agent (adapted from references 13, 34, 42-44; not to scale). NO's antibacterial properties are attributed to both nitrosative and oxidative stress exerted by reactive byproducts such as N_2O_3 and $ONOO^-$ (peroxynitrite). Nitrosative stress leads in part to nitrosation of thiols on proteins as well as DNA deamination, while oxidative stress is responsible for membrane destruction via lipid peroxidation. Notably, increased NO and O_2 concentrations in lipid membranes leads to enhanced production of both nitrosative and oxidative species such as N_2O_3 and NO_2 in the membrane..... 150

Figure 4.12. Toxicity of 45 mol% AHAP3 control (dark gray) and NO-releasing (light gray) silica nanoparticles to L929 mouse fibroblasts as measured by (A) membrane permeability to propidium iodide and (B) lactate dehydrogenase leaching 153

Figure 4.13. Cytotoxicity of PROLI/NO against L929 fibroblast cells as measured by propidium iodide viability assay. The backbone of PROLI/NO (the amino acid proline) demonstrated no toxicity to L929 cells at concentrations up to 16 mg/mL..... 155

Figure 5.1. Nitric oxide release in phosphate buffered saline (pH 7.4) at 37 °C from 40% AHAP3 (v/v) xerogel polymer (balance BTMOS). Inset: total NO released..... 173

Figure 5.2. Optical micrographs (20x magnification) of *P. aeruginosa* proliferation at control (left column) and NO-releasing (right column) 40% AHAP3 xerogel substrates..... 175

Figure 5.3. Surface colonization of control and NO-releasing 40% AHAP3 xerogel substrates (v/v, balance BTMOS) by *P. aeruginosa* in a parallel plate flow cell maintained at 37 °C. Percent surface coverage was determined via threshold analysis of phase-contrast optical micrographs..... 176

Figure 5.4. Optical micrographs (20x magnification) of *P. aeruginosa* proliferation of NO-releasing 40% AHAP3 xerogel substrates at two different locations on the same substrate over 24 h. Bacterial proliferation and surface colonization are indicated by the white asterisk(s) in each image 177

Figure 5.5. Nitric oxide release profiles of (A) 45 mol% AHAP3 and (B) 70 mol% MAP3 silica nanoparticles (balance TEOS). Insets represent total NO release. $[NO]_m$ = maximum NO flux; t_m = time to reach maximum NO flux; t[NO] = total NO released; $t_{1/2}$ = half life of NO release 181

Figure 5.6. Anti-biofilm efficacy of 45 mol% AHAP3 silica nanoparticles (control and NO-releasing) and NO-releasing 70 mol% MAP3 silica nanoparticles against established *P. aeruginosa* biofilms on medical-grade silicone rubber substrates 182

Figure 5.7. Broad spectrum anti-biofilm properties of 70 mol% MAP3 silica nanoparticles (balance TEOS) against (A) *P. aeruginosa* and (B) *E. coli* (gram-negative); (C) *S. aureus* and (D) *S. epidermidis* (gram-positive); and (D) *C. albicans* (pathogenic fungus) biofilms..... 185

Figure 5.8. Viable cells recovered from biofilms of (A) *P. aeruginosa*, (B) *E. coli*, (C) *S. aureus*, (D) *S. epidermidis*, and (E) *C. albicans* after no treatment (Blank) and exposure to 8 mg/mL control 70 mol% MAP3 (balance TEOS) silica nanoparticles depleted of NO (Control) 187

Figure 5.9. Viability of L929 mouse fibroblasts exposed to control and NO-releasing 70 mol% MAP3 silica nanoparticles (balance TEOS) at various concentrations. Viability was measured via MTT reduction by metabolically-active (viable) fibroblast cells and is expressed normalized to untreated fibroblasts 189

LIST OF ABBREVIATIONS AND SYMBOLS

~	approximately
°C	degree(s) Celsius
μg	microgram(s)
μL	microliter(s)
μm	micrometer(s)
μM	micromolar
δ	NMR chemical shift (parts per million)
%	percent
γ_x	surface free energy of substrate x
λ_{max}	wavelength of maximum absorption
AFM	atomic force microscopy/microscope
Ag^+	silver ion
$AgNO_3$	silver nitrate
AHAP3	*N*-(6-aminohexyl)aminopropyltrimethoxysilane
AHAP3/NO	diazeniumdiolate-modified AHAP3
AIDS	acquired immune deficiency syndrome
Ang-1	angiopoietin-1
APTMS	3-aminopropyltrimethoxysilane
Ar	argon gas
ATCC	American Type Culture Collection
atm	atmosphere
bFGF	basic fibroblast growth factor

BP	band pass
br	broad
BSA	bovine serum albumin
BTMOS	isobutyltrimethoxysilane
C. albicans	*Candida albicans*
Ca^{2+}	calcium ion
$CaCl_2$	calcium chloride
CD_3OD	tetradeuteromethanol
CDI	collagen density index
CFU	colony forming unit
cGMP	cyclic guanosine monophosphate
cm	centimeter
CO_2	carbon dioxide
CP/MAS	cross-polarization/magic angle spinning
CVC	central venous catheter
d	day(s), doublet
DAF-2	4,5-diaminofluorescein
DAF-2 DA	4,5-diaminofluorescein diacetate
DCP-OES	direct current plasma optical emission spectrometry
DET3	diethylenetriamine
DETA/NO	diazeniumdiolate-modified DETA
DI	deionized
DNA	deoxyribonucleic acid

E. coli	*Escherichia coli*
e.g.	for example
EDRF	endothelium-derived relaxing factor
ELISA	enzyme-linked immunosorbent assay
eNOS	endothelial nitric oxide synthase
et al.	and others
EtOH	ethanol
FBGC	foreign body giant cell
FBR	foreign body response
FBS	fetal bovine serum
FDA	U.S. Food and Drug Administration
Fig.	Figure
FITC	fluorescein isothiocyanate
GST	glutathione-*S*-transferase
^{1}H	proton
h	hour(s)
H&E	hematoxylin and eosin
H_2O	water
HA	hyaluronic acid
HCl	hydrochloric acid
HeNe	helium neon
HEPES	4-(2-hydroxyethyl)-1-piperazineethanesulfonic acid
HPLC	high performance liquid chromatography

Hz	hertz
i.e.	that is
IgG	immunoglobulin G
IL-6	interleukin-6
IL-8	interleukin-8
iNOS	inducible nitric oxide synthase
IRF	inflammatory response factor
KCl	potassium chloride
kg	kilogram(s)
KGF	keratinocyte growth factor
KH_2PO_4	potassium phosphate monobasic
kHz	kilohertz
KRH	Krebs-Ringer-HEPES
LDH	lactate dehydrogenase
L-NAME	*N*-nitro-L-arginine methyl ester
LP	long-pass
m	meter(s), multiplet
M	molar
MAHMA	*N*,*N*′-dimethyl-1,6-hexanediamine
MAHMA/NO	diazeniumdiolate-modified MAHMA
MALDI-TOF	matrix-assisted laser desorption ionization time of flight
MAP3	*N*-methylaminopropyltrimethoxysilane
MAP3/NO	diazeniumdiolate-modified MAP3

MBC	minimum bactericidal concentration
MBEC	minimum biofilm eradication concentration
MCP-1	macrophage chemoattractant protein-1
MEM	minimal essential media
MeOH	methanol
mg	milligram(s)
$MgSO_4$	magnesium sulfate
MHz	megahertz
MIC	minimum inhibitory concentration
min	minute(s)
mL	milliliter(s)
mm	millimeter(s)
mM	millimolar
mmol	millimole(s)
mol	mole(s)
MRSA	methicillin-resistant *Staphylococcus aureus*
MTT	3-(4,5-dimethylthiazol-2-yl)-2,5-diphenyltetrazolium bromide
MΩ	megohm
N	newton
N.A.	numerical aperature
n_0	% surface coverage of bacterial cells at t=0
N_2	nitrogen gas
N_2O_3	dinitrogen trioxide

N_2O_4	dinitrogen tetroxide
NaCl	sodium chloride
$NADH/NAD^+$	nicotinamide adenine dinucleotide
Nanoparticle/NO	diazeniumdiolate-modified AHAP3/TEOS silica nanoparticle
$NaOCH_3$	sodium methoxide
NH_4OH	ammonium hydroxide
nm	nanometer(s)
nmol	nanomole(s)
NMR	nuclear magnetic resonance spectroscopy
nNOS	neuronal nitric oxide synthase
NO	nitric oxide
NO_2	nitrogen dioxide
$[NO]_m$	maximum NO flux
NOS	nitric oxide synthase
NSAID	non-steroidal anti-inflammatory drug
n_t	% surface coverage of bacterial cells at time t
O_2	oxygen gas
O_2^-	superoxide
OH	hydroxyl radical
$ONOO^-$	peroxynitrite
P. aeruginosa	*Pseudomonas aeruginosa*
P. mirabilis	*Proteus mirabilis*
P. vulgaris	*Proteus vulgaris*

PBS	phosphate buffered saline, pH 7.4
PDGF	platelet-derived growth factor
PET	poly(ethylene terephthalate)
PFA	polyfluoroalkoxy alkane
pg	picogram(s)
pH	-log of proton concentration
PI	propidium iodide; 3,8-diamino-5-[3-(diethylmethylammonio)propyl]-6-phenylphenanthridinium diiodide
PLG	poly(lactide-*co*-glycolide)
PLGA	poly(lactide-*co*-glycolic acid)
pM	picomolar
PMMA	poly(methyl methacrylate)
pmol	picomole(s)
ppb	parts per billion
ppm	parts per million
PROLI/NO	diazeniumdiolate-modified proline
PRP	platelet-rich plasma
P/S	penicillin/streptomycin
Pt	platinum
PTFE	polytetrafluoroethylene
PVC	poly(vinyl) chloride
PVP-I	polyvinylpyrrolidone iodine complex (povidone iodine)
qt	quartet
rev	revolution

rNO_x	reactive nitrogen oxide
rpm	revolutions per minute
s	second(s), singlet
S. aureus	*Staphylococcus aureus*
S. epidermidis	*Staphylococcus epidermidis*
SEM	scanning electron microscopy/microscope
^{29}Si	silicon isotope with mass number 29
SiR	silicone rubber
SSD	silver sulfadiazene
t	triplet
t	time
t[NO]	total amount of NO released
$t_{1/2}$	NO release half life
t_d	doubling time
TEOS	tetraethoxysilane
TGF-β	transforming growth factor-β
TiO_2	titanium(IV) oxide; titanium dioxide
t_m	time of maximum NO flux
TMS	tetramethylsilane
TSA	tryptic soy agar
TSB	tryptic soy broth
U.S.	United States
UV	ultraviolet

UV-Vis	ultraviolet-visible spectroscopy
v/v	volume/volume
VEGF	vascular endothelial growth factor
wt	weight
YPD	yeast-peptone-dextrose broth
ZI	zone of inhibition
Zn^{+}	zinc ion

Chapter 1:

Recent Advances in the Design of More Biocompatible and Antimicrobial Biomaterials

1.1 Biomedical implants and associated biocompatibility issues

Modern perspectives relating to biomaterials and biocompatibility can be traced to World War II, when ophthalmologists observed that fragments of windshields composed of poly(methyl methacrylate) (PMMA) healed without permanent adverse reactions in the eyes of pilots.[1] Since that observation, scientists have attempted to design biomaterials that integrate into healthy tissue upon implantation without an unfavorable host response (e.g., chronic inflammation). Examples of biomaterials in use today that are designed to interact with human tissue include catheters, stents, pacemakers, sensors, prostheses, and orthopedic and dental implants.[1] Despite the efforts of countless chemists, engineers, biologists, and physicians, the utility and efficacy of almost all indwelling medical devices continue to be plagued by the body's response to foreign materials and the threat of microbial infection.

1.1.1 Foreign body response. The foreign body response (FBR) is the manner in which the wound-healing cascade proceeds in the presence of a foreign body such as a medical implant or device. The physiological processes associated with the FBR have been extensively reviewed[1-3] and are best understood in the context of the wound healing cascade. In the absence of a foreign material, the chronological process of wound healing consists of: 1) cessation of bleeding; 2) acute inflammation; 3) formation of granulation tissue; and, 4) tissue remodeling.[4] Implantation of a foreign material creates injury to tissue and initiates

the wound-healing sequence, which is altered from the process described above due to the presence of the foreign material. As shown in Figure 1.1, plasma proteins rapidly adsorb to the surface of the implant[1] and the inflammatory response begins with neutrophils and monocytes accumulating at the site of implantation to clear the wound of microbes and other microscopic materials via phagocytosis. After recognizing the implanted biomaterial as "foreign", neutrophils attempt to digest it. However, biomaterial clearance by phagocytes is most often unsuccessful due to the size disparity between the microscopic neutrophils and macroscopic implant.

For "normal" wounds (i.e., not created due to biomaterial implantation), the associated inflammation effectively eliminates microbial cells and other foreign material, allowing tissue remodeling to proceed and with time, the acute inflammatory response subsides.[4] In contrast, the foreign body remains for biomaterial-induced wounds and rather than subsiding, the acute inflammatory response evolves into a chronic inflammatory response. The chronic inflammatory response is characterized by an abundance of inflammatory cells, particularly macrophages, that are recruited to the site of implantation over the course of several days.[3] Like neutrophils during the acute inflammatory response, macrophages attempt to digest or otherwise destroy the implant, but are unsuccessful due to size disparities. In response, the macrophages undergo frustrated phagocytosis, whereby individual macrophages fuse together to form multinucleated foreign body giant cells (FBGC) that may remain at the tissue/material interface for the lifetime of the implant.[1] Still unsuccessful in their attempts to digest the implant, FBGCs secrete cytokines that trigger fibroblasts to deposit a dense layer of collagen around the implant. This foreign body collagen capsule, also known as scar tissue, is typically devoid of blood capillaries and serves

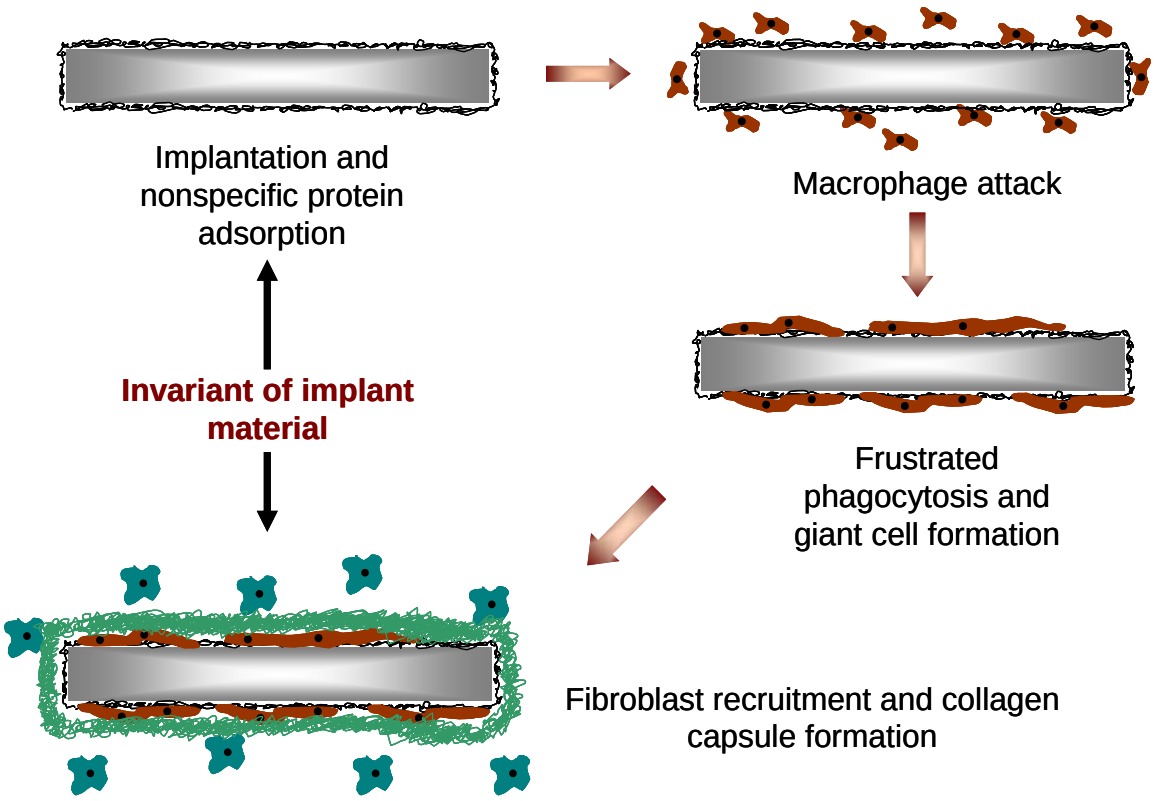

Figure 1.1. The progression of the foreign body response from device implantation to collagen capsule formation. Following protein adsorption to the implant, macrophages interrogate the foreign material, leading to frustrated phagocytosis and foreign body giant cell formation. Finally, fibroblasts form a collagen capsule around the implant, sequestering the foreign material from surrounding tissue. Adapted from Ratner, B.D., *J. Controlled Release*, **2002**, *78*, 211-218.

to sequester the implant from the surrounding tissue for the lifetime of the implant. The collagen capsule, coupled with the lack of proximal blood vessels and the persistent inflammatory response, is the root cause of many of the issues that plague implantable medical devices today. For example, chronic inflammation and scar tissue formation often lead to pain and discomfort for patients who receive artificial prostheses or cosmetic implants. More specifically, the dense collagen capsule prevents implantable drug delivery devices from functioning properly.[5] Likewise, the collagen capsule and the lack of blood vessels reduce the utility of implantable biosensors by decreasing the diffusion of blood analytes (e.g., glucose) to the sensor surface (Fig. 1.2).[6-8]

1.1.2 Device-associated infection. In addition to the deleterious effect of the foreign body response, medical devices and implants are highly susceptible to infection. Indeed, the presence of a foreign body drastically reduces the threshold of bacterial cells necessary to cause infection. Zimmerli et al. reported a 100% infection rate at subcutaneous implant sites inoculated with *Staphylococcus aureus* at a cell concentration of 1.0×10^3 colony forming units (CFUs). Without the subcutaneous implant, infections were not observed even up to 1.0×10^8 CFU *S. aureus* inoculations,[9] demonstrating that the threshold number of bacterial cells necessary to induce infection was decreased by 5 orders of magnitude in the presence of a foreign material. In a similar study, Wei and coworkers found that the threshold of bacterial cells necessary to induce pneumococcal meningitis was significantly lower in rats that had a cochlear implant than in those without an implant.[10] The authors concluded that the presence of a foreign body was an independent risk factor for bacterial infection.

Medical devices increase the likelihood of infection because they provide a substrate on which microbial cells can adhere and proliferate.[11] At the cellular level, device-associated

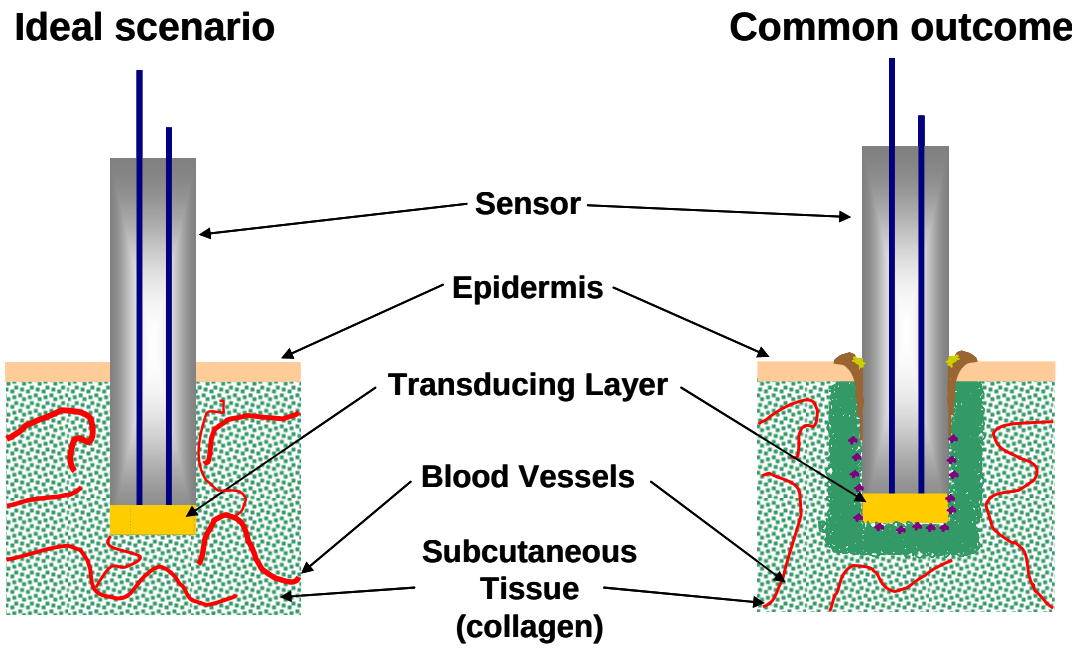

Figure 1.2. The foreign body response as it relates to the utility of implantable subcutaneous sensors. In the ideal scenario, the sensor heals within healthy vascularized tissue, ensuring sufficient mass transport of analytes from the blood to the sensor surface and adequate sensitivity. The typical foreign body response, however, sequesters the sensor within a dense capsule of avascular collagen, drastically reducing analyte diffusion to the sensor and severely limiting sensor performance.

infections are the result of bacterial adhesion to a biomaterial surface.[12] Upon implantation, a competition exists between integration of the material into the surrounding tissue and adhesion of bacteria to the implant surface.[13] For a successful implant, tissue integration occurs prior to appreciable bacterial adhesion, thereby inhibiting any colonization of the implant. Host defenses are often not capable of preventing further colonization if bacterial adhesion occurs before tissue integration.[13] A 6-h post-implantation "decisive period" has been identified during which prevention of bacterial adhesion is critical to the long-term success of an implant.[14] Over this period, the implant is particularly susceptible to surface colonization. At extended periods, certain species of adhered bacteria are capable of forming a biofilm at the implant-tissue interface. Biofilms are remarkably resistant to both the host immune response and systemic antibiotic intervention, resulting in life-threatening device-associated infection. Since the formation of a pathogenic biofilm ensues from the initial adhesion of bacteria to an implant surface, inhibiting bacterial adhesion is often regarded as the most critical step for preventing device-associated infection.

Infectious bacteria can be traced to several sources including the ambient atmosphere of the operating room, surgical equipment, clothing worn by medical professionals, the patient's skin, and bacteria already in the body.[15] Although sterilization and the use of aseptic techniques greatly reduces the levels of bacteria found in hospital settings, pathogenic microorganisms are still found at the site of approximately 90% of all implants.[16] The most common pathogens that cause implant infections include gram-positive *S. aureus* and *Staphylococcus epidermidis*, two species responsible for up to 60% of all prosthetic hip implant infections since 1980.[15] *S. aureus* infections proceed rapidly and are generally more severe than *S. epidermidis* infections. However, *S. epidermidis* has more accessibility as an

opportunistic pathogen since it is found ubiquitously on the skin. Other bacteria that have been implicated in device-associated infections include gram-negative *Escherichia coli*, *Pseudomonas aeruginosa*, and those from the *Proteus* group (e.g., *P. mirabilis* and *P. vulgaris*).[15]

Due to its fundamental role in the development of implant infections, the process of bacterial adhesion has been well-studied.[12] The adhesion of bacteria is preceded by the surface adsorption of a conditioning film of small organic compounds and macromolecules including proteins. Subsequently, the physicochemical forces that mediate bacterial adhesion can be divided into two time-dependent phases (Fig. 1.3). Phase I involves reversible cellular association with the surface over the first 1–2 h post-implantation. This non-specific association is mediated through long (e.g., gravitational, van der Waals, and electrostatic interactions) and short (e.g., hydrogen bonding, dipole-dipole, ionic, and hydrophobic interactions) range forces. Phase II begins approximately 2–3 h later and is characterized by stronger adhesion between the bacterial cells and the foreign material. Specific chemical interactions between compounds on the cell and substrate surfaces result in irreversible molecular bridging.[11] Both polysaccharides on and adhesin proteins within the bacterial membrane facilitate attachment to substrate surfaces. Beyond Phase II, certain bacterial strains are capable of forming a biofilm by self-secreting an exopolysaccharide matrix that retains nutrients and protects the microorganisms from the immune response.[12] With the protective polysaccharide coating and sequestered nutrients, bacteria in biofilms exhibit extreme resistance to antibiotics. In some cases, it has been found that killing bacteria in a biofilm requires approximately 1000 times the antibiotic dose necessary to achieve the same results in a suspension of cells.[17]

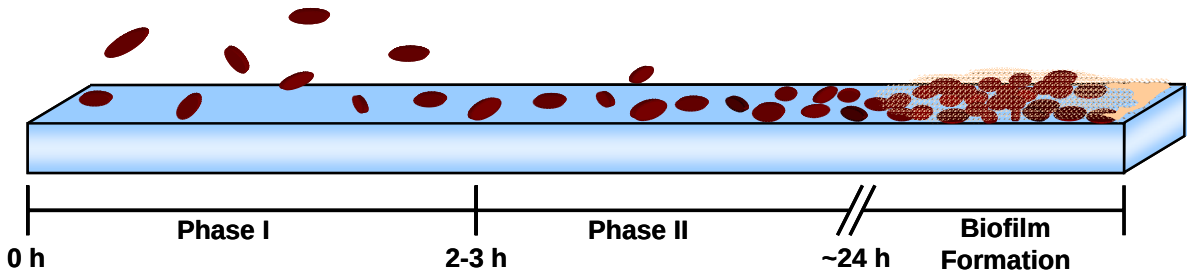

Figure 1.3. Representation of bacterial adhesion to a biomaterial substrate. Phase I adhesion involves reversible cellular association with the surface. During Phase II, bacteria undergo irreversible molecular bridging with the substrate through cell surface adhesin compounds. After approximately 1 d, certain bacterial species are capable of secreting a protective exopolysaccharide matrix (biofilm) that protects the adhered bacteria from host defenses and systemically-administered antibiotics.

1.2 Overview of current methods to mitigate the foreign body response

Since protein adsorption is one of the first events to occur when a biomaterial is placed in the body,[3] some researchers have hypothesized that changing the surface chemistry of the implant to limit or alter protein adsorption may reduce the ensuing foreign body response. For example, implants coated with tetraglyme (tetraethylene glycol dimethyl ether) were found to reduce fibrinogen adsorption to the implant surface. Unfortunately, in vivo studies demonstrated little difference in capsule formation between tetraglyme-coated implants and controls.[18] In fact, in a seminal in vivo study using ten different biomaterials, the thickness of the foreign body capsule formed at each implant proved invariant of the surface hydrophobicity or protein adsorption profile of each implant (Fig. 1.1).[18] Thus, it is evident that strategies to alter the foreign body response cannot rely solely on manipulating the surface chemistry of the implant. As a result, researchers have adopted approaches that include controlling the microarchitecture of the implant surface and/or engineering implants to elute compounds that play critical roles in the foreign body response.

1.2.1 Control over implant surface microarchitecture. Manipulation of the microarchitecture of the implant has proven useful for reducing the effects of the foreign body response.[19-23] For example, Picha and Drake[19] modified the surface of silicone rubber implants to include "pillar" microstructures with well-defined dimensions (100 μm diameter, 500 μm height, 100 μm inter-pillar distance). In vivo tissue compatibility studies showed a drastic decrease in the foreign body response and an increase in vascularization at implants with pillar microstructures versus control implants with smooth surfaces. Histology analysis indicated that smooth surface control implants resulted in the formation of 140 μm thick avascular collagen capsules. In contrast, the microstructure/pillar-modified substrates had

much thinner capsules (~10 μm thick) with higher degrees of vascularization. Indeed, blood vessels were found much closer to the microstructured implants than to the corresponding smooth control implants. For substrates implanted into the right posterior section of rats, the nearest blood vessel to control implants was on average 85 μm from the implant surface. Conversely, the nearest blood vessel to microstructured implants was only 5 μm from the implant surface. The foreign body response was thus shown to be drastically reduced at microstructured implants compared to smooth surface controls.

In a separate study, DeFife et al. used a templating approach to generate model biomaterial implants with controlled pore size.[21] As the pore size was increased from 66 to 157 μm, both the inflammatory response and foreign body giant cell index decreased by 56 and 21%, respectively. Collectively, the results suggest that capsule formation may be reduced by modulating the pore size of an implant. Instead of using pores, Sahlin et al. micropatterned TiO_2 dots with dimensions of 5, 10, 30, and 100 μm on polished quartz substrates.[22] In vitro studies performed with neutrophils and macrophages showed a significant reduction in the inflammatory response at micropatterned surfaces compared to non-patterned (i.e., smooth) surfaces.

The exact mechanism by which micropatterned surfaces enhance implant biocompatibility is not clearly understood.[24] As shown in Figure 1.4, it is generally accepted that the physical constraints imposed on inflammatory cells by the surface microarchitecture plays an important role.[24, 25] At smooth implants, macrophages fuse together to create multinucleated foreign body giant cells. This change in inflammatory cell phenotype alters the wound healing response, prompting the body to sequester the implant with a foreign body collagen capsule. Upon interrogating a micropatterned implant, however, macrophages are

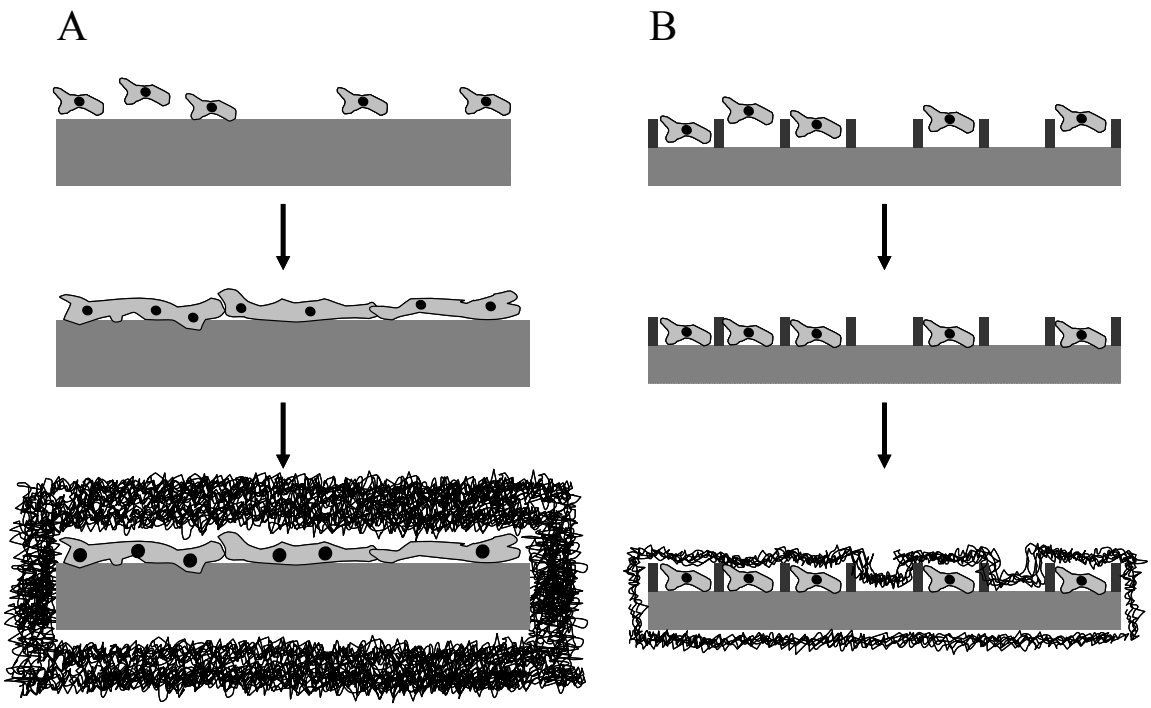

Figure 1.4. A) At smooth implant surfaces, macrophage attack is followed by the formation of foreign body giant cells and eventual collagen capsule formation. B) At micropatterned implants, it has been proposed that macrophages become spatially confined within the microstructures and are unable to fuse together to form foreign body giant cells. As a result, foreign body capsule formation at the micropatterned implant is significantly reduced.

physically constrained either within the microstructures or by the surface microarchitecture. As such, they are unable to fuse together into foreign body giant cells and do not change phenotype or trigger capsule formation.[25] A similar cell-confinement explanation has been provided for the reduced inflammatory response observed at micropatterned TiO_2 dots.[22] Picha and Drake suggest that the difference may be due to differential tissue formation within the microporous structures.[19] They propose that adipose tissue initially occupies the microstructures, thereby preventing inflammatory cells from entering the area. The intervening layer of adipose tissue reduces the shear forces between the implant and surrounding subcutaneous tissue, thereby moderating the fibrotic response that generally arises due to shear forces. While different rationalizations exist, the above studies clearly demonstrate the impact of micropatterned surfaces on the inflammatory and foreign body responses.

1.2.2 Implants engineered to elute anti-inflammatory and pro-angiogenic compounds. A more aggressive approach for mitigating the foreign body response involves modifying implants to release compounds that reduce inflammation and/or promote blood vessel growth (e.g., pharmaceutical agents and/or growth factors). The advantage of local active release of such compounds is that high doses may be delivered directly to the desired site of action while avoiding systemic toxicity concerns.[26, 27] Systemic administration also suffers from rapid clearance from the body, while elution directly from the implant allows sustained delivery over days or weeks.[26]

Since the formation of a fibrous tissue capsule is linked to the presence of neutrophils, macrophages, and foreign body giant cells (i.e., inflammation) at the tissue/implant interface, compounds that reduce the inflammatory response may also

decrease capsule thickness. For example, dexamethasone, a potent anti-inflammtory glucocorticoid that functions by reducing the migration of inflammatory cells and blocking the release of pro-inflammatory chemokines,[26, 28] limits fibroblast proliferation,[28] making it an attractive release compound for reducing collagen capsule formation at the site of implants. Due to its anti-inflammatory activity and ability to limit fibrosis, several groups have exploited dexamethasone to reduce the foreign body response at biomedical implants.

Hickey et al. incorporated dexamethasone into poly(lactide-*co*-glycolide) (PLGA) microspheres via an oil-in-water emulsion/solvent evaporation technique.[29] The release of dexamethasone from the PLGA microspheres, monitored via reverse-phase HPLC with UV detection, was continuous for >30 d, with a total of approximately 10 μg of dexamethsone released per mg of microspheres. Both control and dexamethasone-loaded microspheres were injected subcutaneously into the backs of rats adjacent to a cotton thread (included to simulate an implantable glucose sensor). The tissue inflammatory response was monitored via histological staining. As observed from tissue sections stained with hematoxylin & eosin (H&E), the inflammatory response at the site of dexamethasone-releasing microspheres was significantly reduced compared to control microspheres after both one week and one month.[29] After one month, thick fibrotic tissue was observed at the control microspheres, while the dexamethasone-releasing microspheres were characterized by significantly reduced fibrotic deposits.[29] The authors concluded that dexamethasone release may prove useful for improving the function of implantable subcutaneous glucose sensors.

Blanco et al. examined the ability of dexamethasone to improve the functionality of an implantable drug-delivery device.[26] Specifically, the ability of dexamethasone-releasing PLGA millirods to reduce collagen capsule formation at the tissue/implant interface of

radiofrequency-ablated liver tissue was investigated. Dexamethasone-modified millirods were synthesized via a compression-heat molding procedure.[30] The millirod composition with optimal release profile eluted 80% of the loaded dexamethasone after soaking in phosphate buffered saline for 6 h (as monitored via UV absorption spectroscopy). Roughly 95% of the drug was released after 4 d.[26] The investigators then implanted control and dexamethasone-releasing millirods into radiofrequency-ablated rat livers. To determine the effect of sustained dexamethasone release from the millirods, one set of control millirods received a bolus injection of dexamethasone in saline. After 4 d, the collagen capsules observed at control millirods both with and without injected dexamethasone were 0.13 ± 0.01 mm thick, while the capsules that formed at the dexamethasone-releasing millirods were only 0.02 ± 0.01 mm thick. These results indicate that sustained delivery of dexamethasone is required to reduce capsule thickness, as simply injecting an equivalent amount of dexamethasone adjacent to the millirods did not reduce capsule thickness. After 8 d, the collagen capsules that formed at control millirods, control millirods with injected aqueous dexamethasone, and dexamethasone-releasing millirods were 0.29 ± 0.08, 0.26 ± 0.07, and 0.04 ± 0.01 mm thick, respectively. The inflammatory response observed at the dexamethosone-releasing implants was also reduced compared to the control implants after 8 d. Blanco et al. suggest that by reducing collagen capsule thickness, the dexamethaxone release may be beneficial for improving the efficacy of other drug-delivery devices designed to release chemotherapeutic agents at the site of tumors.[26] Despite the success of dexamethasone release, concerns exist regarding the potentially serious side-effects of glucocorticoids,[31] including diabetes, hypertension, osteoporosis, and perhaps most alarmingly, infection and the inhibition of wound repair.[31, 32] Indeed, active-release implant

coatings designed to alter the inflammatory response may increase the likelihood of wound infection by limiting the body's natural defense mechanisms, thereby delaying wound healing, a potentially serious drawback of anti-inflammatory implant coatings.[32]

In addition to polymeric dexamethasone release, other strategies have focused on the controlled release of pro-angiogenic cytokines to increase vascularization in the tissue surrounding implants. This approach is employed most often in the context of implantable tissue-based biosensors, whose utility is severely limited by the formation of a hypovascular foreign body collagen capsule.[33, 34] The goal of pro-angiogenic cytokine release is to increase vascularization within the collagen capsule and decrease the distance between the indwelling sensor and blood vessels, thereby increasing analyte mass transfer from the blood to the sensor. The most commonly-employed pro-angiogenic cytokine to date is vascular endothelial growth factor (VEGF), which acts by initiating endothelial capillary formation.[35]

Multiple studies have demonstrated that controlled VEGF release from subcutaneous implants enhances vascularization in the tissue surrounding the implant.[35-37] Recent reports have focused on combination approaches to further boost angiogenesis, as well as fundamental studies to determine the spatial efficacy of controlled VEGF release.[37, 38] For example, Riley and coworkers loaded hyaluronic acid (HA) hydrogels with both VEGF and angiopoietin-1 (Ang-1) and tested their ability to promote blood vessel formation in a mouse ear angiogenesis model.[37] The authors predicted that VEGF, which initially stimulates new blood vessel formation, coupled with Ang-1, which aids in later blood vessel maturation,[37, 39] would lead to long-term vascularization at the implant site. Significantly more microvessels were observed at implants loaded with both cytokines compared to control sites. It was also found that VEGF and Ang-1 slowly released from a HA hydrogel elicited a significantly

greater angiogenic response than equivalent concentrations of cytokines delivered as aqueous solutions, the latter not resulting in increased blood vessel formation compared to controls. The data suggest that sustained release from a biomaterial is likely necessary to sustain angiogenesis.[37] A similar study by the same group demonstrated that HA hydrogels loaded with both VEGF and keratinocyte growth factor (KGF) also enhanced angiogenesis compared to blank HA hydrogels and hydrogels loaded with only VEGF or KGF.[39]

In another example of dual growth factor-loaded biomaterials, Richardson et al. created PLGA scaffolds that released both VEGF and platelet-derived growth factor (PDGF) for >30 days.[40] When implanted into the hindlimbs of mice, PLGA implants loaded with only VEGF resulted in a significant increase in angiogenesis after two weeks, but the vessels observed were small with little evidence of stabilization within the extracellular matrix. Delivery of PDGF alone did not increase the density of blood vessels observed near the implant, but did lead to larger vessels than control implants. When both VEGF and PDGF were released simultaneously, significantly more blood vessels were observed after both 2 and 4 weeks (approximately 110 and 115 vessels/mm^2 at 2 and 4 weeks, respectively), and were both larger and more mature than vessels formed at controls. Biomaterials designed to release dual growth factors simultaneously may represent the best approach for promoting the formation of large, stable blood vessels in the surrounding tissue.

Ward et al. reported on the spatial efficacy of VEGF release from a model biosensor implant.[41] Using a rat model, infusion of VEGF at 0.45 μm/day led to a 2- to 3-fold increase in blood vessel density at a distance of 1 mm from the infusion site compared to saline-releasing controls. A non-significant increase in blood vessel density was observed at 13 mm from the point of infusion, while at 25 mm no difference was observed between VEGF and

saline infusion. Systemic administration of VEGF influenced neither the capsule thickness nor the extent of inflammation at the implant site. Using an enzyme-linked immunosorbent assay (ELISA), the authors found that subcutaneous VEGF infusion also did not lead to elevated levels of VEGF in serum compared to saline-infused rats (71 ± 48 vs. 57 ± 52 pg/mL at 1 week for VEGF- and saline-treated rats, respectively). The data suggest that local delivery of VEGF likely does not provoke systemic secondary reactions.[41] Despite these findings, concerns remain regarding possible side-effects of VEGF administration.[41] For example, VEGF has been implicated in diabetic retinopathy,[42-44] rheumatoid arthritis,[45] and certain skin diseases,[46] and may play a role in the promotion or metastasis of select cancers.[47, 48]

1.3 Overview of current methods to prevent device-associated infections

Due to the critical role that bacterial adhesion plays in the pathogenesis of medical device-associated infections and wound healing, much effort has focused on developing polymeric device coatings that resist bacterial adhesion.[49] For in vivo applications, a competition exists between bacterial adhesion to the device surface and integration of the device into surrounding tissue.[13] If bacterial cells adhere to the device prior to tissue integration, the body's natural defense mechanisms may not be capable of preventing bacterial colonization and device infection. If, however, bacterial adhesion can be prevented for a certain period after device insertion (the typical goal is 6 h[14]), effective tissue integration may ensue and thus prevent colonization of the device surface. This competition between bacterial adhesion and tissue integration has been described as a "race for the surface".[13, 50] Several strategies have been developed in an attempt to reduce bacterial

adhesion and tip the balance in favor of effective tissue integration. Strategies to inhibit or reduce bacterial adhesion may be divided into three general approaches: 1) altering the surface physicochemical properties of the device; 2) incorporating or anchoring antimicrobial agents into/on a polymeric device coating; and, 3) engineering polymeric coatings to actively release antimicrobial agents.

1.3.1 Passive strategies for polymeric device coatings. One of the most straightforward methods for reducing bacterial adhesion involves altering the physicochemical properties of the device surface such that bacteria-substrate interactions are unfavorable. Several polymer coatings have been developed in this manner to passively reduce bacterial adhesion.[51] In general, increasing surface hydrophilicity correlates with reduced bacterial adhesion,[51] possibly by interrupting the hydrophobic effect between proteins on the surface of bacterial cells and hydrophobic substrates.[50] Approaches that have involved modifying polymers with hydrophilic functional groups have shown promise at reducing bacterial adhesion. For example, surfaces modified with poly(ethylene glycol),[52] poly(ethylene oxide) brushes,[53] and hydrophilic polyurethanes[54] have demonstrated reduced bacterial adhesion in vitro. Other approaches have exploited the negative surface charge of bacterial cell membranes at neutral pH.[51] For example, Harkes and coworkers demonstrated the influence of surface charge by testing the adhesion of three different strains of *E. coli* to polymers with varying zeta potentials.[55] The authors observed an increase in bacterial adhesion of each bacterial strain that corresponded directly with an increase in polymeric surface charge. Building on that observation, Kohnen et al. modified polyurethane with acrylic acid to generate a negatively-charged surface and observed decreased *S. epidermidis* adhesion compared to unmodified polyurethane.[51]

Yet another passive approach involves altering the surface free energy of the substrate to make bacterial adhesion unfavorable.[56] In situations where the surface tension of the medium in which bacterial cells are suspended is less than the surface free energy of the bacterial cells themselves, bacterial adhesion trends with the free energy of the substrate surface, i.e., lower surface free energy is expected to result in bacterial adhesion becoming more unfavorable.[57] As such, research efforts have focused on developing polymer coatings with low surface free energy. For antibacterial applications, the most commonly-employed low surface energy coatings are fluoropolymers,[56] which exhibit very low surface free energies due to the electronegativity of fluorine atoms.[56, 58] Indeed, the surface free energies (γ) of the $–CH_2–$, $–CH_3$, $–CF_2–$, and $–CF_3$ constituent groups are 36, 30, 23, and 15 $mJ \cdot m^{-2}$, respectively.[56, 59] Tsibouklis et al. developed poly(methylpropenoxyfluoroalkylsiloxane) and poly(perfluoroacrylate) coatings with surface free energies as low as 12.2 and 5.6 $mJ \cdot m^{-2}$, respectively, depending on the number of fluorine atoms in the polymer side-chains (with greater fluorine substitution resulting in lower surface energies).[60] The fluoropolymer coatings were compared to glass controls with respect to bacterial adhesion (γ_{glass} = 42.9 $mJ \cdot m^{-2}$).[61] Adhesion of *S. aureus* was reduced >95% compared to the glass controls.[60] In a separate study, Pereni et al. found that fluoropolymers (e.g., perfluoroalkoxy alkane [PFA, γ_{PFA} = 17.18 $mJ \cdot m^{-2}$] and polytetrafluoroethylene [PTFE, γ_{PTFE} = 21.35 $mJ \cdot m^{-2}$]) resulted in significantly lower *P. aeruginosa* adhesion than higher surface energy stainless steel (SS, γ_{SS} = 43.30 $mJ \cdot m^{-2}$) commonly used for orthopedic devices.[62]

Despite the success of passive device coatings at reducing bacterial adhesion in vitro, the formation of protein conditioning layers limits their effectiveness at reducing bacterial adhesion and related infection in vivo.[49, 63] Likewise, modulating the free energy of a

substrate surface is not always effective for reducing bacterial adhesion. Bacterial cells with low surface free energy are expected to adhere more readily to low free energy surfaces.[56] Indeed, studies have shown that hydrophobic bacteria adhere more preferentially to hydrophobic substrates, despite the low surface energy of those substrates.[64] Clearly, passive strategies alone are not sufficient to reduce bacterial adhesion and prevent device infection in vivo.

1.3.2 Antimicrobial agents covalently anchored to polymers. A further level of sophistication involving anti-infective device coatings involves modifying the surface of polymers with antimicrobial agents.[65, 66] Examples include adding biocides to polymers either during or after synthesis, constructing polymerizable monomers with antimicrobial activity, or grafting antimicrobial agents onto naturally-occurring polymers.[66] A primary advantage of these types of polymer coatings is that their efficacy is independent of traditional antibiotics, whose use continues to be questioned due to the ongoing threat of antibiotic-resistant bacteria.[67] Of all covalently-bound antimicrobial polymer systems, polymeric quaternary alkylammonium salts have received the most attention due to their broad-spectrum bactericidal activity and the relatively straightforward approaches for incorporating them into polymers.[66] For example, Ola et al.[68] have created antimicrobial polymers by employing a quaternary ammonium compound with both a long 18-carbon hydrophobic tail and a trimethoxysilyl group (3-(trimethoxysilyl)-propyldimethyloctadecyl ammonium chloride; Fig. 1.5) amenable to polymerization via the sol-gel process.[69] The polymer demonstrated >99.5% killing of planktonic *E. coli* within 1 h.[68] The mechanism by which quaternary alkylammonium salts kill bacterial cells involves insertion of the lipophilic

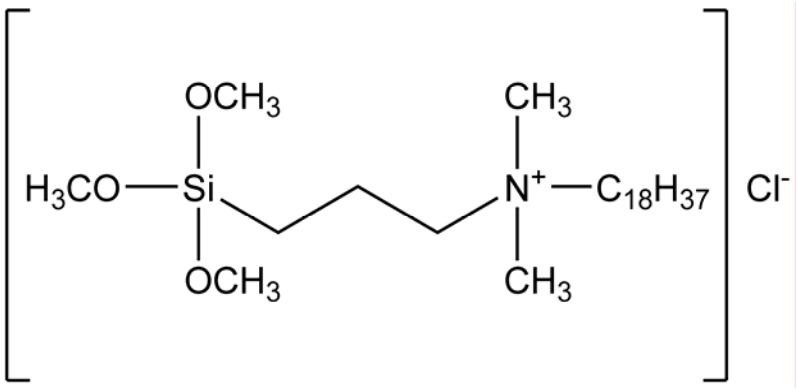

Figure 1.5. Structure of 3-(trimethoxysilyl)-propyldimethyloctadecyl ammonium chloride.

alkyl chain into the cell membrane followed by membrane disruption via the charged quaternary ammonium group.[70]

A polymer that has received a great deal of attention recently in the field of anti-infective coatings is chitosan.[66] Derived from chitin obtained from the shells of crustaceans, chitin is known for both its antimicrobial activity and wound-healing properties.[71] An advantage of chitosan polymers is that each monomer contains a free primary amine group amenable to modification with electrophilic reagents (Fig. 1.6). In a recent study, Kenawy et al.[71] covalently grafted chitosan polymers with vanillin, *p*-hydroxybenzaldehyde, *p*-chlorobenzaldehyde, anisaldehyde, methyl 4-hydroxybenzoate, methyl 2,4-dihydroxybenzoate, propyl 3,4,5-trihydroxybenzoate, and methyl 2-hydroxylbenzoate. The authors used a standard Kirby-Bauer disk-diffusion assay to measure the zone of inhibition (ZI) of microbial growth around each polymer, with greater antimicrobial activity resulting in a larger ZI. The *p*-hydroxy benzaldehyde-modified chitosan was found to be most effective against the pathogenic fungus *Candida albicans* (ZI = 45.0 mm), while vanillin-modified chitosan demonstrated the greatest antibacterial efficacy against *E. coli* (ZI = 26.0 mm) and *S. aureus* (ZI = 18.0 mm). Despite the promise of covalently-grafted antimicrobial polymers such as quaternary alkylammonium salts and chitosan, such coatings suffer similar decreased efficacy in vivo as passive coatings due to the potential masking properties of protein-conditioning films.[49, 63]

1.3.3 Silver-releasing device coatings. Yet a further level of sophistication in creating antimicrobial device coatings involves engineering polymers to slowly elute antibiotics and other antimicrobial agents. Perhaps the most widespread of such polymers are those designed to release silver ions. Many antibiotics operate specifically against certain

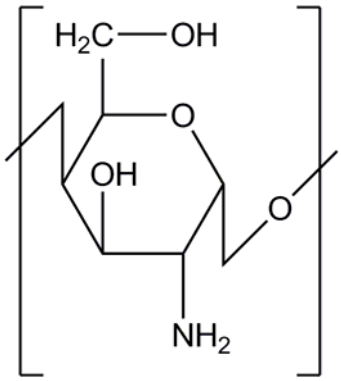

Figure 1.6. Structure of unmodified chitosan.

species of bacteria and show limited efficacy against others. In contrast, the antimicrobial properties of silver have been known for centuries,[72] and while nontoxic to mammalian cells and tissue,[73] the chemical nature of silver ions affords antibacterial activity via multiple mechanisms. Biomolecules such as proteins, enzymes, and cell-membrane components generally contain nucleophilic sulfhydryl, hydroxyl, and amine functionalities that are capable of coordinating ionic silver (Ag^+). As a result, Ag^+ reacts with and disrupts the function of bacterial cell membranes and crucial metabolic proteins and enzymes, ultimately leading to cell death. Silver cations also displace other metal ions that are essential to cell survival, including Zn^+ and Ca^{2+}. The bactericidal activity of Ag^+ is thus general and, to date, Ag^+ has demonstrated antibacterial efficacy against a broad spectrum of pathogens found at implant sites including *P. aeruginosa*, *E. coli*, *S. aureus*, and *S. epidermidis*.

Studies have already evolved to coating catheters[73] and orthopedic fixation pins[74] with metallic silver. While colonization was significantly reduced for silver-coated catheters in vitro,[73] in vivo studies with silver-coated fixation pins failed to demonstrate decreased bacterial adhesion.[74] Likewise, Sheehan et al. reported that silver coatings applied to model orthopedic implants did not result in decreased adhesion of *S. epidermidis* or *S. aureus*.[75] An explanation for the limited antibacterial efficacy of such silver coatings is that they do not actively release silver ions. Indeed, the antibacterial properties of silver have been attributed to its oxidized form (i.e., Ag^+), a form of silver that is not necessarily present at high concentrations at surfaces simply coated with metallic silver. Polymers that actively release silver in the oxidized state, however, have exhibited strong antibacterial activity. Such coatings act as reservoirs of silver and are capable of releasing bactericidal levels of Ag^+ for extended periods (>3 months).[76]

Recently, Furno and coworkers created antibacterial polymer coatings doped with silver particles ranging from 10-100 nm in diameter.[63] Organic silver complexes were dissolved in supercritical carbon dioxide and permeated into medical grade silicone rubber at high pressure. The release of Ag^+, measured by inductively coupled plasma mass spectrometry, was greatest over the first three days, with lower levels of release over the next two days. The initial burst of Ag^+ was found to be critical with respect to the antibacterial properties of the coatings. To explore if such release originated from silver particles existing at or near the polymer surface, sample coatings were washed after doping to remove surface-bound silver. Indeed, the washed coatings showed no inhibitory zones against *S. epidermidis*, analogous to control polymers that did not contain silver nanoparticles. The antibacterial activity of these coatings was also tested in the presence of a human plasma-derived protein conditioning film at the substrate surface to better mimic in vivo conditions. Although Ag^+ generally reacts rapidly with proteins, the bactericidal activity of the coatings was not eliminated in the presence of the in vitro protein coating, suggesting that such materials would maintain their antibacterial activity upon protein adsorption in vivo.[63] Indeed, this finding (i.e., reduced bacterial adhesion in the presence of a protein conditioning film) represents a primary advantage of active release coatings, as passive coatings have shown reduced efficacy in the presence of protein conditioning films.[49, 63]

Dowling and coworkers focused on methods to increase the level of Ag^+ delivered from silver surface coatings by incorporating platinum into the coating.[77] Since platinum is more cathodic than silver in the galvanic series, silver oxidation is enhanced when the two metals are in contact. The authors demonstrated that the addition of 3 wt% Pt to a metallic silver coating increased Ag^+ formation by a factor of two compared to standard silver

coatings. As expected, the Pt-doped silver coatings resulted in enhanced antibacterial efficacy due to increased Ag^+ release. In vitro experiments demonstrated that inclusion of 1 wt% Pt in a silver coating on polyurethane reduced *S. epidermidis* adhesion by almost two orders of magnitude compared to similar silver coatings without Pt. As well, the toxicity of such coatings to healthy fibroblast cells was not altered by the inclusion of platinum. Despite the proven in vitro antibacterial efficacy of Ag^+-releasing coatings, concerns about the development of Ag^+-resistant bacteria remain.[78, 79] Indeed, Ag^+-resistant mutants of *E. coli* have been identified that have active Ag^+ efflux systems and accumulate four times less Ag^+ than their Ag^+-susceptible counterparts.[79]

1.3.4 Antibiotic-releasing device coatings. Perhaps the most direct approach for improving the efficacy of conventional antibiotics against implant-associated infections is to deliver the antibiotics in a controlled manner at the implant from a surface coating. The topic of controlled drug release from implanted medical devices has been reviewed by Wu and Grainger.[27] The primary advantage of delivering antibiotics directly at the site of implantation is that high local doses may be administered without exceeding the systemic toxicity level of the drug. Localized administration also allows for the tailored selection of antibiotics toward specific pathogens associated with implant infections. As an example of antibiotic-releasing device coatings, Price and coworkers reported the synthesis of a biodegradable PLGA coating that actively released gentamicin.[80] Gentamicin sulfate and PLGA were dissolved in methylene chloride. The resulting solution was deposited onto stainless steel fracture plates by a standard coating/evaporation procedure. Gentamicin release, monitored via a fluorescence polarization immunoassay, was evaluated in vitro for coatings loaded with 10, 20, and 30 wt% gentamicin. The 20 and 30% coatings were both

characterized by an initial burst of antibiotic release (~250 and 2000 μg/mL, respectively) over the first 9–12 days. Burst release was not observed for the 10% formulation. The average daily release was dictated by initial antibiotic loading levels (10, 20, and 30% mixtures exhibited average daily release of 21, 133, and 374 μg/mL, respectively, over 20 d). For each coating, antibiotic release remained above the minimum inhibitory concentration (1-4 μg/mL) for pathogens commonly found to infect orthopedic devices (e.g., *S. aureus* and *S. epidermidis*) up to 20 d. An in vitro assay demonstrated that coatings with 20 wt% gentamicin reduced *S. aureus* viability by >99% over 24 d compared to uncoated control surfaces.[80] Despite the promising in vitro efficacy of antibiotic-releasing implant coatings, reluctance regarding their clinical application remains due to the fear that such coatings may foster antibiotic-resistant bacteria.[81]

1.3.5 Antibody-eluting device coatings. Immunotherapy (i.e., clinical delivery of externally-derived antibodies) has been an effective treatment for many diseases since the 1800s, exploiting the high specificity of antibody-antigen interactions to achieve therapeutic efficacy for patients with various medical conditions, including AIDS and other immune deficiency disorders.[82] Of the five major classes of human antibodies, IgG antibodies have proven to be the most useful as immunotherapeutics. IgG is directly involved in the natural immune response to infection through opsonization and phagocytosis. Pooled IgG antibodies possess specificity for a wide variety of epitopes expressed on bacterial cell surfaces. Through opsonization (i.e., antibody recognition of and binding to bacterial cell-surface antigens), IgG binds to invading bacterial cells, targeting them for phagocytic destruction by immune system components including neutrophils, monocytes, and macrophages (Fig. 1.7). IgG opsonization inhibits bacterial adhesion by blocking cell-surface attachment factors and

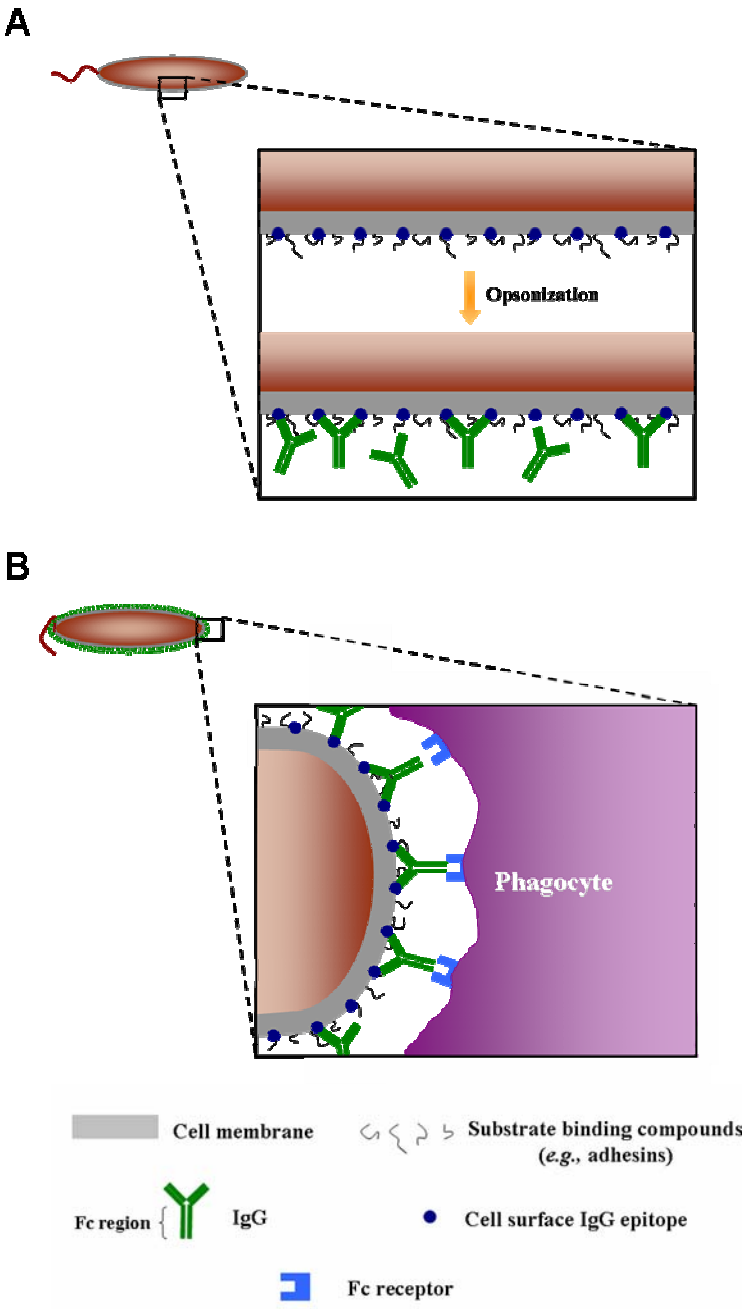

Figure 1.7. A) Opsonization of a bacterial cell via IgG binding to specific cell-surface epitopes, thereby blocking adhesin compounds. B) Opsonized bacteria are targeted to phagocytes for destruction.

altering the surface hydrophobicity of the cell. The motility of flagellar bacteria such as *E. coli* is also reduced upon opsonization, thereby inhibiting their mechanism of transport.[83] Due to these characteristics, treatment with exogenously-supplied IgG has been shown to diminish the severity of infections and reduce bacterial adhesion to model surfaces.[82]

To exploit the antimicrobial properties of IgG for possible application to medical devices, Rojas et al. developed a polyurethane coating that controllably released bioactive IgG for up to 25 h.[83] Lyophilized-pooled human IgG was homogenously dispersed in biomedical grade polyurethane solution and applied to latex tubing substrates through a dip-coating process. Following curing at 40 °C, antibody release from the coatings was measured in PBS via an enzyme-linked immunosorbent assay (ELISA). As with other controlled release coatings,[84] IgG was released in an initial burst over the first 7 h, with lower levels of release through 25 h. The total antibody flux was largely dependent on the initial loading levels. For example, IgG loaded at 15% (w/w in polyurethane) released roughly 50 $\mu g/cm^2$, while coatings loaded with 10% IgG released only ~17 $\mu g/cm^2$.[83] The anti-bacterial adhesion efficacy of the IgG release coatings was then evaluated in vitro. *E. coli* adhesion to IgG-releasing polyurethane coatings was reduced by two orders of magnitude compared to blanks after incubation in a bacterial suspension for 4, 8, and 24 h. The authors attributed the reduction in adhesion to steric blockage of bacterial attachment factors and decreased flagellar motility as a result of IgG opsonization. Of note, coatings that released IgG had lower levels of bacterial colonization than blank polyurethane coatings exposed to suspension of *E. coli* pre-treated with IgG. Polymer-released IgG also maintained its ability to direct phagocytic killing of bacteria. An in vitro assay with blood neutrophils showed that IgG released from polyurethane coatings killed 70-90% of *E. coli* cells, compared to <10%

for control surfaces. These results were attributed to the IgG-initiated targeting of bacteria to neutrophils (via opsonization) for destruction. Antibody released from the polyurethane coatings resulted in greater bacterial killing than aqueous phase IgG added to a bacterial suspension with blank polyurethane. Such data further substantiates the suggestion that IgG released from a polymer coating is more successful at mitigating implant-associated infection than exogenously-administered antibody treatments.[83] The same research group extended these findings to an in vivo study demonstrating that the controlled release of IgG from a hydrogel matrix reduced *P. aeruginosa* and *S. aureus* implant infection in a mouse model.[85] Despite the promise that controlled antibody release holds as a strategy for preventing implant-associated infection, clinical application may be limited due to possible overselectivity of antibodies for specific antigens and the high costs associated with immunotherapy.[86]

1.4 Nitric oxide

Despite the advances that have been made recently toward the development of more biocompatible and anti-infective device coatings, successes are tempered by potential side effects, drawbacks, or limited efficacy as discussed above. Moreover, most strategies are designed to address only one issue associated with biocompatibility (e.g., capsule thickness, the inflammatory response, angiogenesis, or infection). Indeed, relatively few strategies follow a multi-faceted approach towards improving biocompatibility.[87]

A more recent strategy that has proven effective at battling bacterial infection involves the release of nitric oxide (NO), a physiological signaling molecule endogenously produced by mammals.[88] One of the main advantages of NO-based therapies is that NO is

already synthesized within humans at picomolar to micromolar levels,[88] depending on the source and mode of action. Nitric oxide is a potent antimicrobial agent,[89-92] and has been shown to participate in all aspects of the foreign body response including inflammation,[72, 93] collagen deposition,[94, 95] and angiogenesis.[96, 97] In addition, NO plays an important role in the processes of wound-healing.[93, 98] For these reasons, studies focused on elucidating the ability of NO-releasing materials to fight infection and promote implant biocompatibility have generated great interest.

1.4.1 Physiological sources of NO. Nitric oxide is produced by a class of heme-containing enzymes known as nitric oxide synthases (NOSs).[88, 99] Three forms of NOS exist, the first two named for the cell type in which they were first discovered: neuronal NOS (nNOS), endothelial NOS (eNOS), and inducible NOS (iNOS). In contrast to iNOS, whose expression is induced by endotoxins and cytokines,[99] nNOS and eNOS are considered constitutive and thus always expressed.[88] Inducible NOS is found in neutrophils, macrophages, and other cells involved in the inflammatory response,[94] and is capable of producing high (μM) quantities of NO.[92] Unlike iNOS, constitutive NOSs operate in a Ca^{2+}-dependent manner and produce lower (pM) quantities of NO.[88] Despite the differences between inducible and constitutive NOSs, each enzyme produces NO in a remarkably similar manner via the oxidation of L-arginine to L-citrulline as shown in Figure 1.8.

1.4.2 Physiological roles of NO. The first physiological role of NO to be discovered was as the long-elusive endothelium-derived relaxing factor (EDRF), responsible for vasodilation and blood pressure regulation.[100, 101] This finding explained the efficacy of nitrovasodillatory drugs such as nitroglycerin and sodium nitroprusside.[88] Briefly, the mechanism of NO-induced vasodilation involves NO reacting with iron in the heme

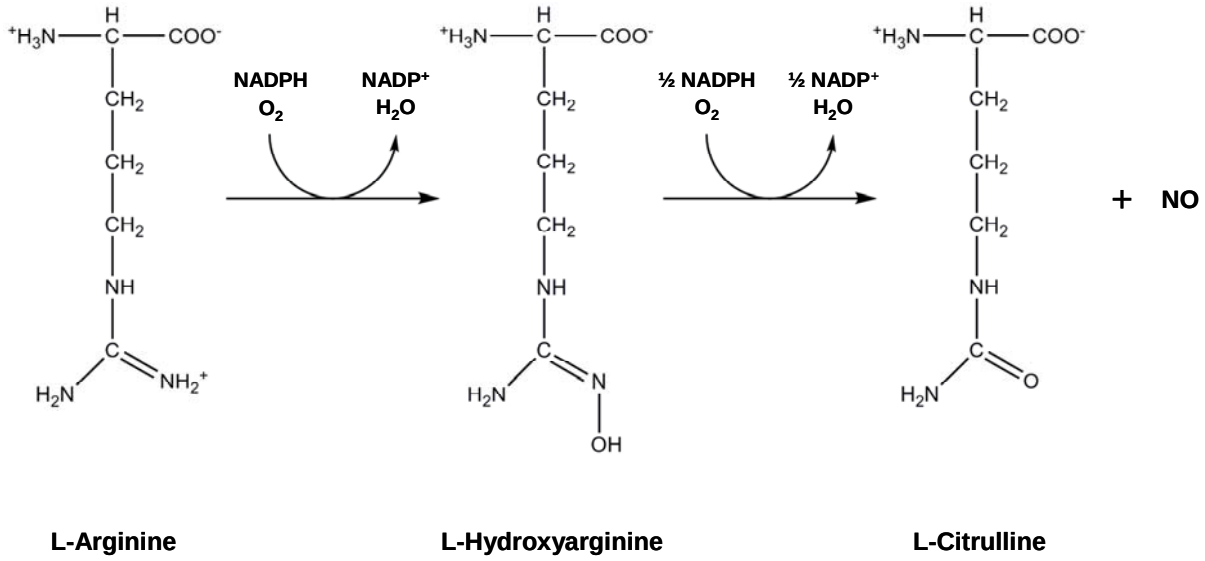

Figure 1.8. Reaction for the nitric oxide synthase-catalyzed conversion of L-arginine to L-hydroxyarginine, which is then oxidized to yield L-citrulline and nitric oxide.

prosthetic group of soluble guanylate cyclase, thus activating the enzyme which then catalyzes the production of cyclic guanosine monophosphate (cGMP), the compound ultimately responsible for vascular relaxation.[88] As a corollary, NOS inhibitors such as *N*-nitro-L-arginine methyl ester (L-NAME), an arginine mimic, are potent vasoconstrictors. Another important role of NO in the cardiovascular system is its ability to inhibit platelet aggregation, which also occurs via a cGMP-dependent mechanism.[88]

The discovery of a neuronal NOS isoform,[99] coupled with the detection of NO in all areas of animal and human brains[99, 102, 103] has highlighted NO's action in the central and peripheral nervous systems. Nitric oxide has been shown to play a role in the formation of memory,[104, 105] and inhibiting nNOS impairs learning behavior.[106] Nitric oxide is also involved in other sensory pathways including vision and olfaction.[88] In the peripheral nervous system, NO facilitates sensory transmission and helps regulate multiple digestive processes.[88]

In contrast to the roles that NO plays in the vascular and nervous systems (at pM concentrations generated by constitutive NOSs), antibacterial concentrations of NO (μM) are generated by the inducible isoform of NOS in inflammatory cells such as neutrophils and macrophages, which act as the body's first line of defense against microbial infection.[88, 92] Microbial infection and the presence of cytokines stimulate macrophages to produce NO, which acts as a strong oxidizing agent at such concentrations inducing oxidative stress both directly and indirectly through multiple reactive intermediates. The most lethal of these reactive species is peroxynitrite ($ONOO^-$), formed via the reaction between NO and superoxide (O_2^-), a species also produced by macrophages. Peroxynitrite has been implicated in cell membrane damage through lipid peroxidation.[107] Nitric oxide is also capable of

targeting important structures within bacterial cells, including DNA and proteins, upon diffusion across their cell membranes. Oxidation of DNA by NO either directly or via reactive intermediates is capable of irreparable damage by breaking the DNA strand. Nitric oxide can also nitrosate tyrosine and cysteine residues of proteins, primarily through its reaction products (e.g., N_2O_3 and N_2O_4). Nitrosation of even one amino acid residue is capable of altering protein function.[92] Indeed, macrophage-derived NO is so important in fighting infection that mice lacking iNOS are significantly more susceptible to bacterial infection than those with full NO-production capabilities.[90, 91]

1.4.3 Nitric oxide, infection, and the foreign body response. Due to the many roles that NO plays in physiology, research has focused on understanding the potential of NO-based therapies. While these efforts are multifaceted and span a range of potential clinical applications, a limited extent of research has centered on antimicrobial applications as well as those related to the foreign body response. For example, Raulli et al. have reported on the antibacterial properties of a small molecule NO donor, diazeniumdiolate-modified diethylenetriamine (DETA/NO), against several bacterial species.[11] The authors determined the minimum inhibitory concentration (MIC) of DETA/NO against both gram-negative and gram-positive pathogens, and found MICs ranging from 0.2 mg/mL for *S. epidermidis* to 12.0 mg/mL for *Enterococcus faecalis* and *Serratia maloescens*. In related work, Ghaffari et al. tested gaseous NO (200 ppm) against gram-negative and gram-positive bacteria (including methicillin-resistant *S. aurues* [MRSA]) and found NO to be effective against all species tested.[108] Moreover, the broad-spectrum antimicrobial properties of NO have been further established by McElhaney-Feser et al., who determined the MIC of DETA/NO against pathogenic fungal species including *Candida albicans* (MIC = 2.00 mg/mL), *Candida krusei*

(MIC = 1.20 mg/mL), and *Candida tropicalis* (MIC = 2.20 mg/mL).[11] Clearly, the therapeutic potential of NO release holds great promise as a strategy for battling microbial infections.

In addition to its antimicrobial properties, the influence of NO on multiple aspects of the foreign body response has been established. Most notably, NO has been shown to play a role in angiogenesis, inflammation, and collagen deposition. With respect to angiogenesis, NO promotes new blood vessel formation by modulating VEGF production.[96, 97] Related to inflammation, Amadeu et al. observed decreased recruitment of inflammatory cells with the administration of an exogenous NO donor to a cutaneous wound in a rat model.[93] The exact mechanism by which NO reduces inflammation is unclear, however, it may involve regulation of key inflammatory cytokines such as macrophage chemoattractant protein-1 (MCP-1) and interleukin-6 (IL-6),[94] or the formation of nitrosated proteins.[109] Nitric oxide also plays a critical role in collagen deposition by fibroblasts, and studies have demonstrated that collagen synthesis at a wound site was decreased in a dose-dependent manner with the application of an exogenous NO donor.[95] Studies have shown that NO's modulation of a key collagen-regulating cytokine, transforming growth factor-β (TGF-β), may be responsible for the observed decrease in collagen deposition.[94, 110, 111] Due to the ability of NO to influence angiogenesis, inflammation, and collagen deposition, it is apparent that NO applied at the site of subcutaneous implants may help mitigate the foreign body response. However, a thorough study of NO's effects on the foreign body response has yet to be conducted due to the lack of NO-releasing materials capable of delivering sustained NO release at the site of a subcutaneous implant.

1.5 Nitric oxide-releasing materials for enhanced biocompatibility and antimicrobial applications

Due to the diversity of its physiological roles in vivo and particularly those that may influence wound healing, compounds and materials capable of controlled NO release are warranted to design more biocompatible and anti-infective implant materials. Application of NO, whether in vitro or in vivo, requires stable NO donors that store biologically-relevant doses of NO and release it under physiological conditions. As a result, a wide variety of NO donors have been synthesized and their NO release characterized.[112, 113] Major classes of NO donors include metal-NO complexes, nitrosamines, nitrosothiols, and diazeniumdiolates.[112,113] Of all classes of NO donors, those that have found the most widespread application are diazeniumdiolates, due to their stability, ability to generate NO spontaneously under physiological conditions, and widely varying NO release kinetics (based on the structure of the NO donor precursor).[113] First described by Drago and Paulik in 1960,[114] *N*-diazeniumdiolates are formed via the reaction of polyamines with NO at high pressure (Figure 1.9**)**. When exposed to a proton source such as buffer or water, the diazeniumdiolate decomposes to generate 2 molecules of NO and the parent amine. The kinetics of diazeniumdiolate decomposition are accelerated at low pH and high temperature, illustrating the two major pathways for NO generation from diazeniumdiolates (i.e., proton-initiated and thermal decomposition).[113] As such, diazeniumdiolates are stable in the absence of a proton source at low temperature. Diazeniumdiolates have been formed on small molecules such as proline (PROLI/NO)[115] and diethylenetriamine (DETA/NO),[113] and larger macromolecular scaffolds such as dendrimers[116] and proteins such as bovine serum albumin (BSA).[117]

A

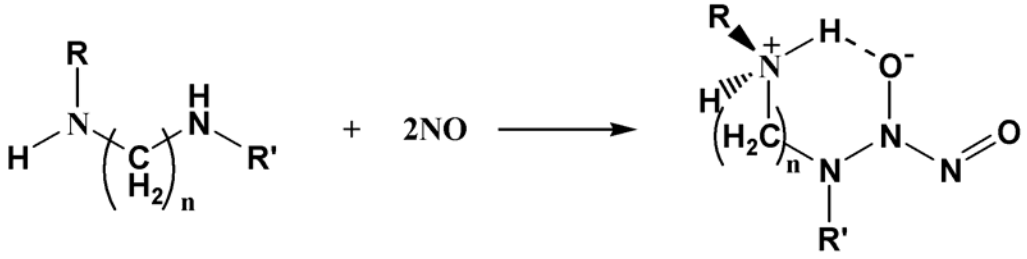

B

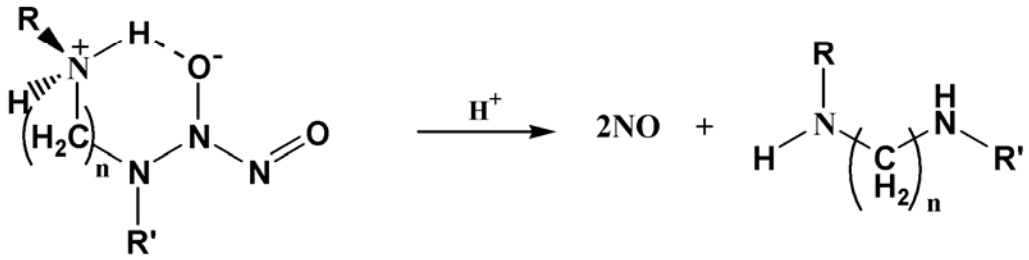

Figure 1.9. A) Reaction of NO with amines to produce diazeniumdiolate NO-donors; and B) diazeniumdiolate decomposition and NO release in the presence of a proton source such as water or buffer.

1.5.1 Nitric oxide-releasing polymers for blood-contacting devices. Due to the versatility of diazeniumdiolates as NO donors and NO's anti-thrombotic properties,[118] several diazeniumdiolate-based NO-releasing polymers have been designed to improve the thromboresistivity of blood-contacting biomaterials.[119] Mowery et al. synthesized NO-releasing polymers (e.g., polyurethane and poly(vinyl) chloride)) by three different methods: 1) dispersion of a small molecule diazeniumdiolate NO donor throughout the polymer matrix; 2) covalent attachment of the NO donor to the polymer backbone; and, 3) blending organic-soluble diazeniumdiolated heparin into the polymer.[120] The resulting polymers released NO for periods ranging from 10–72 h depending on the NO donor and polymer composition. To test blood compatibility, the NO-releasing polymers were exposed to platelet-rich plasma (PRP) obtained from sheep blood and the extent of platelet adhesion to each polymer system was analyzed via scanning electron microscopy (SEM) analysis. Compared to control (i.e., non-NO-releasing) samples, polymers doped with small molecule NO donor (diazeniumdiolate-modified *N*,*N*′-dimethyl-1,6-hexanediamine; MAHMA/NO), and those covalently modified with diazeniumdiolates were characterized by significantly less platelet adhesion. In contrast to control samples, the few platelets that adhered to the NO releasing samples were not activated, thereby demonstrating the thromboresistivity conferred to polymers modified to release NO. The polymer containing diazeniumdiolated heparin did not reduce platelet adhesion or activation, possibly due to polymer roughness or heparin's ability to induce platelet adhesion.[120] In related work, Schoenfisch et al. tested the analytical performance of NO-releasing oxygen sensors in a canine model.[121] The oxygen sensors modified to release NO demonstrated better analytical accuracy than control sensors, and less thrombus formation compared to controls, further demonstrating that the thromboresistivity

of NO release coatings is maintained in vivo. Despite these promising findings, the NO donor (MAHMA/NO) was found to leach from the polymer films, presenting potential toxicity concerns for clinical application.[120, 122]

1.5.2 Xerogel films. To improve on the strategies that employed small molecule NO donors simply doped into sensor membranes, Marxer et al. synthesized xerogel polymers whereby the NO donor precursor was covalently attached to the backbone of sol-gel derived (i.e., xerogel) polymers.[122] In this respect, leaching of amine decomposition byproducts was minimized. Briefly, the NO-releasing xerogel coatings were synthesized by reacting alkylalkoxysilanes (e.g. iso-butyltrimethoxysilane [BTMOS]) with aminoalkoxysilanes (e.g., (3-trimethoxysilylpropyl)-ethylenetriamine [DET3] and *N*-(6-aminohexyl)-aminopropyltri-methoxysilane [AHAP3]) through the sol-gel process (Fig. 1.10), creating a crosslinked glass-like polymer with covalently-linked NO donor precursors (amines) throughout the matrix. Subsequent exposure to high pressures of NO (~5 atm) facilitated the formation of diazeniumdiolate NO-donors at amines throughout the xerogel. In the presence of a proton source such as water or buffer, the xerogel released NO with a highly tunable NO flux (1-60 pmol cm^{-2} s^{-1}) based on the identity (structure) and amount of aminosilane precursor in the xerogel formulation. The NO release profiles for most formulations exhibited trends similar to other controlled-release coatings,[83, 84] with the maximal flux occurring soon after solution immersion, followed by a gradual decrease in NO release over time. Of note, the NO release from certain xerogel formulations was maintained at relatively consistent levels through 24 h. For example, a 40 v/v% DET3/BTMOS coating initially released ~60 pmol cm^{-2} s^{-1}, a flux that diminished to only ~50 pmol cm^{-2} s^{-1} after 24 h. The duration of NO release was also found to be dependent on the identity and amount of the aminosilane: 40% AHAP3/BTMOS

A

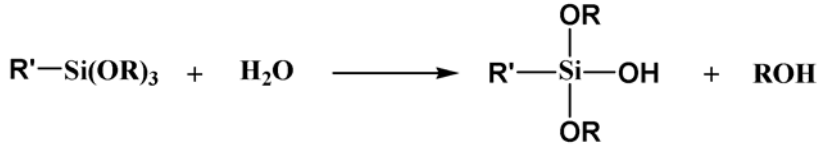

B

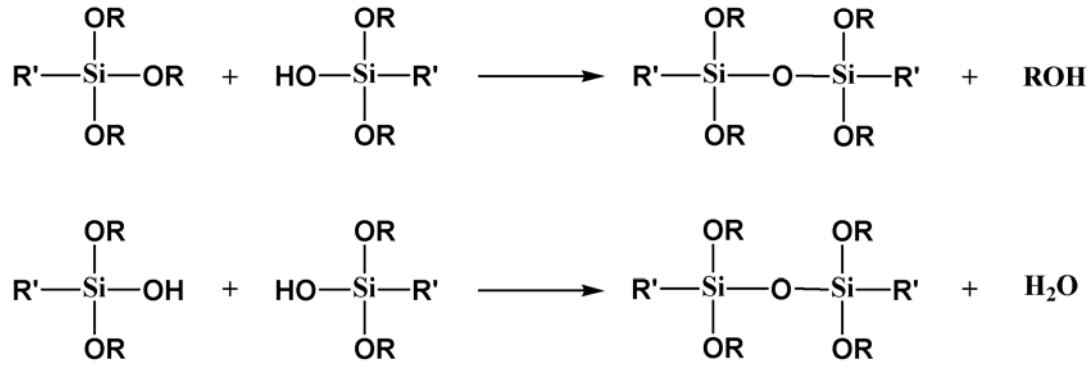

Figure 1.10. A) Hydrolysis of silane precursors; and B) subsequent condensation to form a xerogel polymer where R is typically a methyl or ethyl group and R′ is the amine-containing NO-donor precursor.

coatings released measurable quantities of NO up to 20 d.[122] Unfortunately, the maximum aminosilane concentration for the xerogels was limited by xerogel stability. As measured by direct current plasma optical emission spectroscopy (DCP-OES), aminosilane concentrations above 40% (v/v) led to polymer fragmentation at extended soak periods.[122]

The effectiveness of NO release from xerogel films at preventing bacterial adhesion was also investigated.[123-125] Nitric oxide-releasing xerogels were cast onto glass microscope slides and immersed in concentrated suspensions (10^8 CFU/mL) of *P. aeruginosa*.[123] Phase-contrast optical microscopy analysis revealed extensive bacterial adhesion at control surfaces (i.e., those that did not release NO) after only a 30 min incubation period. In some instances, clusters of bacterial cells were observed, representing possible nucleation sites for biofilm formation. In contrast, NO-releasing surfaces (1-20 pmol cm^{-2} s^{-1}) exhibited significantly reduced levels of *P. aeruginosa* adhesion (up to 93% reduction in bacterial adhesion at NO-releasing surfaces compared to controls). Bacteria present at the surface of NO release coatings were generally dispersed with minimal indication of biofilm nucleation sites.[123]

Nablo et al. modified stainless-steel substrates with xerogels to assess their efficacy as antibacterial coatings for orthopedic implant applications.[124] Nitric oxide-releasing xerogel-coated stainless steel was shown to significantly reduce *P. aeruginosa* adhesion compared to control (xerogel) and blank (bare steel) surfaces. A similar significant NO-mediated reduction was observed for *S. aureus* and *S. epidermidis*, although both adhered to controls at lower levels than *P. aeruginosa*.

To understand the flux of NO necessary to reduce bacterial adhesion, Nablo et al. synthesized xerogels of variable aminosilane compositions and NO release characteristics.[125] Poly(vinyl chloride) coatings were applied over the xerogels to ensure consistent surface

properties across samples. *P. aeruginosa* adhesion was reduced in a linear manner with increasing NO release up to ~20 pmol·cm^{-2}·s^{-1} (75% adhesion reduction). At fluxes >20 pmol cm^{-2} s^{-1}, NO had diminished effectiveness at further reducing adhesion.[125] The authors thus concluded that xerogels releasing NO at fluxes >20 pmol cm^{-2} s^{-1} exhibited the greatest anti-adhesion efficacy against *P. aeruginosa*. The collective results from these studies suggest that NO-release polymers may represent a new strategy for reducing the surface adhesion of medically-relevant gram-negative and gram-positive opportunistic pathogens. Moreover, control xerogel surfaces not modified to release NO have shown reduced bacterial and platelet adhesion compared to both glass and other biomaterial substrates,[122] demonstrating the inherent biocompatibility of xerogels themselves.

The in vivo efficacy of NO-releasing coatings against implant-associated infection was subsequently studied.[16] Xerogel coatings (40% AHAP3/BTMOS) were applied to medical-grade silicone elastomer via a dip coating process. Following sterilization, control and NO-releasing implants were placed in the subcutaneous tissue of adult male rats. Prior to wound closure, the implant sites were challenged with *S. aureus* (10 μL of a 10^8 CFU/mL suspension in PBS). After 8 d, the tissue surrounding each implant was analyzed for infection. Bacteria were present in 11 of the 15 tissue samples surrounding control implants. In contrast, bacteria were found in only 2 of the 15 samples surrounding the NO-releasing implants, indicating that sustained NO release may aid natural defense mechanisms to help clear bacteria and prevent implant-associated infection. Indeed, histological analysis revealed the formation of *S. aureus* biofilms at the sites of uncoated control implants. Such biofilms were not observed at any of the NO-releasing implants. The tissue surrounding NO-releasing implants appeared similar to that adjacent to uninfected controls.[16]

The in vitro and in vivo antibacterial studies outlined above demonstrate the promise that NO-releasing polymers hold as a strategy to prevent implant-associated infections. Certain questions remain, however, regarding the efficacy and mechanism of antibacterial activity. For example, the bacterial adhesion assays were conducted under "static" conditions, which require passing the substrate with adhered bacteria through an air/liquid interface. Previous studies have demonstrated that passage through an air/liquid interface presents sufficient shear force to remove loosely adhered bacteria,[126, 127] raising the question of whether NO release actually prevents bacterial adhesion or if it simply prevents bacterial retention.[128] A more recent innovation in bacterial adhesion testing involves the use of parallel plate flow cells, which prevent the passage of an air-liquid interface and allow real-time imaging of bacterial adhesion and biofilm formation.[14, 53, 129-131] Moreover, it is still uncertain as to if a low surface flux of NO can kill adhered bacterial cells in addition to preventing their adhesion. Killing adhered bacteria represents a more important step than merely preventing bacterial adhesion with respect to reducing biofilm formation.[132] Equally important is understanding the effect of NO release on tissue integration. As discussed above, NO plays multiple roles in the foreign body response.[72, 93-97, 110, 111] However, the influence of sustained NO delivery from an implant coating on the foreign body response in an animal model has yet to be studied.

1.5.3 Silica nanoparticles. While initial studies have focused on small molecule NO donors, one of the most recent advances in the field of NO-releasing materials is the development of nanoparticles that store and release large payloads of NO.[116, 133-137] Indeed, nitric oxide-releasing gold,[133] dendrimer,[116, 135] and silica[136, 137] nanoparticles have recently been synthesized. Building off the sol-gel approach used to create NO-releasing xerogels,[122]

the synthesis of NO-releasing silica particles represents one of the most versatile advances in the field of NO-based nanomaterials.[136, 137] Initially conceived of as an improvement over previously-developed fumed silica microparticles onto which NO donor precursors were grafted,[138] Shin et al. synthesized silica nanoparticles capable of storing extraordinarily large amounts of NO per mg.[137] Formed via the co-condensation of aminoalkoxysilanes with either tetramethoxy- or tetraethoxysilane, multiple types of silica nanoparticles have been prepared with varying sizes, NO release kinetics, and total NO storage capacity.[136, 137]

One of the most prominent areas of research receiving a great deal of current attention is the field of nanoparticle-based drug delivery.[139, 140] Indeed, the promising potential of silica nanoparticles as drug delivery agents is based on the chemical and physical versatility of silica, and the ability to tailor surface properties of the particles via functionalization.[136] While NO-releasing macromolecules have been proposed for anticoagulation,[135] restinosis,[17] and inhalation[141] therapies, one of the most pressing areas that NO-releasing nanoparticles are poised to influence is the field of antimicrobial therapy. At a time when antibiotic-resistant infections are becoming more prevalent, fewer new drugs for treating bacterial infections are being developed by the pharmaceutical industry and achieving FDA approval.[81] This alarming predicament has resulted in bacterial infections becoming the most common cause of infectious disease-related death in the U.S..[81, 142] Of the 2 million hospital-acquired infections that occur each year in the U.S., approximately 90,000 cases result in death.[81]

To address the shortage of effective antimicrobial agents, basic research has focused on engineering nanoparticles capable of killing pathogenic microbes. Examples of nanoparticle-based antimicrobial strategies include vancomycin-capped gold,[143] silver,[144-146]

and ionic liquid-releasing mesoporous silica[147] nanoparticles. While such particles have shown great promise at killing pathogenic bacteria, the use of conventional antibiotics (e.g., vancomycin) or classical antibacterial agents (e.g., Ag^{+}) continues to raise concern over the potential development of resistant bacteria.[78, 79, 81] As such, novel antibacterial nanoparticles that do not employ conventional antibiotics or classical antibacterial agents are highly desirable. Nitric oxide-releasing silica nanoparticles fit these criteria, and the rapid diffusion of NO through solution, tissue, and lipid membranes makes NO-releasing nanoparticles attractive for study as antimicrobial agents.[89, 148] Recent reports also suggest that the mechanisms of NO's antimicrobial properties are such that development of bacterial resistance to NO may be limited.[149] Although the antimicrobial properties of NO itself have been documented,[89-92, 150] the effectiveness of NO-releasing silica nanoparticles as bactericidal agents remains unknown. It is in this context that fundamental studies regarding the antibacterial efficacy of NO-releasing nanoparticles are urgently warranted.

1.6 Summary of dissertation research

Broadly, the goals of my dissertation research were to study the antimicrobial and wound-healing properties of NO-releasing materials. Specifically, the antibacterial and anti-biofilm properties of NO-releasing xerogel polymers and silica nanoparticles were characterized in vitro, and the influence of implant-derived NO on the foreign body response was examined in vivo. To determine the ability of NO-releasing xerogels to prevent bacterial adhesion under flowing conditions without the passage of an air-liquid interface, studies were conducted in a parallel plate flow cell. A secondary advantage of using the flow cell was the ability to monitor bacterial adhesion in real-time, providing important information regarding

the temporal aspects of the antibacterial efficacy of NO-releasing xerogels. Two separate methods were employed to determine the viability of bacterial cells adhered to the NO-releasing surfaces. Next, the foreign body response at implants modified to release NO was characterized in vivo. Although NO has been shown to influence multiple aspects of the foreign body response individually (e.g., inflammation, angiogenesis, and collagen deposition), limitations in NO-releasing materials have prevented a thorough study of the effect of sustained NO release on the entire foreign body response. Here, NO-releasing xerogel coatings were applied to model implants, which were then implanted into the subcutaneous tissue of rats. Following explantation, the foreign body response at control and NO-releasing implants was characterized in terms of capsule formation, collagen density, angiogenesis, and inflammation. Due to the great demand for novel antibacterial therapeutics, the ability of NO-releasing silica nanoparticles to kill both planktonic and biofilm-based pathogenic microbes was also studied. A portion of these studies was dedicated to understanding the antibacterial efficacy of NO-releasing nanoparticles in comparison to a previously-developed small molecule NO-donor. The efficacy of NO delivery to bacterial cells from both nanoparticles and a small molecule NO donor was studied, along with the toxicity of both systems to mammalian fibroblasts.

To summarize, the specific aims of my research included determining:

1) the ability of NO-releasing xerogels to prevent bacterial adhesion under flow conditions;
2) the viability of bacterial cells adhered to NO-releasing xerogels;

3) the influence of implant-derived NO on the foreign body response at subcutaneous implants in a rat model, with a focus on collagen capsule formation, angiogenesis, and the inflammatory response;
4) the ability of NO-releasing silica nanoparticles to kill planktonic bacterial cells, with a comparison of both the bactericidal activity and NO-delivery efficacy of silica nanoparticles with a small molecule NO donor;
5) the influence of surface-derived NO on bacterial proliferation and surface colonization; and,
6) the ability of NO-releasing silica nanoparticles to kill a broad spectrum of biofilm-based pathogens.

The goal of this introduction chapter was to provide an overview of the current strategies employed to mitigate the foreign body response, prevent bacterial adhesion and infection at indwelling medical devices, and to address the issue of antibiotic resistance and bacterial infections. In Chapter 2, the ability of NO-releasing xerogels to prevent bacterial adhesion under flowing conditions and kill bacterial cells that manage to adhere to the surface is presented. Chapter 3 presents the results of an in vivo study designed to examine the foreign body response at NO-releasing subcutaneous implants. The efficacy of NO-releasing silica nanoparticles against pathogenic microbial cells in their planktonic and biofilm states is presented in Chapters 4 and 5, respectively. Finally, Chapter 6 summarizes my work collectively and provides several avenues of future studies required to develop a more complete understanding of the potential of NO-based therapies for wound healing, tissue integration, and anti-infective applications.

1.7 References

(1) Ratner, B. D.; Bryant, S. J. "Biomaterials: Where we have been and where we are going." *Annu. Rev. Biomed. Eng.* **2004,** *6*, 41-75.

(2) Castner, D. G.; Ratner, B. D. "Biomedical surface science: Foundations to frontiers." *Surf. Sci.* **2002,** *500*, 28-60.

(3) Anderson, J. M. "Biological responses to materials." *Annu. Rev. Biomed. Eng.* **2001,** *31*, 81-110.

(4) Ryan, T. J. "Infection following soft tissue injury: Its role in wound healing." *Curr. Opin. Infect. Dis.* **2007,** *20*, 124-128.

(5) Ratner, B. D. "Reducing capsular thickness and enhancing angiogenesis around implant drug release systems." *J. Controlled Release* **2002,** *78*, 211-218.

(6) Wilson, G. S.; Hu, Y. "Enzyme-based biosensors for in vivo measurements." *Chem. Rev.* **2000,** *100*, 2693-2704.

(7) Frost, M. C.; Meyerhoff, M. E. "Implantable chemical sensors for real-time chemical monitoring: Progress and challenges." *Curr. Opin. Chem. Biol.* **2002,** *6*, 633-641.

(8) Wilson, G. S.; Gifford, R. "Biosensors for real-time in vivo measurements." *Biosens. Bioelectron.* **2005,** *20*, 2388-2403.

(9) Zimmerli, W.; Waldvogel, F. A.; Vaudaux, P.; Nydegger, U. E. "Pathogenesis of foreign body infection: Description and characteristics of an animal model." *J. Infect. Dis.* **1982,** *146*, 487-497.

(10) Wei, B. P. C.; Shepherd, R. K.; Robins-Browne, R. M.; Clark, G. M.; O'Leary, S. J. "Threshold shift: Effects of cochlear implantation on the risk of pneumococcal meningitis." *Otolaryngol. Head Neck Surg.* **2007,** *136*, 589-596.

(11) McElhaney-Feser, G. E.; Raulli, R. E.; Cihlar, R. L. "Synergy of nitric oxide and azoles against *Candida* species in vitro." *Antimicrob. Agents Chemother.* **1998**.

(12) Vacheethasanee, K.; Marchant, R. E., "Nonspecific *Staphylococcus epidermidis* adhesion: Contributions of biomaterial hydrophobicity and charge." In *Handbook of Bacterial Adhesion: Principles, Methods, and Applications*, An, Y. H.; Friedman, R. J., Eds. Humana Press: Totowa, NJ, 2000; p 74.

(13) Gristina, A. G. "Biomaterial-centered infection: Microbial adhesion versus tissue integration." *Science* **1987,** *237*, 1588-1595.

(14) Poelstra, K. A.; van der Mei, H. C.; Gottenbos, B.; Grainger, D. W.; van Horn, J. R.; Busscher, H. J. "Pooled human immunoglobulins reduce adhesion of *Pseudomonas aeruginosa* in a parallel plate flow chamber." *J. Biomed. Mater. Res.* **2000,** *51*, 224-232.

(15) An, Y. H.; Friedman, R. J. "Prevention of sepsis in total joint arthroplasty." *J. Hosp. Infect.* **1996,** *33*, 93-108.

(16) Nablo, B. J.; Prichard, H. L.; Butler, R. D.; Klitzman, B.; Schoenfisch, M. H. "Inhibition of implant-associated infections via nitric oxide release." *Biomaterials* **2005,** *26*, 6984-6990.

(17) Pulfer, S. K.; Ott, D.; Smith, D. J. "Incorporation of nitric oxide-releasing crosslinked polyethyleneimine microspheres into vascular grafts." *J. Biomed. Mater. Res.* **1997,** *37*, 182-189.

(18) Ratner, B. D. In "Biomaterials, biocompatibility, inflammation, and wound healing technology: Rules to live by," 1st International Symposium on Wound Healing and Technology (WHAT I), Seattle, WA, August 30th, 2006; Seattle, WA, **2006**.

(19) Picha, G. J.; Drake, R. F. "Pillared-surface microstructure and soft-tissue implants: Effect of implant site and fixation." *J. Biomed. Mater. Res.* **1996,** *30*, 305-312.

(20) Anderson, J. M.; DeFife, K.; McNally, A.; Collier, T.; Jenney, C. "Monocyte, macrophage, and foreign body giant cell interactions with molecularly engineered surfaces." *J. Mater. Sci. Mater. Med.* **1999,** *10*, 579-588.

(21) DeFife, K. M.; Colton, E.; Nakayama, Y.; Matsuda, T.; Anderson, J. M. "Spatial regulation and surface chemistry control of monocyte/macrophage adhesion and foreign body giant cell formation by photochemically micropatterned surfaces." *J. Biomed. Mater. Res.* **1999,** *45*, 148-154.

(22) Sahlin, H.; Contreras, R.; Gaskill, D. F.; Bjursten, L. M.; Frangos, J. A. "Anti-inflammatory properties of micropatterned titanium coatings." *J. Biomed. Mater. Res.* **2006,** *77A*, 43-49.

(23) Bezuidenhout, D.; Davies, N.; Zilla, P. "Effect of well defined dodecahedral porosity on inflammation and angiogenesis." *ASAIO Journal* **2002,** *48*, 465-471.

(24) Rosengren, A.; Bjursten, L. M. "Pore size in implanted polypropylene filters is critical for tissue organization." *J. Biomed. Mater. Res.* **2003,** *67A*, 918-926.

(25) Sanders, J. E.; Lamont, S. E.; Karchin, A.; Golledge, S. L.; Ratner, B. D. "Fibroporous meshes made from polyurethane micro-fibers: Effects of surface charge on tissue response." *Biomaterials* **2005,** *26*, 813-818.

(26) Blanco, E.; Weinberg, B. D.; Stowe, N. T.; Anderson, J. M.; Gao, J. "Local release of dexamethasone from polymer millirods effectively prevents fibrosis after radiofrequency ablation." *J. Biomed. Mater. Res.* **2006,** *76A*, 174-182.

(27) Wu, P.; Grainger, D. W. "Drug/device combinations for local drug therapies and infection prophylaxis." *Biomaterials* **2006,** *27*, 2450-2467.

(28) Schimmer, B.; Parker, K., "Adrenocorticotropic hormone; adrenocortical steroids and their synthetic analogs; inhibitors of the synthesis and actions of adrenocortical hormones." In *The Pharmacological Basis of Therapeutics*, 9th ed.; Hardman, J.; Limbird, L.; Molinoff, P.; Ruddon, R.; Gilman, A., Eds. McGraw-Hill: New York, 1996; pp 1459-1485.

(29) Hickey, T.; Kreutzer, D.; Burgess, D. J.; Moussy, F. "In vivo evaluation of a dexamethasone/PLGA microsphere system designed to suppress the inflammatory tissue response to implantable medical devices." *J. Biomed. Mater. Res.* **2002,** *61*, 180-187.

(30) Qian, F.; Szymanski, A.; Gao, J. "Fabrication and characterization of controlled release poly(D,L-lactide-co-glycolide) millirods." *J. Biomed. Mater. Res.* **2001,** *55*, 512-522.

(31) Miner, J. N.; Ardecky, B.; Benbatoul, K.; Griffiths, K.; Larson, C. J.; Mais, D. E.; Marschke, K.; Rosen, J.; Vajda, E.; Zhi, L.; Negro-Vilar, A. "Antiinflammatory glucocorticoid receptor ligand with reduced side effects exhibits an altered protein-protein interaction profile." *Proc. Natl. Acad. Sci. U.S.A.* **2007,** *104*, 19244-19249.

(32) Rosen, J.; Miner, J. N. "The search for safer glucocorticoid receptor ligands." *Endocr. Rev.* **2005,** *26*, 452-464.

(33) Wisniewski, N.; Moussy, F.; Reichert, W. M. "Characterization of implantable biosensor membrane biofouling." *Fresenius' J. Anal. Chem.* **2000,** *366*, 611-621.

(34) Koschwanez, H. E.; Reichert, W. M. "In vitro, in vivo, and post explantation testing of glucose-detecting biosensors: Current methods and recommendations." *Biomaterials* **2007,** *28*, 3687-3703.

(35) Zisch, A. H.; Lutolf, M. P.; Hubbell, J. A. "Biopolymeric delivery matrices for angiogenic growth factors." *Cariovasc. Path.* **2003,** *12*, 295-310.

(36) Dellian, M.; Witwer, B. P.; Salehi, H. A.; Yuan, F.; Jain, R. K. "Quantitation and physiological characterization of angiogenic vessels in mice." *Am. J. Path.* **1996,** *149*, 59-71.

(37) Riley, C. M.; Fuegy, P. W.; Firpo, M. A.; Shu, X. Z.; Prestwich, G. D.; Peattie, R. A. "Stimulation of in vivo angiogenesis using dual growth factor-loaded crosslinked glycosaminoglycan hydrogels." *Biomaterials* **2006,** *27*, 5935-5943.

(38) Ravin, A. G.; Olbrich, K. C.; Levin, L. S.; Usala, A. L.; Klitzman, B. "Long- and short-term effects of biological hydrogels on capsule microvascular density around implants in rats." *J. Biomed. Mater. Res.* **2001,** *58*, 313-318.

(39) Peattie, R. A.; Rieke, E. R.; Hewett, E. M.; Fisher, R. J.; Shu, X. Z.; Prestwich, G. D. "Dual growth factor-induced angiogenesis in vivo using hyaluronan hydrogel implants." *Biomaterials* **2006,** *27*, 1868-1875.

(40) Richardson, T. P.; Peters, M. C.; Ennett, A. B.; Mooney, D. J. "Polymeric system for dual growth factor delivery." *Nat. Biotech.* **2001,** *19*, 1029-1034.

(41) Ward, W. K.; Quinn, M. J.; Wood, M. D.; Tiekotter, K. L.; Pidikiti, S.; Gallagher, J. A. "Vascularizing the tissue surrounding a model biosensor: How localized is the effect of a subcutaneous infusion of vascular endothelial growth factor (VEGF)?" *Biosens. Bioelectron.* **2003,** *19*, 155-163.

(42) Funatsu, H.; Yamashita, H.; Ikeda, T.; Nakanishi, Y.; Kitano, S.; Hori, S. "Angiotensin II and vascular endothelial growth factor in the vitreous fluid of patients with diabetic macular edema and other retinal disorders." *Am. J. Ophthalmol.* **2002,** *133*, 537-543.

(43) Noma, H.; Funatsu, H.; Yamashita, H.; Kitano, S.; Mishima, H. K.; Hori, S. "Regulation of angiogenesis in diabetic retinopathy: Possible balance between vascular endothelial growth factor and endostatin." *Arch. Ophthalmol.* **2002,** *120*, 1075-1080.

(44) Simo, R.; Lecube, A.; Segura, R. M.; Garcia Arumi, J.; Hernandez, C. "Free insulin growth factor-I and vascular endothelial growth factor in the vitreous fluid of patients with proliferative diabetic retinopathy." *Am. J. Ophthalmol.* **2002,** *134*, 376-382.

(45) Afuwape, A. O.; Kiriakidis, S.; Paleolog, E. M. "The role of the angiogenic molecule VEGF in the pathogenesis of rheumatoid arthritis." *Histol. Histopathol.* **2002,** *17*, 961-972.

(46) Brown, L. F.; Harrist, T. J.; Yeo, K. T.; Stahle-Backdahl, M.; Jackman, R. W.; Berse, B.; Tognazzi, K.; Dvorak, H. F.; Detmar, M. "Increased expression of vascular permeability factor (vascular endothelial growth factor) in bullous pemphigoid, dermatitis herpetiformis, and erythema multiforme." *J. Invest. Dermatol.* **1995,** *104*, 744-749.

(47) Paley, P. J.; Goff, B. A.; Gown, A. M.; Greer, B. E.; Sage, E. H. "Alterations in SPARC and VEGF immunoreactivity in epithelial ovarian cancer." *Gynecol. Oncol.* **2000,** *78*, 336-341.

(48) Niedergethmann, M.; Hildenbrand, R.; Wostbrock, B.; Hartel, M.; Sturm, J. W.; Richter, A.; Post, S. "High expression of vascular endothelial growth factor predicts early recurrence and poor prognosis after curative resection for ductal adenocarcinoma of the pancreas." *Pancreas* **2002,** *25*, 122-129.

(49) Hetrick, E. M.; Schoenfisch, M. H. "Reducing implant-related infections: Active release strategies." *Chem. Soc. Rev.* **2006,** *35*, 780-789.

(50) An, Y. H.; Dickinson, R. B.; Doyle, R. J., "Mechanisms of bacterial adhesion and pathogenesis of implant and tissue infections." In *Handbook of Bacterial Adhesion: Principles, Methods, and Applications*, An, Y. H.; Friedman, R. J., Eds. Humana Press: Totowa, NJ, 2000; pp 1-27.

(51) Kohnen, W.; Jansen, B., "Changing material surface chemistry for preventing bacterial adhesion." In *Handbook of Bacterial Adhesion: Principles, Methods, and Applications*, An, Y. H.; Friedman, R. J., Eds. Humana Press: Totowa, NJ, 2000; pp 581-589.

(52) Kingshott, P.; Wei, J.; Bagge-Ravn, D.; Gadegaard, N.; Gram, L. "Covalent attachment of poly(ethylene glycol) to surfaces, critical for reducing bacterial adhesion." *Langmuir* **2003,** *19*, 6912-6921.

(53) Kaper, H. J.; Busscher, H. J.; Norde, W. "Characterization of poly(ethylene oxide) brushes on glass surfaces and adhesion of *Staphylococcus epidermidis*." *J. Biomater. Sci. Pol. Ed.* **2003,** *14*, 313-324.

(54) Nagel, J. A.; Dickinson, R. B.; Cooper, S. L. "Bacterial adhesion to polyurethane surfaces in the presence of pre-adsorbed high molecular weight kininogen." *J. Biomater. Sci. Pol. Ed.* **1996,** *7*, 769-770.

(55) Harkes, G.; Feijen, J.; Dankert, J. "Adhesion of *Escherichia coli* on to a series of poly(methacrylates) differing in charge and hydrophobicity." *Biomaterials* **1991,** *12*, 853-860.

(56) Roosjen, A.; Norde, W.; van der Mei, H.; Busscher, H. J. "The use of positively charged or low surface energy coatings versus polymer brushes in controlling biofilm formation." *Progr. Colloid. Polym. Sci.* **2006,** *132*, 138-144.

(57) Quirynen, M.; Dierickx, K.; van Steenberghe, D., "Effects of surface roughness and free energy on oral bacterial adhesion." In *Handbook of Bacterial Adhesion: Principles, Methods, and Applications*, An, Y. H.; Friedman, R. J., Eds. Humana Press: Totowa, NJ, 2000; pp 91-102.

(58) Thomas, R. R., "Material properties of fluoropolymers and perfluoroalkyl-based polymers." In *Fluoropolymers 2: Properties*, Hougham, G.; Cassidy, P. E.; Johns, K.; Davidson, T., Eds. Plenum Press: New York, 1999; pp 47-65.

(59) Tsibouklis, J.; Nevell, T. G. "Ultra-low surface energy polymers: The molecular design requirements." *Adv. Mater.* **2003,** *15*, 647-650.

(60) Tsibouklis, J.; Stone, M.; Thorpe, A. A.; Graham, P.; Nevell, T. G.; Ewen, R. J. "Inhibiting bacterial adhesion onto surfaces: The non-stick coating approach." *Int. J. Adhesion Adhesives* **2000,** *20*, 91-96.

(61) Dhathathreyan, A.; Maheshwari, R. "Surface energy, wettability, and water vapor permeability of Langmuir-Blodgett films of protein-polymer composites." *Langmuir* **2002,** *18*, 10039-10041.

(62) Pereni, C. I.; Zhao, Q.; Liu, Y.; Abel, E. "Surface free energy effect on bacterial retention." *Colloids Surf., B* **2006,** *48*, 143-147.

(63) Furno, F.; Morley, K. S.; Wong, B.; Sharp, B. L.; Arnold, P. L.; Howdle, S. M.; Bayston, R.; Brown, P. D.; Winship, P. D.; Reid, H. J. "Silver nanoparticles and polymeric medical devices: A new approach to prevention of infection?" *J. Antimicrob. Chemother.* **2004,** *54*, 1019-1024.

(64) Bakker, D. P.; Huijs, F. M.; de Vries, J.; Klijnstra, J. W.; Busscher, H. J.; van der Mei, H. "Bacterial deposition to fluoridated and non-fluoridated polyurethane coatings with different elastic modulus and surface tension in a parallel plate and a stagnation point flow chamber." *Colloids Surf., B* **2003,** *32*, 179-190.

(65) Worley, S. D.; Sun, G. "Biocidal polymers." *Trends Polym. Sci.* **1996,** *4*, 364-370.

(66) Kenawy, E. R.; Worley, S. D.; Broughton, R. "The chemistry and applications of antimicrobial polymers: A state-of-the-aret review." *Biomacromolecules* **2007,** *8*, 1359-1384.

(67) Kurt, P.; Wood, L.; Ohman, D. E.; Wynne, K. J. "Highly effective contact antimicrobial surfaces via polymer surface modifiers." *Langmuir* **2007,** *23*, 4719-4723.

(68) Ola, S. M. A. E.; Kotek, R.; White, W. C.; Reeve, J. A.; Hauser, P.; Kim, J. H. "Unusual polymerization of 3-(trimethoxysilyl)-propyldimethyloctadecyl ammonium chloride on PET substrates." *Polymer* **2004,** *45*, 3215-3225.

(69) Livage, J.; Sanchez, C. "Sol-gel chemistry." *J. Non-Cryst. Solids* **1992,** *145*, 11-19.

(70) Kuroda, K.; DeGrado, W. F. "Amphiphilic polymethacrylate derivatives as antimicrobial agents." *J. Am. Chem. Soc.* **2005,** *127*, 4128-4129.

(71) Kenawy, E. R.; Abdel-Hay, F. I.; El-Magd, A. A.; Mahmoud, Y. "Biologically active polymers: Modification and anti-microbial activity of chitosan derivatives." *J. Bioact. Compat. Polym.* **2005,** *20*, 95-111.

(72) Gifford, R.; Batchelor, M. M.; Lee, Y.; Gokulrangan, G.; Meyerhoff, M. E.; Wilson, G. S. "Mediation of in vivo glucose sensor inflammatory response via nitric oxide release." *J. Biomed. Mater. Res.* **2005,** *75A*, 755-766.

(73) Bologna, R. A.; Tu, L. M.; Polansky, M.; Fraimow, H. D.; Gordon, D. A.; Whitmore, K. E. "Hydrogel/silver ion-coated urinary catheter reduces nosocomial urinary tract infection rates in intensive care unit patients: A multicenter study." *Urology* **1999,** *54*, 982-987.

(74) Masse, A.; Bruno, A.; Bosetti, M.; Biasibetti, A.; Cannas, M.; Gallinaro, P. "Prevention of pin track infection in external fixation with silver coated pins: Clinical and microbiological results." *J. Biomed. Mater. Res.* **2000,** *53*, 600-604.

(75) Sheehan, E.; McKenna, J.; Mulhall, K. J.; Marks, P.; McCormack, D. "Adhesion of *Staphylococcus* to orthopedic metals, an in vivo study." *J. Orthop. Res.* **2004,** *22*, 39-43.

(76) Kumar, R.; Munstedt, H. "Silver ion release from antimicrobial polyamide/silver composites." *Biomaterials* **2005,** *26*, 2081-2088.

(77) Dowling, D. P.; Betts, A. J.; Pope, C.; McConnell, M. L.; Eloy, R.; Arnaud, M. N. "Anti-bacterial silver coatings exhibiting enhanced activity through the addition of platinum." *Surf. Coat. Technol.* **2003,** *163-164*, 637.

(78) Silver, S. "Bacterial silver resistance: Molecular biology and uses and misuses of silver compounds." *FEMS Microbiol. Rev.* **2003,** *27*, 341-353.

(79) Li, X. Z.; Nikaido, H.; Williams, K. E. "Silver-resistant mutants of *Escherichia coli* display active efflux of Ag^{+} and are deficient in porins." *J. Bacteriol.* **1997,** *179*, 6127-6132.

(80) Price, J. S.; Tencer, A. F.; Arm, D. M.; Bohach, G. A. "Controlled release of antibiotics from coated orthopedic implants." *J. Biomed. Mater. Res.* **1996,** *30*, 281-286.

(81) "Bad bugs, no drugs: As antibiotic discovery stagnates, a public health crisis brews." Infectious Diseases Society of America: Arlington, VA, **2004**, pp 1-35.

(82) Grainger, D. W. "Controlled-release and local delivery of therapeutic antibodies." *Expert Opin. Biol. Ther.* **2004,** *4*, 1029-1044.

(83) Rojas, I. A.; Slunt, J. B.; Grainger, D. W. "Polyurethane coatings release bioactive antibodies to reduce bacterial adhesion." *J. Controlled Release* **2000,** *63*, 175-189.

(84) Kwok, C. S.; Wan, C.; Hendricks, S.; Bryers, J. D.; Horbett, T. A.; Ratner, B. D. "Design of infection-resistant antibiotic-releasing polymers: I. Fabrication and formulation." *J. Controlled Release* **1999,** *62*, 289-299.

(85) Poelstra, K. A.; Barekzi, N. A.; Rediske, A. M.; Felts, A. G.; Slunt, J. B.; Grainger, D. W. "Prophylactic treatment of gram-positive and gram-negative abdominal implant infections using locally delivered polyclonal antibodies." *J. Biomed. Mater. Res.* **2002,** *60*, 206-215.

(86) Tomioka, H. "Adjunctive immunotherapy of mycobacterial infections." *Curr. Pharm. Design* **2004,** *10*, 3297-3312.

(87) Hetrick, E. M.; Prichard, H. L.; Klitzman, B.; Schoenfisch, M. H. "Reduced foreign body response at nitric oxide-releasing subcutaneous implants." *Biomaterials* **2007,** *28*, 4571-4580.

(88) Moncada, S.; Higgs, A. "The L-arginine-nitric oxide pathway." *N. Engl. J. Med.* **1993,** *329*, 2002-2012.

(89) Fang, F. C. "Mechanisms of nitric oxide-related antimicrobial activity." *J. Clin. Invest.* **1997,** *99*, 2818-2825.

(90) MacMicking, J.; Xie, Q.; Nathan, C. "Nitric oxide and macrophage function." *Annu. Rev. Immunol.* **1997,** *15*, 323-350.

(91) MacMicking, J. D.; Nathan, C.; Hom, G.; Chartrain, N.; Fletcher, D. S.; Trumbauer, M.; Stevens, K.; Xie, Q.; Sokol, K.; Hutchinson, N.; Chen, H.; Mudgett, J. S. "Altered responses to bacterial infection and endotoxic shock in mice lacking inducible nitric oxide synthase." *Cell* **1995,** *81*, 641-650.

(92) Miranda, K. M.; Espey, M. G.; Jourd'heuil, D.; Grisham, M. B.; Fukuto, J.; Freelisch, M.; Wink, D. A., "The chemical biology of nitric oxide." In *Nitric Oxide: Biology and Pathobiology*, Ignarro, L. J., Ed. Academic Press: New York, 2000; pp 41-55.

(93) Amadeu, T. P.; Seabra, A. B.; de Oliveira, M. G.; Costa, A. M. A. "*S*-nitrosoglutathione-containing hydrogel accelerates rat cutaneous wound repair." *J. Eur. Acad. Derm. Vener.* **2007,** *21*, 629-637.

(94) Schwentker, A.; Vodovotz, Y.; Weller, R.; Billiar, T. R. "Nitric oxide and wound repair: Role of cytokines?" *Nitric Oxide* **2002,** *7*, 1-10.

(95) Shukla, A.; Rasik, A. M.; Shankar, R. "Nitric oxide inhibits wound collagen synthesis." *Mol. Cell Biochem.* **1999,** *200*, 27-33.

(96) Cooke, J. P. "NO and angiogenesis." *Atherosclerosis Suppl.* **2003,** *4*, 53-60.

(97) Dulak, J.; Jozkowicz, A. "Regulation of vascular endothelial growth factor synthesis by nitric oxide: Facts and controversies." *Antioxid. Redox Signal.* **2003,** *5*, 123-132.

(98) Luo, J. D.; Chen, A. F. "Nitric oxide: A newly discovered function on wound healing." *Acta Pharm. Sinica* **2005,** *26*, 259-264.

(99) Rosen, G. M.; Tsai, P.; Pou, S. "Mechanism of free-radical generation by nitric oxide synthases." *Chem. Rev.* **2002,** *102*, 1191-1199.

(100) Ignarro, L. J.; Buga, G. M.; Wood, K. S.; Byrns, R. E.; Chaudhuri, G. "Endothelium-derived relaxing factor produced and released from artery and vein is nitric oxide." *Proc. Natl. Acad. Sci. U.S.A.* **1987,** *84*, 9265-9269.

(101) Furchgott, R. F. "Endothelium-derived relaxing factor: Discovery, early studies, and identification as nitric oxide (Nobel Lecture)." *Angew. Chem. Int. Ed.* **1999,** *38*, 1870-1880.

(102) Forstermann, U.; Gorsky, L. D.; Pollack, J. S.; Schmidt, H. H.; Heller, M.; Murad, F. "Regional distribution of EDRF/NO-synthesizing enzyme(s) in rat brain." *Biochem. Biophys. Res. Commun.* **1990,** *168*, 727-732.

(103) Bredt, D. S.; Hwang, P. M.; Snyder, S. H. "Localization of nitric oxide synthase indicating a neural role for nitric oxide." *Nature* **1990,** *347*, 768-770.

(104) Shibuki, K.; Okada, D. "Endogenous nitric oxide release required for long-term synaptic depression in the cerebellum." *Nature* **1991,** *349*, 326-328.

(105) Schuman, E. M.; Madison, D. V. "A requirement for the intercellular messenger nitric oxide in long-term potentiation." *Science* **1991,** *254*, 1503-1506.

(106) Chapman, P. F.; Atkins, C. M.; Allen, M. T.; Haley, J. E.; Steinmetz, J. E. "Inhibition of nitric oxide synthesis impairs two different forms of learning." *Neuroreport* **1992,** *3*, 567-570.

(107) Rubbo, H.; Radi, R.; Trujillo, M.; Telleri, R.; Kalyanaraman, B.; Barnes, S.; Kirk, M.; Freeman, B. A. "Nitric oxide regulation of superoxide and peroxynitrite-dependent lipid peroxidation. Formation of novel nitrogen-containing oxidized lipid derivatives." *J. Biol. Chem.* **1994,** *269*, 26066-26075.

(108) Ghaffari, A.; Miller, C. C.; McMullin, B.; Ghahary, A. "Potential application of gaseous nitric oxide as a topical antimicrobial agent." *Nitric Oxide* **2006,** *14*, 21-29.

(109) Bogdan, C. "Nitric oxide and the immune response." *Nat. Immunol.* **2001,** *2*, 907-916.

(110) Chu, A. J.; Prasad, J. K. "Up-regulation by human recombinant transforming growth factor B-1 of collagen production in cultured dermal fibroblasts is mediated by the inhibition of nitric oxide signaling." *J. Am. Coll. Surg.* **1999,** *188*, 271-280.

(111) Craven, P. A.; Studer, R. K.; Felder, J.; Phillips, S.; DeRubertis, F. R. "Nitric oxide inhibition of transforming growth factor-B and collagen synthesis in mesangial cells." *Diabetes* **1997,** *46*.

(112) Wang, P. G.; Xian, M.; Tang, X.; Wu, X.; Wen, Z.; Cai, T.; Janczuk, A. J. "Nitric oxide donors: Chemical activities and biological applications." *Chem. Rev.* **2002,** *102*, 1091-1134.

(113) Hrabie, J. A.; Keefer, L. K. "Chemistry of the nitric oxide-releasing diazeniumdiolate ("nitrosohydroxylamine") functional group and its oxygen-substituted derivatives." *Chem. Rev.* **2002,** *102*, 1135-1154.

(114) Drago, R. S.; Paulik, F. E. "The reaction of nitrogen(II) oxide with diethylamine." *J. Am. Chem. Soc.* **1960,** *82*, 96-98.

(115) Saavedra, J. E.; Southan, G. J.; Davies, K. M.; Lundell, A.; Markou, C.; Hanson, S. R.; Adrie, C.; Hurford, W. E.; Zapol, W. M.; Keefer, L. K. "Localizing antithrombotic and vasodilatory activity with a novel, ultrafast nitric oxide donor." *J. Med. Chem.* **1996,** *39*, 4361-4365.

(116) Stasko, N. A.; Schoenfisch, M. H. "Dendrimers as a scaffold for nitric oxide release." *J. Am. Chem. Soc.* **2006,** *128*, 8265-8271.

(117) Hrabie, J. A.; Saavedra, J. E.; Roller, P. P.; Southan, G. J.; Keefer, L. K. "Conversion of proteins to diazeniumdiolate-based nitric oxide donors." *Bioconjugate Chem.* **1999,** *10*, 838-842.

(118) Radomski, M. W.; Palmer, R. M. J.; Moncada, S. "The role of nitric oxide and cGMP in platelet adhesion to vascular endothelium." *Biochem. Biophys. Res. Commun.* **1987,** *148*, 1482-1489.

(119) Frost, M. C.; Reynolds, M. M.; Meyerhoff, M. E. "Polymers incorporating nitric oxide releasing/generating substances for improved biocompatibility of blood-contacting medical devices." *Biomaterials* **2005,** *26*, 1685-1693.

(120) Mowery, K. A.; Schoenfisch, M. H.; Saavedra, J. E.; Keefer, L. K.; Meyerhoff, M. E. "Preparation and characterization of hydrophobic polymeric films that are thromboresistant via nitric oxide release." *Biomaterials* **2000,** *21*, 9-21.

(121) Schoenfisch, M. H.; Mowery, K. A.; Rader, M. V.; Baliga, N.; Wahr, J. A.; Meyerhoff, M. E. "Improving the thromboresistivity of chemical sensors via nitric oxide release: Fabrication and in vivo evaluation of NO-releasing oxygen-sensing catheters." *Anal. Chem.* **2000,** *72*, 1119-1126.

(122) Marxer, S. M.; Rothrock, A. R.; Nablo, B. J.; Robbins, M. E.; Schoenfisch, M. H. "Preparation of nitric oxide (NO)-releasing sol-gels for biomaterial applications." *Chem. Mater.* **2003,** *15*, 4193-4199.

(123) Nablo, B. J.; Schoenfisch, M. H. "Antibacterial properties of nitric oxide-releasing sol-gels." *J. Biomed. Mater. Res.* **2003,** *67A*, 1276-1283.

(124) Nablo, B. J.; Rothrock, A. R.; Schoenfisch, M. H. "Nitric oxide-releasing sol-gels as antibacterial coatings for orthopedic implants." *Biomaterials* **2005,** *26*, 917-924.

(125) Nablo, B. J.; Schoenfisch, M. H. "Poly(vinyl chloride)-coated sol-gels for studying the effects of nitric oxide release on bacterial adhesion." *Biomacromolecules* **2004,** *5*, 2034-2041.

(126) Gomez-Suarez, C.; Busscher, H. J.; van der Mei, H. C. "Analysis of bacterial detachment from substratum surfaces by the passage of air-liquid interfaces." *Appl. Environ. Microbiol.* **2001,** *67*, 2531-2537.

(127) Pitt, W. G.; McBride, M. O.; Barton, A. J.; Sagers, R. D. "Air-water interface displaces adsorbed bacteria." *Biomaterials* **1993,** *14*, 605-608.

(128) Gomez-Suarez, C.; Busscher, H. J.; van der Mei, H. C. "Analysis of bacterial detachment from substratum surfaces by the passage of air-liquid interfaces." *Appl. Environ. Microbiol.* **2001,** *67*, 2531-2537.

(129) Busscher, H. J.; van der Mei, H. C. "Microbial adhesion in flow displacement systems." *Clin. Microbiol. Rev.* **2006,** *19*, 127-141.

(130) Roosjen, A.; de Vries, J.; van der Mei, H. C.; Norde, W.; Busscher, H. J. "Stability and effectiveness against bacterial adhesion of poly(ethylene oxide) coatings in biological fluids." *J. Biomed. Mater. Res.* **2005,** *73*, 347-354.

(131) Rodrigues, L.; van der Mei, H.; Banat, I. M.; Teixeira, J.; Oliveira, R. "Inhibition of microbial adhesion to silicone rubber treated with biosurfactant from *Streptococcus thermophilus*." *FEMS Immunol. Med. Microbiol.* **2006,** *46*, 107-112.

(132) Fu, J.; Ji, J.; Yuan, W.; Shen, J. "Construction of anti-adhesive and antibacterial multilayer films via layer-by-layer assembly of heparin and chitosan." *Biomaterials* **2005,** *26*, 6684-6692.

(133) Rothrock, A. R.; Donkers, R. L.; Schoenfisch, M. H. "Synthesis of nitric oxide-releasing gold nanoparticles." *J. Am. Chem. Soc.* **2005,** *127*, 9362-9363.

(134) Polizzi, M. A.; Stasko, N. A.; Schoenfisch, M. H. "Water-soluble nitric oxide-releasing gold nanoparticles." *Langmuir* **2007,** *23*, 4938-4943.

(135) Stasko, N. A.; Fischer, T. H.; Schoenfisch, M. H. "*S*-nitrosothiol-modified dendrimers as nitric oxide delivery vehicles." *Biomacromolecules* **2008,** *9*, 834-841.

(136) Shin, J. H.; Metzger, S. K.; Schoenfisch, M. H. "Synthesis of nitric oxide-releasing silica nanoparticles." *J. Am. Chem. Soc.* **2007,** *129*, 4612-4619.

(137) Shin, J. H.; Schoenfisch, M. H. "Inorganic/organic hybrid silica nanoparticles as a nitric oxide delivery scaffold." *Chem. Mater.* **2008,** *20*, 239-249.

(138) Zhang, H.; Annich, G. M.; Miskulin, J.; Stankiewicz, K.; Osterholzer, K.; Merz, S. I.; Bartlett, R. H.; Meyerhoff, M. E. "Nitric oxide-releasing fumed silica particles: Synthesis, characterization, and biomedical application." *J. Am. Chem. Soc.* **2003,** *125*, 5015-5024.

(139) Kawashima, Y. "Nanoparticulate systems for improved drug delivery." *Adv. Drug Delivery Rev.* **2001,** *47*, 1-2.

(140) Kohane, D. S. "Microparticles and nanoparticles for drug delivery." *Biotechnol. Bioeng.* **2007,** *96*, 203-209.

(141) Jeh, H. S.; Lu, S.; George, S. C. "Encapsulation of PROLI/NO in biodegradable microparticles." *J. Microencapsulation* **2004,** *21*, 3-13.

(142) Robson, M. C. "Wound infection: A failure of wound healing caused by an imbalance of bacteria." *Surg. Clin. North Am.* **1997,** *77*, 637-659.

(143) Gu, H.; Ho, P. L.; Tong, E.; Wang, L.; Xu, B. "Presenting vancomycin on nanoparticles to enhance antimicrobial activities." *Nano Lett.* **2003,** *3*, 1261-1263.

(144) Morones, J. R.; Elechiguerra, J. L.; Camacho, A.; Holt, K.; Kouri, J. B.; Ramirez, J. T.; Yacaman, M. J. "The bactericidal effect of silver nanoparticles." *Nanotechnology* **2005,** *16*, 2346-2353.

(145) Sambhy, V.; MacBride, M. M.; Peterson, B. J.; Sen, A. "Silver bromide nanoparticle/polymer composites: Dual action tunable antimicrobial materials." *J. Am. Chem. Soc.* **2006,** *128*, 9798-9808.

(146) Panacek, A.; Kvitek, L.; Prucek, R.; Kolar, M.; Vecerova, R.; Pizurova, N.; Sharma, V. K.; Nevecna, T.; Zboril, R. "Silver colloid nanoparticles: Synthesis, characterization, and their antibacterial activity." *J. Phys. Chem. B* **2006,** *110*.

(147) Trewyn, B. G.; Whitman, C. M.; Lin, V. S. Y. "Morphological control of room-temperature ionic liquid templated mesoporous silica nanoparticles for controlled release of antibacterial agents." *Nano Lett.* **2004,** *4*, 2139-2143.

(148) Lancaster, J. R. "A tutorial on the diffusibility and reactivity of free nitric oxide." *Nitric Oxide: Biology and Chemistry* **1997,** *1*, 18-30.

(149) Carlsson, S.; Weitzberg, E.; Wiklund, P.; Lundberg, J. O. "Intravesical nitric oxide delivery for prevention of catheter-associated urinary tract infections." *Antimicrob. Agents Chemother.* **2005,** *49*, 2352-2355.

(150) Fang, F. C. "Antimicrobial reactive oxygen and nitrogen species: Concepts and controversies." *Nat. Rev. Microbiol.* **2004,** *2*, 820-832.

Chapter 2:

Antibacterial Nitric Oxide-Releasing Xerogels: Cell Viability and Parallel Plate Flow Cell Adhesion Studies

2.1 Introduction

Roughly half of the ~2,000,000 hospital-acquired infections per year in the United States occur at the site of indwelling medical devices.[1] Despite sterilization, annual cases of orthopedic implant infections exceed 110,000 while the number associated with central venous catheters has been estimated to be 250,000.[1, 2] Of the latter, the mortality rate approaches 25%.[2] Device-associated infections are particularly resistant to systemic antibiotics, and persistent infections often require device removal. The direct medical costs associated with bacterial infections at the site of implanted devices exceed $3 billion annually in the U.S. alone.[1] Due to an aging worldwide population and advances in medical technology, cases of device-associated infections and their related burdens are expected to continue to rise.

Medical device infections are the direct result of bacterial adhesion to a material surface.[3] Initially, bacterial adhesion is mediated by reversible bacteria-substrate interactions, while at longer times irreversible molecular bridging occurs.[4] Once adhered, certain bacteria are capable of forming a protective biofilm by self-secreting an exopolysaccharide matrix that retains nutrients and protects the bacteria from components of

the natural immune response. Biofilms are an important defense mechanism for bacteria and provide remarkable resistance to traditional antibiotic therapies.[5]

Since the formation of a pathogenic biofilm is attributed to the initial adhesion of bacteria to a biomaterial surface, a great deal of research has focused on methods to prevent bacterial adhesion. To date, research has focused on both passive coatings that alter the physiochemical properties of the substrate as well as coatings that actively release antibacterial agents.[6] While passive coatings such as hydrophilic polyurethanes[7] have been shown to reduce bacterial adhesion, they provide no mechanism by which to kill bacteria that manage to adhere. Since even low levels of adhered bacteria, if viable, present the threat of eventual implant infection, it is desirable to develop coatings that are also capable of killing adhered bacteria.[8] The active release of antibiotics,[9] silver ions,[10] bioactive antibodies,[11] and nitric oxide[12] have all been shown to reduce bacterial adhesion. In addition, active-release coatings also provide an avenue toward killing bacteria that manage to adhere, an important characteristic for preventing biofilm formation.

Nitric oxide (NO), a diatomic free radical produced by macrophages as part of the natural immune response to bacterial infection,[13, 14] has several properties that make it an attractive agent for use in antibacterial coatings. With a short half life in physiological milieu (on the order of seconds), NO exhibits broad reactivity and rapid diffusion properties through solution and lipid membranes.[15] In the presence of oxygen, NO forms reactive intermediates (e.g., N_2O_3 and N_2O_4) that are capable of nitrosating nucleophilic amino acid residues, thereby altering normal protein function.[16] Likewise, the reaction of NO with superoxide (O_2^-) forms peroxynitrite ($ONOO^-$), a potent oxidizing agent whose downstream reaction products (OH and NO_2 radicals) cause lipid peroxidation that can disrupt the structural

integrity of bacterial cell membranes.[17] The wide-ranging antibacterial properties of NO have been demonstrated by Raulli and co-workers in a series of solution-based in vitro assays that show NO-mediated inhibition of a wide variety of gram-negative and gram-positive bacterial species.[18]

Based on NO's potential to reduce bacterial adhesion, our lab has focused on the synthesis of xerogel polymers modified to contain diazeniumdiolate NO donors as NO release scaffolds.[19] These polymers have shown promise as coatings for biomedical devices such as orthopedic implants[20] and subcutaneous sensors,[21] both of which are negatively impacted by bacterial adhesion. The influence of NO on *Pseudomonas aeruginosa, Proteus mirabilis, Staphylococcus aureus,* and *Staphylococcus epidermidis* adhesion has been reported.[12, 20, 22, 23] While a reduction in adhesion has been observed at NO-releasing surfaces, the viability of bacteria adhered to such polymers has not been investigated. Additionally, the in vitro adhesion studies conducted thus far have been performed under conditions of mild agitation ("static") requiring the substrate and adhered bacteria to be passed through an air-liquid interface. Other work has shown that passage through an air-liquid interface presents sufficient shear force to remove adhered bacteria from the substrate.[24, 25] Such experiments therefore measure bacterial *retention* rather than bacterial *adhesion*.[24]

A common strategy to avoid the inconsistencies generated by the passage of an air-liquid interface is the use of a parallel plate flow cell.[26-29] Flow experiments also allow for reproducible mass transport of bacteria to the substrate surface, controlled wall shear rates, real-time image-acquisition capabilities, and the ability to achieve reproducible surface coverage values of adhered bacteria.[30] Herein, a parallel plate flow cell was employed to

study *P. aeruginosa* adhesion as a function of NO release. As well, the viability of *P. aeruginosa* cells adhered to NO-releasing xerogels was assessed with fluorescent viability probes and by cell removal via sonication and determination of the number of colony forming units in the resulting suspension.

2.2 Methods and materials

Isobutyltrimethoxysilane (BTMOS) and *N*-(6-aminohexyl)aminopropyl-trimethoxysilane (AHAP3) were purchased from Gelest (Morrisville, PA) and stored under nitrogen. Ethanol (absolute), hydrochloric acid, and tetrahydrofuran were purchased from Fisher Scientific (Pittsburgh, PA) and used as received. Low molecular weight poly(vinyl chloride) (PVC) was purchased from Aldrich. Nitric oxide and argon were purchased from National Welders (Raleigh, NC). *P. aeruginosa* (ATCC #19143) was purchased from American Type Culture Collection (Manassas, VA). BacLight LIVE/DEAD fluorescent viability probes were purchased from Molecular Probes (Eugene, OR).

2.2.1 Synthesis of AHAP3/BTMOS xerogel films. Nitric oxide-releasing AHAP3/BTMOS xerogel films were synthesized as described by Marxer et al.[19] Briefly, H_2O (60 μL), ethanol (200 μL), 0.5 M HCl (10 μL) and BTMOS (120 – 180 μL) were mixed for 1 h, followed by addition of AHAP3 (20 – 80 μL) with additional mixing for 1 h. The volume percentage of aminosilane (i.e., AHAP3) relative to the total silane volume was varied from 10 – 40% (v/v). Glass microscope slides were cut to approximately 2.6 x 0.8 cm^2, sonicated in ethanol (20 min), dried under nitrogen, and UV-cleaned in a BioForce TipCleaner (Ames, IA) for 20 min. Sol-gel solution (30 μL) was deposited onto the clean glass slides via a spread-cast method. Xerogel films were allowed to solidify at room

temperature for 30 min then transferred to a 70 ºC oven for 3 d. After removal from the oven, xerogel-coated glass slides were stored in a desiccator at room temperature.

2.2.2 Diazeniumdiolate formation. Diazeniumdiolate NO-donors were synthesized within the xerogel network by exposing the films to high pressures of NO. Xerogel-coated glass slides were placed in a 500 mL hydrogenation bomb, which was subsequently flushed with Ar to remove O_2. The chamber was then pressurized to 5 atm of NO. After 3 d, unreacted NO was flushed from the chamber with Ar. Diazeniumdiolate-modified xerogel films were stored under N_2 at -20 ºC to prevent NO-donor decomposition.

2.2.3 Poly(vinyl chloride)-coated xerogels. Poly(vinyl chloride)-coated xerogels were prepared following procedures described previously by Nablo et al.[23] Briefly, low molecular weight PVC (500 mg) was dissolved in tetrahydrofuran (10 mL). Exactly 500 μL of the polymer solution was cast onto both control and diazeniumdiolate-modified xerogels at 3000 rpm for 10 s using a CHEMAT Technology KW-4A Precision Spin-Coater (Northridge, CA). The PVC-coated xerogels were stored at -20 °C until further use.

2.2.4 Nitric oxide release measurements. Real-time NO release data were obtained using a Sievers 280 chemiluminescent NO analyzer (Boulder, CO). The instrument was calibrated with an atmospheric sample that had been passed through a NO zero filter and a 24.1 ppm NO gas standard (balance N_2). Xerogel-coated glass slides were immersed in deoxygenated phosphate buffered saline (PBS; pH 7.4) at 25 °C, and NO was carried from the buffer to the analyzer with a stream of N_2 bubbled into the solution at a flow rate of 80 mL/min. In the instrument, NO was detected via its chemiluminescent reaction with ozone.[31]

2.2.5 Bacterial adhesion in a parallel plate flow chamber. *P. aeruginosa* was cultured at 37 ºC in tryptic soy broth (TSB), pelleted by centrifugation, resuspended in 15%

glycerol (v/v in PBS), and stored at -80 ºC. Cultures for bacterial adhesion studies were grown from a -80 ºC stock at 37 ºC in TSB overnight. A 1 mL aliquot of overnight culture was inoculated into 100 mL fresh TSB, incubated at 37 ºC with rotation, and grown to a concentration of ~10^8 colony forming units (CFU)/mL (verified by serial 10-fold dilutions in PBS, plating on tryptic soy agar nutrient plates, and subsequent CFU enumeration). The bacteria were pelleted by centrifugation, rinsed with ultrapure water, and resuspended in sterile PBS. Glass slides coated with xerogel films (NO-releasing and control) were affixed in custom-machined polycarbonate flow cells (chamber dimensions = 2.1 x 0.6 x 0.08 cm^3). Each flow cell apparatus consisted of three individual chambers for replicate analyses (see Fig. 2.1 for schematic of flow cell design and setup). Two flow cells were connected in series with PVC tubing and a three-channel peristaltic pump was used to pass the suspension of *P. aeruginosa* through the flow chambers (i.e., over the xerogel films) at a controlled rate of 0.2 mL/min. Adhesion to 40% AHAP3 xerogels was also evaluated at a flow rate of 0.6 mL/min. Each flow cell was placed on the stage of a Zeiss Axiovert 200 inverted microscope (Chester, VA). Bacterial adhesion was monitored in real time by capturing phase-contrast optical micrographs (20x magnification) of the xerogel surface with a Zeiss Axiocam digital camera (Chester, VA). Images were taken at discrete intervals of 5, 20, 40, 60, 90, and 120 min. To determine the percent surface coverage of bacteria, each image was digitally processed by applying a threshold value to differentiate the adhered cells from the background. In this manner, bacterial adhesion to each xerogel surface was determined as a function of time.

2.2.6 Bacterial adhesion under static conditions. *P. aeruginosa* was cultured as described above to a concentration of ~10^8 CFU/mL. Aliquots (5 mL) of the bacterial

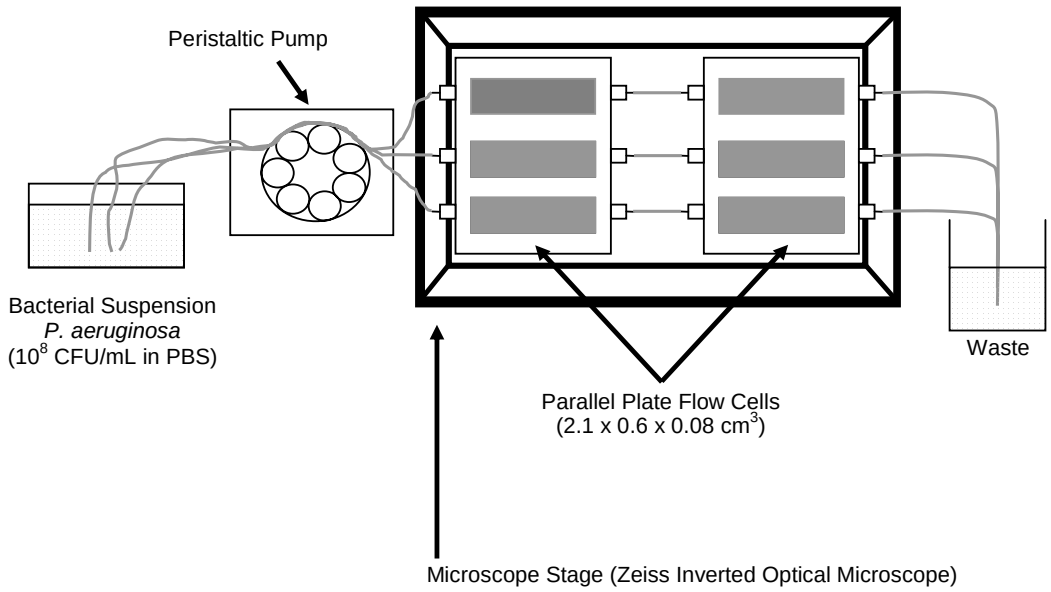

Figure 2.1. Schematic representation of flow cell design used to study *P. aeruginosa* adhesion to xerogel polymer coatings. A peristaltic pump was used to flow a suspension of *P. aeruginosa* (10^8 colony forming units per mL) through custom-machined flow cells that were placed on the stage of an inverted optical microscope. The suspension was exposed to control xerogel films prior to NO-releasing xerogels.

suspension in PBS were distributed to 15 mL polypropylene test tubes. Control and NO-releasing xerogels were placed in the test tubes and gently agitated at 25 °C for either 1 or 2 h. The xerogel slides were then removed, rinsed gently with ultrapure water to remove loosely adhered cells, and dried under a stream of N_2. Quantification of bacterial adhesion was performed via phase contrast optical microscopy and digital thresholding as described above.

2.2.7 Fluorescent viability staining of adhered bacteria. The viability of adhered bacteria was qualitatively determined using BacLight fluorescence probes. Bacterial viability was studied both immediately after the adhesion event and at discrete time intervals after adhesion (time-based studies). The latter experiments allowed viability information to be obtained after the adhered bacteria were exposed to a flux of NO from the xerogel coating for an extended period. *P. aeruginosa* was cultured in TSB as described above to a concentration of ~10^8 CFU/mL. The bacteria were pelleted by centrifugation and resuspended in sterile PBS. Glass microscope slides coated on one side with 40% AHAP3 (balance BTMOS) xerogel were placed in 5 mL of the bacterial suspension and incubated for 2 h to achieve thorough bacterial adhesion to the xerogel surface. The slides with adhered bacteria were removed from the bacterial suspension and transferred to either sterile PBS (to maintain NO release for time-based studies) or into 50 mL of suspended BacLight fluorescent probes (propidium iodide and Syto 9) in PBS. After 30 min incubation with the fluorescent probes, the slides were removed and rinsed gently with DI water. Bright field and fluorescence micrographs (20x magnification) of the slides were obtained using a Zeiss Axiovert 200 inverted microscope equipped with propidium iodide and Syto 9 filter sets from Chroma (Battleboro, VT). For time-based studies, xerogel-coated slides with adhered *P.*

aeruginosa were allowed to incubate in sterile PBS for fixed periods (1 – 15 h). After incubation, the adhered bacteria were fluorescently labeled and images were acquired as described above.

2.2.8 Quantification of viable adhered bacteria. Flow cell bacterial adhesion data were used to facilitate quantitative determination of adhered bacterial viability. Glass microscope slides coated with NO-releasing AHAP3 xerogels (10 – 40% v/v) were placed in the parallel plate flow chambers as described above. A ~10^8 CFU/mL suspension of *P. aeruginosa* in PBS was passed through the chambers at a flow rate of 0.2 mL/min. Each xerogel composition was exposed to the bacterial suspension for the time required to achieve 20% surface coverage (i.e., 12, 38, 60, and 180 min for 10, 20, 30, and 40% AHAP3 xerogels, respectively). Upon obtaining 20% surface coverage (verified by threshold analysis of optical micrographs), the bacterial suspension was exchanged with sterile PBS without the passage of an air-liquid interface. The xerogel films with adhered bacteria were left undisturbed at ambient temperature for 15 h. The sterile PBS was subsequently removed from the flow chambers, and the xerogel-coated slides were removed and imaged at 20x magnification. Each slide was then placed in 5 mL of sterile PBS and adhered bacteria were removed from the substrate surface via sonication (40 kHz, 15 min).[11] The resulting bacterial suspensions were subjected to serial 10-fold dilutions in sterile PBS, and 100 μL aliquots of each dilution were plated on tryptic soy agar (TSA) nutrient plates. The plates were incubated at 37 ºC and the number of live bacteria was determined by counting the number of colonies that grew on each plate overnight.

2.3 Results and discussion

2.3.1 Nitric oxide release. Nitric oxide-releasing AHAP3/BTMOS xerogels were selected as NO release surfaces for these studies because they have been well-characterized in terms of material properties[19] and bacterial adhesion.[20, 22, 23] As shown in Figure 2.2, the flux of NO from diazeniumdiolate-modified AHAP3/BTMOS xerogel films is tunable based on the amount of aminoalkoxysilane (i.e., AHAP3) in the xerogel. Indeed, the initial flux of NO varied between 1 and 24 pmol·cm^{-2}·s^{-1} as a function of aminoalkoxysilane concentration.

The initial rapid release of NO upon immersion in PBS is attributed to decomposition of diazeniumdiolates at or near the xerogel surface. Continued NO release at lower levels is the result of extended water diffusion that decomposes NO-donors within the xerogel matrix. These NO-release properties are ideal for preventing bacterial adhesion to an implant surface. The high NO flux at early time points (< 6 h) may reduce initial adhesion of bacteria throughout the critical period where immune and other cells interrogate the implant preceding tissue integration.[32] The prolonged release of low levels of NO may serve to kill bacteria that manage to adhere to the implant surface, and potentially augment the host's natural defense mechanisms. Of note, the NO-release data presented herein were collected at 25 ºC to correspond with the conditions present in the subsequent parallel plate flow cell experiments. Previous studies have shown that at physiological temperature (i.e., 37 ºC), NO release from 40% AHAP3 xerogels is higher initially and decays more rapidly than the flux of NO from the same xerogel system at 25 ºC.[20]

2.3.2 Nitric oxide-mediated reduction in bacterial adhesion under flowing conditions. Figure 2.3 shows phase contrast optical micrographs (20x magnification) of *P. aeruginosa* adhered to control and NO-releasing xerogel polymers after 1 h exposure to a flowing

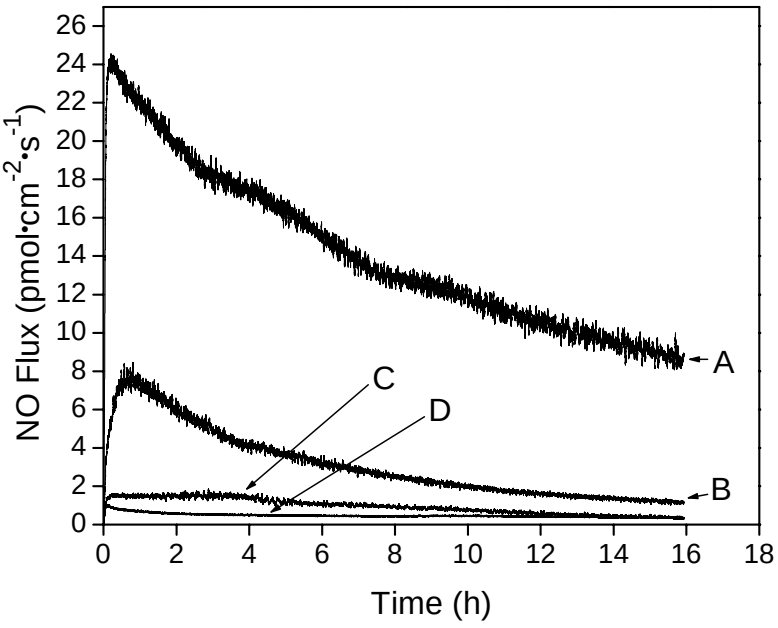

Figure 2.2. Nitric oxide release in PBS (pH 7.4) at 25 °C from 40 (A), 30 (B), 20 (C) and 10% (D) AHAP3 (v/v) xerogel polymers (balance BTMOS).

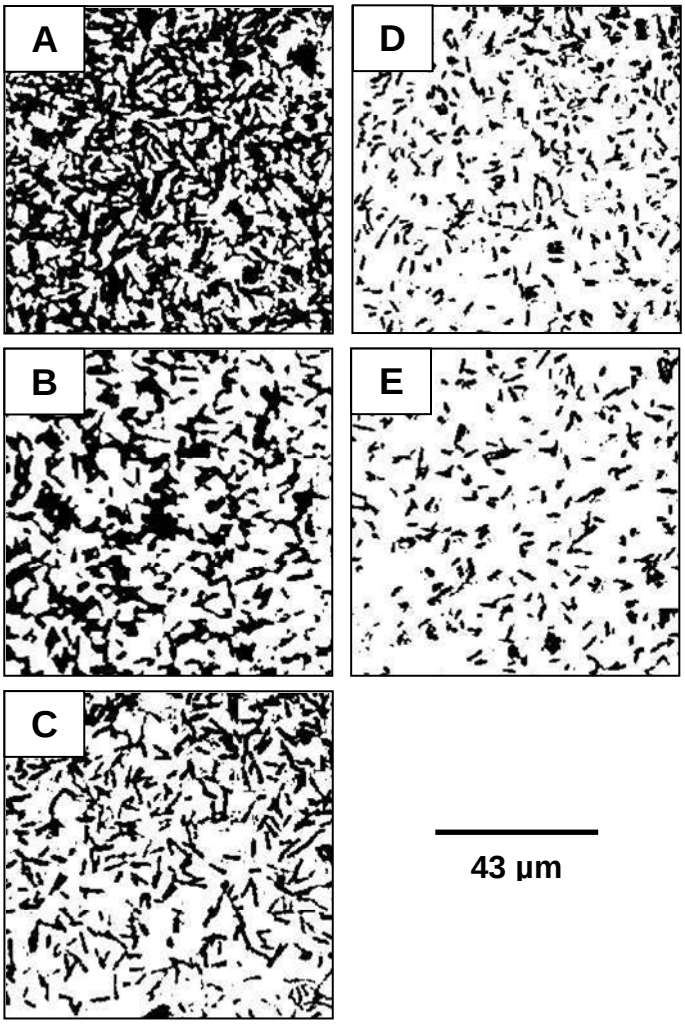

Figure 2.3. Phase contrast optical micrographs of *P. aeruginosa* adhesion to control (A), and NO-releasing 10 (B), 20 (C), 30 (D), and 40% (E) AHAP3 (v/v) xerogels (balance BTMOS) after 1 h exposure to a flowing suspension of *P. aeruginosa*. Flow rate = 0.2 mL/min. Control is non-NO-releasing 40% AHAP3/BTMOS.

suspension (10^8 CFU/mL) of *P. aeruginosa*. As observed in previous static experiments, the NO-releasing xerogels were characterized by reduced bacterial adhesion at a flow rate of 0.2 mL/min in an NO flux-dependent fashion.

Phase contrast optical microscopy and black/white threshold image analysis were used to quantify the extent of bacterial adhesion to control and NO-releasing xerogels in the parallel plate flow chamber.[33] Real-time image acquisition was facilitated by placing the flow cell apparatus with optically-transparent xerogel films directly on the imaging stage of an inverted optical microscope. In this manner, the temporal dynamics of bacterial adhesion to control and NO-releasing xerogel surfaces was determined. As shown in Figure 2.4, bacterial adhesion to control surfaces proceeded rapidly, with ~23% of the surface covered with *P. aeruginosa* cells within 5 min of exposure to the bacterial suspension. In contrast, surfaces that released NO were characterized by significantly lower levels of bacterial adhesion over the initial 5 min. Bacterial surface coverage at 10% AHAP3 NO-releasing xerogels was only 14%, while NO-releasing 20, 30, and 40% AHAP3 xerogels had significantly lower levels of adhered *P. aeruginosa* (7, 6, and 4%, respectively). After 5 min, the surface coverage of *P. aeruginosa* to NO-releasing 40% AHAP3 was reduced by >84% compared to control surfaces. Reducing bacterial adhesion during the first several minutes of exposure to the bacterial suspension proved important in preventing further bacterial adhesion because the initial reduction of adhered cells diminished potential nucleation sites for further bacterial adhesion.[32] While the low levels of NO released from 10% AHAP3 xerogels resulted in significantly reduced bacterial adhesion over the first 1 h, *P. aeruginosa* adhesion increased quickly thereafter, and by 1.5 h was statistically indistinguishable from that at controls. In contrast, the NO flux from 20, 30, and 40% AHAP3 NO-releasing

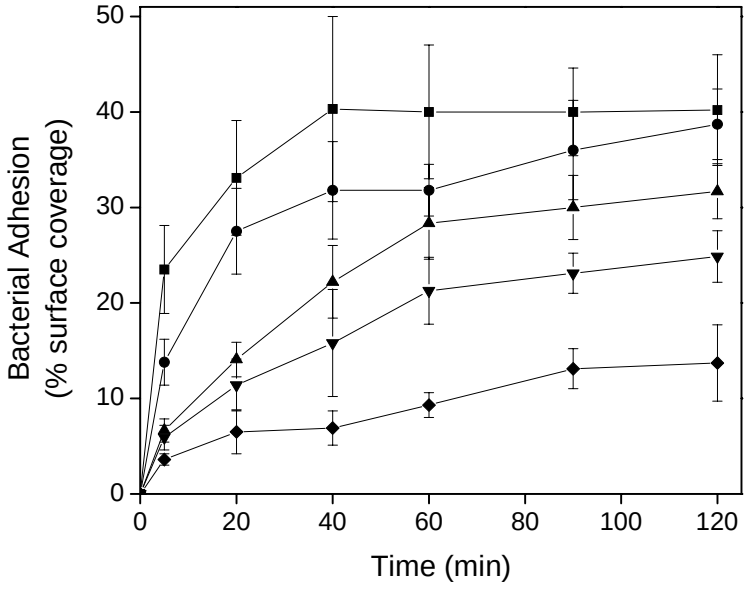

Figure 2.4. *P. aeruginosa* adhesion under flowing conditions (0.2 mL/min) to xerogel films with average 2 h NO flux values of 0 (■), 0.42 (●), 1.9 (▲), 10.8 (▼), and 21.3 (◆) pmol·cm^{-2}·s^{-1}. Nitric oxide release was achieved with 10 (●), 20 (▲), 30 (▼), and 40% (◆) AHAP3 (v/v) xerogel films (balance BTMOS). For clarity, the data presented for controls (■) represent the average of all control samples at each time point (surface coverage values for all controls were identical (within error) at each time point).

xerogels mediated a significant reduction in *P. aeruginosa* adhesion over the entire experiment, indicating that fluxes in excess of ~1.5 pmol·cm^{-2}·s^{-1} are required to maintain a significant reduction in bacterial adhesion over 2 h. After 2 h, NO-releasing 40% AHAP3 xerogels were characterized by <14% *P. aeruginosa* surface coverage, while adhesion to controls reached 40% coverage, representing a 65% decrease in bacterial adhesion for interfaces releasing NO. Clinically, the NO-based reduction in bacterial adhesion during the acute phase following implantation of a coated device may allow for more effective tissue integration and hinder biofilm formation at the implant-tissue interface.[32]

An NO-mediated reduction in *P. aeruginosa* adhesion was also observed at higher flow rates, albeit to a lesser extent (Fig. 2.5). The bacterial surface coverage of control 40% AHAP3 xerogels at a flow rate of 0.6 mL/min after 2 h was approximately half that observed at a flow rate of 0.2 mL/min. This reduction in cell adhesion is attributed to greater wall shear rates. In contrast, *P. aeruginosa* adhesion to NO-releasing 40% AHAP3 xerogels was greater at 0.6 mL/min after 1 h (surface coverage of 16 vs. 9% at flow rates of 0.6 and 0.2 mL/min, respectively), indicating that the anti-bacterial adhesion effect of NO-releasing xerogels was diminished. This reduction in antibacterial efficacy is attributed to faster removal of interfacial NO and other reactive nitrogen oxide (rNO_x) species at higher flow rates. In turn, the effective concentrations of NO and rNO_x species at the xerogel surface-solution interface are reduced. Nevertheless, *P. aeruginosa* adhesion at the NO-releasing xerogel remained less than controls (by ~65 and 29% at 0.2 and 0.6 mL/min, respectively).

2.3.3 Bacterial adhesion under static conditions. Bacterial adhesion studies were performed at 25 °C under static conditions for comparison with experiments carried out under the controlled flow conditions using the parallel plate flow chamber. After 1 and 2 h

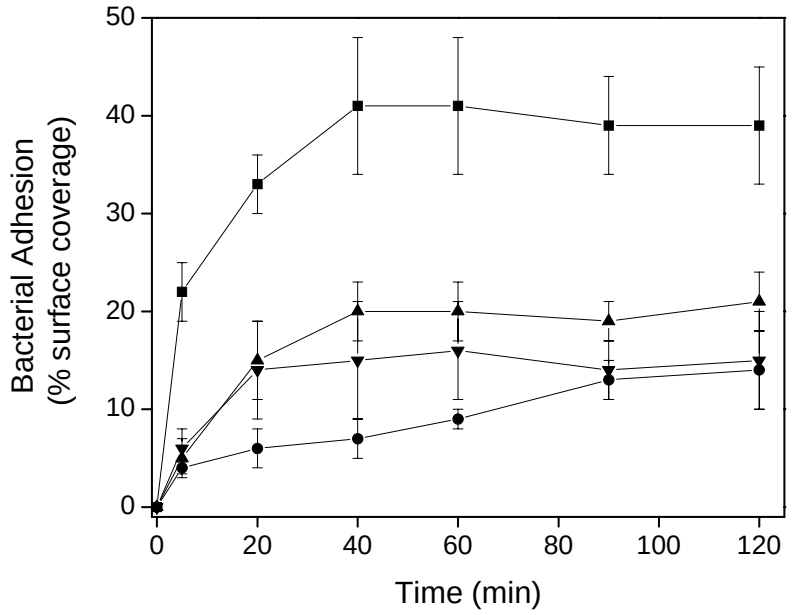

Figure 2.5. *P. aeruginosa* adhesion to control (■ and ▲) and NO-releasing (▼ and ●) 40% AHAP3 (v/v) xerogel films (balance BTMOS). Adhesion was studied at controlled flow rates of 0.2 mL/min (■ and ●) and 0.6 mL/min (▲ and ▼).

exposure to the concentrated suspension of *P. aeruginosa*, control xerogels were characterized by identical (within error) percent bacterial surface coverage (Table 2.1), indicating that the extent of bacterial adhesion to control xerogels is invariant of the amount of aminosilane included in the xerogel synthesis. The levels of *P. aeruginosa* adhesion to NO-releasing 10, 20, and 30% AHAP3 xerogels were significantly lower in the static experiment at 1 and 2 h relative to the same samples in the parallel plate flow chamber (Table 2.2). A potential factor for this behavior may be the build-up of high concentrations of NO and reactive nitrogen species over time in the bacterial suspension in the static experiments. In contrast, the continuous passage of fresh buffer through the flow cell carries away NO and reactive byproducts, effectively lowering the concentration immediately at the xerogel surface. Further evidence for this explanation is the fact that in the static experiments, bacterial adhesion to NO-releasing 10% AHAP3 xerogels was significantly reduced compared to controls after 2 h (Table 2.1), while adhesion to the same xerogel composition in the parallel plate flow chamber was not significantly different from controls after 2 h (Table 2.2). These differences may also be the result of passing samples from the static experiment through an air-liquid interface. The forces exerted during this step of the static experiments may dislodge more loosely adhered bacteria, thereby lowering surface coverage values.

2.3.4 Adhered bacterial viability. While reducing initial bacterial adhesion represents an important step toward preventing biofilm formation, bacteria that do adhere still present the threat of implant infection. Fu et al. emphasized that the ideal coating to prevent implant infection both reduces bacterial adhesion and kills bacteria that adhere.[8] To study the bactericidal effects of NO release on adhered *P. aeruginosa*, a BacLight LIVE/DEAD

Table 2.1. *P. aeruginosa* adhesion (percent surface coverage) under static conditions.

	1 h			2 h		
% AHAP3[a]	Control	NO-releasing	ANOVA P-value	Control	NO-releasing	ANOVA P-Value
10	35 ± 10	23 ± 7	4.42×10^{-5}	41 ± 5	33 ± 6	9.64×10^{-5}
20	34 ± 9	19 ± 4	2.95×10^{-6}	42 ± 7	25 ± 9	3.66×10^{-7}
30	35 ± 8	13 ± 4	2.17×10^{-12}	39 ± 6	18 ± 6	1.12×10^{-13}
40	34 ± 4	9 ± 3	1.16×10^{-20}	43 ± 7	9 ± 3	1.28×10^{-18}

[a]v/v, balance BTMOS.

Table 2.2. *P. aeruginosa* adhesion (percent surface coverage) in parallel plate flow chamber.[a]

Xerogel Composition[b]	1 h	ANOVA P-Value With Control	2 h	ANOVA P-Value With Control
Control[c]	40 ± 7	--	40 ± 6	--
10	32 ± 3	1.44×10^{-3}	39 ± 4	4.50×10^{-1}
20	28 ± 4	2.54×10^{-5}	32 ± 3	1.19×10^{-3}
30	21 ± 4	2.46×10^{-7}	25 ±3	7.01×10^{-10}
40	9 ± 1	1.56×10^{-17}	14 ± 4	4.40×10^{-17}

[a]Flow rate = 0.2 mL/min.
[b]Volume percentage of AHAP3 (balance BTMOS).
[c]Control xerogels consist of the same silane compositions without NO-release capabilities. Adhesion to controls at both time points was invariant of composition. For clarity, these values represent the average of adhesion to all controls.

fluorescent viability kit was used to distinguish live and dead cells. After exposure to the fluorescent nucleic acid stains, live bacteria fluoresce green (Syto 9, $\lambda_{max} \approx 533$ nm) while red fluorescence (propidium iodide, $\lambda_{max} \approx 622$ nm) indicates dead cells. Bright field and fluorescent (Syto 9 and propidium iodide) images of bacteria adhered to control 40% AHAP3 xerogels are shown in Figure 2.6. Separate samples were stained either immediately after the 2 h adhesion procedure (Fig. 2.6 A, B, C) or after additional incubation of the surface-adhered bacteria for 7 h in PBS (Fig. 2.6 D, E, F). The Syto 9 fluorescent images (Fig. 2.6 B, E) indicate that at each time point, the vast majority of bacteria adhered to control surfaces were alive. Propidium iodide fluorescent images of the same fields (Fig. 2.6 C, F) were dark (i.e., no fluorescence), indicating that none of the adhered bacteria were dead either immediately after adhesion or after 7 h incubation. Thus, control xerogel surfaces were not bactericidal to adhered *P. aeruginosa*.

Similar experiments were conducted with NO-releasing 40% AHAP3 xerogels (Fig. 2.7). Syto 9 fluorescent images (Fig. 2.7 B) of adhered bacteria after the 2 h adhesion procedure indicate that the majority of bacteria were viable. In contrast, Syto 9 fluorescence was not observed for adhered cells at 7 h (Fig. 2.7 E). Images of the same field using the propidium iodide filter (Fig. 2.7 F) showed strong fluorescence, indicating that the adhered bacteria were killed by 7 h. Similar fluorescence viability studies indicated that after 5 h incubation, the adhered bacteria were still viable (data not shown), suggesting that the dose of NO necessary to kill adhered *P. aeruginosa* is between 375 nmol·cm^{-2} and 425 nmol·cm^{-2} (the total amount of NO released from 40% AHAP3 xerogels after 5 h and 7 h, respectively). Further examination revealed that only those bacteria cells adhered directly to the NO-releasing xerogel were killed by the NO. *P. aeruginosa* cells adhered to the bare glass side

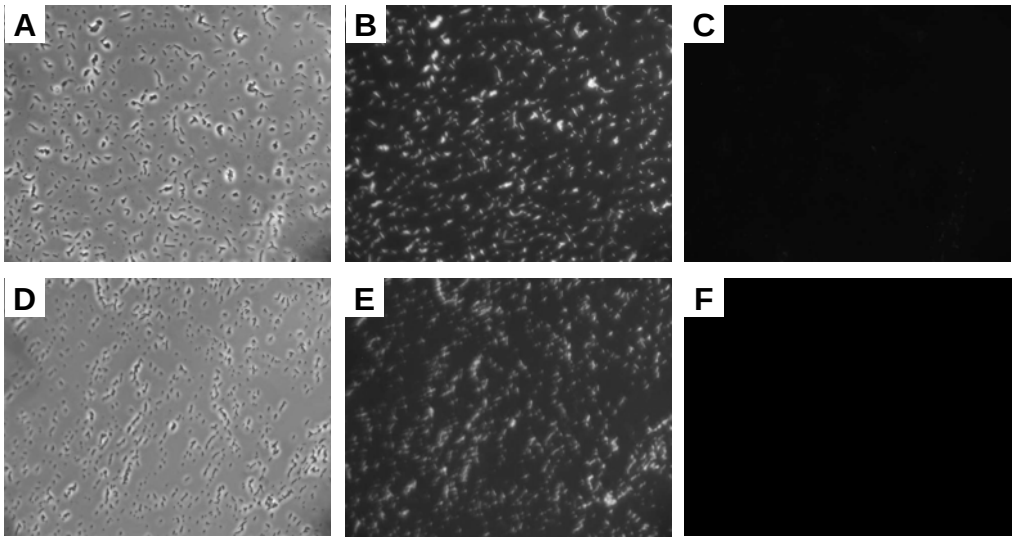

Figure 2.6. Bright field (A, D), Syto 9 fluorescent (B, E), and propidium iodide fluorescent (C, F) micrographs (20x magnification) of *P. aeruginosa* adhered to control (non-NO-releasing) 40% AHAP3 (v/v) xerogels (balance BTMOS). Images were acquired immediately (A, B, C) and 7 h after (D, E, F) initial bacterial adhesion.

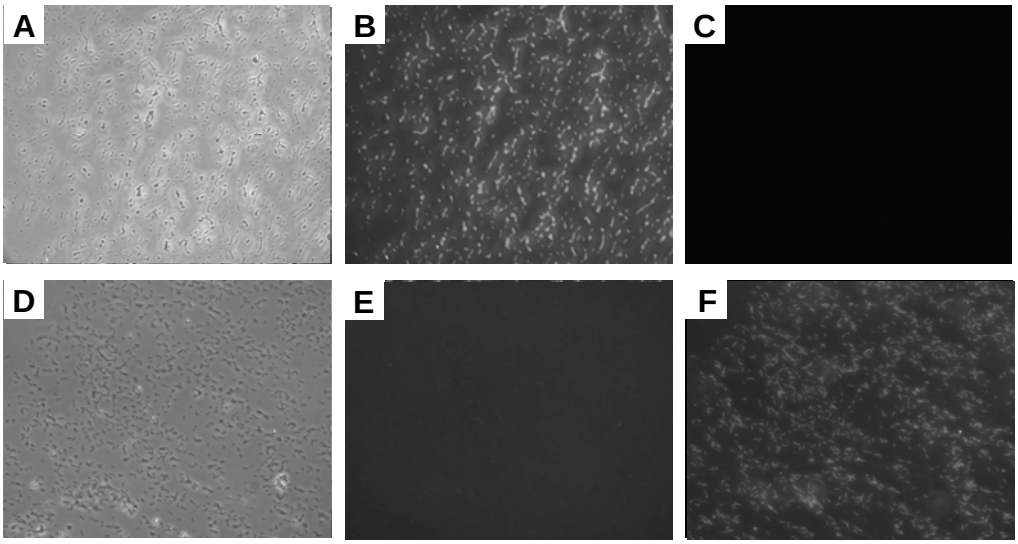

Figure 2.7. Bright field (A, D), Syto 9 fluorescent (B, E), and propidium iodide fluorescent (C, F) micrographs (20x magnification) of *P. aeruginosa* adhered to NO-releasing 40% AHAP3 (v/v) xerogels (balance BTMOS). Images were acquired immediately (A, B, C) and 7 h after (D, E, F) initial bacterial adhesion.

opposite the NO-releasing xerogel-coated side remained viable at 7 h (Fig. 2.8). Cells adhered directly to the glass substrate exhibited strong Syto 9 fluorescence, while no fluorescence was observed from propidium iodide. Thus, only bacterial cells in direct contact with the surface that released the NO were killed at 7 h, while cells adhered farther from the source of NO remained viable. Collectively, these results suggest that NO-releasing xerogels may mitigate biofilm formation even when bacteria manage to adhere.

Previous studies have shown that NO-releasing xerogels coated with a PVC overlayer maintained their ability to reduce bacterial adhesion despite a ~20% reduction in the 24 h NO flux.[23] As such, the antibacterial efficacy of such materials was attributed solely to NO and not the xerogel matrix, for example. To further isolate the effect of NO on bacteria, we evaluated the viability of bacteria adhered to PVC-coated xerogels. Of note, the thickness of the PVC overlayer used for these studies was ~10 μm. As expected, a significant reduction in bacterial adhesion was observed after only 1 h at PVC-coated NO-releasing xerogels compared to PVC-coated controls (8 ± 3% vs. 25 ±4% surface coverage, respectively; ANOVA *P*-value = 3.9×10^{-6}). Moreover, the NO release was cytotoxic to adhered *P. aeruginosa*. The propidium iodide fluorescence observed from *P. aeruginosa* cells adhered to PVC-coated NO-releasing xerogels for 7 h was intense, indicating cell death (data not shown). In contrast, bacteria adhered to PVC-coated controls remained viable through 7 h as evidenced by Syto 9 fluorescence. In addition to further corroborating NO's role as an antibacterial agent, the data indicate that NO release may prove effective at rendering a range of polymers antibacterial.

To further characterize the antibacterial properties of NO-releasing xerogels, the viability of adhered *P. aeruginosa* was examined as a function of the total amount of NO

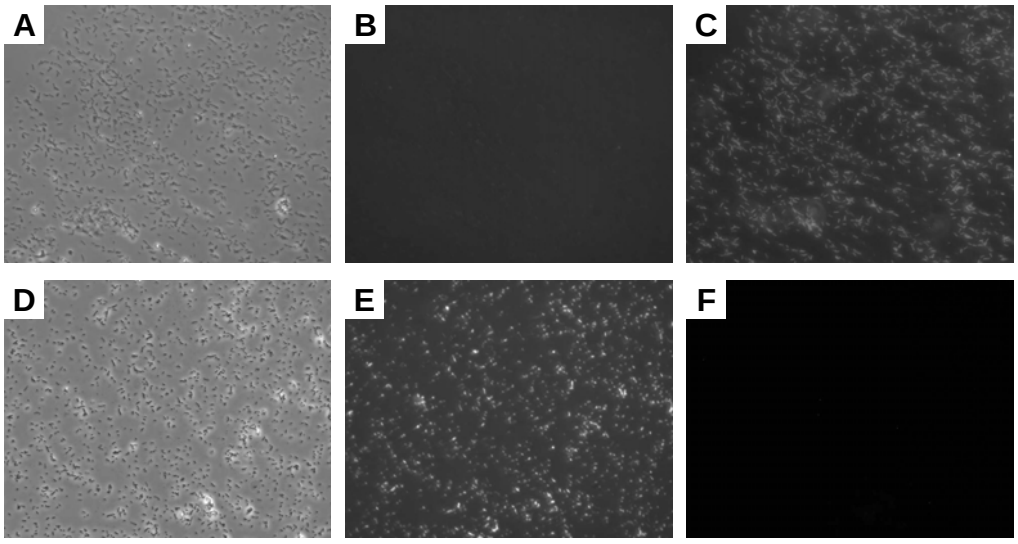

Figure 2.8. Bright field (A, D), Syto 9 fluorescent (B, E), and propidium iodide fluorescent (C, F) images of *P. aeruginosa* adhered to the xerogel-coated side (A, B, C) and the glass side (D, E, F) of a glass microscope slide (20x magnification). Images were acquired after 7 h incubation in PBS. The cells adhered to the glass remain viable, while those adhered to the NO-releasing xerogel were killed after 7 h. Xerogel coating is 40% AHAP3 (v/v, balance BTMOS).

released. Due to both blurring during the exposure times required to obtain fluorescent images of adhered bacteria and the widely variable fluorescent intensities of Syto 9 and propidium iodide, the threshold/image analysis procedure used to determine percent bacterial surface coverage was not a valid method for obtaining quantitative viability information as a function of total NO release. Such information was instead obtained by removing adhered bacteria from the xerogel surfaces via sonication, and determining the extent of bacterial survival with a reproductive viability assay.[11] Identical surface coverage values were obtained with the parallel plate flow cells by exposing each xerogel to the flowing bacterial suspension for the time required to achieve 20% coverage (verified by optical microscopy). The flowing bacterial suspension was then replaced with sterile PBS to facilitate the continued release of NO from the xerogels for 15 h. Over this period, the total NO release from 10, 20, 30, and 40% AHAP3 xerogels was 25, 53, 170, and 750 nmol·cm^{-2}, respectively. After the 15 h incubation, the bacteria were removed from the substrate surface by sonication, serially diluted (10-fold dilutions), and plated on nutrient agar plates. The number of colonies counted on each plate after overnight incubation were then used to calculate the number of viable cells removed from the xerogel surface. As shown in Figure 2.9, a dramatic decrease in viability was observed with increasing total NO release. The number of viable *P. aeruginosa* cells removed from the surface of 10% AHAP3 xerogels was 6.9 x 10^6 while only 2.7 x 10^5 viable cells were removed from the 40% AHAP3 xerogels, representing a 96% decrease in viability upon increasing the total amount of NO released from 25 nmol·cm^{-2} to 750 nmol·cm^{-2} over 15 h.

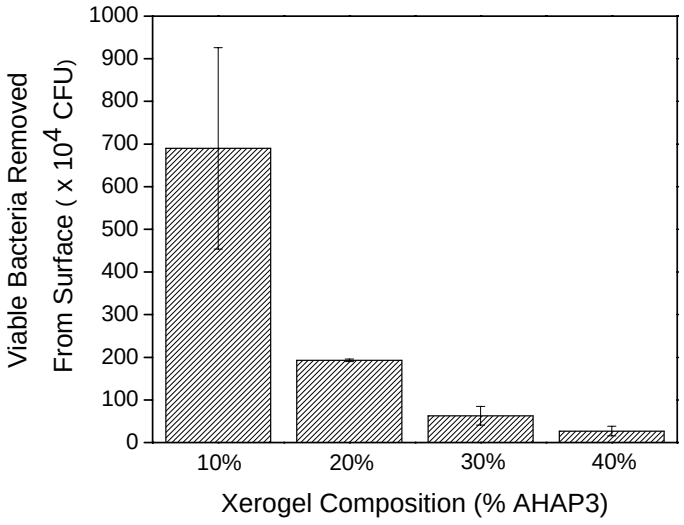

Figure 2.9. Viable *P. aeruginosa* adhered to AHAP3 xerogels with varying NO release capabilities removed by sonication after 15 h incubation in sterile PBS. Initial levels of *P. aeruginosa* adhered to each substrate were identical (20% surface coverage). Values represent average ± standard error of the mean.

2.4 Conclusions

Herein, NO-releasing xerogels were shown to reduce the initial adhesion of *P. aeruginosa* under dynamic flow conditions. After 2 h exposure to a flowing bacterial suspension (0.2 mL/min), NO-releasing 40% AHAP3 xerogels reduced *P. aeruginosa* adhesion by ~65% compared to controls. Nitric oxide release was also shown to kill adhered bacteria in a dose-dependent fashion over extended periods (> 7h). By initially reducing bacterial adhesion and killing bacteria that manage to adhere to the surface, NO-releasing xerogels applied as coatings to implantable medical devices may drastically reduce the possibility of biofilm formation and subsequent device infection. Notably, recent studies have shown that NO plays a key role in wound healing,[34] partly due to its antibacterial properties. Thus, the continued release of antibacterial levels of NO from a polymer coating may play a defining role in the healing process at the site of coated implants.

Experiments to elucidate the mechanism by which NO prevents bacterial adhesion are currently underway. We hypothesize that NO, through reactive intermediate species such as N_2O_3 and N_2O_4, destroys the function of bacterial adhesin proteins that mediate surface adhesion. A similar effect could be achieved by the NO reaction product peroxynitrite ($ONOO^-$), which has been implicated in cell membrane destruction via the mechanism of lipid peroxidation[13]. Destruction of the bacterial membrane may compromise cell attachment and thereby contribute to lower levels of bacterial adhesion. In addition, studies are underway to explore the effect of NO release on protein-mediated bacterial adhesion to better mimic the in vivo pathways that lead to implant infections and biofouling.

2.5 References

(1) Darouiche, R. O. "Treatment of infections associated with surgical implants." *N. Engl. J. Med.* **2004,** *350*, 1422-1429.

(2) O'Grady, N. P.; Alexander, M.; Dellinger, E. P.; Gerberding, J. L.; Heard, S. O.; Maki, D. G.; Masur, H.; McCormick, R. D.; Mermel, L. A.; Pearson, M. L.; Raad, I. I.; Randolph, A.; Weinstein, R. A. "Guidelines for the prevention of intravascular catheter-related infections." *MMWR Recommendations Recommendations and Reports* **2002,** *51 (RR-10)*, 1-26.

(3) Vacheethasanee, K.; Marchant, R. E., "Nonspecific *Staphylococcus epidermidis* adhesion: Contributions of biomaterial hydrophobicity and charge." In *Handbood of Bacterial Adhesion: Principles, Methods, and Applications*, An, Y. H.; Friedman, R. J., Eds. Humana Press: Totowa, NJ, 2000; p 74.

(4) An, Y. H.; Friedman, R. J. "Concise review of mechanisms of bacterial adhesion to biomaterial surfaces." *J. Biomed. Mater. Res.* **1998,** *43*, 338-348.

(5) Smith, A. W. "Biofilms and antibiotic therapy: Is there a role for combating bacterial resistance by the use of novel drug delivery systems?" *Adv. Drug Del. Rev.* **2005,** *57*, 1539-1550.

(6) Hetrick, E. M.; Schoenfisch, M. H. "Reducing implant-related infections: Active release strategies." *Chem. Soc. Rev.* **2006,** *35*, 780-789.

(7) Nagel, J. A.; Dickinson, R. B.; Cooper, S. L. "Bacterial adhesion to polyurethane surfaces in the presence of pre-adsorbed high molecular weight kiniogen." *J. Biomaterials Sci. Polym. Edn.* **1996,** *7*, 769-770.

(8) Fu, J.; Ji, J.; Yuan, W.; Shen, J. "Construction of anti-adhesive and antibacterial multilayer films via layer-by-layer assembly of heparin and chitosan." *Biomaterials* **2005,** *26*, 6684-6692.

(9) Hendricks, S. K.; Kwok, C.; Shen, M.; Horbett, T. A.; Ratner, B. D.; Bryers, J. D. "Plasma-deopsited membranes for controlled release of antibiotic to prevent bacterial adhesion and biofilm formation." *J. Biomed. Mater. Res.* **2000,** *50*, 160-170.

(10) Kumar, R.; Munstedt, H. "Silver ion release from antimicrobial polyamide/silver composites." *Biomaterials* **2005,** *26*, 2081-2088.

(11) Rojas, I. A.; Slunt, J. B.; Grainger, D. W. "Polyurethane coatings release bioactive antibodies to reduce bacterial adhesion." *J. Controlled Release* **2000,** *63*, 175-189.

(12) Nablo, B. J.; Chen, T.; Schoenfisch, M. H. "Sol-gel derived nitric oxide releasing materials that reduce bacterial adhesion." *J. Am. Chem. Soc.* **2001,** *123*, 9712-9713.

(13) Fang, F. C. "Perspectives series: Host/pathogen interactions." *J. Clin. Invest.* **1997,** *99*, 2818-2825.

(14) MacMicking, J.; Xie, Q.; Nathan, C. "Nitric oxide and macrophage function." *Annu. Rev. Immunol.* **1997,** *15*, 323-350.

(15) Lancaster, J. R. "A tutorial on the diffusibility and reactivity of free nitric oxide." *Nitric Oxide* **1997,** *1*, 18-30.

(16) Miranda, K. M.; Espey, M. G.; Jourd'heuil, D.; Brisham, M. B.; Fukuto, J.; Freelisch, M.; Wink, D. A., "The chemical biology of nitric oxide." In *Nitric Oxide: Biology and Pathobiology*, Ignarro, L. J., Ed. Academic Press: New York, 2000; pp 41-55.

(17) Wink, D.; Mitchell, J. B. "Chemical biology of nitric oxide: Insights into regulatory, cytotoxic, and cytoprotective mechanisms of nitric oxide." *Free Radical Biol. Med.* **1998,** *25*, 434-456.

(18) Raulli, R.; McElhaney-Feser, G.; Hrabie, J. A.; Cihlar, R. L. "Antimicrobial properties of nitric oxide using diazeniumdiolates as the nitric oxide donor." *Rec. Res. Devel. Microbiol.* **2002,** *6*, 177-183.

(19) Marxer, S. M.; Rothrock, A. R.; Nablo, B. J.; Robbins, M. E.; Schoenfisch, M. H. "Preparation of nitric oxide (NO)-releasing sol-gels for biomaterial applications." *Chem. Mater.* **2003,** *15*, 4193-4199.

(20) Nablo, B. J.; Rothrock, A. R.; Schoenfisch, M. H. "Nitric oxide-releasing sol-gels as antibacterial coatings for orthopedic implants." *Biomaterials* **2005,** *26*, 917-924.

(21) Shin, J. H.; Marxer, S. M.; Schoenfisch, M. H. "Nitric oxide-releasing sol-gel particle/polyurethane glucose biosensors." *Anal Chem.* **2004,** *76*, 4543-4549.

(22) Nablo, B. J.; Schoenfisch, M. H. "Antibacterial properties of nitric oxide-releasing sol-gels." *J. Biomed. Mater. Res.* **2003,** *67*, 1276-1283.

(23) Nablo, B. J.; Schoenfisch, M. H. "Poly(vinyl chloride)-coated sol-gels for studying the effects of nitric oxide release on bacterial adhesion." *Biomacromolecules* **2004,** *5*, 2034-2041.

(24) Gomez-Suarez, C.; Busscher, H. J.; van der Mei, H. C. "Analysis of bacterial detachment from substratum surfaces by the passage of air-liquid interfaces." *Appl. Environ. Microbiol.* **2001,** *67*, 2531-2537.

(25) Pitt, W. G.; McBride, M. O.; Barton, A. J.; Sagers, R. D. "Air-water interface displaces adsorbed bacteria." *Biomaterials* **1993,** *14*, 605-608.

(26) Poelstra, K. A.; van der Mei, H. C.; Gottenbos, B.; Grainger, D. W.; van Horn, J. R.; Busscher, H. J. "Pooled human immunoglobulins reduce adhesion of *Pseudomonas aeruginosa* in a parallel plate flow chamber." *J. Biomed. Mater. Res.* **2000,** *51*, 224-232.

(27) Kaper, H. J.; Busscher, H. J.; Norde, W. "Characterization of poly(ethylene oxide) brushes on glass surfaces and adhesion of *Staphylococcus epidermidis*." *J. Biomaterials Sci. Polym. Edn.* **2003,** *14*, 313-324.

(28) Roosjen, A.; de Vries, J.; van der Mei, H. C.; Norde, W.; Busscher, H. J. "Stability and effectiveness against bacterial adhesion of poly(ethylene oxide) coatings in biological fluids." *J. Biomed. Mater. Res.* **2005,** *73*, 347-354.

(29) Rodrigues, L.; van der Mei, H.; Banat, I. M.; Teixeira, J.; Oliveira, R. "Inhibition of microbial adhesion to silicone rubber treated with biosurfactant from *Streptococcus thermophilus*." *FEMS Immunol. Med. Microbiol.* **2006,** *46*, 107-112.

(30) Busscher, H. J.; van der Mei, H. C. "Microbial adhesion in flow displacement systems." *Clin. Microbiol. Rev.* **2006,** *19*, 127-141.

(31) Beckman, J. S.; Conger, K. A. "Direct measurement of dilute nitric oxide in solution with an ozone chemiluminescent detector." *Methods Enzymol.* **1995,** *7*, 35-39.

(32) Gristina, A. G. "Biomaterial-centered infection: Microbial adhesion versus tissue integration." *Science* **1987,** *237*, 1588-1597.

(33) Busscher, H. J.; van der Mei, H. C. "Use of flow chamber devices and image analysis methods to study microbial adhesion." *Methods Enzymol.* **1995,** *253*, 455-477.

(34) Luo, J.; Chen, A. F. "Nitric oxide: A newly discovered function on wound healing." *Acta Pharmacol. Sinica* **2005,** *26*, 259-264.

Chapter 3:

Reduced Foreign Body Response at Nitric Oxide-Releasing Subcutaneous Implants

3.1 Introduction

While a great deal of research has focused on the design of more biocompatible tissue-based sensors, their utility and function continue to be impaired by the body's response to foreign materials.[1-4] The foreign body response is a physiological cascade triggered upon implantation that begins with protein adsorption to the implant surface and the recruitment of inflammatory cells.[5, 6] Neutrophils modulate the host response initially (minutes to hours) whereas macrophages respond over a longer period (days).[6, 7] While macrophages efficiently rid the wound site of microscopic matter such as bacteria and dead cells, they are unable to digest macroscopic implants, leading to chronic inflammation and macrophage fusion into foreign body giant cells (FBGC) that can perpetually remain at the tissue/implant interface.[6, 7] Still unsuccessful in their attempt to digest the implant, FBGC secrete cytokines that trigger fibroblasts to deposit a dense avascular layer of collagen (termed a 'capsule') around the implant to permanently sequester it from the surrounding tissue.[5, 6]

All aspects of the foreign body response conspire to impede the performance of implanted sensors. For example, macrophages and other inflammatory cells recruited to the implant are known to consume oxygen and glucose and produce reactive oxygen species, all of which may influence sensor response.[1] Both adsorbed proteins and the hypovascular collagen capsule isolate the implant and act as substantial barriers to analyte diffusion from

blood capillaries to the sensor. To circumvent such problems, a great deal of research has focused on mitigating the body's response to foreign materials. Strategies to reduce the inflammatory response include altering the microarchitecture of the implant surface[8-10] and applying compounds such as osteopontin that are known to inhibit FBGC formation.[11] Likewise, administering pro-angiogenic cytokines such as vascular endothelial growth factor (VEGF)[12, 13] and inhibitors of type I collagen synthesis such as halofuginone[14] have been proposed as methods to increase angiogenesis and diminish capsule formation, respectively. While several treatments have shown promise at addressing certain facets of the foreign body response, few approaches deal collectively with the entire cascade.

Recently, polymers that slowly release the biological mediator nitric oxide (NO), an endogenously-produced free radical, have proven useful in the design of more biocompatible sensors.[3, 15, 16] For example, NO-releasing polymer coatings have been shown to drastically improve the function of intravascular gas sensors[17] and prevent implant-associated infection in vivo[18] by reducing both platelet and bacterial adhesion to surfaces.[19,20] Nitric oxide also plays a vital role in multiple processes of the wound healing cascade,[21] and promotes angiogenesis by modulating VEGF production.[22, 23] Amadeu et al. reported that exogenous application of a NO donor to a wound site decreased recruitment of inflammatory cells and accelerated re-epithelialization.[24] In related work, Gifford et al. reported that the inflammatory response to implanted NO-releasing sensors was reduced compared controls.[25] Nitric oxide also plays a critical role in collagen deposition by fibroblasts,[26] and studies have demonstrated that collagen synthesis at a wound site was decreased in a dose-dependent manner with the application of an exogenous NO donor.[27] Taken together, these studies suggest that NO administration at the site of a subcutaneous implant may limit the foreign

body response by promoting angiogenesis, diminishing the inflammatory response, and reducing collagen capsule formation.

Herein, we report the effect of NO on the foreign body response to subcutaneous implants in a rat model. Nitric oxide release was conferred to medical-grade silicone elastomer implants via coating with a well-characterized NO-releasing xerogel polymer.[18, 28] Capsule formation, angiogenesis, and the inflammatory response were monitored at 1, 3, and 6 weeks via histological examination of explanted tissue samples. The results indicate that NO release is an attractive strategy to promote wound healing and improve the tissue integration properties of subcutaneous implants.

3.2 Methods and materials

N-(6-Aminohexyl)aminopropyltrimethoxysilane (AHAP3) and isobutyltrimethoxysilane (BTMOS) were purchased from Gelest (Morrisville, PA) and stored under nitrogen. Ethanol (absolute) and hydrochloric acid were purchased from Fisher Scientific (Pittsburgh, PA) and used as received. Distilled water was purified with a Millipore Milli-Q Gradient A-10 water purification system (Bedford, MA) to a final resistivity of 18.2 MΩ•cm and a total organic content of <6 ppb. Nitric oxide and argon were purchased from National Welders (Raleigh, NC). Class VI medical-grade silicone elastomer was purchased from McMaster-Carr (Atlanta, GA).

3.2.1 NO-releasing xerogel-coated implants. Nitric oxide-releasing xerogel coatings were applied to medical-grade silicone elastomer as described by Nablo et al.[18] Briefly, xerogel solutions were prepared by mixing ethanol (1.2 mL), water (640 μL), and 0.5 M HCl (110 μL) followed by dropwise addition of BTMOS (1.28 mL). The solution was mixed for

18 h followed by addition of AHAP3 (860 μL) and additional mixing for 30 h. Class VI medical grade silicone elastomer was cut into square sections 8 x 8 x 2 mm^3 and cleaned by sonicating in ethanol, water, and ethanol again for 30 min each. The silicone squares were sterilized in a steam autoclave at 121 ºC for 25 min, and then coated with sol via a dip-coating procedure. The initial sol coating was allowed to solidify into a xerogel prior to the application of a second coating of sol. To ensure even coating, the squares were spun at ~1 rev/s for 3 d while drying. The xerogel-coated silicone squares (i.e., implants) were then placed in a 55 ºC oven for 1 d followed by storage in a desiccator.

Half of the xerogel-coated implants were modified with diazeniumdiolate NO-donors, while the others were left unmodified to serve as controls. To facilitate diazeniumdiolate synthesis, xerogel-coated implants were placed in an in-house NO reaction vessel that was subsequently sealed and flushed with Ar to remove atmospheric O_2. The vessel was then pressurized to 5 atm NO for 2.5 d, and then flushed copiously with Ar.[18] The diazeniumdiolate-modified implants were removed and stored at -20 ºC until use.

3.2.2 Nitric oxide release measurements. Nitric oxide release from implants coated with diazeniumdiolate-modified xerogel was monitored with a Sievers 280 chemiluminescent NO analyzer (Boulder, CO). The instrument was calibrated with an atmospheric sample that had been passed through a NO zero filter and a 24.1 ppm NO gas standard (balance N_2). Xerogel-coated implants were immersed in deoxygenated phosphate buffered saline (PBS; 10 mM, pH 7.4) at 37 ºC. The NO released was carried from the buffer to the analyzer by a stream of N_2 bubbled into the solution at a flow rate of 80 mL/min. In the instrument, NO was detected via its formation of a chemiluminescent byproduct upon reaction with ozone.

Discrete NO-release measurements were taken over 6 weeks. Between measurements, implants were stored in sealed vials of PBS at 37 ºC.

3.2.3 In vivo studies to examine the foreign body response. The effect of NO release on the foreign body response was evaluated in adult male Sprague-Dawley rats (250 – 300 g; Charles River Laboratories, Raleigh, NC). The animal protocol was approved by the Institutional Animal Care and Use Committee at Duke University. Prior to implantation, all implants were sterilized by exposure to germicidal UV light in a sterile biosafety cabinet.[18] After sterilization, all implants were stored in sterile petri dishes on dry ice.

Rats were anesthetized with 2.5% isoflurane (v/v in O_2), administered a subcutaneous injection of flunixin (2.5 mg/kg), and their backs were shaved. Betadine was applied to the shaved region and the rats were placed on a heating pad in a sterile operating field. Six transverse 1 cm incisions were made approximately 1 cm from the dorsal midline along both sides of the animal. Using blunt dissection, subcutaneous pockets were created at the site of each incision. Each subcutaneous pocket received one of the following implants: NO-releasing xerogel-coated silicone, xerogel-coated silicone not capable of NO release (control), or uncoated bare silicone (blank). Each rat received two of each type of implant, and position was controlled for with 72 implants over 12 total rats. The wounds were closed with non-absorbable sutures and cleaned with hydrogen peroxide. Care was taken to ensure that each rat recovered, flunixin was administered every 12 h for 2 d (2.5 mg/kg), and each rat was given ad libitum access to food and water.

At 1, 3, and 6 weeks, 4 of the rats were anesthetized with 2.5% isoflurane (v/v in O_2) and shaved, and the implants were removed with surrounding tissue. Tissue samples were placed in 10% buffered formalin for 24 h, embedded in paraffin, and sectioned into 5 μm-

thick slices. Tissue samples for histological analysis were stained with Gomori's trichrome, hematoxylin & eosin (H&E), and CD-31 immunohistochemical stain. Images of the trichrome and H&E samples were collected using 10x and 20x objectives with an Olympus optical microscope (Melville, NY) equipped with a SPOT RT KE Slider digital color camera (Diagnostic Instruments; Sterling Heights, MI). Tissue samples treated with the CD-31 immunohistochemical stain were examined with a Zeiss Axiovert 200 inverted microscope equipped with a Syto 9 filter set. Images were captured with a 20x objective with a Zeiss Axiocam digital camera (Chester, VA).

3.2.4 Histological evaluation and data analysis. Capsule thickness data were obtained from trichrome-stained tissue samples. The foreign body capsule was defined as the region of dense collagen oriented parallel to the implant. Regardless of implant type, characteristic foreign body capsules were not observed at 1 week. Tissue samples collected at 3 and 6 weeks exhibited developed capsules in contrast to the loosely-deposited randomly-oriented collagen farther away from the implant. Capsule thickness was determined by direct comparison with the scale bar on each image. For all implant types, 3 images were analyzed from each of 4 rats with 3 capsule thickness measurements per image (36 total measurements). Collagen density was calculated by applying a digital threshold with Photoshop (Adobe Software; San Jose, CA) to images of tissue in regions within 100 μm or 200 μm of the implant surface. The threshold was applied such that all pixels resulting from tissue were converted to black pixels to allow differentiation from the white background. The number of black pixels was then normalized to the total number of pixels in the image and reported as the collagen density index (CDI). At each time point, the CDI was calculated from 3 images analyzed from each of 4 rats (12 total measurements). The number of blood

vessels in proximity to each implant was determined by capturing images of the CD-31-stained samples at pre-determined locations around each implant. Each image was situated such that tissue/implant interface comprised one edge of the field and the tissue section imaged extended one visual field (~330 μm) into the tissue away from the implant. A blinded observer counted the number of CD-31-stained blood vessels per field for each image. The average number of blood vessels was calculated from 6 images collected from 4 rats at each time point (24 total measurements per implant type per time point). The inflammatory response was analyzed from the H&E-stained tissue samples. Images were cropped to display tissue within 50 μm of the implant surface. By applying a digital filter with Photoshop, pixels corresponding to the nuclei of inflammatory cells were selected based on their unique purple color imparted by the H&E stain. The number of pixels corresponding to inflammatory cells was then digitally counted and normalized to the total number of pixels in the image, and reported as the inflammatory response factor (IRF). Average IRF values were calculated from a minimum of 16 images taken from 4 rats. Data are expressed as mean values ± standard error of the mean, and were analyzed for significance ($p < 0.05$) with a nonparametric Kruskal-Wallis *H*-test.[29]

3.3 Results and discussion

3.3.1 Nitric oxide releasing xerogel coatings. Diazeniumdiolate-modified xerogels have been studied previously as coatings to reduce both platelet and bacterial adhesion via NO release.[28] Herein, the tissue and wound healing properties of NO-releasing xerogel coatings were evaluated in a subcutaneous implant rat model. Nitric oxide release from an optimized 40% AHAP3 (v/v balance BTMOS) xerogel coating is shown in Figure 3.1. In

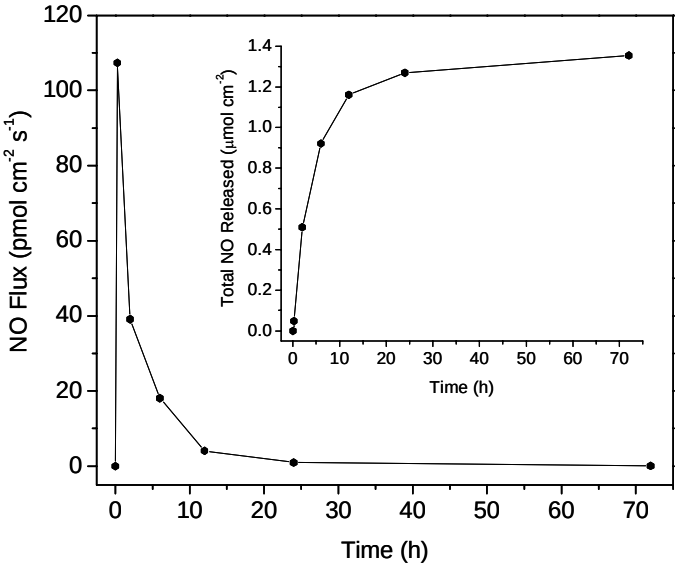

Figure 3.1. Nitric oxide release from silicone elastomer implants coated with diazeniumdiolate-modified 40% AHAP3/BTMOS (v/v) xerogels. Inset: Total NO release.

total, approximately 1.35 μmol of NO was delivered per cm^2 of surface area from the xerogel-coated silicone implants. The release of NO from diazeniumdiolate-modified xerogels is initiated upon immersion in aqueous solution and continues as water diffuses deeper within the xerogel matrix to further decompose diazeniumdiolates.[28] Notably, ~50% of the total NO was released within the first 5 h for the materials used in these studies and >99% of the release was complete after 72 h. Small fluxes of NO (< 1 pmol cm^{-2} s^{-1}) were detectable up to 1 week (data not shown), after which no signal was observed above the baseline response of the chemiluminescent NO analyzer. This NO release profile is similar to that of other controlled release systems including polymers designed to elute antibiotics[30] or therapeutic antibodies,[31] where the majority of the active compound is released within several hours of immersion in aqueous solution. The flux of NO from diazeniumdiolate-modified xerogels is tunable based on the amount of aminosilane NO-donor precursor (i.e., AHAP3) used to prepare the coatings.[28] While it may be possible to achieve higher NO fluxes and longer sustained release by further increasing the volume percentage of AHAP3, stability testing has shown that inclusion of aminosilanes at concentrations greater than 40% (v/v with alkylsilane) results in poor material stability.[28]

3.3.2 Effect of NO release on foreign body capsule formation and collagen deposition. The decrease in sensitivity of subcutaneous sensors has been attributed to both biofouling (i.e., surface-adsorbed proteins) and tissue encapsulation.[4, 32] While both responses (i.e., biofouling and encapsulation) are detrimental to sensor performance, the primary impediment to analyte transport through implanted sensor membranes has been shown to be due to tissue and not the adsorbed biofouling layer.[32] Indeed, tissue effects were found to contribute 3-5 times more resistance to analyte transport than protein biofouling.

Wisniewski and coworkers suggest that efforts to develop more biocompatible sensor membranes should focus on altering the tissue response as opposed to protein biofouling.[32] In light of these findings, we examined both capsule thickness and collagen density over a period of 6 weeks at NO-releasing, control, and blank (uncoated silicone elastomer) implants. The foreign body capsule was identified by its characteristic densely-packed collagen oriented parallel to the implant surface (Fig. 3.2). Since capsule formation generally begins 2-3 weeks after implantation,[6] it was not observed for any implants until the 3 week time point. Qualitatively, the capsules surrounding NO-releasing implants (Fig. 3.2 C) appeared thinner than those surrounding blank and control implants (Fig. 3.2 A, B). These observations were confirmed by calculating the average capsule thickness from 12 images taken across 4 rats for each implant type at each time point. As shown in Figure 3.3, capsule thickness at NO-releasing implants was significantly less ($p < 0.05$) than at xerogel-coated controls and bare silicone elastomer implants at both 3 and 6 weeks. The reduced capsule thickness observed between xerogel-coated controls (i.e., xerogel-coated implants not capable of NO release) and NO-releasing samples indicates that the decrease in capsule thickness is attributable to NO release. The reason that capsule thickness at xerogel-coated controls was reduced compared to bare silicone elastomer implants is not entirely understood. However, it is likely due to differences in surface chemistry such as charge and hydrophobicity. Previous studies have shown that protein adsorption is greatly influenced by surface properties,[33, 34] and that initial protein adsorption to an implanted biomaterial may partially dictate the ensuing foreign body response.[5, 6] Thus, altered protein adsorption may account for the observed reduction in capsule thickness between xerogel-coated controls and

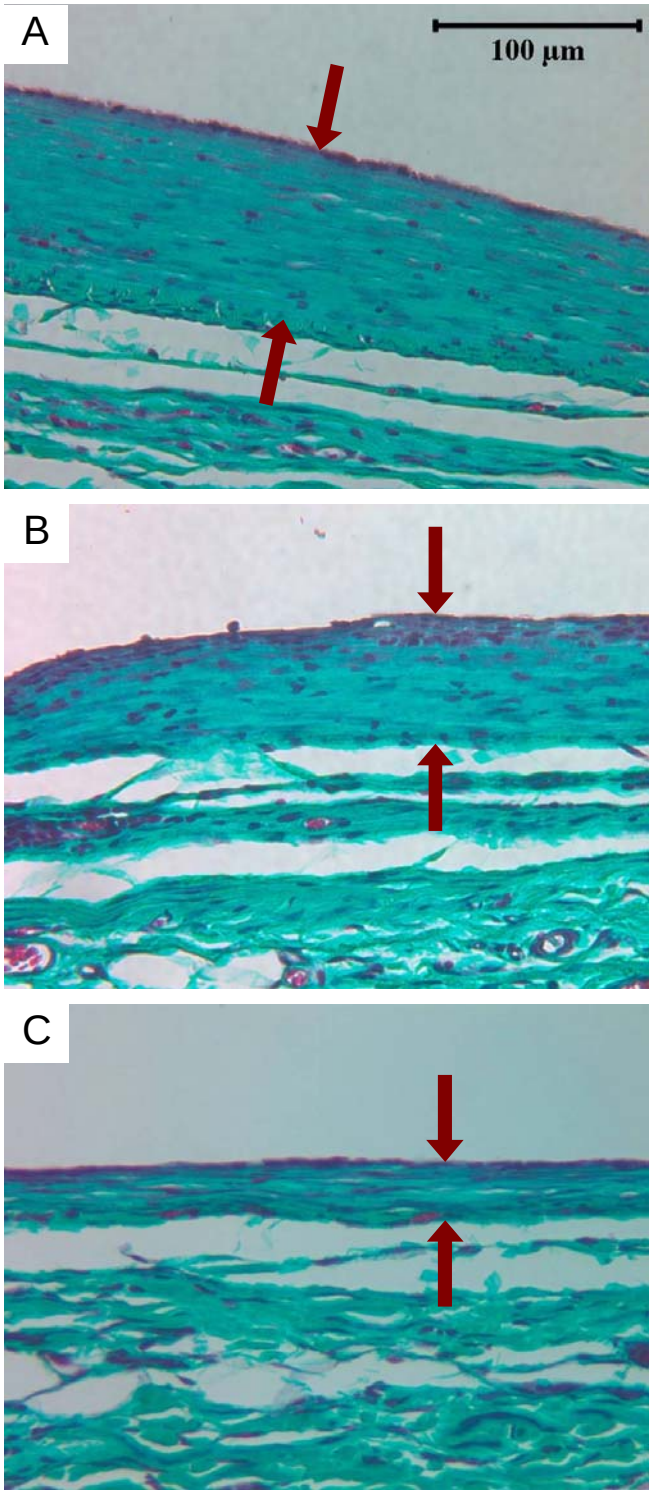

Figure 3.2. Optical micrographs showing foreign body capsule formation after 6 weeks at (A) bare silicone elastomer; (B) xerogel-coated control; and, (C) NO-releasing xerogel-coated subcutaneous implants. Xerogel polymer coating was 40% AHAP3/BTMOS (v/v). Scale is the same in each image and arrows denote the foreign body capsule. The implant was located in the upper white region of each image.

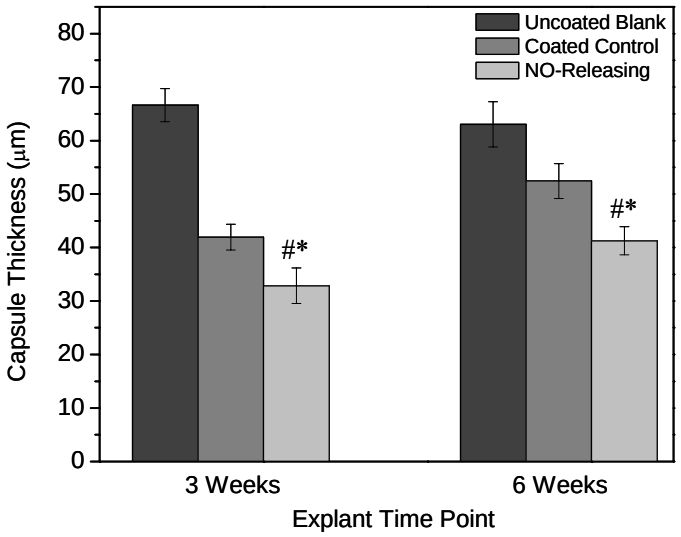

Figure 3.3. Foreign body capsule thickness at uncoated blank, xerogel-coated control, and NO-releasing xerogel-coated subcutaneous implants. Xerogel polymer coating was 40% AHAP3/BTMOS (v/v). Significant differences ($p < 0.05$) between NO-release implants and blanks (#), and NO-release and controls (*) are indicated.

bare silicone elastomer implants. Previous work from our laboratory has shown reduced bacterial and platelet adhesion at control xerogel surfaces.[28]

Figure 3.3 shows that the capsule thickness at bare silicone elastomer implants did not change significantly between 3 and 6 weeks (67 ± 3 μm vs. 63 ± 4 μm, respectively). As such, capsule formation at uncoated implants was essentially complete after 3 weeks. In contrast, the capsules at xerogel-coated control and NO-releasing implants continued to develop between 3 and 6 weeks, indicating that capsule formation at those implants was delayed compared to bare silicone elastomer implants. Future experiments will be conducted to determine if the decrease in capsule thickness at NO-releasing implants is temporary (i.e., observed only at time points ≤ 6 weeks) or if short-term NO-release permanently reduces capsule thickness.

In addition to directly measuring capsule thickness, the density of collagen near the implant surfaces was also evaluated. To obtain quantitative data, a method of digital thresholding was used to differentiate tissue from the image background. The number of pixels resulting from tissue (versus background) was normalized to the total number of pixels in the image. Since the primary tissue component within the analysis area was collagen, the resulting quotient was reported as the "collagen density index" (CDI), with a CDI value of 100 indicating that every pixel within the selected image area represented tissue. As shown in Figure 3.4, NO-releasing implants were characterized by significantly reduced collagen density at distances up to both 100 and 200 μm from the implant surface at 1 week compared to bare silicone elastomer and xerogel-coated control implants. The CDI within 100 μm remained significantly lower compared to bare silicone elastomer implants at both 3 and 6 weeks, due in part to the reduction in capsule thickness as noted above.

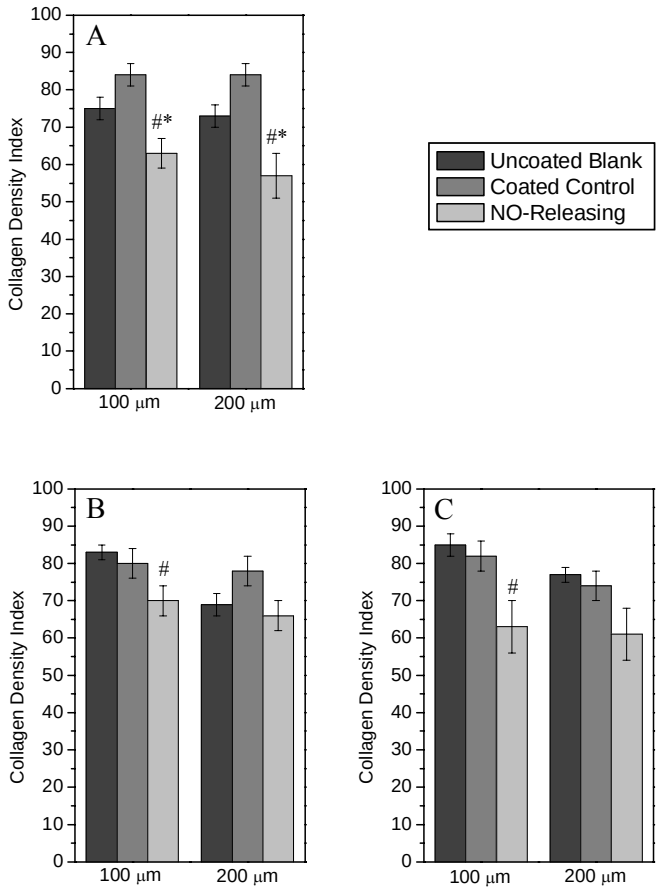

Figure 3.4. Collagen density indexes observed at (A) 1 week; (B) 3 weeks; and, (C) 6 weeks at uncoated blank, xerogel-coated control, and NO-releasing xerogel-coated subcutaneous implants. Xerogel polymer coating was 40% AHAP3/BTMOS (v/v). Significant differences ($p < 0.05$) between NO-release implants and blanks (#), and NO-release and controls (*) are indicated.

The exact mechanism by which NO-release decreases capsule thickness and collagen density at the tissue interface remains unclear. Previous work has shown that NO's modulation of cytokines involved in the wound healing response alters collagen deposition.[26] The cytokine most often associated with collagen production is transforming growth factor-β (TGF-β).[26] TGF-β has been shown to upregulate collagen production by both human dermal fibroblasts[35] and rat mesangial cells.[36] In the same studies, application of exogenous NO donors decreased TGF-β secretion and collagen deposition.[35, 36] Other studies have also shown that inhibitors of TGF-β signaling decrease collagen content in foreign body capsules in vivo.[14] Thus, NO may act directly to modulate cytokines such as TGF-β to decrease collagen deposition.

3.3.3 Effect of NO release on angiogenesis. Over the course of the foreign body response, an implanted biomaterial becomes sequestered within a dense foreign body capsule that is void of blood capillaries.[6] Analogous to the dense collagen layer, the lack of capillaries also presents negative consequences for tissue-based sensors, which require constant transport of analytes from the blood to ensure accurate and consistent function.[1] Sufficient vascularization is also critical for effective wound healing[37, 38] and tissue regeneration[39] to sustain cellular proliferation and vitality. Thus, polymers that enhance new blood vessel formation (i.e., angiogenesis) are desirable as coatings for indwelling medical devices. Notably, NO has been shown to play a key role in angiogenesis by promoting the expression of vascular endothelial growth factor (VEGF), a potent pro-angiogenic cytokine.[23] In the present study, angiogenesis was monitored by treating explanted tissue samples with a CD-31 immunohistochemical staining technique, where blood vessels are fluorescently labeled. Representative images of tissue samples explanted after 1 week and treated with

CD-31 are shown in Figure 3.5. Tissue adjacent to bare silicone elastomer and xerogel-coated controls (Fig. 3.5 A, B) exhibited reduced vascularization compared to tissue adjacent to NO-releasing implants (Fig. 3.5 C). Evaluation of 24 images per implant type per time point allowed for quantitative determination of the number of blood vessels in tissue adjacent to each implant. As shown in Figure 3.6, ~77% more blood vessels were observed within ~330 μm of the NO-releasing implants compared to xerogel-coated control implants after 1 week. Likewise, NO release resulted in significantly greater angiogenesis compared to controls after 3 weeks as well.

While a greater number of blood vessels were also observed at NO-releasing implants at 6 weeks compared to both control and bare silicone elastomer implants, the difference in blood vessel density was not significant due to variability across samples. Significantly enhanced angiogenesis was thus observed at early time points (i.e., 1 and 3 weeks) for NO-releasing implants but not at later periods. Such data is consistent with the temporal efficacy of other angiogenic therapies.[40] Silva and Mooney have reported that VEGF delivered as an injected bolus was quickly cleared from the site of administration and led to lower levels of angiogenesis at 6 weeks than VEGF slowly released from an implanted hydrogel.[41] The xerogel implant coatings described in our study deliver NO as a bolus (Fig. 3.1), with the vast majority of NO released over the initial 10 h post-implantation. Such delivery stimulates angiogenesis at early time points (i.e., 1 and 3 weeks). By 6 weeks, however, the NO release is complete and the coatings no longer promote angiogenesis. Methods to deliver NO for longer periods are currently being explored in our laboratory to evaluate the effect of extended NO release on angiogenesis.

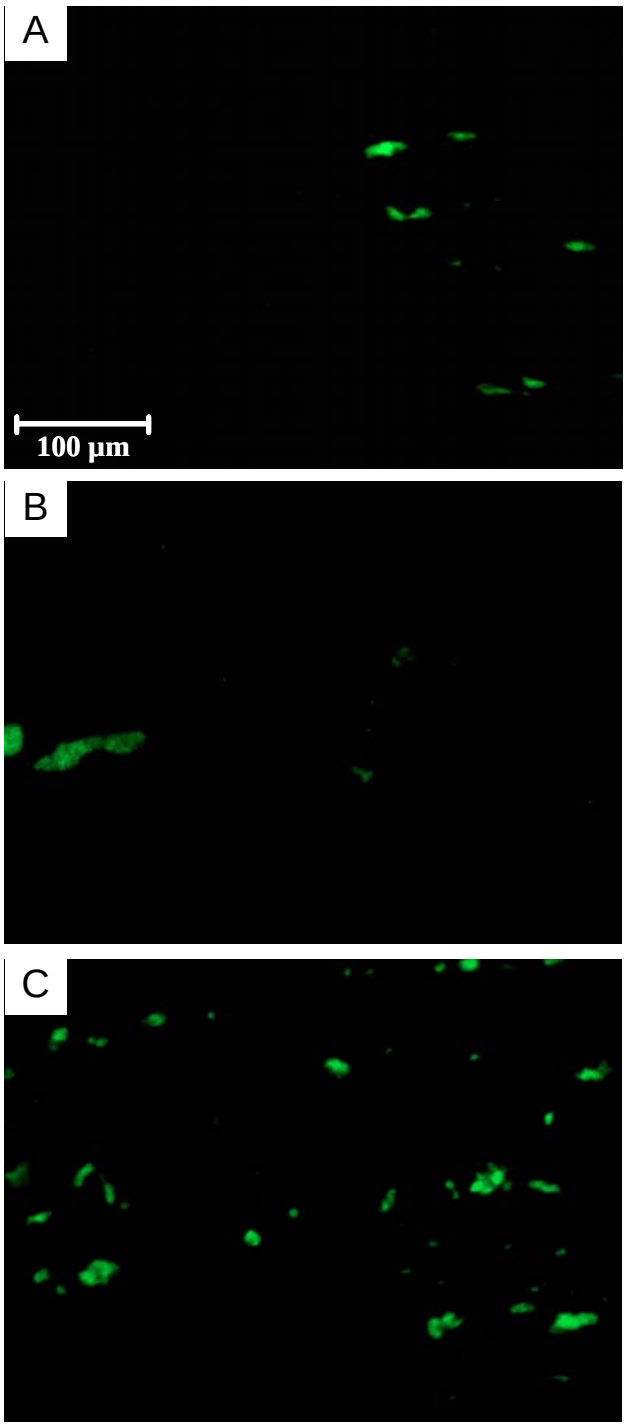

Figure 3.5. Fluorescence micrographs of CD-31-stained tissue samples adjacent to (A) bare silicone elastomer; (B) xerogel-coated control; and, (C) NO-releasing xerogel-coated subcutaneous implants after 1 week. Xerogel polymer coating was 40% AHAP3/BTMOS (v/v). The green fluorescence represents blood vessel presence via positive labeling of endothelial cells with CD-31 immunohistochemical stain. Scale is the same in each image. Each image shows tissue within approximately 340 µm of the implant, which was located at the bottom of each image.

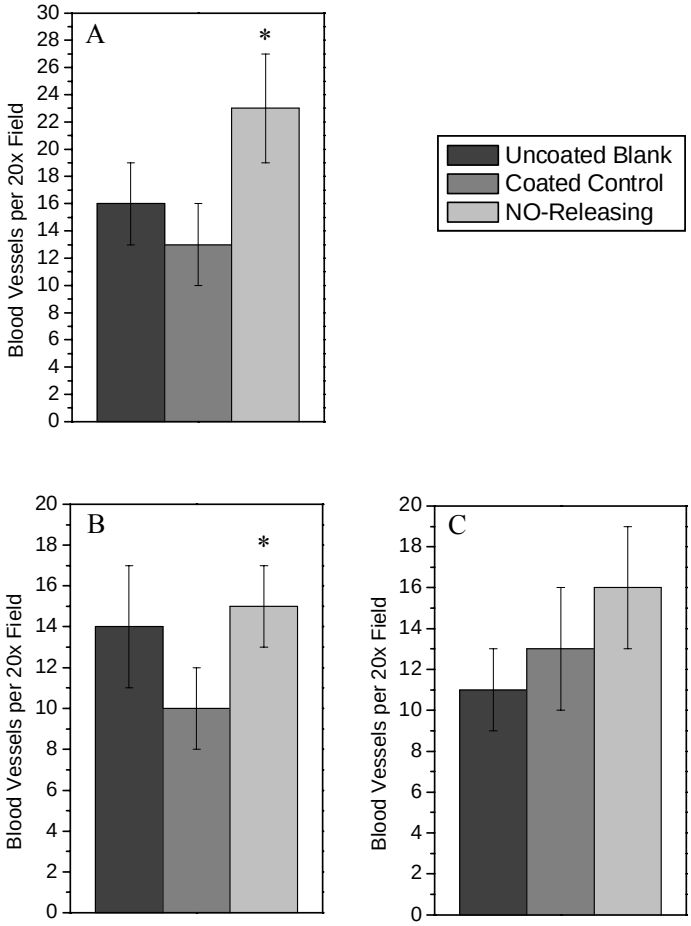

Figure 3.6. Blood vessels observed per 20x field at (A) 1 week; (B) 3 weeks; and, (C) 6 weeks at uncoated blank, xerogel-coated control, and NO-releasing xerogel-coated subcutaneous implants. Xerogel polymer coating was 40% AHAP3/BTMOS (v/v). Significant differences ($p < 0.05$) between NO-release implants and controls (*) are indicated.

3.3.4 Effect of NO release on the inflammatory response. Implantation of a subcutaneous biomaterial creates a wound that inevitably triggers the host inflammatory response and recruitment of phagocytic cells such as monocytes, neutrophils, and macrophages.[6] While such a response is necessary for effective wound healing, the presence of phagocytic cells negatively impacts implanted sensors via their surface adhesion and the release of interfering species. To improve the analytical performance of such devices, it is desirable to mitigate the inflammatory response in tissue adjacent to the sensor. Gifford et al. have reported that a needle-type glucose sensor capable of releasing NO reduced the recruitment of inflammatory cells after 24 h in subcutaneous tissue,[25] thereby demonstrating the feasibility of NO release as a means to control the inflammatory response. However, implanted sensors would ideally function accurately for periods beyond 24 h and we thus monitored the inflammatory response at NO-releasing subcutaneous implants over 6 weeks. Representative H&E-stained tissue samples are shown in Figure 3.7, with inflammatory cells clearly identifiable by the characteristic purple color imparted to their nuclei by the H&E stain. The tissue/implant interface of bare silicone elastomer and xerogel-coated control implants was characterized by an abundance of inflammatory cells. In contrast, the tissue adjacent to the NO-releasing implants exhibited a markedly lower inflammatory response as evidenced by fewer cells. To quantitatively assess the progression of the inflammatory response at each type of implant, an inflammatory response factor (IRF) was determined at each time point. Figure 3.8 shows that while NO-releasing implants did not significantly reduce the inflammatory response at 1 week (Fig. 3.8 A), a significant decrease was observed at both 3 and 6 weeks compared to both bare silicone elastomer and xerogel-coated control implants (Fig. 3.8 B and C). Indeed, the IRF at NO-releasing implants was reduced by

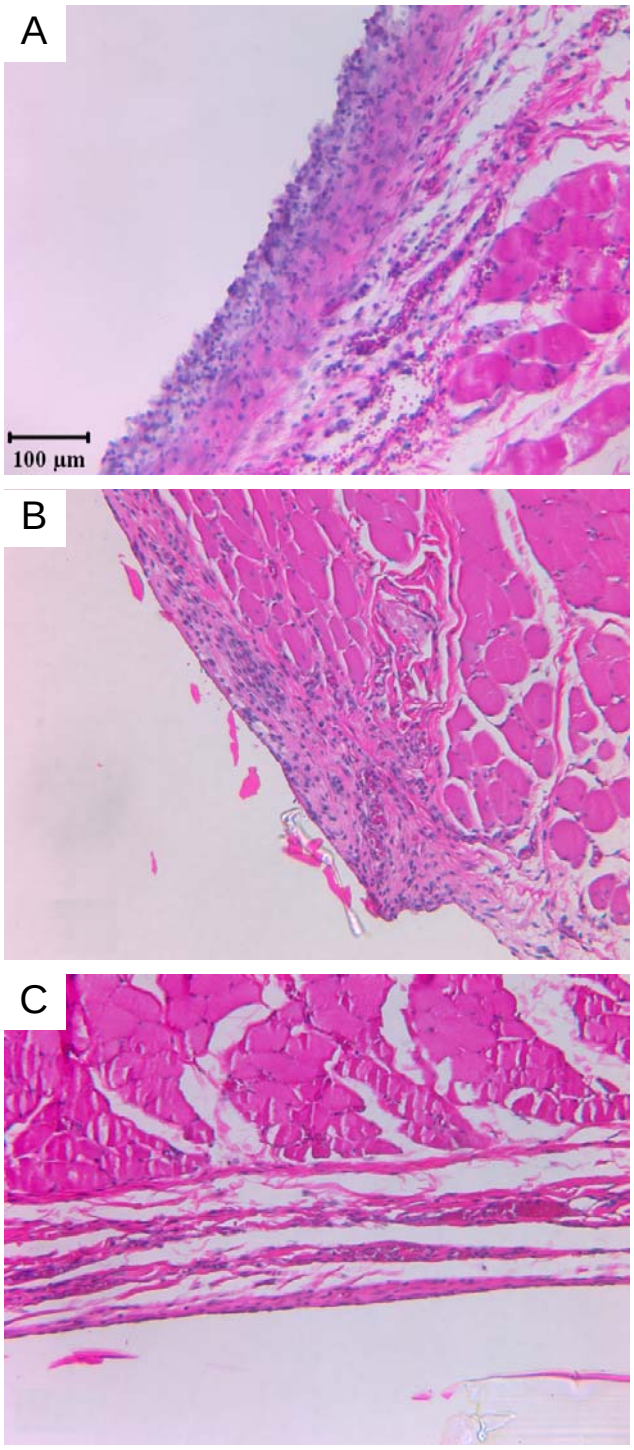

Figure 3.7. Optical micrographs of hematoxylin & eosin (H&E)-stained tissue samples showing the inflammatory response after 3 weeks at (A) bare silicone elastomer; (B) xerogel-coated control; and, (C) NO-releasing xerogel-coated subcutaneous implants. Xerogel polymer coating was 40% AHAP3/BTMOS (v/v). Nuclei stain purple while collagen appears pink with H&E stain. Scale is the same in each image. The implants were located in the white region at the left (A, B) or bottom (C) of each image.

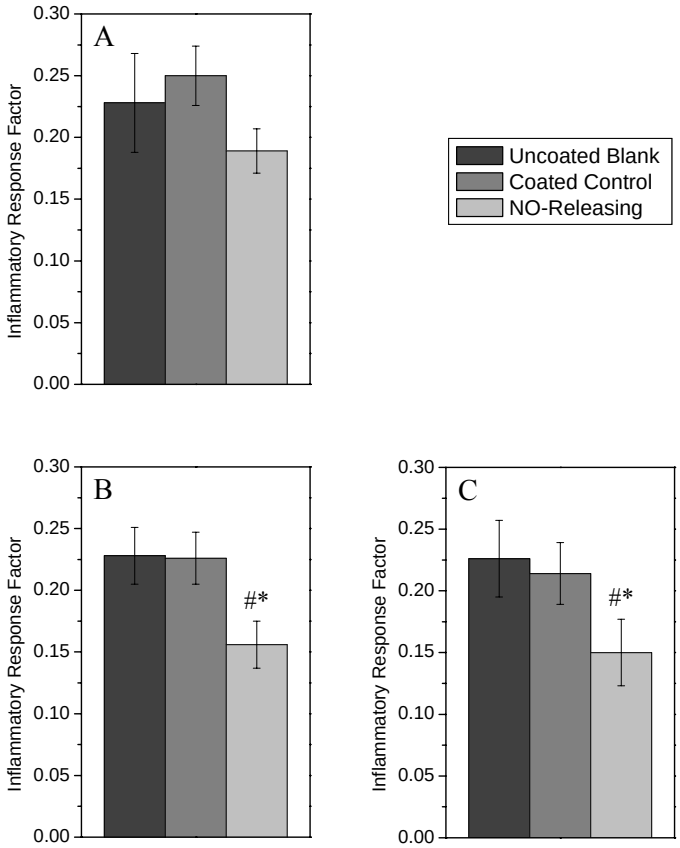

Figure 3.8. Inflammatory response factors observed at (A) 1 week; (B) 3 weeks; and, (C) 6 weeks at uncoated blank, xerogel-coated control, and NO-releasing xerogel-coated subcutaneous implants. Xerogel polymer coating was 40% AHAP3/BTMOS (v/v). Significant differences ($p < 0.05$) between NO-release implants and blanks (#) and NO-release implants and controls (*) are indicated.

>30% relative to bare and control implants at both 3 and 6 weeks. The IRF for each implant type did not change significantly between 3 and 6 weeks, indicating that a reduced chronic inflammatory response due to NO release may be long-lasting. Of note, the analgesic provided to the rats during the experiment (flunixin) belongs to a class of compounds known as non-steroidal anti-inflammatory drugs (NSAIDs) that derive their efficacy by modulating the inflammatory response.[42, 43] All rats were treated with the same dose of flunixin throughout the experiment. As such, differences in the IRF can be attributed solely to differences in implant chemistry and not the analgesic itself. Similar experiments conducted with non-NSAID analgesics may result in different inflammatory responses to the subcutaneous implants.

A further question that remains is understanding the mechanism by which short-term (≤ 1 week) NO release modulates the chronic inflammatory response at extended periods (i.e., 3 and 6 weeks) after NO release has subsided. The fact that the inflammatory response at all three implant types was not statistically different at 1 week may be expected since it has been suggested that the initial inflammatory response to implanted materials is primarily the result of surgical trauma and not the implant itself.[10] The significant decrease in inflammatory response at 3 and 6 weeks at NO-releasing implants may be due to NO's ability to downregulate pro-inflammatory cytokines such as macrophage chemoattractant protein-1 (MCP-1) and interleukin-6 (IL-6).[26] It has also been suggested that a reduction in the inflammatory response may be mediated by nitrosated proteins.[44] Such modified proteins may form near the implant during the early period of high NO release. The ability of NO to regulate other inflammatory modulators may translate short-term NO release into longer-term anti-inflammatory activity. Studies to determine the effect of xerogel-derived NO on

cytokine regulation and protein nitrosation are currently planned. Also of interest is the fact that some inflammatory cells such as macrophages and neutrophils are capable of generating NO themselves to battle microbial infection and orchestrate wound healing.[26] Previous studies have shown that NO production by macrophages may be a self-regulating pathway.[44] The application of an exogenous NO donor to murine macrophages exerted biphasic regulation of the expression of inducible nitric oxide synthase (iNOS), the enzyme responsible for high-output NO production.[45] Likewise, it has been suggested that NO may also regulate iNOS expression in neutrophils via modulation of the cytokine IL-8.[26] While it is clear that NO production by inflammatory cells is regulated in part by NO itself, it is not yet certain what dose of NO and timing of administration are necessary for optimal tissue integration for subcutaneous implants. Such studies are currently planned in our laboratory.

3.4 Conclusions

Nitric oxide-releasing polymer coatings applied to subcutaneous implants were shown to influence multiple aspects of the foreign body response in a rat model. Delivery of ~1.35 μmol NO per cm^2 of implant surface area resulted in a drastic reduction in both capsule thickness and collagen density at the tissue/implant interface. The NO release was also shown to increase angiogenesis and reduce the chronic inflammatory response. Decreased tissue resistance and enhanced angiogenesis may lead to improved transport of analytes to an implanted sensor, while a reduced inflammatory response would likely enhance sensor function. Thus, NO-releasing sensor membranes may represent a new paradigm for improving the analytical performance of implantable subcutaneous sensors. The potential application of NO-releasing coatings extends well beyond sensors to include other

biomedical implants that would benefit from improved tissue integration. For example, drug delivery devices may function more reliably when encapsulation by dense collagen is avoided, while pain and unsightly scarring may be minimized by reducing inflammation and undesirable collagen deposition at artificial prostheses and cosmetic implants.

The mechanisms by which short-term NO release influences the longer-term course of the foreign body response are not entirely understood. It is likely that in addition to any direct physiological effects, NO's role as a key signaling molecule in the wound-healing process may facilitate its long-term effects. The initial modulation of inflammatory and wound-healing cytokines by implant-released NO may lead to the observed differences in the inflammatory and foreign body responses at 3 and 6 weeks. It is possible that in addition to directly participating in certain aspects of the foreign body response (e.g., collagen deposition), NO's influence on one facet may indirectly influence others. For example, the reduced inflammatory response observed at NO-releasing implants may play a critical role in altering capsule formation since fewer macrophages may lead to lower levels of cytokines that trigger collagen deposition. Likewise, thinner capsules may allow blood vessels to form closer to the implants, thereby leading to enhanced vascularization in tissue proximal to the implant. Studies are planned to evaluate the effect of NO on cytokine production, as well as to understand the effect of extended NO release durations on the foreign body response.

3.5 References

(1) Wilson, G. S.; Hu, Y. "Enzyme-based biosensors for in vivo measurements." *Chem. Rev.* **2000,** *100*, 2693-2704.

(2) Frost, M. C.; Meyerhoff, M. E. "Implantable chemical sensors for real-time clinical monitoring: progress and challenges." *Curr. Opin. Chem. Biol.* **2002,** *6*, 633-641.

(3) Frost, M. C.; Batchelor, M. M.; Lee, Y.; Zhang, H.; Kang, Y.; Oh, B.; Wilson, G. S.; Gifford, R.; Rudich, S. M.; Meyerhoff, M. E. "Preparation and characterization of implantable sensors with nitric oxide release coatings." *Microchem. J.* **2003,** *74*, 277-288.

(4) Wilson, G. S.; Gifford, R. "Biosensors for real-time in vivo measurements." *Biosens. Bioelectron.* **2005,** *20*, 2388-2403.

(5) Ratner, B. D. "Reducing capsular thickness and enhancing angiogenesis around implant drug release systems." *J. Controlled Release* **2002,** *78*, 211-218.

(6) Ratner, B. D.; Bryant, S. J. "Biomaterials: Where we have been and where we are going." *Annu. Rev. Biomed. Eng.* **2004,** *6*, 41-75.

(7) Xia, Z.; Triffitt, J. T. "A review on macrophage responses to biomaterials." *Biomed. Mater.* **2006,** *1*, R1-R9.

(8) DeFife, K. M.; Colton, E.; Nakayama, Y.; Matsuda, T.; Anderson, J. M. "Spatial regulation and surface chemistry control of monocyte/macrophage adhesion and foeign body giant cell formation by photochemically micropatterned surfaces." *J. Biomed. Mater. Res.* **1999,** *45*, 148-154.

(9) Bezuidenhout, D.; Davies, N.; Zilla, P. "Effect of well defined dodecahedral porosity on inflammation and angiogenesis." *ASAIO Journal* **2002,** *48*, 465-471.

(10) Sahlin, H.; Contreras, R.; Gaskill, D. F.; Bjursten, L. M.; Frangos, J. A. "Anti-inflammatory properties of micropatterned titanium coatings." *J. Biomed. Mater. Res.* **2006,** *77A*, 43-49.

(11) Tsai, A. T.; Rice, J.; Scatena, M.; Liaw, L.; Ratner, B. D.; Giachelli, C. M. "The role of osteopontin in foreign body giant cell formation." *Biomaterials* **2005,** *26*, 5835-5843.

(12) Leach, J. K.; Kaigler, D.; Wang, Z.; Krebsbach, P. H.; Mooney, D. J. "Coating of VEGF-releasing scaffolds with bioactive glass for angiogenesis and bone regeneration." *Biomaterials* **2006,** *27*, 3249-3255.

(13) Riley, C. M.; Fuegy, P. W.; Firpo, M. A.; Shu, X. Z.; Prestwich, G. D.; Peattie, R. A. "Stimulation of in vivo angiogenesis using dual growth factor-loaded crosslinked glycosaminoglycan hydrogels." *Biomaterials* **2006,** *27*, 5935-5943.

(14) Olbrich, K. C.; Meade, R.; Bruno, W.; Heller, L.; Klitzman, B.; Levin, L. S. "Halofuginone inhibits collagen deposition in fibrous capsules around implants." *Ann. Plast. Surg.* **2005,** *54*, 293-296.

(15) Frost, M. C.; Reynolds, M. M.; Meyerhoff, M. E. "Polymers incorporating nitric oxide releasing/generating substances for improved biocompatibility of blood-contacting medical devices." *Biomaterials* **2005,** *26*, 1685-1693.

(16) Shin, J. H.; Schoenfisch, M. H. "Improving the biocompatibility of in vivo sensors via nitric oxide release." *Analyst* **2006,** *131*, 609-615.

(17) Schoenfisch, M. H.; Mowery, K. A.; Rader, M. V.; Baliga, N.; Wahr, J. A.; Meyerhoff, M. E. "Improving the thromboresistivity of chemical sensors via nitric oxide release: Fabrication and in vivo evaluation of NO-releasing oxygen-sensing catheters." *Anal. Chem.* **2000,** *72*, 1119-1126.

(18) Nablo, B. J.; Prichard, H. L.; Butler, R. D.; Klitzman, B.; Schoenfisch, M. H. "Inhibition of implant-associated infections via nitric oxide release." *Biomaterials* **2005,** *26*, 6984-6990.

(19) Mowery, K. A.; Schoenfisch, M. H.; Saavedra, J. E.; Keefer, L. K.; Meyerhoff, M. E. "Preparation and characterization of hydrophobic polymeric films that are thromboresistant via nitric oxide release." *Biomaterials* **2000,** *21*, 9-21.

(20) Hetrick, E. M.; Schoenfisch, M. H. "Antibacterial nitric oxide-releasing xerogels: Cell viability and parallel plate flow cell adhesion studies." *Biomaterials* **2007,** *28*, 1948-1956.

(21) Luo, J. D.; Chen, A. F. "Nitric oxide: A newly discovered function on wound healing." *Acta Pharm. Sinica* **2005,** *26*, 259-264.

(22) Cooke, J. P. "NO and angiogenesis." *Atherosclerosis Supplements* **2003,** *4*, 53-60.

(23) Dulak, J.; Jozkowicz, A. "Regulation of vascular endothelial growth factor synthesis by nitric oxide: facts and controversies." *Antioxid. Redox Signal.* **2003,** *5*, 123-132.

(24) Amadeu, T. P.; Seabra, A. B.; de Oliveira, M. G.; Costa, A. M. A. "S-nitrosoglutathione-containing hydrogel accelerates rat cutaneous wound repair." *J. Eur. Acad. Derm. Vener.* **2007,** *21*, 1-9.

(25) Gifford, R.; Batchelor, M. M.; Lee, Y.; Gokulrangan, G.; Meyerhoff, M. E.; Wilson, G. S. "Mediation of in vivo glucose sensor inflammatory response via nitric oxide release." *J. Biomed. Mater. Res.* **2005,** *75A*, 755-766.

(26) Schwentker, A.; Vodovotz, Y.; Weller, R.; Billiar, T. R. "Nitric oxide and wound repair: role of cytokines?" *Nitric Oxide* **2002,** *7*, 1-10.

(27) Shukla, A.; Rasik, A. M.; Shankar, R. "Nitric oxide inhibits wound collagen synthesis." *Mol. Cell. Biochem.* **1999,** *200*, 27-33.

(28) Marxer, S. M.; Rothrock, A. R.; Nablo, B. J.; Robbins, M. E.; Schoenfisch, M. H. "Preparation of nitric oxide (NO)-releasing sol-gels for biomaterial applications." *Chem. Mater.* **2003,** *15*, 4193-4199.

(29) Pett, M. A., *Nonparametric statistics for health care research*. SAGE Publications: Thousand Oaks, CA, 1997.

(30) Kwok, C. S.; Wan, C.; Hendricks, S.; Bryers, J. D.; Horbett, T. A.; Ratner, B. D. "Design of infection-resistant antibiotic-releasing polymers: I. Fabrication and formulation." *J. Controlled Release* **1999,** *62*, 289-299.

(31) Rojas, I. A.; Slunt, J. B.; Grainger, D. W. "Polyurethane coatings release bioactive antibodies to reduce bacterial adhesion." *J. Controlled Release* **2000,** *63*, 175-189.

(32) Wisniewski, N.; Klitzman, B.; Miller, B.; Reichert, W. M. "Decreased analyte transport through implanted membranes: Differentiation of biofouling from tissue effects." *J. Biomed. Mater. Res.* **2001,** *57*, 513-521.

(33) Chapman, R. G.; Ostuni, E.; Takayama, S.; Holmlin, R. E.; Yan, L.; Whitesides, G. M. "Surveying for surfaces that resist the adsorption of proteins." *J. Am. Chem. Soc.* **2000,** *122*, 8303-8304.

(34) Raffaini, G.; Ganazzoli, F. "Sequential adsorption of proteins and the surface modification of biomaterials: a molecular dynamics study." *J. Mater. Sci. Mater. Med.* **2007,** *18*, 309-316.

(35) Chu, A. J.; Prasad, J. K. "Up-regulation by human recombinant transforming growth factor β−1 of collagen production in cultured dermal fibroblasts is mediated by the inhibition of nitric oxide signaling." *J. Am. Coll. Surg.* **1999,** *188*, 271-280.

(36) Craven, P. A.; Studer, R. K.; Felder, J.; Phillips, S.; DeRubertis, F. R. "Nitric oxide inhibition of transforming growth factor-β and collagen synthesis in mesangial cells." *Diabetes* **1997,** *46*, 671-681.

(37) Gordillo, G. M.; Sen, C. K. "Revisiting the essential role of oxygen in wound healing." *Am. J. Surg.* **2003,** *186*, 259-263.

(38) Li, J.; Zhang, Y.; Kirsner, R. S. "Angiogenesis in wound repair: Angiogenic growth factors and the extracellular matrix." *Microsc. Res. Tech.* **2003,** *60*, 107-114.

(39) Laschke, M. W.; Harder, Y.; Amon, M.; Martin, I.; Farhadi, J.; Ring, A.; Torio-Padron, N.; Schramm, R.; Rucker, M.; Junker, D.; Haufel, J. M.; Carvalho, C.; Herberer, M.; Germann, G.; Vollmar, B.; Menger, M. D. "Angiogenesis in tissue engineering: breathing life into constructed tissue substitutes." *Tiss. Eng.* **2006,** *12*, 2093-2104.

(40) Fischbach, C.; Mooney, D. J. "Polymers for pro- and anti-angiogenic therapy." *Biomaterials* **2007,** *28*, 2069-2076.

(41) Silva, E. A.; Mooney, D. J. "Spatiotemporal control of vascular endothelial growth factor delivery from injectable hydrogels enhances angiogenesis." *J. Thromb. Haemost.* **2007,** *5*, 590-598.

(42) Botting, R.; Botting, J., "Non-steroidal anti-inflammatory drugs." In *Principles of Immunopharmacology*, Nijkamp, F. P.; Parnham, M. J., Eds. Birkhauser Verlag: Basel, 2005; pp 499-510.

(43) Ogino, T.; Arai, T. "Pharmacokinetic interactions of flunixin meglumine and enrofloxacin in ICR mice." *Exp. Anim.* **2007,** *56*, 79-84.

(44) Bogdan, C. "Nitric oxide and the immune response." *Nat. Immunol.* **2001,** *2*, 907-916.

(45) Connelly, L.; Palacios-Callender, M.; Ameixa, C.; Moncada, S.; Hobbs, A. J. "Biphasic regulation of NF-κB activity underlies the pro- and anti-inflammatory actions of nitric oxide." *J. Immunol.* **2001,** *166*, 3873-3881.

Chapter 4:

Bactericidal Efficacy of Nitric Oxide-Releasing Silica Nanoparticles

4.1 Introduction

Antibiotic resistance has resulted in bacterial infections becoming the most common cause of infectious disease-related death.[1, 2] In the United States alone, nearly 2 million people per year acquire infections during a hospital stay, of which approximately 90,000 die.[2] The primary culprits behind such deadly infections are antibiotic-resistant pathogens, which are responsible for approximately 70% of all lethal nosocomial infections. The growing danger of life-threatening infections and the rising economic burden of resistant bacteria have created a demand for new antibacterial therapeutics.

The use of nanoparticles as delivery vehicles for bactericidal agents represents a new paradigm in the design of antibacterial therapeutics. To date, most antibacterial nanoparticles have been engineered using traditional antibiotics that are either incorporated within the particle scaffold or attached to the exterior of the particle. In many cases, such particles have exhibited greater efficacy than their constituent antibiotics alone. For example, Gu et al. reported that vancomycin-capped gold nanoparticles exhibited a 64-fold improvement in efficacy over vancomycin alone.[3] Similarly, silver nanoparticles have shown greater antibacterial activity than silver ion (Ag^+) in solution due to the direct toxicity of the particles and tunable release of Ag^+ based on nanocomposite size.[4-6] Mesoporous silica has also been used to deliver antibacterial agents. For example, Lin and co-workers

employed mesoporous silica nanoparticles to controllably release ionic liquids with proven bactericidal efficacy.[7]

While antibacterial nanoparticles have shown great promise, the use of conventional antibiotics (e.g., vancomycin) or classical antibacterial agents (e.g., Ag^+) does not address bacterial resistance concerns.[2, 8, 9] Nitric oxide (NO), a diatomic free radical that plays a key role in the natural immune system response to infection,[10] may represent an alternative approach in the design of antibacterial nanoparticles. Macrophages and other inflammatory cells produce NO to battle infection[11] and mice lacking the ability to endogenously produce NO have been found to be more susceptible to microbial infection than mice with full NO-production capabilities.[12] Nitric oxide has been shown to possess broad spectrum antibacterial activity, primarily due to its reactive byproducts such as peroxynitrite ($ONOO^-$) and dinitrogen trioxide (N_2O_3).[13] Both gram-positive and gram-negative bacteria have been found to be susceptible to gaseous NO, including methicillin-resistant *Staphylococcus aureus* (MRSA).[14] The doses of NO required to kill bacteria proved non-toxic to human dermal fibroblasts. Using diazeniumdiolate small molecule NO donors, Raulli et al. reported the minimum inhibitory concentrations against several bacterial species.[15] These initial studies illustrate NO's tremendous potential as an antibacterial agent with broad spectrum activity.

Unfortunately, the utility of NO as an antibacterial agent is hindered by the lack of suitable vehicles for NO storage and delivery. Indeed, NO is an extremely reactive gas and difficult to administer as a therapeutic. To address delivery issues, Schoenfisch and coworkers have synthesized nanoparticle-based scaffolds capable of storing large payloads of NO.[16-18] The nanoparticles spontaneously release tunable levels of NO under aqueous conditions at physiological temperature and pH, and thus represent attractive vehicles for delivering NO. Nanoparticle delivery of NO has two main advantages over previously-

developed small molecule NO donor systems (e.g., diazeniumdiolates, nitrosothiols, and metal-NO complexes[19, 20]). First, the rate of NO release is easily modulated as a function of nanoparticle size, composition, and/or surface hydrophobicity, thereby allowing for control over the duration of NO release. Second, the versatility of the chemistry used to synthesize the nanoparticles allows for specific tailoring of particles with functional groups to minimize their toxicity and enable imaging and/or cell-specific targeting, while retaining the ability to deliver therapeutic levels of NO. Herein, we report the efficacy of NO-releasing silica nanoparticles against *Pseudomonas aeruginosa*, an opportunistic pathogen problematic in burn and chronic wound infections.[21-23] Both the bactericidal efficacy and cytotoxicity of nanoparticle-derived NO is compared to NO release from a small molecule NO donor to illustrate the advantage of delivering NO from silica nanoparticles.

4.2 Methods and materials

Tetraethoxysilane (TEOS) and sodium methoxide ($NaOCH_3$) were purchased from Fluka (Buchs, Switzerland). *N*-(6-Aminohexyl)aminopropyltrimethoxysilane (AHAP3) and 3-aminopropyltrimethoxysilane (APTMS) were purchased from Gelest (Tullytown, PA). Methanol (MeOH), ethanol (EtOH), and ammonia solution (NH_4OH, 30 wt% in water) were purchased from Fisher Scientific (Fair Lawn, NJ). Tryptic soy broth (TSB, soybean-casein digest) was purchased from Becton, Dickinson and Company (Sparks, MD). Nitric oxide (NO, 99.5%) was obtained from Linde (Raleigh, NC), and argon (Ar) and nitrogen (N_2) gases were purchased from National Welders (Raleigh, NC). *P. aeruginosa* (ATCC #19143) and L929 mouse fibroblast cells were purchased from American Type Culture Collection (Manassas, VA). 4,5-Diaminofluorescein diacetate (DAF-2 DA) was purchased from Calbiochem (San Diego, CA). Fluorescein isothiocyanate (FITC), proline and reagents for

the propidium iodide and lactate dehydrogenase cytotoxicity assays were purchased from Sigma (St. Louis, MO). Other solvents and chemicals were analytical-reagent grade and used as received. A Millipore Milli-Q UV Gradient A-10 System (Bedford, MA) was used to purify distilled water to a final resistivity of 18.2 MΩ·cm and a total organic content of ≤6 ppb.

4.2.1 Synthesis of NO-releasing silica nanoparticles. The synthesis and characterization of NO-releasing silica nanoparticles has been described previously.[18] Briefly, an aminoalkoxysilane solution was prepared by dissolving AHAP3 (2.3 mmol) in 20 mL of EtOH and 4 mL of MeOH in the presence of $NaOCH_3$ (2.3 mmol). The solution was then placed into 10 mL vials equipped with stir bars. The vials were placed in a Parr bottle, connected to an in-house NO reactor, and flushed with Ar six times to remove O_2 in the solution. The reaction bottle was pressurized to 5 atm NO for 3 d with continuous stirring of the silane solution. Prior to removing the diazeniumdiolate-modified AHAP3 silane sample (AHAP3/NO), unreacted NO was purged from the chamber with Ar. Silane solutions were prepared by mixing TEOS (2.8 mmol) and AHAP3/NO (2.3 mmol; corresponding to 45 mol%, balance TEOS) in the EtOH/MeOH solution for 2 min (Scheme 4.1). The silane solution was then added into 22 mL of EtOH and 6 mL ammonia catalyst (30 wt% in water), and mixed vigorously for 30 min at 4 ºC. The precipitated nanoparticles were collected by centrifugation (5000 rpm, 5 min), washed with EtOH several times, dried under ambient conditions for 1 h, and stored in a sealed container at -20 ºC until used. Diazeniumdiolate incorporation into the nanoparticle scaffold was confirmed by UV absorbance spectroscopy. The UV absorbance spectra of nanoparticles (both NO-releasing and controls depleted of diazeniumdiolates) suspended in phosphate buffered saline (PBS) at 160 $\mu g \cdot mL^{-1}$ were recorded on a Perkin-Elmer Lambda 40 UV/Vis Spectrometer.

Scheme 4.1. Synthesis of AHAP3 NO donor and co-condensation with TEOS to form NO-releasing silica nanoparticles. R = $-(CH_2)_3Si\equiv$ and R' = $H_2N(CH_2)_6-$.

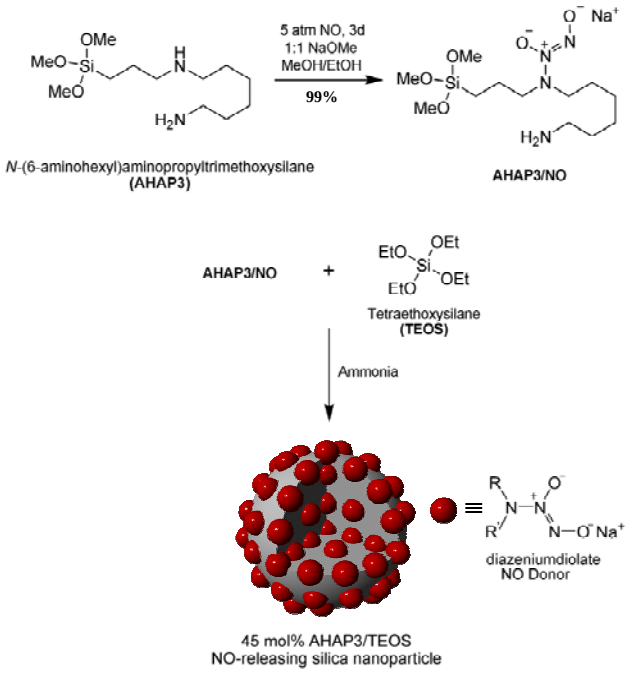

4.2.2 Characterization of diazeniumdiolate-modified silane (AHAP3/NO). ^{1}H NMR (CD_3OD, δ): 0.61 (br, $SiCH_2$), 1.32 (qt, $NRCH_2CH_2CH_2CH_2CH_2CH_2NH_2$), 1.43 (m, $SiCH_2CH_2CH_2$, $NRCH_2CH_2$), 1.56 (m, $CH_2CH_2CH_2NH_2$), 2.56 (m, $CH_2CH_2NH_2$), 2.84 (br,CH_2NRCH_2), 4.88 (s, $Si(OCH_3)_3$) where R = $NONO^-Na^+$. UV-Vis (EtOH): λ_{max} = 253 nm. ^{29}Si nuclear magnetic resonance (NMR) spectroscopy was also employed to characterize AHAP3/NO. Cross-polarization/magic angle spinning (CP/MAS) ^{29}Si NMR spectra of the AHAP3/NO were obtained at 20 ºC on a Bruker 360 MHz DMX spectrometer (Billerica, MA) equipped with wide-bore magnets (triple-axis pulsed field gradient double-resonance probes). The alcoholic solution of diazeniumdiolate-modified silane (i.e., AHAP3/NO) was loaded into 4 mm rotors (double-resonance frequency of 71.548 MHz) and spun at a speed of 8.0 kHz. The chemical shifts were determined in ppm relative to a TMS external standard.

4.2.3 Synthesis of fluorescently-labeled NO-releasing silica nanoparticles. The synthesis of fluorescently-labeled NO-releasing silica nanoparticles was adapted from a previously reported literature procedure.[24] Briefly, FITC (10 μmol) was reacted with neat APTMS (200 μmol) overnight in the dark to yield the FITC-modified silane. ^{1}H NMR (CD_3OD, δ): 0.32 (br, $SiCH_2$), 1.52 (qt, $SiCH_2CH_2CH_2NH$-FITC), 2.73 (t, $SiCH_2CH_2CH_2NH$-FITC), 3.69 (m, $SiCH_2CH_2CH_2NH$-FITC), 4.81 (s, $Si(OCH_3)_3$), 6.46 (m, aromatic), 7.01 (m, aromatic) 7.11 (d, aromatic) 7.45 (d, aromatic) 7.57 (d, aromatic). UV-Vis (EtOH): λ_{max} = 493 nm.

Next, 100 μL of the FITC-modified silane solution was co-condensed with AHAP3/NO (2.3 mmol) and TEOS (2.8 mmol) in the EtOH/ammonia solution as described above to yield FITC-labeled NO-releasing silica nanoparticles (Scheme 4.2). Incorporation

Scheme 4.2. Synthesis of FITC-modified NO-releasing 45 mol% AHAP3 silica nanoparticles (balance TEOS). Abbreviations: AHAP3 = *N*-(6-aminohexyl)aminopropyltrimethoxysilane; APTMS = 3-aminopropyltrimethoxysilane; FITC = fluorescein isothiocyanate; TEOS = tetraethoxysilane.

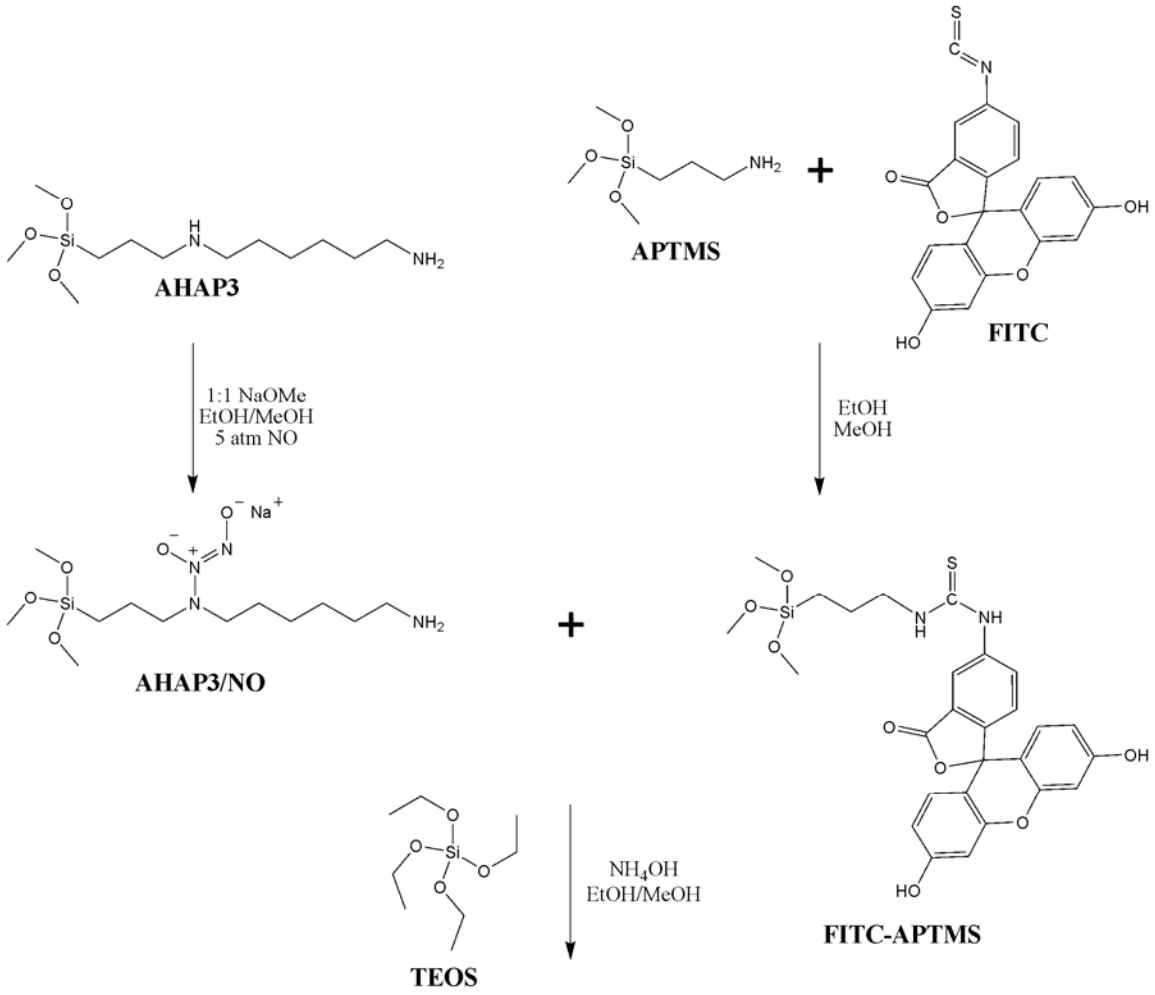

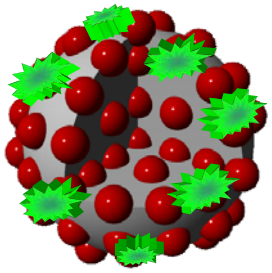

of FITC was confirmed by exciting the particles at 488 nm and observing the characteristic fluorescence due to FITC at 500 – 530 nm.

4.2.4 Size characterization of silica nanoparticles. The size of control, NO-releasing, and FITC-modified silica nanoparticles was characterized via atomic force microscopy (AFM). Prior to analysis, the particles were suspended in toluene, deposited on a freshly cleaved mica surface (SPI; West Chester, PA), and dried under ambient conditions for 3 h. Contact mode AFM images were obtained in air using a Molecular Force Probe 3D AFM (Asylum Research; Santa Barbara, CA) controlled with MFP-3D software running under Igor Pro (Wavemetrics; Lake Oswego, OR). Triangular silicon nitride cantilevers with a nominal spring constant of 0.12 $N \cdot m^{-1}$ and resonance frequency of 20 kHz (Veeco; Santa Barbara, CA) were used to acquire height/topography images at a scan rate of 1.0 Hz.

4.2.5 Synthesis of 1-[2-(carboxylato)pyrrolidin-1-yl]diazen-1-ium-1,2-diolate (PROLI/NO) (adapted from a previously reported procedure[25]). Proline (300 mg, 2.6 mmol) was dissolved in a 50:50 mixture of methanol:ether and treated with 281 mg (5.2 mmol) of $NaOCH_3$. The basic solution was placed in a glass hydrogenation bomb and stirred. The bomb was copiously flushed with Ar to remove atmospheric O_2, followed by introduction of NO gas at 5 atm. After 3 d, the glass vial was removed from the vessel after thorough flushing with Ar. The solution was treated with cold ether to precipitate the product (PROLI/NO). The NO donor precipitate was then filtered, and dried under vacuum at -70 ºC (dry ice/acetone bath) to yield 299 mg PROLI/NO.

4.2.6 Nitric oxide release measurements. Nitric oxide release from both the diazeniumdiolate-modified silica nanoparticles and PROLI/NO was measured in deoxygenated phosphate-buffered saline (PBS, 0.01 M; 37 ºC) at pH 7.4 using a Sievers NOA 280i chemiluminescence NO analyzer (Boulder, CO). Nitric oxide released from the

donors was transported to the analyzer by a stream of N_2 (70 mL·min^{-1}) passed through the reaction cell. The instrument was calibrated with air passed through a NO zero filter (0 ppm NO) and a 24.1 ppm NO standard gas (balance N_2).

4.2.7 Bactericidal assays under static conditions. To test the bactericidal properties of PROLI/NO and NO-releasing 45 mol% AHAP3/TEOS silica nanoparticles under non-growth ("static") conditions, *P. aeruginosa* was cultured to a concentration of 10^8 colony-forming-units (CFUs) per mL in tryptic soy broth (TSB), resuspended in sterile PBS, and adjusted to a concentration of 10^3 CFU·mL^{-1}. Silica nanoparticles (NO-releasing and control), PROLI/NO, and proline were added to separate aliquots of the bacterial suspension over a concentration range optimized for each system. After 1 h incubation at 37 ºC with gentle agitation, 100-µL aliquots from each suspension were plated on tryptic soy agar. After overnight incubation at 37 ºC, the colonies on each plate were counted, allowing for calculation of the number of viable *P. aeruginosa* cells in each vial at the time of plating.

4.2.8 Time-based bactericidal assays under nutrient growth conditions. To test the temporal efficacy of the NO-releasing silica nanoparticles, time-based antibacterial assays were conducted in TSB nutrient media. *P. aeruginosa* was cultured in TSB to a concentration of 10^8 CFU·mL^{-1} and diluted to 10^4 CFU·mL^{-1} in additional TSB. Silica nanoparticles (control and NO-releasing), PROLI/NO, and proline were added to separate aliquots of the 10^4 bacterial suspension over concentration ranges optimized for each system. Every 30 min for 2 h, 100-µL aliquots of each suspension were removed, diluted 10-fold in PBS, and plated on tryptic soy agar. Bacterial viability was determined as described above after incubating the plates overnight at 37 ºC.

4.2.9 Interaction between nanoparticles and bacterial cells. *P. aeruginosa* was cultured in TSB to 10^8 CFU·mL^{-1}, pelleted by centrifugation, resuspended in PBS, and

adjusted to a concentration of 10^6 CFU·mL^{-1} in PBS. The bacterial suspension was seeded onto a glass microscope slide where the bacteria were allowed to adhere to the slide for 30 min. The microscope slide was placed on the stage of a Zeiss LSM 510 confocal fluorescence microscope (Chester, VA) and bright-field and fluorescence images of the bacteria were acquired with a 63x N.A. 1.4 planapochromat oil immersion lens. Next, an aliquot of FITC-modified NO-releasing silica nanoparticles (final concentration = 100 μg·mL^{-1}) was added and bright-field and fluorescence images of the same field were captured after 0, 10, 20, 30, and 60 min. The FITC fluorophores were excited with the 488 nm line of an Ar laser and the fluorescence was collected using a BP 500-530 nm bandpass filter.

4.2.10 Confocal fluorescence microscopy for detection of intracellular NO and cell killing. Confocal microscopy experiments were conducted to simultaneously monitor intracellular concentrations of NO within *P. aeruginosa* cells and the kinetics of cell killing using 4,5-diaminofluorescein diacetate (DAF-2 DA, a NO-sensitive fluorescence probe), and propidium iodide (PI, a fluorescence viability dye that enters only cells with compromised membranes and emits bright red fluorescence after binding to DNA[26]). An aliquot of *P. aeruginosa*, cultured as described above, was resuspended at 10^6 CFU·mL^{-1} in PBS supplemented with DAF-2 DA (10 μM) and incubated at 37 °C for 30 min. 500 μL of the cells loaded with DAF-2 were transferred onto a glass microscope slide affixed in a circular microscope cell to allow capture of initial images. 500 μL of PBS containing 10 μM DAF-2 DA, 60 μM PI and either NO-releasing silica nanoparticles (200 μg·mL^{-1}) or PROLI/NO (388 μg·mL^{-1}) was then introduced. Images were immediately collected with a 63x objective every minute for 2.5 h. The fluorescent reaction product of NO and DAF-2 (excitation λ_{max} = 495 nm, emission λ_{max} = 515 nm)[27] was excited with the 488 line of an argon laser. Fluorescence was collected using a BP 500-530 nm bandpass filter. PI fluorescence was

excited with the 543 nm line of a HeNe laser and collected with a long-pass (LP 560) filter. All confocal microscopy experiments were performed at 25 °C. At 25 °C, the half life of NO release from 45 mol% AHAP3 silica nanoparticles increased to >1 h. Thus, the initial level of NO release was reduced, extending the duration of NO release.

4.2.11 Propidium iodide cytotoxicity assay. L929 mouse fibroblasts were plated on 24-well tissue culture treated dishes (BD Bioscience #353047) at a density of 3.0 x 10^5 cells·mL^{-1} (150 x 10^3 cells per well) and incubated overnight at 37 ºC in 5% CO_2/95% air. For the PI assay, the incubation buffer (Minimum Essential Medium) was aspirated from each of the wells and replaced with 500 μL of Krebs-Ringer-HEPES (KRH) buffer containing 115 mM NaCl, 5 mM KCl, 1 mM $CaCl_2$, 1 mM KH_2PO_4, 1.2 mM $MgSO_4$, 25 mM HEPES, pH 7.4, supplemented with 30 μM PI.[28] Control or NO-releasing silica nanoparticles were added to the wells at 0, 50, 200, 400, 600, 800, or 1000 μg·mL^{-1}, or PROLI/NO was added at 0, 4, 8, or 12 mg·mL^{-1}. The fluorescence resulting from PI complexation with intracellular nucleic acid material[26] in cells with compromised membranes was acquired for a total of 120 min. Upon completion of these measurements, the cells were incubated with digitonin (40 μM) for 20 min to completely permeabilize the plasma membranes and achieve a maximum PI fluorescence. Cell viability is presented as the increase in PI fluorescence from each well expressed as the percentage of maximal fluorescence obtained from cells treated with digitonin (100% cell death).

4.2.12 Lactate dehydrogenase cytotoxicity assay. The lactate dehydrogenase (LDH) cytotoxicity assay was performed concomitantly with the same cells used for the PI assay described above. Every 15 min, 20-μL aliquots of KRH buffer were removed from the plate used for the PI assay and stored at -20 ºC in black 96-well plates (Greiner; Monroe, NC) for subsequent LDH analysis. The 96-well plates containing aliquots of incubation buffer were

warmed to 37 ºC. Lactate dehydrogenase activity was measured from the rate of NADH production after adding 180 μL of KRH buffer containing 0.22 mM NAD^+, 11.1 mM sodium lactate and 11.1 mM hydrazine, pH 8.0 into each well.[29] The NADH fluorescence was monitored with a FluoStar Galaxy plate reader using 340 nm excitation and 460 nm emission filters. The LDH activity is expressed as the change in relative fluorescence per min per well. The data are normalized to maximal LDH activity in each well obtained from samples treated with 40 μM digitonin for 20 min.

4.2.13 Statistics. For the bactericidal assays conducted in PBS, n = 3 and data are expressed as mean values ± standard deviation. Data from both the PI and LDH cytotoxicity assays are presented as mean values ± standard error of the mean.

4.3 Results and discussion

4.3.1 Characterization of NO-releasing silica nanoparticles and PROLI/NO. Shin et al. previously reported the synthesis and characterization of NO-releasing silica nanoparticles.[30] Briefly, diazeniumdiolate NO donors were synthesized on aminoalkoxysilane precursors prior to nanoparticle construction (Scheme 4.1), enabling the formation of particles with superior NO release ability. By synthesizing diazeniumdiolate-modified aminoalkoxysilanes prior to nanoparticle synthesis, particle aggregation was reduced due to decreased hydrogen bonding interactions between amines. The synthesis resulted in ~99% amine-to-diazeniumdiolate conversion efficiency and greater yields of NO per mol of aminoalkoxysilane precursor compared to previous synthetic procedures used to generate NO-releasing silica nanoparticles.[18] ^{29}Si NMR spectroscopy of the AHAP3/NO product was used to determine whether the presence of sodium methoxide would lead to self-condensation of the AHAP3/NO precursors during the diazeniumdiolate formation step (Step

1 of Scheme 4.1). Notably, no significant T^n peaks characteristic of organosilane polymerization were observed,[18] indicating that the AHAP3/NO molecules did not pre-condense under such reaction conditions. ^{1}H NMR of AHAP3/NO revealed that the protons adjacent to the secondary amine where diazeniumdiolate formation occurs became deshielded in the presence of the zwitterionic NO donor, shifting downfield from 2.45 ppm to 2.84 ppm. The presence of the diazeniumdiolate on AHAP3/NO was also confirmed via UV-Vis spectroscopy (λ_{max} = 253 nm, characteristic of the diazeniumdiolate absorption maximum[17, 31]) and direct observation of the released NO via chemiluminescence.[32]

The presence of the diazeniumdiolate functional group in the nanoparticle scaffold was confirmed via UV absorbance spectroscopy and the direct measurement of NO release. As shown in Figure 4.1, diazeniumdiolate-modified 45 mol% AHAP3/TEOS silica nanoparticles (Nanoparticle/NO) exhibited a similar λ_{max} of 257 nm. Nitric oxide release due to diazeniumdiolate decomposition[33] was monitored in phosphate buffered saline (PBS; 10 mM, pH 7.4) at 37 °C using a chemiluminescence NO analyzer.[32] As shown in Figure 4.2 A, the total amount of NO released (t[NO]) and maximum NO flux ($[NO]_m$) from the AHAP3 nanoparticle system were ~3.8 μmol·mg^{-1} and ~21700 ppb·mg^{-1}, respectively. The NO release kinetics from the AHAP3 silica nanoparticles were relatively rapid compared to other NO-releasing silica nanoparticle systems,[18] with a NO release half life ($t_{1/2}$) of 18 min. As a result of the rapid NO release from the 45 mol% AHAP3 nanoparticles, the time required to reach the maximum NO flux (t_m) of ~21700 ppb·mg^{-1} was only 8 min after immersion in buffer solution. The initial burst of NO allows for the relatively rapid delivery of micromolar quantities of NO that produce the reactive nitrogen and oxygen species that mediate NO's

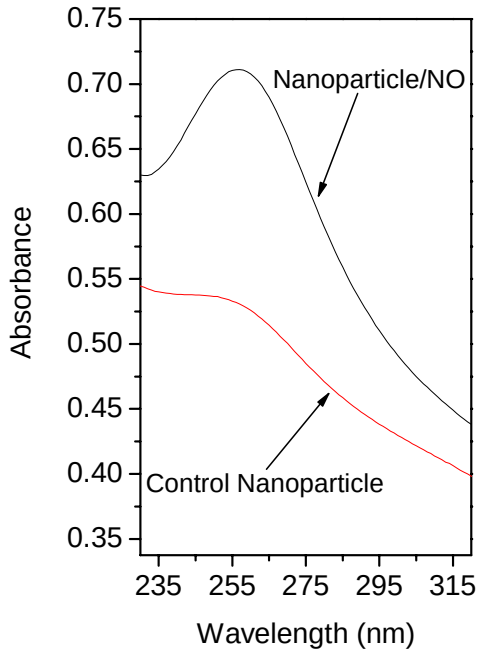

Figure 4.1. UV absorbance of control and diazeniumdiolate-modified (Nanoparticle/NO) 45 mol% AHAP3/TEOS silica nanoparticles (concentration = 160 $\mu g \cdot mL^{-1}$ in phosphate buffered saline).

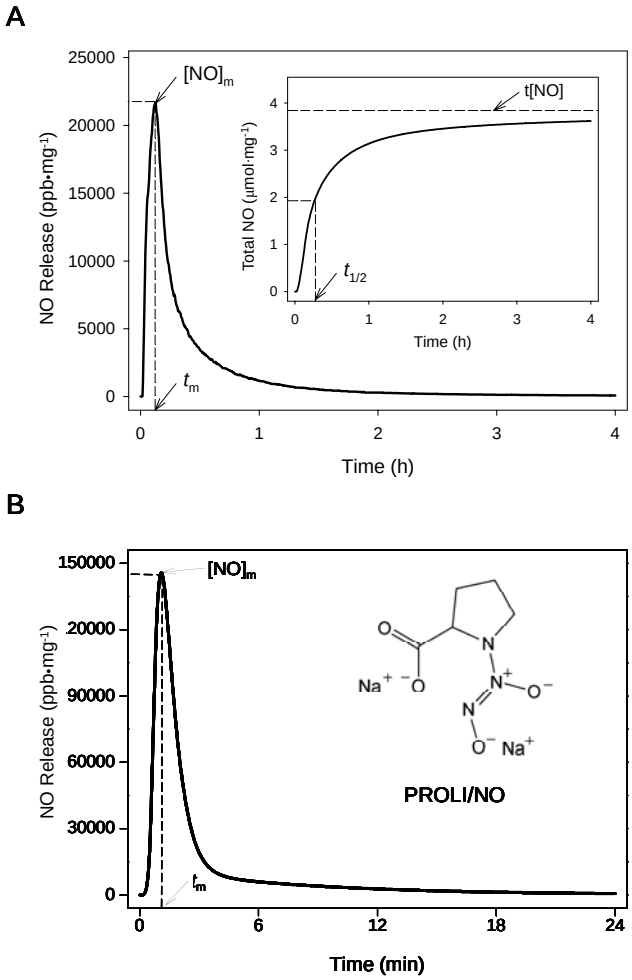

Figure 4.2. Nitric oxide release profiles of (A) 45 mol% AHAP3 silica nanoparticles and (B) PROLI/NO in PBS, pH 7.4, 37 °C. Inset of (A) represents total NO release. $[NO]_m$ = maximum NO flux; t_m = time to reach maximum NO flux; t[NO] = total NO released; $t_{1/2}$ = half life of NO release.

bactericidal actions.[34] As characterized by atomic force microscopy (AFM), the size and homogeneity of the 45 mol% AHAP3 nanoparticles were 136 ± 15 nm (Fig. 4.3). Both the size and NO-release properties of diazeniumdiolate-modified silica nanoparticles proved tunable based on the amount and identity of aminoalkoxysilane precursor employed in the synthesis (data not shown). A full systematic characterization of such properties as a function of NO donor is reported elsewhere.[30]

To facilitate comparison of the bactericidal efficacy of nanoparticle-derived NO with small molecule-derived NO, the amino acid proline was functionalized with diazeniumdiolate NO-donors as described by Saavedra et al.[25] As shown in Figure 4.2 B, the release of NO from PROLI/NO was also extremely rapid, with a $t_{1/2}$ of approximately 1.7 min. On a per mg basis, PROLI/NO released less than half as much total NO as the AHAP3 nanoparticles, with a t[NO] value of 1.8 μmol NO·mg^{-1}. Due to its rapid NO release characteristics, however, the $[NO]_m$ for PROLI/NO (>145000 ppb·mg^{-1}) was more than 6 times greater than the $[NO]_m$ generated by the nanoparticles per mg, with t_m approximately 1 min after addition to buffer. Despite the large bolus of NO released by PROLI/NO, the extended duration of NO release from the AHAP3/TEOS nanoparticle system is more beneficial for antibacterial applications because its NO release capabilities are not immediately lost upon exposure to aqueous conditions. Indeed, effective NO-based antibacterial agents require NO release durations long enough to allow the NO donor vehicle to reach the intended site of action without becoming depleted of NO during transit, while still releasing bactericidal quantities of NO.

4.3.2 Bactericidal efficacy under static conditions. The bactericidal efficacy of the 45 mol% AHAP3 NO-releasing silica nanoparticles was evaluated against *P. aeruginosa*, an opportunistic gram-negative pathogen. Due to a multitude of virulence factors, *P.*

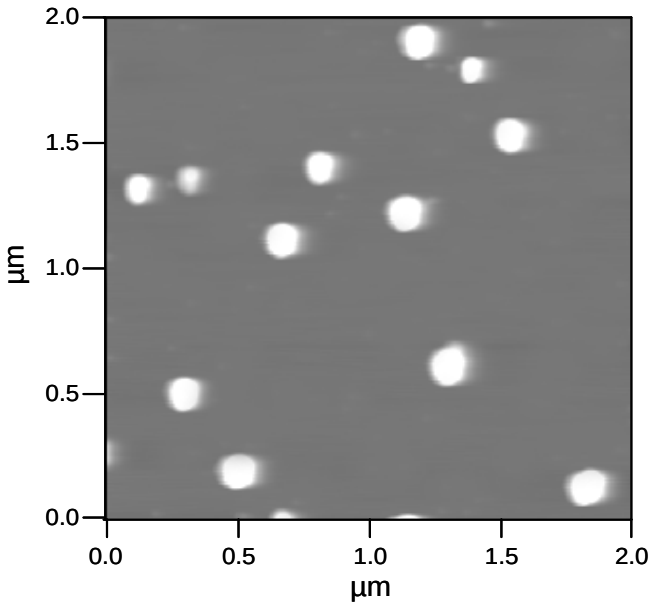

Figure 4.3. AC mode AFM height image of 45 mol% AHAP3 silica nanoparticles (balance TEOS) on a mica surface.

aeruginosa is a common cause of burn wound infections leading to significant morbidity and mortality in burn wound victims.[21,22] Additionally, *P. aeruginosa* plagues >30% of all leg and foot ulcers resulting in chronic wounds with impaired healing.[23] Perhaps most alarming, however, is the emergence of multidrug-resistant *P. aeruginosa* that has been isolated from nosocomial burn wound patients.[22, 35] *P. aeruginosa* clones resistant to both β-lactams and aminoglycosides, two classes of antibiotics that are commonly used to treat *P. aeruginosa* infections are documented.[35] Thus, novel treatments for combating infections resulting from antibiotic-resistant pathogens are urgently needed. We hypothesized that the AHAP3/TEOS silica nanoparticle system, capable of storing multiple NO donors within each delivery vehicle, may represent an attractive new method for killing pathogenic bacteria due to its ability to release high localized doses of NO. To determine the influence of the nanodelivery vehicle on the antibacterial properties of NO, the bactericidal efficacy of 45 mol% AHAP3 nanoparticles was compared to that of PROLI/NO. Although a previous study evaluated the antibacterial properties of the small molecule NO-donor DETA/NO (diazeniumdiolate-modified diethylenetriamine),[15] we observed that the diethylenetriamine backbone alone demonstrated considerable toxicity to *P. aeruginosa* (data not shown), which is consistent with the observations of others.[36] Conversely, the backbone of PROLI/NO (the amino acid proline) exhibited no toxicity to *P. aeruginosa* up to 20 $mg \cdot mL^{-1}$, the highest concentrations tested.

To facilitate direct comparison of the amount of NO necessary to kill *P. aeruginosa*, initial studies were conducted in PBS. The bacterial killing assays conducted in aqueous buffer demonstrate the bactericidal activity of NO under nutrient-free ("static") conditions in which the bacteria were unable to replicate. In this manner, the data collected were not convoluted by the ability of the bacterial culture to proliferate in the medium during the

experiment. Bacterial killing assays were performed instead of the more conventional minimum inhibitory concentration (MIC) assays in order to assess the extent to which NO actually kills *P. aeruginosa* as opposed to simply inhibiting its growth. An understanding of these parameters is important because it has been suggested that bactericidal agents are less likely to foster resistance among pathogens than those that are simply bacteriostatic.[37] As shown in Figure 4.4, the concentrations of PROLI/NO and NO-releasing nanoparticles that proved completely bactericidal (3 logs of killing) to *P. aeruginosa* were 2.5 $mg \cdot mL^{-1}$ and 70 $\mu g \cdot mL^{-1}$, respectively. Thus, by mass, approximately 35 times more PROLI/NO was required than silica nanoparticles to completely kill all *P. aeruginosa* cells in the bacterial suspension. Both the proline and 45 mol% AHAP3 silica controls depleted of NO exhibited no killing of *P. aeruginosa* over the concentration ranges tested, indicating that the toxicity observed from the NO-releasing analogues was due entirely to NO. Real-time chemiluminescent detection of NO released from the two NO-donor systems (Fig. 4.2) allowed for a direct comparison of the amount of NO released into solution over the 1 h time course of the bactericidal assays. Of note, the amount of NO required per mL to elicit a 3 log reduction in bacterial viability was markedly less from the nanoparticle scaffold than from PROLI/NO (0.22 versus 4.5 μmol NO from nanoparticles and PROLI/NO, respectively). The amount of NO delivered is expressed as total μmol NO released instead of a concentration (e.g., mM) because the NO quickly reacts to form other reactive nitrogen and oxygen species. As such, the exact molar concentration of NO and the byproducts in solution are not known.

4.3.3 Time-based bactericidal assays under nutrient growth conditions. While the PBS-based bactericidal assays allow an uncomplicated comparison of the dose of NO from both systems required to kill *P. aeruginosa*, they do not demonstrate the temporal efficacy of

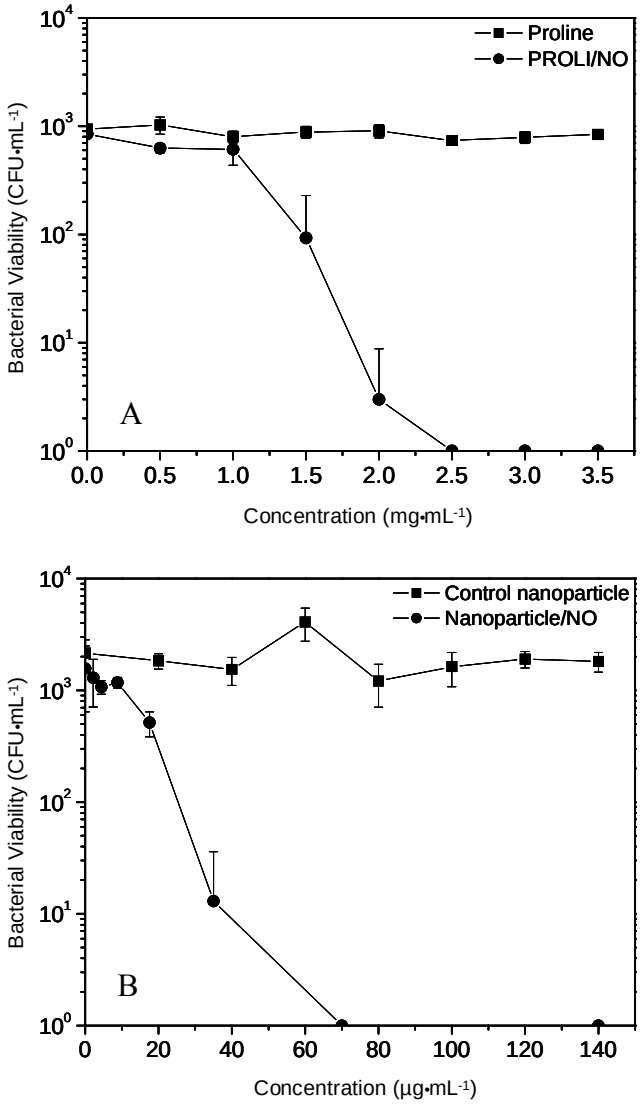

Figure 4.4. Bactericidal efficacy of (A) praline and PROLI/NO and (B) control and NO-releasing 45 mol% AHAP3 silica nanoparticles (balance TEOS) against *P. aeruginosa* in phosphate buffered saline.

each system, or accurately mimic a situation where the bacteria have the ability to replicate. To better understand such parameters, time-based killing assays were performed in tryptic soy broth (TSB) to test the bactericidal efficacy of NO-releasing silica nanoparticles in a culture medium where the bacteria had the capacity to proliferate and present a competition between the rate of bacterial cell killing and replication. Such time-kill studies offer valuable information regarding the temporal efficacy of antimicrobial agents.[38] Conventional antibacterial susceptibility tests such as the MIC and minimum bactericidal concentration (MBC) assays do not allow for acute temporal studies. In the TSB nutrient medium, *P. aeruginosa* exposed to blank and control (proline and silica) solutions proliferated over the 2 h experiment (Fig. 4.5). As expected, the concentration of both NO-releasing silica nanoparticles and PROLI/NO necessary to completely kill *P. aeruginosa* in TSB was greater than the dose necessary to achieve the same result in PBS. This increase is attributed to both the ability of *P. aeruginosa* to proliferate in TSB and the NO scavenging properties of the protein digest that comprises TSB. Indeed, chemiluminescent NO release measurements performed in TSB revealed that a significant amount of NO was scavenged by the TSB media itself (Fig. 4.6), effectively lowering the amount of NO able to act on the *P. aeruginosa* cells.

Despite the scavenging of NO and bacterial proliferation in TSB, complete bacterial killing was still achieved, albeit at higher concentrations of both nanoparticles and PROLI/NO. Similar to the experiments performed in PBS, the amount (by mass) of PROLI/NO necessary to kill all *P. aeruginosa* was greater than that of NO-releasing nanoparticles. Figure 4.5 illustrates the dose- and time-dependent bactericidal activity of both PROLI/NO and NO-releasing silica nanoparticles. At a nanoparticle concentration of 400 $\mu g \cdot mL^{-1}$, ~90% bactericidal efficacy was achieved after 2 h (one log reduction in viable

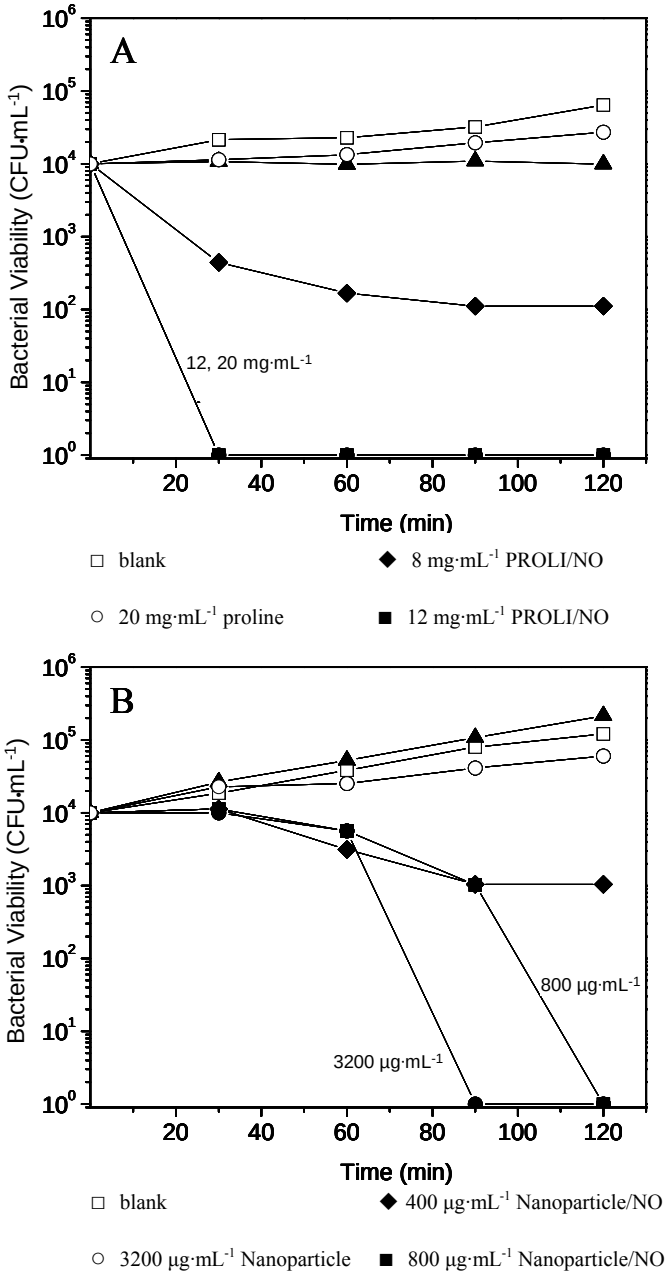

Figure 4.5. Time- and concentration-based bactericidal efficacy of (A) proline (control) and PROLI/NO and (B) control (Nanoparticle) and NO-releasing 45 mol% AHAP3 silica nanoparticles (Nanoparticle/NO).

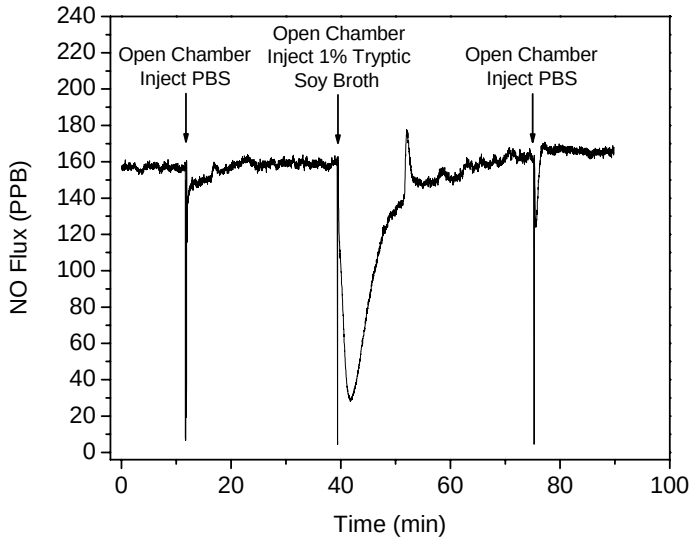

Figure 4.6. Real-time NO release of the small molecule diazeniumdiolate NO-donor DETA/NO before, during, and after injection of 1% tryptic soy broth (TSB), as measured using a chemiluminescent nitric oxide analyzer.

P. aeruginosa; Fig. 4.5 B). Doubling the particle concentration to 800 μg·mL^{-1} resulted in 100% bacterial killing over the same period (4 log reduction in viable *P. aeruginosa*). Complete bactericidal activity was achieved in a shorter period (90 min) using significantly greater concentrations of silica nanoparticles (3200 μg·mL^{-1}). However, particle concentrations >3200 μg·mL^{-1} did not reduce the time necessary for 100% bacterial killing below 90 min (data not shown). In contrast, PROLI/NO achieved more rapid bacterial killing than the 45 mol% AHAP3 nanoparticles, but at significantly greater concentrations. For example, a concentration of 12 mg·mL^{-1} PROLI/NO resulted in complete killing after only 30 min. The difference in the rate of bacterial killing is attributed to the NO-release kinetics of each NO donor. The NO release from PROLI/NO is rapid with a half life ($t_{1/2}$) of 1.7 min, resulting in rapid (≤30 min) bacterial killing at 12 and 20 mg·mL^{-1}. In contrast, the NO release kinetics from 45 mol% AHAP3 silica nanoparticles, which were unchanged in the presence of TSB, are significantly longer ($t_{1/2}$ = 18 min), thereby requiring longer incubation periods at 800 and 3200 μg·mL^{-1} to achieve complete bactericidal activity. Analogous to the results obtained in PBS, complete bacterial killing required a markedly greater amount of NO per mL from PROLI/NO (21.6 μmol) than from the NO-releasing silica nanoparticles (2.8 μmol).

A direct comparison of the amount of NO required from each vehicle to achieve 100% bactericidal efficacy in both PBS and TSB is shown in Figure 4.7. Greater amounts of NO were necessary in TSB to achieve complete bactericidal activity than from the same vehicles in PBS due to both the ability of *P. aeruginosa* to proliferate in TSB and the NO-scavenging properties of TSB as noted above. Regardless of the media, NO delivered from the nanoparticles exhibited significantly greater bactericidal efficacy than NO delivered from the small molecule diazeniumdiolate (i.e., PROLI/NO). Indeed, the amount of NO required

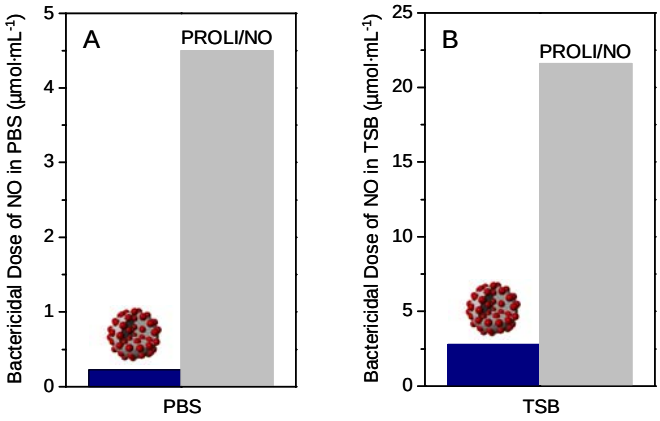

Figure 4.7. Comparison of the NO doses necessary from silica nanoparticles (dark blue) and PROLI/NO (grey) to achieve 100% bactericidal efficacy against *P. aeruginosa* in (A) PBS and (B) TSB.

from PROLI/NO to completely kill *P. aeruginosa* was approximately one order of magnitude greater than that required from the 45 mol% AHAP3 nanoparticles. Since the reactivity of NO is largely dependent on its localized concentration and diffusion properties,[39] NO derived from a small molecule dispersed throughout solution is expected to possess slower diffusion into bacterial cells and correspondingly lessened antibacterial activity compared to the high localized concentrations of NO delivered by silica nanoparticles.

4.3.4 Confocal microscopy studies. To understand the enhanced bactericidal efficacy of NO delivered from nanoparticles compared to PROLI/NO, fluorescein isothiocyanate (FITC)-modified silica nanoparticles were synthesized to visually determine if any nanoparticle interaction with *P. aeruginosa* cells existed. After synthesis of the nanoparticles, characteristic FITC fluorescence was observed at 500 – 530 nm when the particles were excited at 488 nm. Incorporation of FITC into the silica nanoparticle scaffold did not significantly alter the NO-release properties of the nanoparticles (data not shown) or the particle diameter (124 ± 13 nm vs. 136 ± 15 nm with and without FITC, respectively). Using the FITC-modified silica nanoparticles, confocal fluorescence microscopy studies were conducted to determine if the enhanced bactericidal efficacy of the nanoparticles was due to nanoparticle interaction with *P. aeruginosa* cells. As shown in Figure 4.8, nanoparticles began to associate with the *P. aeruginosa* cells as early as 10 min post-injection. The possible mechanism by which this association occurs is not entirely understood, but most likely is attributed to electrostatic[40] and/or hydrophobic[41] interactions between the particles and bacterial membrane.

A NO-sensitive fluorescence probe, 4,5-diaminofluorescein diacetate (DAF-2 DA),[27] was employed to determine if the association between NO-releasing silica nanoparticles and *P. aeruginosa* cells resulted in high local concentrations of NO and more efficient delivery of

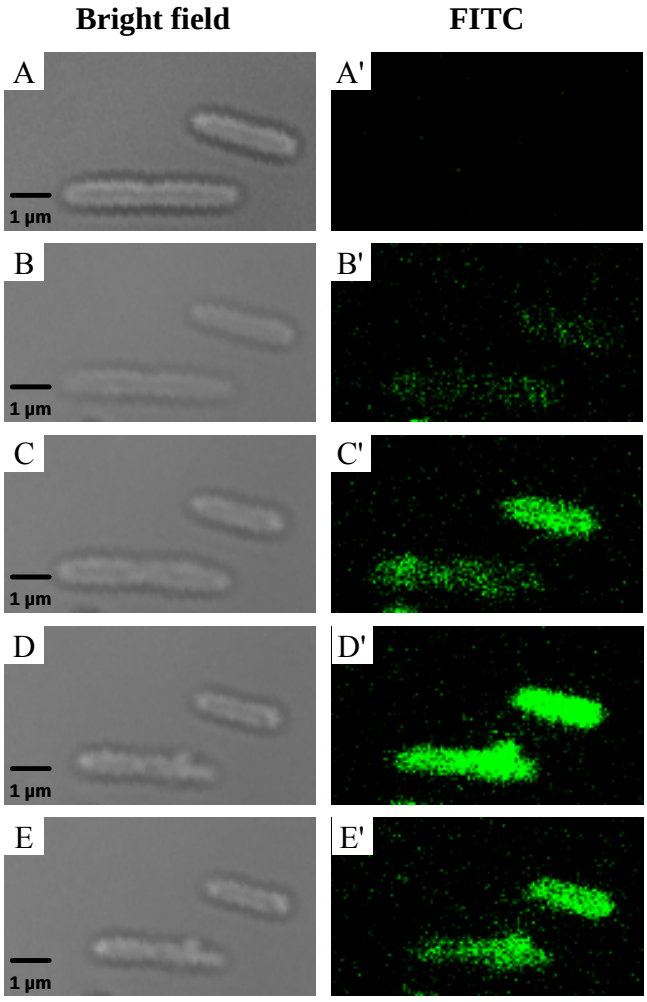

Figure 4.8. Scanning confocal microscopy images of FITC-modified NO-releasing silica nanoparticle association with *P. aeruginosa* cells. Images were acquired in bright-field mode (A-E) and on the FITC fluorescence channel (A′-E′) before injection (A, A′) of 100 µg·mL^{-1} NO-releasing FITC-modified AHAP3 silica nanoparticles, and 10 (B, B′), 20 (C, C′), 30 (D, D′) and 60 (E, E′) minutes post-injection.

NO to the bacterial cells. Once DAF-2 DA permeates the bacterial cell membrane, intracellular esterases hydrolyze the acetate groups to generate the membrane-impermeable DAF-2.[27] In the presence of NO, DAF-2 is nitrosated by reactive nitrogen species (e.g., N_2O_3) and exhibits bright green intracellular fluorescence.[27] Cells loaded with DAF-2 were imaged in the presence of propidium iodide (PI), a nucleic acid viability dye that only enters cells with compromised membranes. Inside the cell, PI exhibits strong red fluorescence upon interaction with nucleic acid material. Red fluorescence due to PI entering cells with disrupted plasma membranes thus indicates cell death.[26] Prior to introduction of NO-releasing silica nanoparticles, no autofluorescence was observed from either DAF-2 DA or DAF-2. However, *P. aeruginosa* cells loaded with DAF-2 exposed to 100 $\mu g \cdot mL^{-1}$ NO-releasing nanoparticles exhibited strong DAF-2 fluorescence (Fig. 4.9 B-E), indicative of a high localized concentration of NO in close proximity to the bacterial cells. As more NO was released from the nanoparticles, the DAF-2 green fluorescence in each cell increased progressively, indicating that the NO level inside each cell was increasing. After reaching a peak intracellular intensity of DAF-2 fluorescence, PI then rapidly entered the bacterial cells due to membrane disruption and cell death. The increase in PI fluorescence coincided with a decrease in DAF-2 fluorescence (Fig. 4.9 C-F), suggesting that the DAF-2 fluorophore leaked from the cytosol through the damaged cell membrane that allowed PI to enter the cells.

In contrast to the strong intracellular green fluorescence observed from DAF-2 in the presence of 100 $\mu g \cdot mL^{-1}$ NO-releasing silica nanoparticles, DAF-2 fluorescence was not observed when an equal amount of NO was delivered with PROLI/NO (data not shown). As indicated by the absence of any PI fluorescence from the bacterial cells over the same period, *P. aeruginosa* cell death was not observed with this dose of NO from PROLI/NO, thus

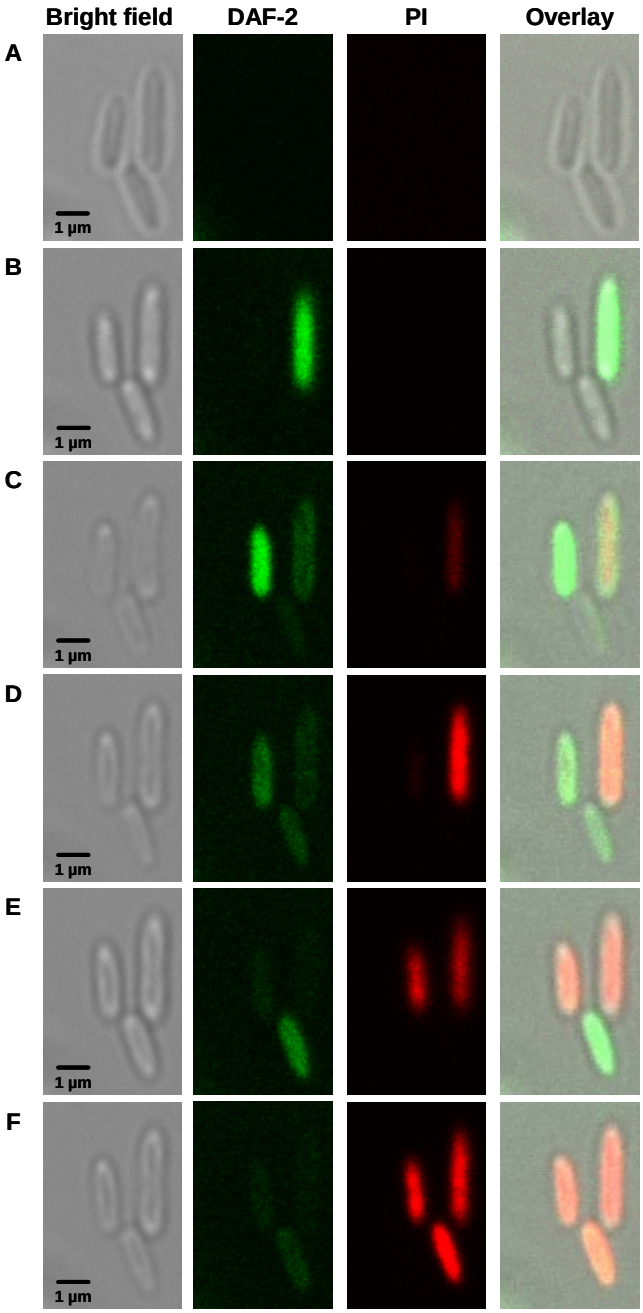

Figure 4.9. Intracellular DAF-2 (green) and propidium iodide (red) fluorescence from *P. aeruginosa* bacterial cells incubated with 100 µg·mL^{-1} 45 mol% AHAP3/TEOS NO-releasing silica nanoparticles. DAF-2 fluorescence indicates the presence of NO and reactive nitrogen species, while propidium iodide fluorescence indicates membrane destruction and cell death. Images were acquired (A) 30 min, (B) 83 min, (C) 113 min, (D) 124 min, (E) 132 min, and (F) 140 min after nanoparticle additio

reaffirming that doses of NO delivered from nanoparticle delivery vehicles were more efficient at killing *P. aeruginosa* cells compared to similar doses from small molecule NO donors. When the amount of PROLI/NO was increased to bactericidal levels (5 $mg \cdot mL^{-1}$), rapid cell death was observed as evidenced by bright red intracellular PI fluorescence in the confocal microscopy images (Fig. 4.10). However, intracellular DAF-2 fluorescence was still not observed prior to cell death (in contrast to the nanoparticles), indicating that the NO concentration surrounding the cells was not high enough to induce intracellular DAF-2 fluorescence. These data reveal that the delivery of NO to *P. aeruginosa* is significantly more efficient from silica nanoparticles than from PROLI/NO. As such, lower doses of NO delivered from silica nanoparticles effectively kill the bacteria.

As shown in Figure 4.11, the ability of the nanoparticles to deliver appreciable NO payloads in close proximity to the bacterial cells allows the NO to more efficiently target cellular components (e.g., cell membrane, DNA, proteins, etc.) critical to cell function, circumventing the need for NO to diffuse across large distances in solution to reach the cell. As a lipophilic molecule, NO is capable of rapidly crossing cell membranes.[13] The release of high levels of NO at or near the cell membrane would be expected to lead to high intracellular concentrations of NO. The antibacterial properties of NO and its reactive byproducts have been thoroughly reviewed,[13, 34, 42-44] and are typically ascribed to either nitrosative or oxidative stress. In addition to causing DNA deamination, nitrosative species such as N_2O_3 may nitrosate thiols (*S*-nitrosation) on proteins and initiate disulfide bridging with other thiols on the protein,[45] thereby directly altering protein function.[13] Due to their lipophilic nature, NO and O_2 tend to concentrate in cell membranes, accelerating NO's oxidation to N_2O_3 and creating greater nitrosative stress within and near the bacterial membrane.[44] Nitrosation of both cell surface proteins and intracellular proteins (including

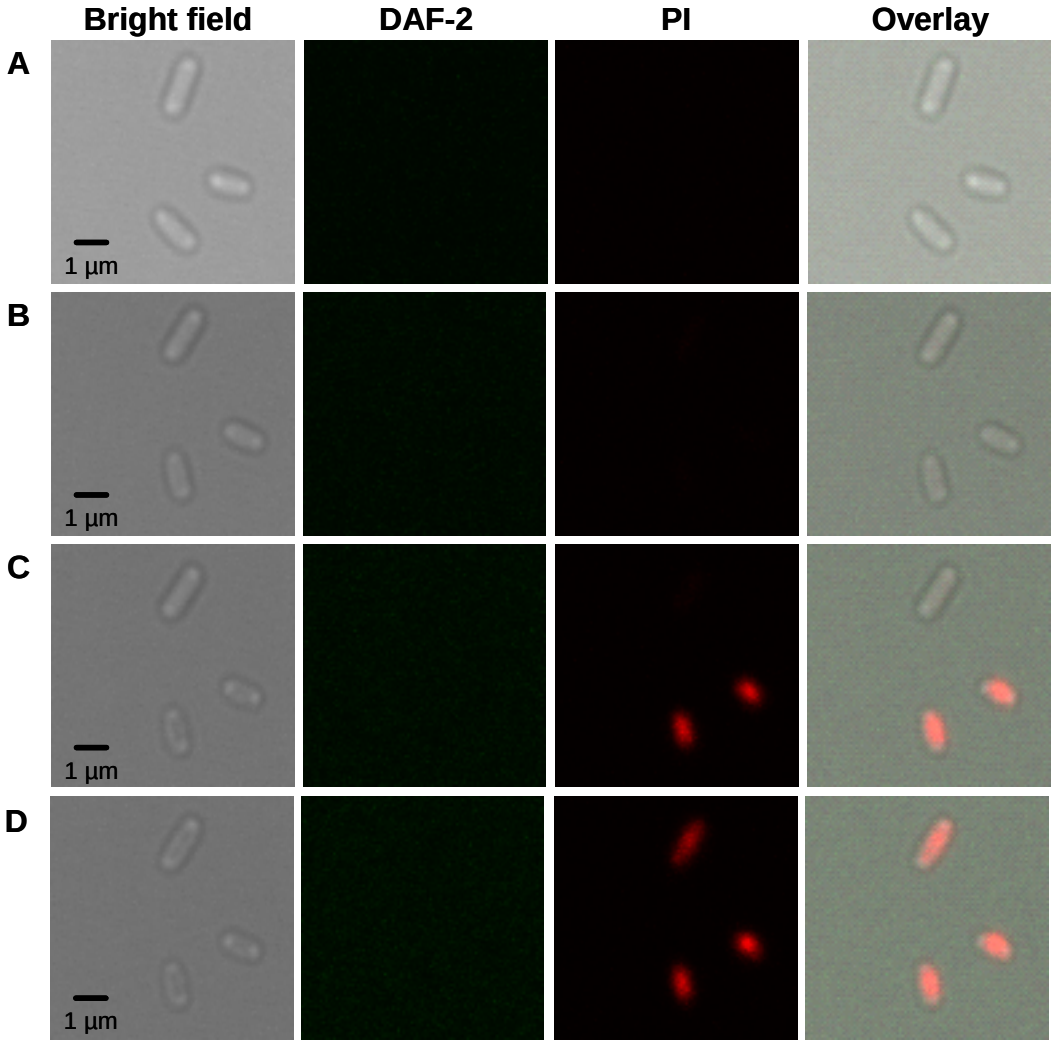

Figure 4.10. Bright field and fluorescence images of *P. aeruginosa* cells treated with 5 mg·mL^{-1} PROLI/NO. Propidium iodide (PI) fluorescence indicates cell death. Images were acquired (A) 0 min, (B) 10.5 min, (C) 21min, and (D) 31 min after addition of 5 mg·mL^{-1} PROLI/NO.

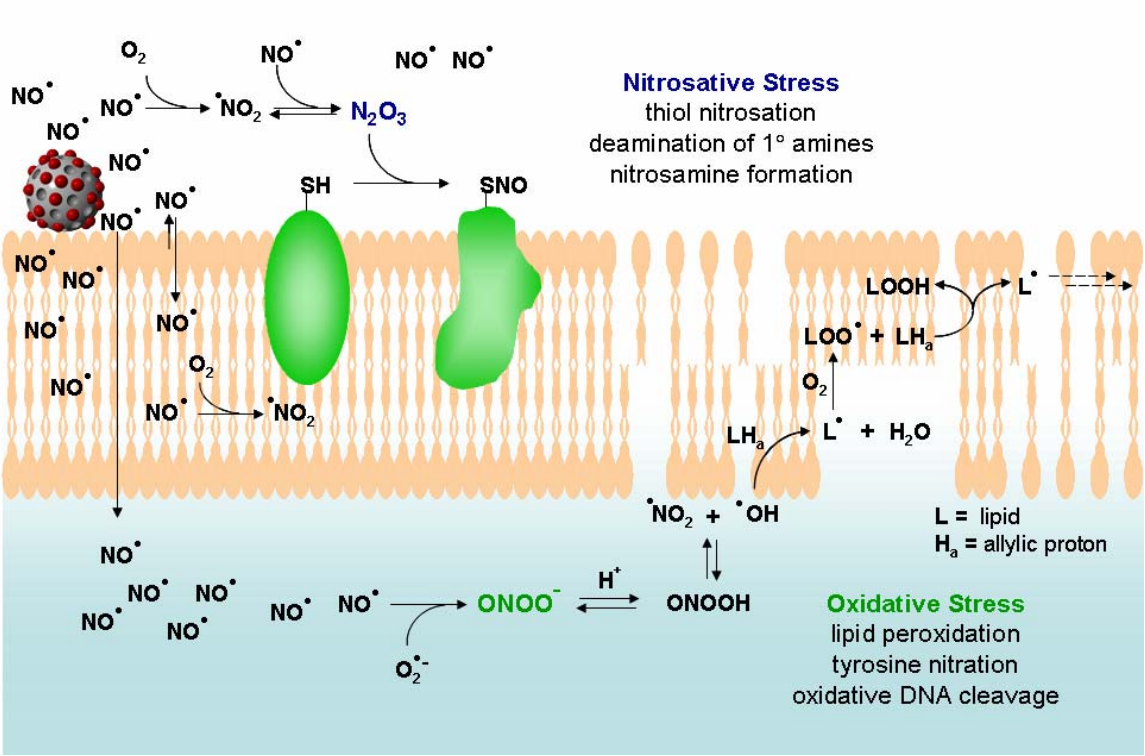

Figure 4.11. Proposed mechanisms by which NO acts as an antibacterial agent (adapted from references 13, 34, 42-44; not to scale). NO's antibacterial properties are attributed to both nitrosative and oxidative stress exerted by reactive byproducts such as N_2O_3 and $ONOO^-$ (peroxynitrite). Nitrosative stress leads in part to nitrosation of thiols on proteins as well as DNA deamination, while oxidative stress is responsible for membrane destruction via lipid peroxidation. Notably, increased NO and O_2 concentrations in lipid membranes leads to enhanced production of both nitrosative and oxidative species such as N_2O_3 and NO_2 in the membrane.

enzymes) has been shown to cause bacterial cell death.[13] Oxidative stress is driven primarily by peroxynitrite ($ONOO^-$), which forms via the reaction of NO with superoxide endogenously derived from the bacterial cellular respiration process.[13, 46-49] Thus, oxidative damage is expected to occur predominantly inside the cell, since superoxide does not readily cross cell membranes.[50] A significant antibacterial process related to oxidative stress is peroxynitrite-dependent lipid peroxidation, which stems from OH and NO_2 radicals derived from peroxynitrous acid (HOONO; Fig. 4.11).[51] The production of NO_2 radical from NO and O_2 is also accelerated in membranes, leading to even greater NO-mediated oxidative stress within bacterial cell membranes.[44] Membrane destruction via lipid peroxidation has been proposed as one of the major mechanisms of NO-mediated bactericidal activity. As a peroxynitrite-dependent process requiring superoxide, NO released in close proximity to a bacterial cell would be expected to exert greater bactericidal effects than NO released diffusely throughout solution by generating a larger intracellular NO concentration.[13] Indeed, we observed direct evidence of membrane destruction during the confocal microscopy experiments by the rapid appearance of intracellular PI fluorescence (Fig. 4.9) in cells treated with NO-releasing silica nanoparticles. By virtue of the extended NO-release half-life of the silica nanoparticles relative to PROLI/NO, a significant portion of the NO is retained until *after* particle association with the *P. aeruginosa* cells. Such high localized NO release in close proximity to the bacterial cells may then facilitate delivery of greater concentrations of NO and other reactive species to the cell membrane and into the cell itself, leading to enhanced bactericidal efficacy of NO delivered from nanoparticles.

4.3.5 Cytotoxicity of AHAP3 nanoparticles and PROLI/NO against L929 mouse fibroblasts. The significant toxicity that NO-releasing 45 mol% AHAP3 silica nanoparticles exhibited against *P. aeruginosa* cells demands study of their effect on healthy mammalian

cells as well. Although Ghaffari et al. have demonstrated that NO gas (200 ppm for 4 h) was not toxic to human dermal fibroblasts,[14] similar studies were conducted to determine the combined effects of NO and the silica nanoparticle scaffold on L929 mouse fibroblast cells. Such cells represent the standard for cytotoxicity testing of novel therapeutic agents.[52, 53] Survival of the L929 cells in the presence of control and NO-releasing silica nanoparticles was monitored via both propidium iodide (PI) and lactate dehydrogenase (LDH) viability assays over 2 h to mimic the time-based bactericidal assays described above. As discussed above, healthy cells with uncompromised membranes exclude PI in the buffer solution, while disrupted plasma membranes allow PI to diffuse into the cell and emit characteristic fluorescence after complexation with intracellular nucleic acids.[26] Positive detection of LDH in the culture medium also indicates compromised cellular membranes that allow larger proteins to leak out of the cell, further indicating membrane disruption and cell death. Both assays thus monitor membrane permeability to assess cell viability, a suitable method to assay for the destructive properties of reactive NO byproducts that are known to form in greater quantities at lipid membranes.[44] A range of nanoparticle concentrations was tested to encompass the bactericidal concentrations of 45 mol% AHAP3 silica in the PBS and TSB assays (70 $\mu g \cdot mL^{-1}$ and 800 $\mu g \cdot mL^{-1}$, respectively). As shown in Figure 4.12, both control and NO-releasing 45 mol% AHAP3 silica nanoparticles were found to present minimal toxicity to the L929 fibroblasts. Remarkably, when exposed to the same concentration of NO-releasing silica nanoparticles required to induce 4 logs of bacterial killing (800 $\mu g \cdot mL^{-1}$; Fig. 4.5 B), L929 cells maintained 92% viability as measured by the PI assay. Thus, *P. aeruginosa* appears to be extremely susceptible to NO-releasing silica nanoparticles, while such delivery vehicles pose minimal threat to healthy mammalian fibroblasts.

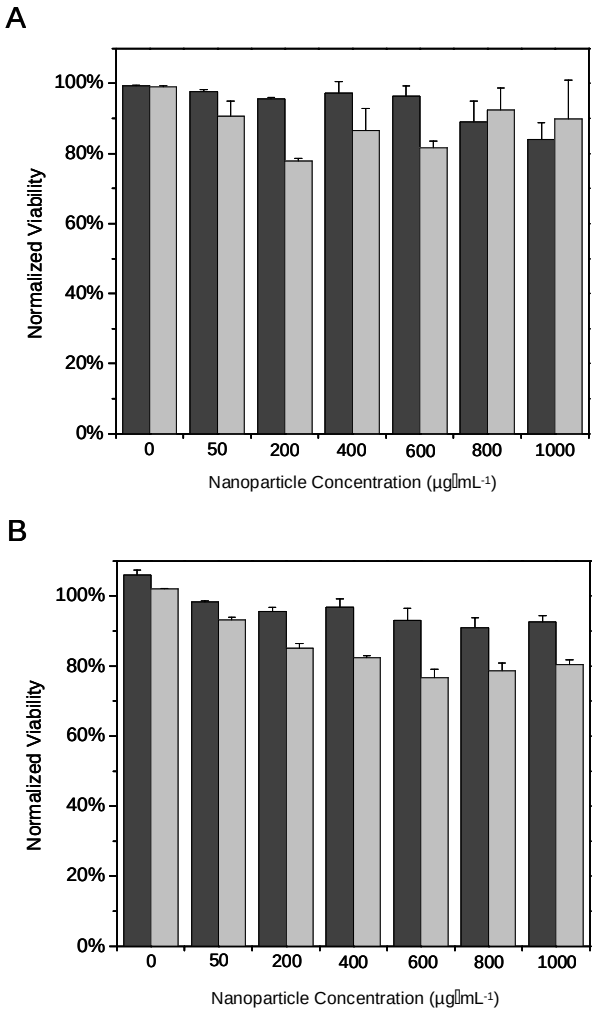

Figure 4.12. Toxicity of 45 mol% AHAP3 control (dark gray) and NO-releasing (light gray) silica nanoparticles to L929 mouse fibroblasts as measured by (A) membrane permeability to propidium iodide and (B) lactate dehydrogenase leaching.

In contrast, PROLI/NO proved toxic to L929 fibroblasts when administered at concentrations required to kill *P. aeruginosa*. When L929 cells were exposed to the dose of PROLI/NO required to induce 4 logs of bacterial killing in TSB within 2 h (12 $mg \cdot mL^{-1}$; Fig. 4.5 A), 100% cell death (i.e., 0% viability) was observed within 45 min (Fig. 4.13). While proline, (the precursor of PROLI/NO) exhibited no toxicity to L929 fibroblasts at concentrations up to 16 $mg \cdot mL^{-1}$ (data not shown), 100% fibroblast cell death was observed within 90 min at a PROLI/NO concentration of 8 $mg \cdot mL^{-1}$. Upon reducing the PROLI/NO concentration to 4 $mg \cdot mL^{-1}$, 100% fibroblast viability was maintained through 2 h, but at the expense of bactericidal efficacy (Fig. 4.5 A). These results reinforce the advantages of delivering NO via nanoparticle scaffolds, as both the amount of NO necessary to kill bacteria and toxicity to healthy mammalian cells are reduced.

4.4 Conclusions

Nitric oxide delivered from silica nanoparticles was shown to be significantly more effective at killing pathogenic *P. aeruginosa* than NO derived from the small molecule NO donor PROLI/NO. Indeed, significantly less NO was required from the nanoparticles to kill *P. aeruginosa* than from PROLI/NO, even though the initial NO release from PROLI/NO was 6-fold greater than from 45 mol% AHAP3 silica nanoparticles. In vitro cytotoxicity experiments conducted with L929 mouse fibroblasts confirmed that NO-releasing silica nanoparticles are largely non-toxic to mammalian fibroblast cells at concentrations capable of killing *P. aeruginosa*, while PROLI/NO presents significant toxicity to such cells when administered at bactericidal concentrations. Such results demonstrate the promise that NO holds as a new strategy for battling bacterial infection. Confirmation of particle association with *P. aeruginosa* cells and the measurement of intracellular NO levels helped elucidate the

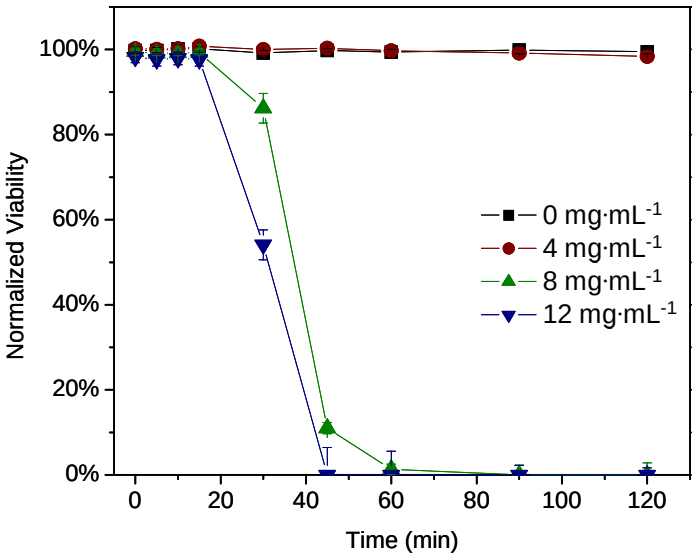

Figure 4.13. Cytotoxicity of PROLI/NO against L929 fibroblast cells as measured by propidium iodide viability assay. The backbone of PROLI/NO (the amino acid proline) demonstrated no toxicity to L929 cells at concentrations up to 16 mg/mL.

differential toxicity observed between macromolecular and small molecule NO donors. The versatility in the synthesis of NO-releasing silica scaffolds allows for both tuning of size and exterior functionality that may further enhance their use as antibacterial agents. Future studies are aimed at identifying the intracellular location of the reactive radical species formed upon NO release and establishing a mechanistic understanding of the interactions between NO-releasing nanoparticles and bacterial cell membranes. As well, experiments are underway to evaluate the antibacterial properties of NO-releasing silica nanoparticles against other species of pathogenic bacteria including gram-positive strains and those that exhibit resistance to conventional antibiotics.

4.5 References

(1) Robson, M. C. "Wound infection: A failure of wound healing caused by an imbalance of bacteria." *Surg. Clin. N. Am.* **1997,** *77*, 637-650.

(2) "Bad bugs, no drugs: As antibiotic discovery stagnates, a public health crisis brews." *Infectious Diseases Society of America* **2004**, 1-35.

(3) Gu, H.; Ho, P. L.; Tong, E.; Wang, L.; Xu, B. "Presenting vancomycin on nanoparticles to enhance antimicrobial activities." *Nano Lett.* **2003,** *3*, 1261-1263.

(4) Morones, J. R.; Elechiguerra, J. L.; Camacho, A.; Holt, K.; Kouri, J. B.; Ramirez, J. T.; Yacaman, M. J. "The bactericidal effect of silver nanoparticles." *Nanotechnology* **2005,** *16*, 2346-2353.

(5) Sambhy, V.; MacBride, M. M.; Peterson, B. R.; Sen, A. "Silver bromide nanoparticle/polymer composites: Dual action tunable antimicrobial materials." *J. Am. Chem. Soc.* **2006,** *128*, 9798-9808.

(6) Panacek, A.; Kvitek, L.; Prucek, R.; Kolar, M.; Vecerova, R.; Pizurova, N.; Sharma, V. K.; Nevecna, T.; Zboril, R. "Silver colloid nanoparticles: Synthesis, characterization, and their antibacterial activity." *J. Phys. Chem. B* **2006,** *110*, 16248-16253.

(7) Trewyn, B. G.; Whitman, C. M.; Lin, V. S.-Y. "Morphological control of room-temperature ionic liquids templated mesoporous silica nanoparticles for controlled release of antibacterial agents." *Nano Lett.* **2004,** *4*, 2139-2143.

(8) Silver, S. "Bacterial silver resistance: Molecular biology and uses and misuses of silver compounds." *FEMS Microbiol. Rev.* **2003,** *27*, 341-353.

(9) Li, X.-Z.; Nikaido, H.; Williams, K. E. "Silver-resistant mutants of *Escherichia coli* display active efflux of Ag^{+} and are deficient in porins." *J. Bacteriol.* **1997,** *179*, 6127-6132.

(10) Marletta, M. A.; Tayeh, M. A.; Hevel, J. M. "Unraveling the biological significance of nitric oxide." *BioFactors* **1990,** *2*, 219-225.

(11) MacMicking, J.; Xie, Q.; Nathan, C. "Nitric oxide and macrophage function." *Annu. Rev. Immunol.* **1997,** *15*, 323-350.

(12) MacMicking, J.; Nathan, C.; Hom, G.; Chartrain, N.; Fletcher, D. S.; Trumbauer, M.; Stevens, K.; Xie, Q.; Sokol, K.; Hutchinson, N.; Chen, H.; Mudgett, J. S. "Altered response to bacterial infection and endotoxic shock in mice lacking inducible nitric oxide synthase." *Cell* **1995,** *81*, 641-650.

(13) Fang, F. C. "Mechanisms of nitric oxide-related antimicrobial activity." *J. Clin. Invest.* **1997,** *99*, 2818-2825.

(14) Ghaffari, A.; Miller, C. C.; McMullin, B.; Ghahary, A. "Potential application of gaseous nitric oxide as a topical antimicrobial agent." *Nitric Oxide* **2006,** *14*, 21-29.

(15) Raulli, R.; McElhaney-Feser, G.; Hrabie, J. A.; Cihlar, R. L. "Antimicrobial properties of nitric oxide using diazeniumdiolates as the nitric oxide donor." *Rec. Res. Devel. Microbiology* **2002,** *6*, 177-183.

(16) Rothrock, A. R.; Donkers, R. L.; Schoenfisch, M. H. "Synthesis of nitric oxide-releasing gold nanoparticles." *J. Am. Chem. Soc.* **2005,** *127*, 9362-9363.

(17) Stasko, N. A.; Schoenfisch, M. H. "Dendrimers as a scaffold for nitric oxide release." *J. Am. Chem. Soc.* **2006,** *128*, 8265-8271.

(18) Shin, J. H.; Metzger, S. K.; Schoenfisch, M. H. "Synthesis of nitric oxide-releasing silica nanoparticles." *J. Am. Chem. Soc.,* **2007,** *129*, 4612-4619.

(19) Hrabie, J. A.; Keefer, L. K. "Chemistry of the nitric oxide-releaseing diazeniumdiolate ("nitrosohydroxylamine") functional group and its oxygen-substituted derivatives." *Chem. Rev.* **2002,** *102*, 1135-1154.

(20) Wang, P. G.; Xian, M.; Tang, X.; Wu, X.; Wen, Z.; Cai, T.; Janczuk, A. J. "Nitric oxide donors: Chemical activities and biological applications." *Chem. Rev.* **2002,** *102*, 1091-1134.

(21) Pruitt, B. A.; McManus, A. T.; Kim, S. H.; Goodwin, C. W. "Burn wound infections: Current status." *World J. Surg.* **1998,** *22*, 135-145.

(22) Lyczak, J. B.; Cannon, C. L.; Pier, G. B. "Establishment of *Pseudomonas aeruginosa* infection: Lessons from a versatile opportunist." *Microbes and Infection* **2000,** *2*, 1051-1060.

(23) Howell-Jones, R. S.; Wilson, M. J.; Hill, K. E.; Howard, A. J.; Price, P. E.; Thomas, D. W. "A review of the microbiology, antibiotic usage and resistance in chronic skin wounds." *J. Antimicrob. Chemother.* **2005,** *55*, 143-149.

(24) Lin, Y.-S.; Tsai, C.-P.; Huang, H.-Y.; Kuo, C.-T.; Hung, Y.; Huang, D.-M.; Chen, Y.-C.; Mou, C.-Y. "Well-ordered mesoporous silica nanoparticles as cell markers." *Chem. Mater.* **2005,** *17*, 4570-4573.

(25) Saavedra, J. E.; Southan, G. J.; Davies, K. M.; Lundell, A.; Markou, C.; Hanson, S. R.; Adrie, C.; Hurford, W. E.; Zapol, W. M.; Keefer, L. K. "Localizing antithrombotic and vasodilatory activity with a novel, ultrafast nitric oxide donor." *J. Med. Chem.* **1996,** *39*, 4361-4365.

(26) Tas, J.; Westerneng, G. "Fundamental aspects of the interaction of propidium diiodide with nucleic acids studied in a model system of polyacrylamide films." *J. Histochem. Cytochem.* **1981,** *29*, 929-936.

(27) Kojima, H.; Nakatsubo, N.; Kikuchi, K.; Kawahara, S.; Kirino, Y.; Nagoshi, H.; Hirata, Y.; Nagano, T. "Detection and imaging of nitric oxide with novel fluorescent indicators: Diaminofluoresceins." *Anal. Chem.* **1998,** *70*, 2446-2453.

(28) Bielinska, A. U.; Chen, C.; Johnson, J.; Baker, J. R. "DNA Complexing with polyamidoamine dendrimers: Implications for transfection." *Bioconj. Chem.* **1999,** *10*, 843-850.

(29) Puranam, K. L.; Boustany, R.-M., "Assessment of cell viability and histochemical methods in apoptosis." In *Apoptosis in Neurobiology*, Hannun, Y. A.; Boustany, R.-M., Eds. CRC Press LLC: Boca Raton, FL, 1998; pp 129-152.

(30) Shin, J. H.; Schoenfisch, M. H. "Inorganic/organic hybrid silica nanoparticles as a nitric oxide delivery scaffold." *Chem. Mater.* **2008,** *20*, 239-249.

(31) Hrabie, J. A.; Klose, J. R.; Wink, D. A.; Keefer, L. K. "New nitric oxide-releasing zwitterions derived from polyamines." *J. Org. Chem.* **1993,** *58*, 1472-1476.

(32) Beckman, J. S.; Conger, K. A. "Direct measurement of dilute nitric oxide in solution with an ozone chemiluminescent detector." *Methods Enzymol.* **1995,** *7*, 35-39.

(33) Davies, K. M.; Wink, D. A.; Saavedra, J. E.; Keefer, L. K. "Chemistry of the diazeniumdiolates. 2. Kinetics and mechanism of dissociation to nitric oxide in aqueous solution." *J. Am. Chem. Soc.* **2001,** *123*, 5473-5481.

(34) Wink, D. A.; Mitchell, J. B. "Chemical biology of nitric oxide: Insights into regulatory, cytotoxic, and cytoprotective mechanisms of nitric oxide." *Free Radical Biol. Med.* **1998,** *25*, 434-456.

(35) Hsueh, P. R.; Teng, L. J.; Yang, P. C.; Chen, Y. C.; Ho, S. W.; Luh, K. T. "Persistence of a multidrug-resistant *Pseudomonas aeruginosa* clone in an intensive care burn unit." *J. Clin. Microbiol.* **1998,** *36*, 1347-1351.

(36) Dukelow, A. M.; Weicker, S.; Karachi, T. A.; Razavi, H. M.; McCormack, D. G.; Joseph, M. G.; Mehta, S. "Effects of nebulized diethylenetetraamine-NONOate in a mouse model of acute *Pseudomonas aeruginosa* pneumonia." *Chest* **2002,** *122*, 2127-2136.

(37) Stratton, C. W. "Dead bugs don't mutate: Susceptibility issues in the emergence of bacterial resistance." *Emerg. Infect. Dis.* **2003,** *9*, 10-16.

(38) Li, R. C.; Zhu, M.; Schentag, J. J. "Achieving an optimal outcome in the treatment of infections: The role of clinical pharmacokinetics and pharmacodynamics of antimicrobials." *Clinical Pharmacokinet.* **1999,** *37*, 1-16.

(39) Lancaster, J. R. "A tutorial on the diffusibility and reactivity of free nitric oxide." *Nitric Oxide* **1997,** *1*, 18-30.

(40) Shai, Y. "From innate immunity to de-novo designed antimicrobial peptides." *Curr. Pharmaceut. Design* **2002,** *8*, 715-725.

(41) Poelstra, K. A.; van der Mei, H. C.; Gottenbos, B.; Grainger, D. W.; van Horn, J. R.; Busscher, H. J. "Pooled human immunoglobulins reduce adhesion of *Pseudomonas aeruginosa* in a parallel plate flow chamber." *J. Biomed. Mater. Res.* **2000,** *51*, 224-232.

(42) Stamler, J. S.; Lamas, S.; Fang, F. C. "Nitrosylation: The prototypic redox-based signaling mechanism." *Cell* **2001,** *106*, 675-683.

(43) Fang, F. C. "Antimicrobial reactive oxygen and nitrogen species: Concepts and controversies." *Nat. Rev. Microbiol.* **2004,** *2*, 820-832.

(44) Moller, M. N.; Li, Q.; Lancaster, J. R.; Denicola, A. "Acceleration of nitric oxide autoxidation and nitrosation by membranes." *IUBMB Life* **2007,** *59*, 243-248.

(45) Stamler, J. S. "*S*-Nitrosothiols and the bioregulatory actions of nitrogen oxides through reactions with thiol groups." *Curr. Top. Microbiol.* **1995,** *196*, 19-36.

(46) Polack, B.; Dacheux, D.; Delic-Attree, I.; Toussaint, B.; Vignais, P. M. "Role of manganese superoxide dismutase in a mucoid isolate of *Pseudomonas aeruginosa*: Adaptation to oxidative stress." *Infect. Immun.* **1996,** *64*, 2216-2219.

(47) Hassett, D. J.; Cohen, M. S. "Bacterial adaptation to oxidative stress: Implications for pathogenesis and interaction with phagocytic cells." *FASEB J.* **1989,** *3*, 2574-2582.

(48) Fridovich, I. "The biology of oxygen radicals." *Science* **1978,** *201*, 875-880.

(49) Hassett, D. J.; Schweizer, H. P.; Ohman, D. E. "*Pseudomonas aeruginosa sodA* and *sodB* mutants defective in manganese- and iron-cofactored superoxide dismutase activity demonstrate the importance of the iron-Cofactored form in aerobic metabolism." *J. Bacteriol.* **1995,** *177*, 6330-6337.

(50) Nunoshiba, T.; deRojas-Walker, T.; Wishnok, J. S.; Tannenbaum, S. R.; Demple, B. "Activation by nitric oxide of an oxidative-stress response that defends *Escherichia coli* against activated macrophages." *Proc. Natl. Acad. Sci. U.S.A.* **1993,** *90*, 9993-9997.

(51) Fukuto, J. M.; Cho, J. Y.; Switzer, C. H., "The chemical properties of nitric oxide and related nitrogen oxides." In *Nitric Oxide: Biology and Pathology*, Ignarro, L. J., Ed. Academic Press: San Diego, 2000.

(52) Turner, T. D.; Spyratou, O.; Schmidt, R. J. "Biocompatibility of wound management products: Standardization of and determination of cell growth rate in L929 fibroblast cultures." *J. Pharm. Pharmacol.* **1989,** *41*, 775-780.

(53) Nablo, B. J.; Schoenfisch, M. H. "In vitro cytotoxicity of nitric oxide-releasing sol-gel derived materials." *Biomaterials* **2005,** *26*, 4405-4415.

Chapter 5:

Anti-Biofilm Efficacy of Nitric Oxide-Releasing Materials: Inhibition of Microbial Surface Proliferation and Activity against Established Microbial Biofilms

5.1 Introduction

A most dangerous threat to patients with indwelling medical devices or chronic wounds is infection due to microbial biofilm formation.[1, 2] Of the 2 million patients suffering from hospital-acquired infections in the U.S. each year, over half are due to biofilms at the site of indwelling medical devices. The most threatening of all device-associated infections are those associated with central venous catheters (CVCs).[3] Approximately 250,000 CVC-associated infections are reported each year, and up to 25% (62,500) of such infections are fatal.[4] Likewise, the wounds most susceptible to infection are those associated with burns, with roughly 50,000 burn injuries requiring hospitalization each year.[5] Alarmingly, 10,000 patients die each year of burn-related infections in the U.S.[5] While current antimicrobial strategies have shown some success at treating infections, novel approaches to both prevent biofilm formation and eradicate established biofilms are urgently needed.

Microbial biofilms are the common cause of both medical device and wound infections. Biofilms are complex communities that form when microorganisms self-secrete a polysaccharide matrix that retains nutrients for the constituent cells and protects them from both the immune response and antimicrobial agents.[6] Biofilms are remarkably resistant to both host defenses and systemic antibiotics. Indeed, in some cases it has been found that

killing bacteria in a biofilm requires up to 1000 times the antibiotic dose necessary to achieve the same results in a suspension of cells.[7] Biofilm-embedded microbial cells communicate with each other via quorum sensing, and phenotypic variations occur that may exacerbate virulence to the host.[6] Water channels throughout the biofilm matrix allow nutrient transport and facilitate signaling between cells.[2] Development of resistance to antibiotics is a greater threat for biofilm-based bacteria, where the close proximity of cells allows facile transfer of resistance-encoding DNA.[8, 9]

5.1.1 Device-associated biofilms: formation and prevention. Indwelling medical devices are particularly susceptible to infection because they provide a substrate on which microbial cells adhere and proliferate to form a biofilm.[1] As detailed in Chapter 1, device-associated infection is the direct result of bacterial adhesion and surface proliferation, eventually resulting in biofilm formation at the device/tissue interface. Strategies to reduce bacterial adhesion have involved modifying devices with passive hydrophilic coatings such as poly(ethylene glycol),[10] poly(ethylene oxide) brushes,[11] and hydrophilic polyurethanes,[12] for example. Unfortunately, such coatings do not always prevent microbial adhesion in vivo,[1] and they possess no mechanism by which to kill pathogens adhered to the surface or in surrounding tissue.[13-15] Thus, new methods for preventing bacterial colonization and biofilm formation at medical devices are needed.

5.1.2 Biofilm-based wound infections. For several years, debate has existed as to whether biofilm formation occurs in infected wounds.[16] However, recent research has presented unequivocal evidence of microbial biofilm formation in chronic wounds.[17-20] Similar to device-associated infections, the presence of foreign materials in a wound promotes bacterial colonization[21] lowering the threshold of bacterial cells necessary to cause

infection. However, wounds can become infected even in the absence of foreign materials.[21] The goal of clinical intervention for promoting wound healing is to reduce the bacterial density within the wound to a host-manageable bioburden. Although no universally-accepted level for a host-manageable bioburden exists, the threshold is generally accepted to be roughly 10^5 bacterial cells per gram of tissue.[2]

In terms of treating biofilm-based wound infections, antiseptic wound dressings are the most common clinical strategy employed.[21] Although systemic antibiotic administration has shown limited efficacy against wound infections,[22-24] application of antibiotics directly to wounds is unacceptable due to the threat of promoting antibiotic resistance.[21] Current clinical protocols call for applying creams, solutions, or wound dressings that contain antiseptics such as silver ions (Ag^+), iodine, or chlorhexidine.[21] Each has demonstrated broad-spectrum activity against both gram-positive and gram-negative bacterial species; however, their efficacy has most often been tested against planktonic bacteria, not biofilms.[20] The silver compounds most commonly employed include silver nitrate ($AgNO_3$) and silver sulfadiazine (SSD), while povidone iodine (polyvinylpyrrolidone iodine complex [PVP-I]) is the most commonly-employed source of biocidal iodine.[21]

Despite some success, antiseptic treatments have distinct drawbacks. In some cases application of Ag^+ has resulted in permanent skin discoloration (argyria).[25] More problematic, bacteria have begun to develop resistance to Ag^+.[26-28] Povidone iodine has been shown to be toxic to fibroblasts in vitro[29] and its efficacy as a safe antimicrobial agent for wound healing has been questioned.[30-35] Furthermore, both PVP-I and chlorhexidine have been shown to be ineffective at treating biofilms of *Pseudomonas aeruginosa* and *Enterococcus faecalis*,[36, 37] both common pathogens found to cause wound infections.

Alarmingly, a growing number of reports document life-threatening anaphylactic shock in response to chlorhexidine treatment.[38-41] New strategies for battling established biofilms are clearly warranted.

5.1.3 Antimicrobial properties of nitric oxide. Recent research has highlighted the antimicrobial properties of nitric oxide (NO),[42-44] a highly reactive free radical that is synthesized by inflammatory cells (e.g., neutrophils and macrophages) to fight infection. Raulli et al. demonstrated that NO possesses broad-spectrum antibacterial properties against both gram-positive and gram-negative bacteria.[45] Ghaffari et al. reported that NO is effective at killing methicillin-resistant *Staphylococcus aureus* (MRSA).[46] In terms of biomaterial-associated infections, surfaces modified with NO-releasing xerogel polymers have been shown to both reduce bacterial adhesion and kill bacterial cells that manage to adhere, two important steps toward preventing biofilm formation.[47] However, the ability of surface-derived NO to inhibit bacterial proliferation at a substrate surface, another critical step in biofilm formation,[48] has not yet been characterized. Other recent work has demonstrated the potent antibacterial properties of NO-releasing silica nanoparticles (e.g., enhanced antibacterial efficacy against planktonic *P. aeruginosa* cells compared to a small molecule NO donor).[49] However, the antimicrobial activity of such nanoparticles has not yet been tested against established biofilms. The rapid diffusion of NO may result in increased efficacy against biofilm-embedded bacteria.[50] Indeed, NO's ability to diffuse through the dense polysaccharide matrix known to inhibit penetration of other antibiotics may prove to be the ultimate solution to biofilm resistance.[8] Herein, the first studies aimed at understanding the ability of NO to both prevent bacterial surface proliferation and eradicate established microbial biofilms are presented.

5.2 Methods and materials

N-Methylaminopropyltrimethoxysilane (MAP3), *N*-(6-aminohexyl)aminopropyl-trimethoxysilane (AHAP3), and isobutyltrimethoxysilane (BTMOS) were obtained from Gelest (Morrisville, PA) and stored under nitrogen or in a desiccator. Tetraethyl orthosilicate (TEOS) was purchased from Fluka (Buchs, Switzerland) and stored in a desiccator. Ethanol (EtOH; absolute), methanol (MeOH), hydrochloric acid (HCl), and ammonia solution (NH_4OH, 30 wt% in water) were purchased from Fisher Scientific (Fair Lawn, NJ). Tryptic soy broth (TSB), tryptic soy agar (TSA), yeast peptone dextrose broth (YPD), and yeast peptone dextrose agar were purchased from Becton, Dickinson and Company (Sparks, MD). Nitrogen (N_2) and argon (Ar) were purchased from National Welders (Raleigh, NC). Nitric oxide (NO, 99.5%) was obtained from Linde (Raleigh, NC). Other solvents and chemicals were analytical-reagent grade and used as received. *Pseudomonas aeruginosa* (ATCC #19143), *Escherichia coli* (ATCC #53323), *Staphylococcus aureus* (ATCC #29213), *Staphylococcus epidermidis* (ATCC #35983), and *Candida albicans* (ATCC #90028) were purchased from American Type Culture Collection (Manassas, VA). Class VI medical-grade silicone rubber (SiR) was purchased from McMaster-Carr (Atlanta, GA). Distilled water was purified with a Millipore Milli-Q Gradient A-10 water purification system (Bedford, MA) to a final resistivity of 18.2 MΩ·cm and a total organic content of <6 ppb. The following standard cell-culture products were obtained from Invitrogen (Carlsbad, CA): Eagles minimal essential medium (MEM), fetal bovine serum (FBS), penicillin/streptomycin (P/S), trypsin and and 3-(4,5-dimethylthiazol-2-yl)-2,5-diphenyltetrazolium bromide (MTT). L929 mouse fibroblasts (ATCC #CCL-1) were purchased from the University of North Carolina Tissue Culture Facility (Chapel Hill, NC).

5.2.1 Xerogel synthesis. Nitric oxide-releasing AHAP3/BTMOS xerogel films were synthesized as described by Marxer et al.[51] Briefly, H_2O (60 mL), ethanol (200 mL), 0.5 M HCl (10 mL), and BTMOS (120 mL) were mixed for 1 h. Next, AHAP3 (80 mL) was added with additional mixing for 1 h. Glass microscope slides were cut to approximately 2.6 x 0.8 cm^2, sonicated in ethanol, dried under nitrogen, and UV-cleaned in a BioForce TipCleaner (Ames, IA) for 20 min prior to use. Sol–gel solution (30 mL) was deposited onto clean glass slides via a spread-cast method. Xerogel films were allowed to solidify at room temperature for 30 min then transferred to a 70 °C oven for 3 d. After removal from the oven, xerogel-coated glass slides were stored in a desiccator at room temperature.

5.2.2 Diazeniumdiolate formation. Diazeniumdiolate NO-donors were synthesized within the xerogel network by exposing the films to high pressures of NO. Xerogel-coated glass slides were placed in a 500 mL hydrogenation bomb, which was subsequently flushed with Ar to remove O_2. The chamber was then pressurized to 5 atm of NO. After 3 d, unreacted NO was flushed from the chamber with Ar. Diazeniumdiolate-modified xerogel films were stored under N_2 at -20 °C to prevent NO-donor decomposition.

5.2.3 Synthesis of NO-releasing silica nanoparticles. The synthesis and characterization of NO-releasing silica nanoparticles have been described previously.[52, 53] Briefly, an aminoalkoxysilane solution was prepared by dissolving either AHAP3 (2.3 mmol) or MAP 3 (6.8 mmol) in 16 mL of EtOH and 4 mL of MeOH in the presence of $NaOCH_3$ (equimolar with either AHAP3 or MAP3). The solution was then placed into 10 mL vials equipped with stir bars. The vials were placed in a Parr bottle, connected to an in-house NO reactor, and flushed with Ar six times to remove O_2 in the solution. The reaction bottle was pressurized to 5 atm NO for 3 days with continuous stirring of the silane solution. Prior to

removing the diazeniumdiolate-modified silane sample (AHAP3/NO or MAP3/NO), unreacted NO was purged from the chamber with Ar. Silane solutions were prepared by mixing TEOS (2.8 mmol) and AHAP3/NO (2.3 mmol; corresponding to 45 mol%, balance TEOS) or MAP3/NO (6.5 mmol; corresponding to 70 mol%, balance TEOS) in the EtOH/MeOH solution for 2 min. The silane solution was then added into EtOH (22 mL) and ammonia catalyst (6 mL, 30 wt % in water) and mixed vigorously for 30 min at 4 °C. The precipitated nanoparticles were collected by centrifugation (5000 rpm, 5 min), washed with EtOH several times, dried under ambient conditions for 1 h, and stored in a sealed container at -20 °C.

5.2.4 Nitric oxide release measurements. Real-time NO release data were obtained using a Sievers 280 chemiluminescent NO analyzer (Boulder, CO). The instrument was calibrated with an atmospheric sample that had been passed through a NO zero filter and a 24.1 ppm NO gas standard (balance N_2). Xerogel-coated glass slides or a known mass of diazeniumdiolate-modified silica nanoparticles were immersed in deoxygenated PBS (pH 7.4) at 37 °C. The released NO was carried from the buffer to the analyzer with a stream of N_2 bubbled into the solution at a flow rate of 80 mL/min. In the instrument, NO was detected via its chemiluminescent reaction with ozone.[54]

5.2.5 Bacterial surface proliferation and doubling-time experiments. P. aeruginosa was cultured at 37 °C in tryptic soy broth (TSB), pelleted by centrifugation, resuspended in 15% glycerol (v/v in PBS), and stored at -80 °C. Cultures for biofilm studies were grown from a -80 °C stock at 37 °C in TSB overnight. A 1 mL aliquot of overnight culture was inoculated into 100 mL fresh TSB, incubated at 37 °C with rotation, and grown to an optical density ($OD_{\lambda=650\ nm}$) of 0.1 (corresponding to ~10^8 colony forming units [CFU] per mL, as

verified by serial 10-fold dilutions and plating on tryptic soy agar nutrient plates). The bacteria were pelleted by centrifugation, rinsed with ultrapure water, and resuspended in sterile phosphate buffered saline (PBS; 10 mM, pH 7.4). Xerogel substrates (control and NO-releasing 40% AHAP3/BTMOS) were affixed in a custom-machined polycarbonate parallel plate flow cell.[47] The 10^8 CFU/mL suspension of *P. aeruginosa* cells was then introduced into the flow cell (i.e., over the xerogel surfaces) at a controlled flow rate of 0.2 mL/min. After 5 min exposure to the bacterial suspension, the flow was stopped, the tube leading from the flow cell to waste was clamped, and the tubing was detached from the front end of the flow cell. New sterile tubing was then connected to the flow cell and immersed in a sterile vial of TSB. The clamp on the waste line was removed, the peristaltic pump was restarted, and the flow cell was immersed in a 37 °C water bath. Every 2 h, the flow of TSB was stopped and the flow cell was removed from the water bath and placed on the stage of a Zeiss Axiovert 200 inverted optical microscope (Chester, VA). Phase-contrast micrographs were captured with a 20x objective with a Zeiss Axiocam digital camera (Chester, VA) at 5 pre-determined locations. The flow cell was then returned to the water bath for 2 h until the next imaging session. After the experiment, the images were analyzed by applying a threshold value to differentiate the adhered cells from the background.[47] The number of pixels associated with adhered bacterial cells was normalized to the total number of pixels in the image to obtain a percent surface coverage of adhered bacterial cells. In this manner, bacterial proliferation at the xerogel surface was determined as a function of time. The time required for the number of cells to double on the xerogel surface was calculated from the following equation:[55]

$$n_t = n_0 \times 2^{\left(\frac{t}{t_d}\right)} \qquad \text{(Equation 5.1)}$$

where n_t is the percent surface coverage of bacterial cells at time t, n_0 is the percent surface coverage of bacterial cells at $t = 0$, t is the time between measurements, and t_d is the doubling time (i.e., the amount of time required for the number of bacterial cells to double). The doubling time of *P. aeruginosa* was determined for both control and NO-releasing 40% AHAP3/BTMOS xerogel substrates as a measure of the rate of bacterial proliferation at each substrate.

5.2.6 Treatment of established biofilms with NO-releasing silica nanoparticles. *P. aeruginosa*, *E. coli, S. aureus*, *S. epidermidis*, and *C. albicans* were cultured at 37 °C in either tryptic soy broth (TSB; bacteria) or yeast-peptone-dextrose broth (YPD; fungi), pelleted by centrifugation, resuspended in 15% glycerol (v/v in PBS), and stored at -80 °C. Cultures for biofilm studies were grown from a -80 °C stock at 37 °C in TSB overnight. A 1 mL aliquot of overnight culture was inoculated into 100 mL fresh TSB, incubated at 37 °C with rotation, and grown to an optical density ($OD_{\lambda=650\ nm}$) required to achieve ~10^8 colony forming units [CFU] per mL, as verified by serial 10-fold dilutions and plating on nutrient agar plates. The bacteria or fungi were pelleted by centrifugation, rinsed with ultrapure water, and resuspended in sterile phosphate buffered saline (PBS; 10 mM, pH 7.4).

Class VI medical-grade silicone rubber (SiR) was sectioned into squares measuring 8 x 6 x 2 mm^2. The SiR squares were cleaned with ethanol, dried, and sterilized in an autoclave at 121 °C for 25 min. Under aseptic conditions, the SiR squares were then immobilized on the end of sterile syringe needles and submerged in 5 mL sterile TSB or YPD in a sterile 10-mL glass vial. Next, the 10^8 CFU/mL microbial suspension was diluted to 10^6 CFU/mL, and 50 μL of the diluted suspension was added to the nutrient broth in each vial containing the SiR squares (final microbial concentration = 10^4 CFU/mL). The vials

were placed in a 37 °C incubator with gentle agitation. After 24 h, the SiR squares were removed from the nutrient broth, rinsed twice in sterile PBS, and individually transferred into new 10-mL glass vials containing a suspension of either 45 mol% AHAP3/TEOS nanoparticles or 70 mol% MAP3/TEOS nanoparticles in PBS. The SiR squares were returned to the 37 °C incubator and gently agitated. After 24 h, the SiR squares were rinsed twice in sterile PBS and aseptically transferred into polypropylene test tubes containing 2 mL of sterile PBS. To remove the biofilm cells from the substrates, each test tube was vortexed for 10 s, sonicated in a 125 W ultrasonic cleaner for 30 min, then vortexed for an additional 10 s. The resulting bacterial suspension was subjected to serial 10-fold dilutions, and 100 μL of appropriate dilutions were plated on either TSA (bacteria) or yeast peptone dextrose agar (fungi). The nutrient agar plates were then incubated at 37 °C. The following day, the colonies that grew on each plate were counted and the number of viable biofilm bacteria removed from each substrate was determined.

5.2.7 In vitro toxicity testing of NO-releasing nanoparticles. L929 mouse fibroblasts were grown to subconfluency in MEM with 10% FBS supplemented with 0.2% P/S at 37 °C and 5% CO_2. Cells were then trypsinized and resuspended in media at a concentration of 2 x 10^4 cells/mL and plated onto tissue culture treated polystyrene 96-well plates. After incubation for 24 h, the media from each well was discarded and control and NO-releasing 70 mol% MAP3/TEOS nanoparticles were added at concentrations of 1, 2, 4, and 8 mg/mL (200 μL). After incubation with the nanoparticles for 24 h, an MTT viability assay was performed.[56] Briefly, 40 μL of a 1 mg/mL MTT solution in sterile PBS was added to each well and incubated for 3 h, after which all solution was removed from the well and 100 μL DMSO was added to solubilize the crystals. The absorbance measured at 570 nm was

proportional to the concentration of viable cells in each well. Fibroblast viability in the presence of control and NO-releasing silica nanoparticles is reported relative to the viability of fibroblasts not exposed to silica nanoparticles.

5.3 Results and discussion

5.3.1 NO release for preventing biofilm formation. The motivation for studying bacterial proliferation at NO-releasing surfaces stems from previous results demonstrating the antibacterial properties of NO-releasing xerogels. Nablo et al. thoroughly documented the ability of NO-releasing xerogels to reduce bacterial adhesion.[57-60] More recent results show that surface-derived NO kills bacterial cells that adhere to the substrate.[47] Taken together, reduced adhesion and decreased bacterial viability may lead to a decrease in bacterial surface proliferation and biofilm formation at NO-releasing surfaces.[13] To investigate this hypothesis, a parallel plate flow cell was employed with the well-characterized 40% AHAP3 (v/v, balance BTMOS) NO-releasing xerogel system.[47, 51] The parallel plate flow cell allows real-time imaging of bacterial adhesion and proliferation on the substrate surface, and also is amenable to switching between different solutions (e.g., buffer and growth media) without introducing an air-liquid interface.[47] The 40% AHAP3 xerogel system has been well-characterized with respect to NO release, stability, and bacterial adhesion.[51] As shown in Figure 5.1, upon immersion in phosphate buffered saline (PBS; 37 °C, pH 7.4), 40% AHAP3 xerogels rapidly reached their maximum NO flux of ~300 pmol cm^{-2} s^{-1}, after which the NO flux decreased exponentially. Approximately 50% of the total NO was released within ~2.5 h after immersion in buffer. Small fluxes of NO (<1 pmol cm^{-2} s^{-1}) were detectable for up to 1 week.[61]

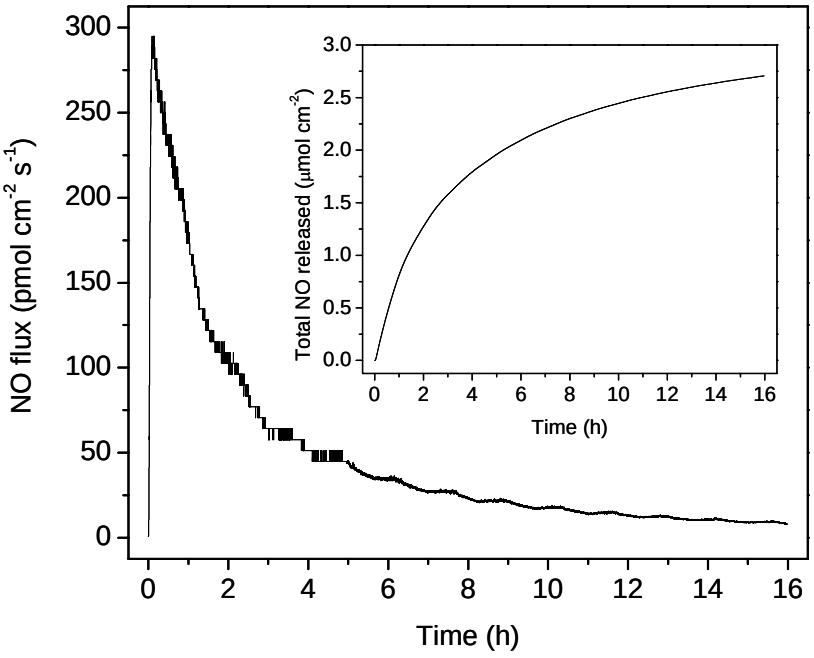

Figure 5.1. Nitric oxide release in phosphate buffered saline (pH 7.4) at 37 °C from 40% AHAP3 (v/v) xerogel polymer (balance BTMOS). Inset: total NO released.

To determine the ability of NO-releasing xerogels to inhibit bacterial surface proliferation, a suspension of *P. aeruginosa* in PBS was introduced to the flow cell for 5 min. Next, sterile nutrient media (i.e., tryptic soy broth) at 37 °C was introduced to allow adhered cells the chance to proliferate. To monitor proliferation, images of the surface were captured at discrete pre-determined locations with a 20x objective. As shown in Figure 5.2, bacterial proliferation at the control xerogel surface proceeded rapidly, while proliferation was not observed at NO-releasing surfaces. Indeed, while the average surface coverage at control xerogels increased from 10 ± 5% to 46 ± 14% from 0.5 to 4 h (Fig. 5.3), no significant increase in surface coverage was observed at the NO-releasing surfaces over a similar period (1.8 ± 0.7% to 1.3 ± 0.4% from 0.5 to 4.8 h). These data indicate that the surface-derived NO either killed the bacterial cells or inhibited the cellular mechanisms necessary for proliferation. Applying Equation 5.1, the doubling time for *P. aeruginosa* on control and NO-releasing xerogel surfaces was ~94 and ~890 min, respectively. Thus, the NO-releasing 40% AHAP3 xerogel surface increased the doubling time of *P. aeruginosa* by approximately one order of magnitude.

Next, experiments were conducted to determine the total time that the NO-releasing xerogels were able to inhibit *P. aeruginosa* proliferation in vitro. The flow cell apparatus was employed as described above, and images of the surface were obtained every 2 h for 24 h. As shown in Figure 5.4, *P. aeruginosa* proliferation was not observed until the 12 h time point at the NO-releasing substrates. Comparison of this finding to the real-time chemiluminescent NO release data from 40% AHAP3 xerogels (Fig. 5.1) reveals that over the initial 12 h period the NO flux was greater than ~15 pmol cm^{-2} s^{-1}, indicating that NO

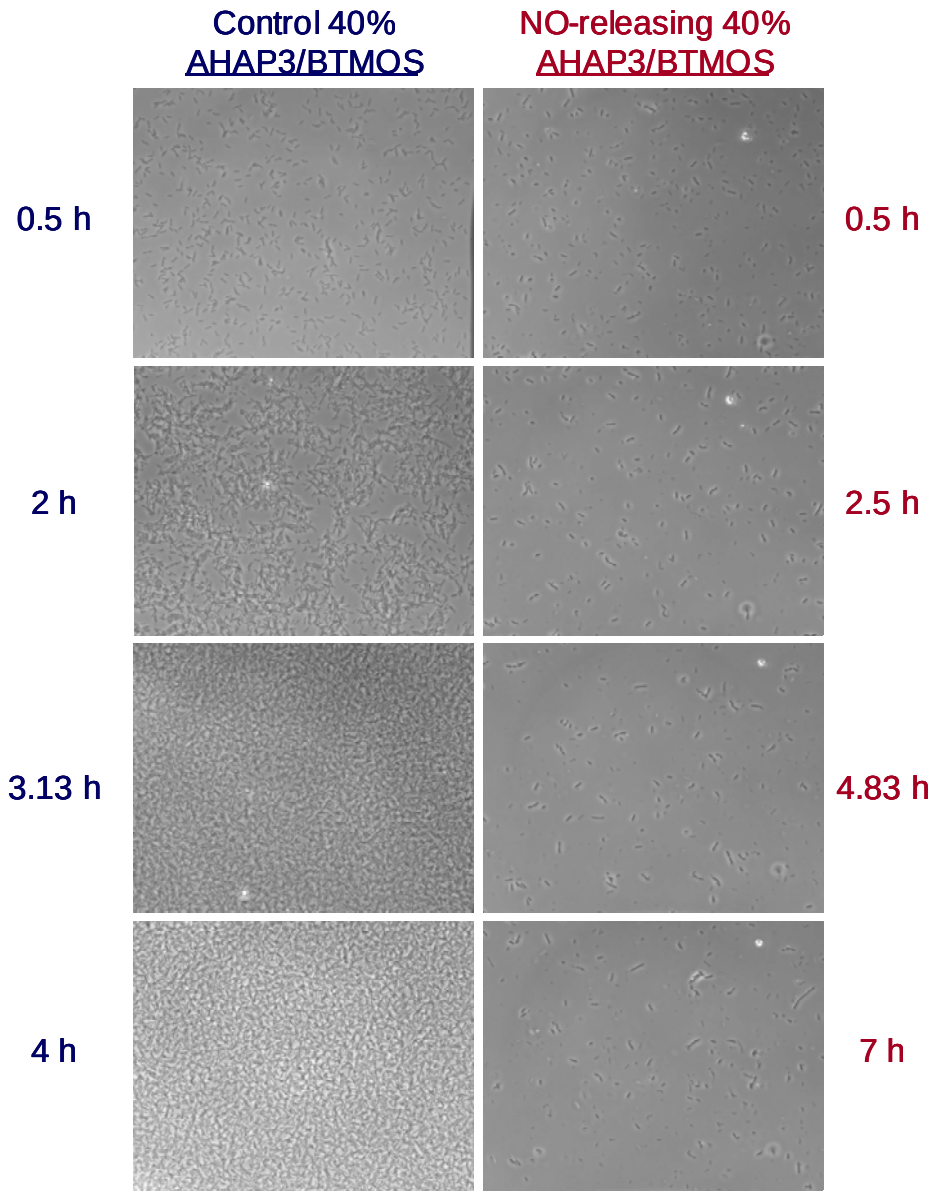

Figure 5.2. Optical micrographs (20x magnification) of *P. aeruginosa* proliferation at control (left column) and NO-releasing (right column) 40% AHAP3 xerogel substrates.

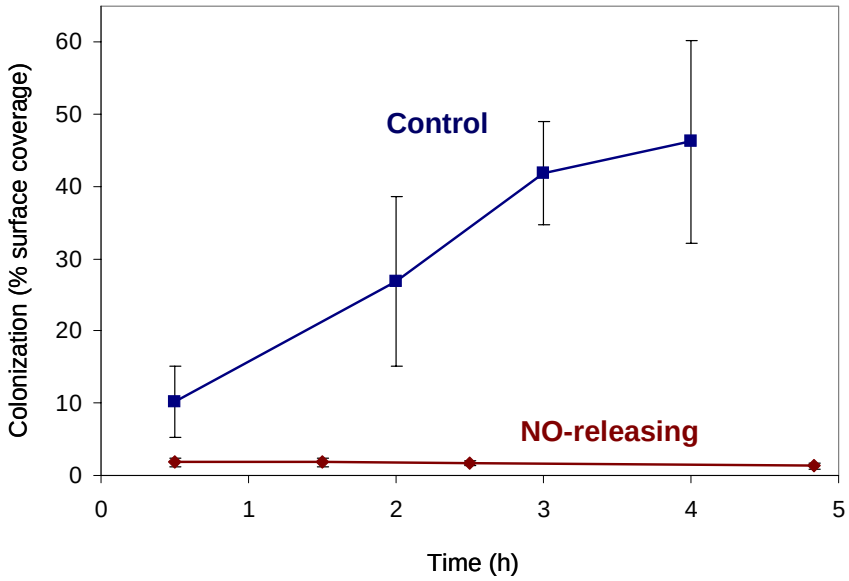

Figure 5.3. Surface colonization of control and NO-releasing 40% AHAP3 xerogel substrates (v/v, balance BTMOS) by *P. aeruginosa* in a parallel plate flow cell maintained at 37 °C. Percent surface coverage was determined via threshold analysis of phase-contrast optical micrographs.

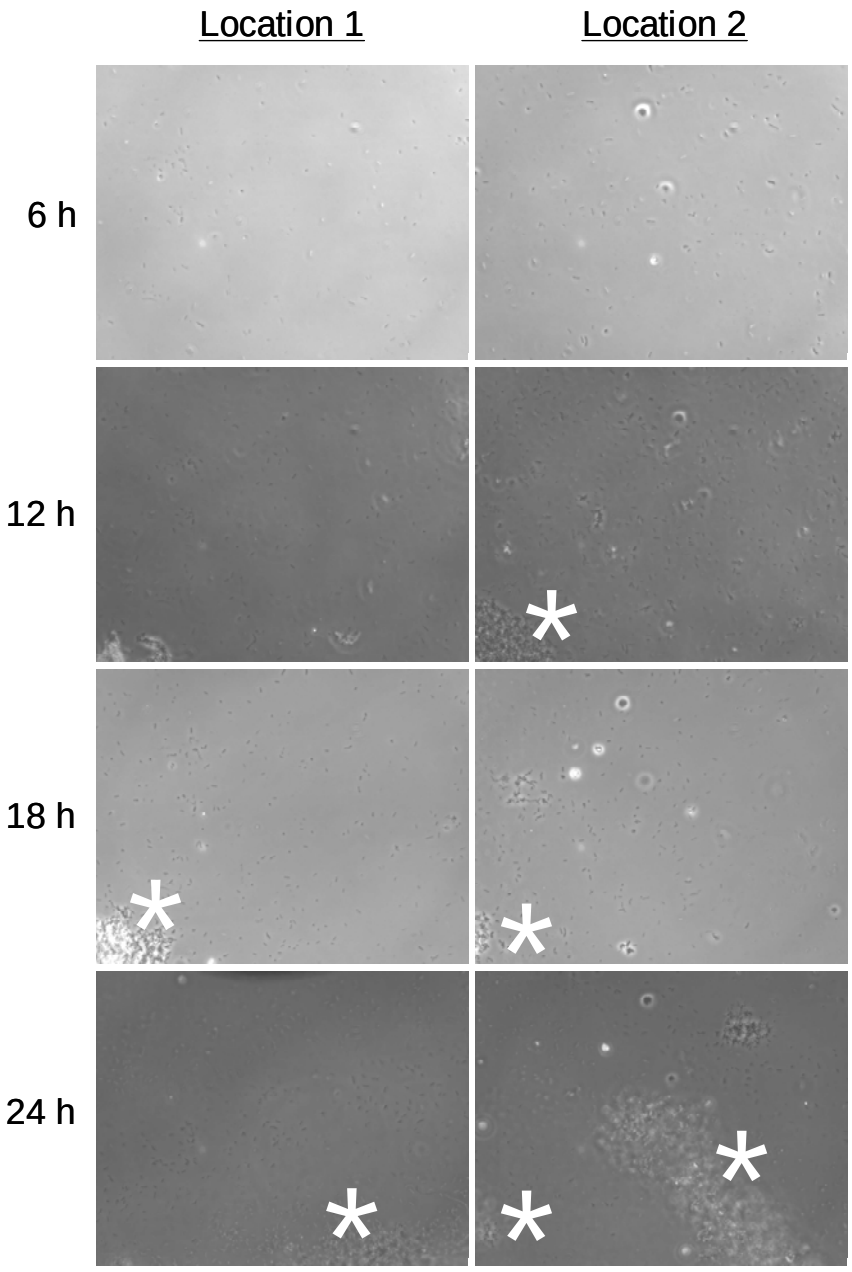

Figure 5.4. Optical micrographs (20x magnification) of *P. aeruginosa* proliferation at NO-releasing 40% AHAP3 xerogel substrates at two different locations on the same substrate over 24 h. Bacterial proliferation is indicated by the white asterisk(s) in each image.

fluxes in excess of this value are necessary to prevent surface proliferation by adhered *P. aeruginosa* cells.

While the mechanism of NO's ability to inhibit surface proliferation is unclear, its bactericidal properties are well-documented.[42, 43, 62, 63] It is likely that the surface flux of NO kills the majority of adhered *P. aeruginosa* cells,[47] leading to an overall decrease in the rate of surface proliferation. It is also possible that sufficient fluxes of NO may directly or indirectly inactivate/alter DNA, enzymes, and/or other components critical to bacterial replication,[62] thus inhibiting proliferation until the NO flux drops below the ~15 pmol cm^{-2} s^{-1} threshold. As shown in Figure 5.4, proliferation ensued from discrete points on the surface as opposed to developing an even bacterial lawn covering the entire surface as seen at controls (Fig. 5.2). It is hypothesized that this may be the result of a limited number of adhered cells beginning to replicate once the NO flux had dropped below ~15 pmol cm^{-2} s^{-1}. It is expected that this would lead to proliferation "islands" as opposed to the complete "lawn" coverage observed at controls. Experiments are planned to confirm this hypothesis with fluorescent viability probes.[47]

Regardless of the mechanism, the anti-proliferation results are encouraging from the standpoint of antimicrobial coatings for medical devices. Bacterial adhesion and device infection have been described as a "race for the surface",[64] with the process of tissue integration competing with bacterial adhesion to the substrate. To avoid infection, tissue integration must occur prior to appreciable bacterial adhesion and colonization at the device surface. If bacterial colonization occurs prior to tissue integration, host defenses may not be capable of preventing infection.[64] A 6-h post-implantation "decisive period" has been identified,[65] where preventing bacterial adhesion and surface proliferation is critical for

effective tissue integration. The finding that NO-releasing xerogels inhibit surface proliferation for up to 12 h (well in excess of the 6-h "critical window") demonstrates the promise that NO release holds as an anti-infective strategy for medical devices.

5.3.2 NO-releasing nanoparticles for treating established biofilms. In addition to causing infections at indwelling medical devices, biofilms are also problematic for wounds, where their presence delays healing and can threaten the life of the patient.[2, 17-20] While useful for treating internal infections, antibiotic administration directly to wounds is clinically unacceptable due to the danger of fostering antibiotic resistance.[21] Indeed, the threat of antibiotic resistance is heightened with biofilm-based infections where microbial cells can easily transfer plasmids that encode for resistance to antimicrobial agents.[8, 9] While antiseptics such as silver ions (Ag^+) and povidone-iodine enhance wound healing by killing wound-based bacteria, concerns over resistance and toxicity to healthy cells remain.[29-35] The concept of using NO to treat wound infections has been proposed by Ghaffari et al., who demonstrated that gaseous NO kills bacteria and enhances wound healing.[46, 66, 67] Barraud et al. also noted that NO-releasing small molecules promote dispersal of *P. aeruginosa* biofilms.[68] As an alternative approach to avoid the use of cumbersome NO gas tanks and extend studies to other species of biofilm-forming pathogens, Chapter 4 described bactericidal NO-releasing silica nanoparticles. Silica nanoparticles modified to release NO killed planktonic *P. aeruginosa* cells more effectively than a small molecule NO donor.[49] To extend these studies to understand the efficacy of NO against established biofilms, biofilms were first formed on medical-grade silicone rubber squares. The biofilms were then exposed to NO-releasing silica nanoparticles suspended in PBS. In this manner, the experimental

protocol mimics the established Minimum Biofilm Eradication Concentration (MBEC) assay.[69]

The NO-releasing silica nanoparticles employed have been characterized and described previously.[52, 53, 70] As shown in Figure 5.5 A, the total amount of NO (t[NO]) released by 45 mol% AHAP3 silica nanoparticles was approximately 3.8 μmol mg^{-1}, with a maximum NO flux ($[NO]_m$) of 21700 ppb mg^{-1} and a NO release half life ($t_{1/2}$) of 18 min. In contrast, NO release from 70 mol% MAP3 nanoparticles was more rapid, with a $t_{1/2}$ of ~6 min. The amount of NO released from the MAP3 nanoparticles was greater than from the AHAP3 nanoparticles, with t[NO] and $[NO]_m$ values of 7.6 μmol mg^{-1} and 190000 ppb mg^{-1}, respectively, for MAP3 (Fig. 5.5 B). As characterized by atomic force microscopy (AFM), the AHAP3 and MAP3 nanoparticles were 136 ± 15 and 90 ± 10 nm in diameter, respectively (data not shown).[49, 70]

To test the influence of the delivery vehicle (i.e., AHAP3 vs. MAP3 silica nanoparticles) on NO's ability to kill biofilm-embedded bacterial cells, *P. aeruginosa* biofilms were grown on silicone rubber substrates and exposed to a range of concentrations of both AHAP3 and MAP3 nanoparticles (0 – 8 mg/mL). After exposure to the NO-releasing nanoparticles, the biofilm cells were removed from the substrates via sonication.[69, 71, 72] The resulting cell suspensions were diluted and plated on nutrient agar to quantitatively determine the number of viable cells recovered from each biofilm. As shown in Figure 5.6, AHAP3 nanoparticles administered at a dose of 8 mg/mL exhibited approximately 2 logs of biofilm eradication (i.e., the number of viable cells was reduced from ~2 x 10^7 to ~3 x 10^5 CFU). A 2-log reduction represents killing 99% of the cells within the biofilm. When administered at an equivalent dose (i.e., 8 mg/mL), MAP3 nanoparticles resulted in >5 logs of eradication,

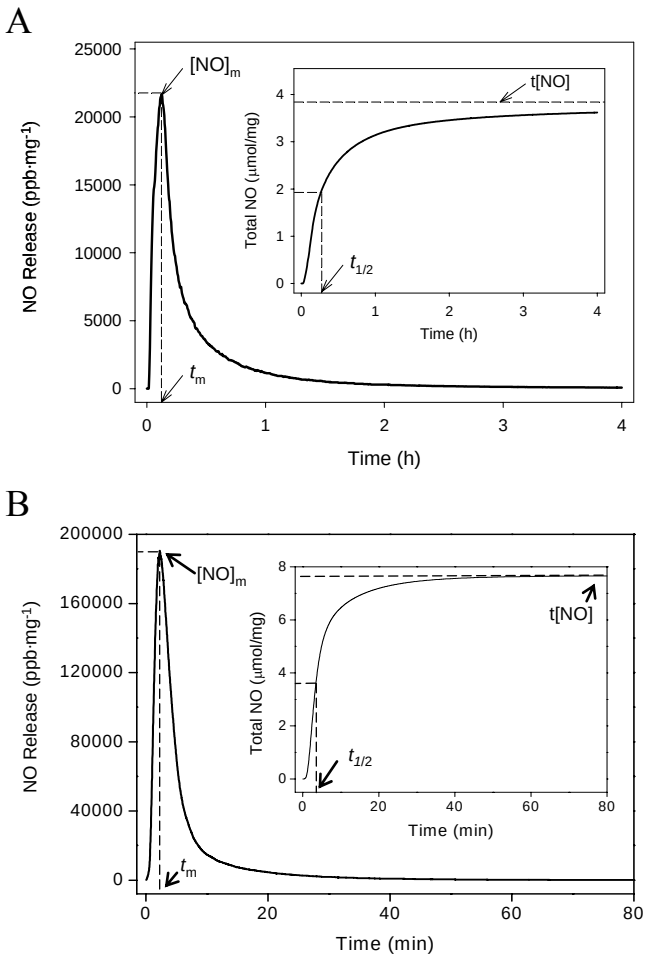

Figure 5.5. Nitric oxide release profiles of (A) 45 mol% AHAP3 and (B) 70 mol% MAP3 silica nanoparticles (balance TEOS). Insets represent total NO release. $[NO]_m$ = maximum NO flux; t_m = time to reach maximum NO flux; t[NO] = total NO released; $t_{1/2}$ = half life of NO release.

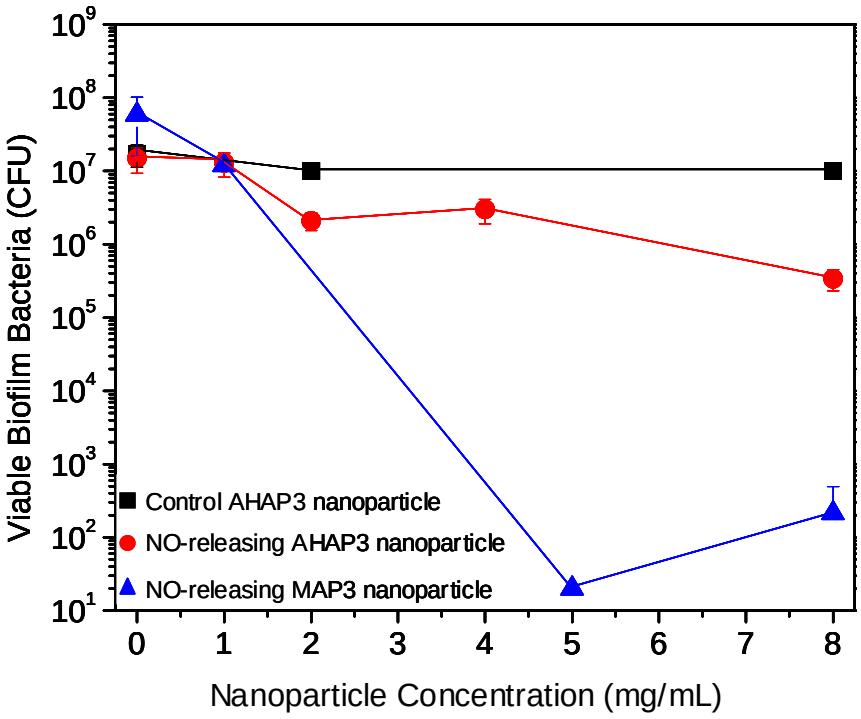

Figure 5.6. Anti-biofilm efficacy of 45 mol% AHAP3 silica nanoparticles (control and NO-releasing) and NO-releasing 70 mol% MAP3 silica nanoparticles against established *P. aeruginosa* biofilms on medical-grade silicone rubber substrates.

reducing the number of viable biofilm bacteria from ~7 x 10^7 to ~3 x 10^2, effectively killing >99.999% of biofilm bacterial cells. Both AHAP3 and MAP3 control nanoparticles (i.e., depleted of NO) exhibited no significant anti-biofilm efficacy, suggesting that the NO itself accounts for the killing.

At equivalent doses (i.e., 8 mg/mL), the MAP3 silica nanoparticles demonstrated ~1000-fold greater efficacy against *P. aeruginosa* biofilms than AHAP3 nanoparticles. While MAP3 nanoparticles release more total NO than AHAP3 nanoparticles per mg (7.6 vs. 3.8 μmol mg^{-1}, respectively), the 1000-fold increase in killing cannot be accounted for by the 2-fold increase in t[NO] alone. It is hypothesized that in addition to the greater amount of NO released by MAP3 nanoparticles, the more rapid delivery, as indicated by shorter $t_{1/2}$, leads to a greater instantaneous concentration of NO in solution. The greater concentration of NO in solution may result in enhanced diffusion of NO into the biofilm matrix, where NO-induced cell death occurs. Other explanations for the improved anti-biofilm efficacy of MAP3 nanoparticles may include their smaller size potentially allowing them to permeate the biofilm matrix more effectively, and/or a possible difference in the surface charge of the particles due to the different identity and amount of synthetic precursors (i.e., AHAP3 vs MAP3) employed. Studies to determine the influence of particle size and surface charge on anti-biofilm efficacy are currently planned. Due to their enhanced efficacy over AHAP3 nanoparticles, MAP3 nanoparticles were used as the NO delivery vehicle for the remainder of the studies.

The anti-biofilm properties of MAP3 nanoparticles were tested against a broad spectrum of biofilm-forming pathogens, including gram-negative (*P. aeruginosa* and *E. coli*), gram-positive (*S. aureus* and *S. epidermidis*), and fungal (*C. albicans*) species. As shown in

Figure 5.7, nanoparticle-derived NO was effective against all species tested. Anti-biofilm efficacy was greatest against the gram-negative species, with >5 logs of killing at the highest dose tested (8 mg/mL) for both *P. aeruginosa* and *E. coli*. Intermediate efficacy was observed for *C. albicans*, with 8 mg/mL MAP3 nanoparticles achieving 3 logs of biofilm killing. The least susceptible biofilms were those formed using gram-positive species (*S. aureus* and *S. epidermidis*), with the highest dose of nanoparticles killing ~2 logs of biofilm bacteria. Nevertheless, a 2-log reduction represents 99% killing of biofilm-embedded cells, a significant decrease that may reduce the bacterial bioburden in an infected wound and help enhance wound healing.[2] The efficacy of the nanoparticles against biofilms of all species tested is summarized in Table 5.1. As shown in Figure 5.8, control MAP3 silica nanoparticles (i.e., depleted of NO) at 8 mg/mL demonstrated no significant anti-biofilm activity against any species, indicating that the NO itself, and not the particle scaffold, is responsible for the observed anti-biofilm properties.

Several aspects of NO-releasing silica nanoparticles show promise with respect to treating wound-based biofilms. Healing is impaired when the bacterial bioburden within a wound is greater than 10^5 bacterial cells per gram of tissue.[2] In all cases, the NO-releasing silica nanoparticles were shown to reduce the number of viable biofilm cells by ≥2 orders of magnitude (i.e., ≥99% killing), a desirable characteristic that may lower the bioburden to levels below the infection threshold, allowing normal healing to progress. A second promising finding is that the anti-biofilm activity of the nanoparticles is broad-spectrum. While NO-releasing nanoparticles were found to be most effective against gram-negative species, the ability to kill multiple pathogens, including gram-positive and fungal-based biofilms, is promising for wound infections that are most often polymicrobial (i.e., caused by

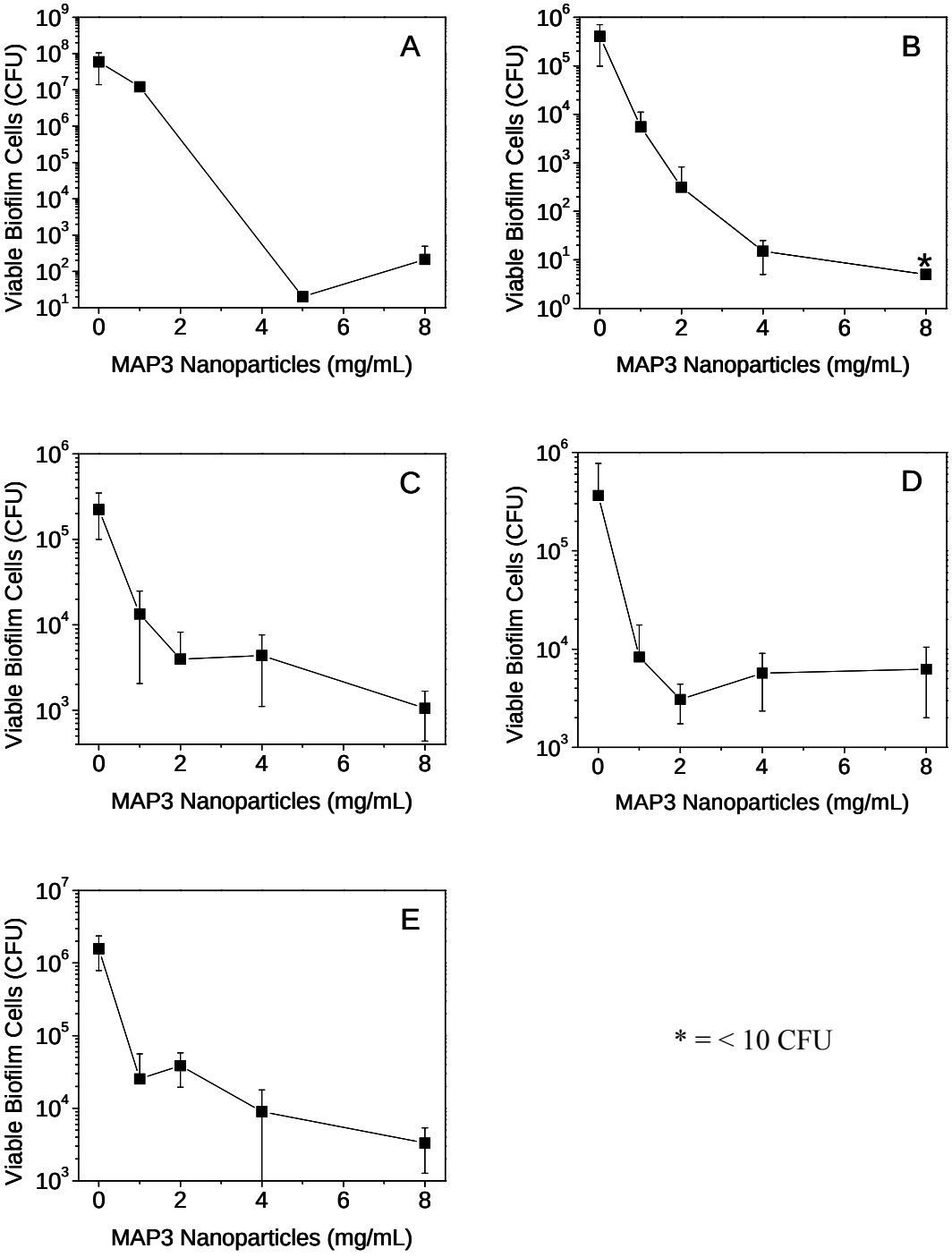

Figure 5.7. Broad spectrum anti-biofilm properties of 70 mol% MAP3 silica nanoparticles (balance TEOS) against (A) *P. aeruginosa* and (B) *E. coli* (gram-negative); (C) *S. aureus* and (D) *S. epidermidis* (gram-positive); and (D) *C. albicans* (pathogenic fungus) biofilms.

Table 5.1. Log-based and percent reductions in biofilm viability at the highest dose of NO-releasing MAP3 silica nanoparticles tested (8 mg/mL) compared to controls (0 mg/mL nanoparticles).

Species	Classification	Log reduction	Percent reduction
P. aeruginosa	gram (-)	5	99.999%
E. coli	gram (-)	5	99.999%
S. aureus	gram (+)	2	99%
S. epidermidis	gram (+)	2	99%
C. albicans	pathogenic fungus	3	99.9%

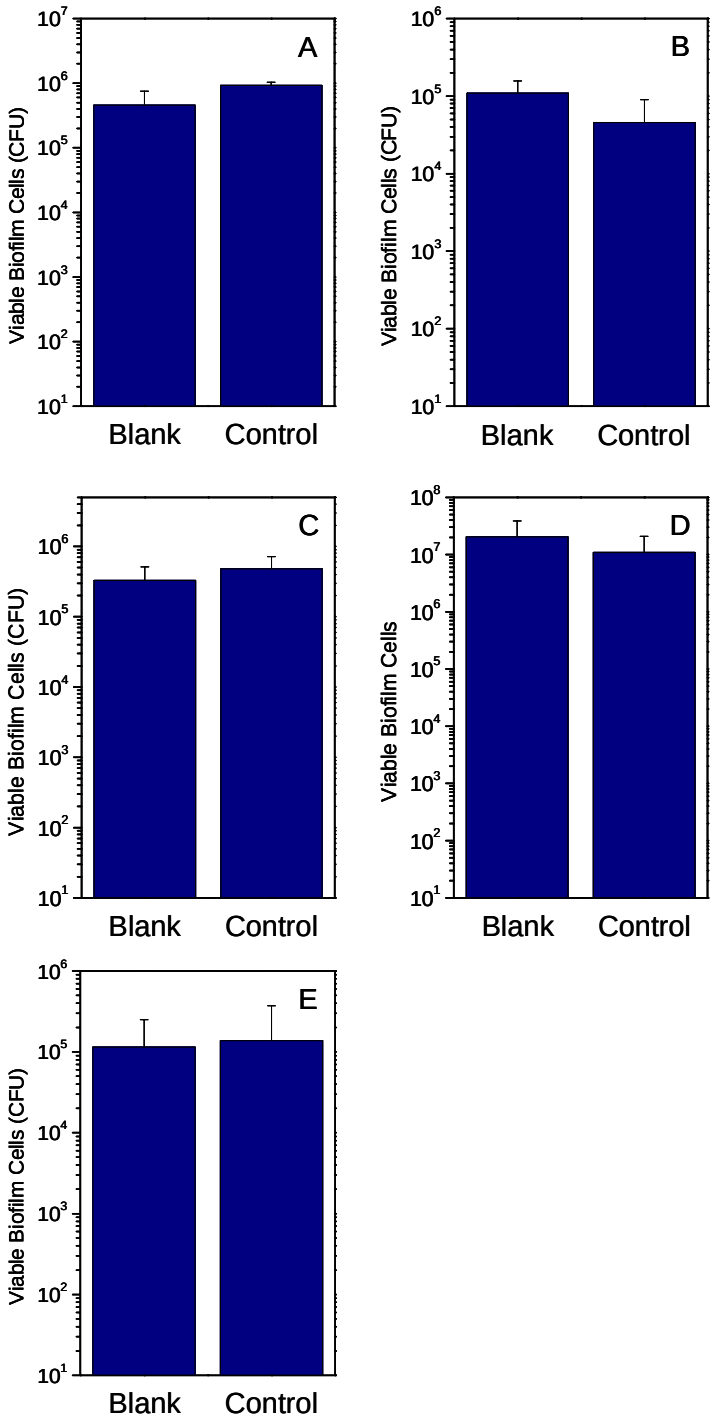

Figure 5.8. Viable cells recovered from biofilms of (A) *P. aeruginosa*, (B) *E. coli*, (C) *S. aureus*, (D) *S. epidermidis*, and (E) *C. albicans* after no treatment (Blank) and exposure to 8 mg/mL control 70 mol% MAP3 (balance TEOS) silica nanoparticles depleted of NO (Control).

more than one species).[73] Finally, the extreme efficacy against both *P. aeruginosa* and *E. coli* (>99.999% biofilm killing for both species) is promising for the treatment of infections due to gram-negative bacteria. Such species are more invasive than gram-positive infections, and thus more difficult to treat.[73] Gram-negative pathogens also exhibit other virulence factors including toxins, proteolytic enzymes, and extracellular polysaccharides[73] that coupled with the increasing antibiotic resistance of gram-negative species[74-76] present a significant threat to implant recipients.

5.3.3 Cytotoxicity of MAP3 nanoparticles to mammalian fibroblasts. In addition to testing the anti-biofilm properties of NO-releasing silica nanoparticles, their toxicity to healthy mammalian cells was also studied. Due to their potential utility as a therapeutic for wound-based infections, the toxicity of the particles was tested against fibroblast cells. Such cells are important to wound healing, helping maintain the extracellular matrix.[77, 78] Previous studies have shown that NO-releasing 45 mol% AHAP3 silica nanoparticles exhibited minimal (<10%) acute toxicity to fibroblasts at concentrations up to 1 mg/mL.[49] In the present study the concentration range was expanded to 8 mg/mL to include the highest dose tested against microbial biofilms. As shown in Figure 5.9, both control and NO-releasing silica nanoparticles reduced the proliferation of L929 fibroblasts at particle concentrations beyond 1 mg/mL. At 8 mg/mL, control and NO-releasing nanoparticles inhibited fibroblast proliferation by approximately 50 and 70%, respectively. Surprisingly, greater amounts of NO did not result in greater toxicity to the fibroblasts. In fact, increasing the NO delivery by increasing the silica nanoparticle concentration from 1 to 8 mg/mL improved the fibroblast viability. Of note, the observed toxicity is minimal compared to other commonly-applied topical antiseptics.[29, 79] For example, Pyo et al. found that administering clinical

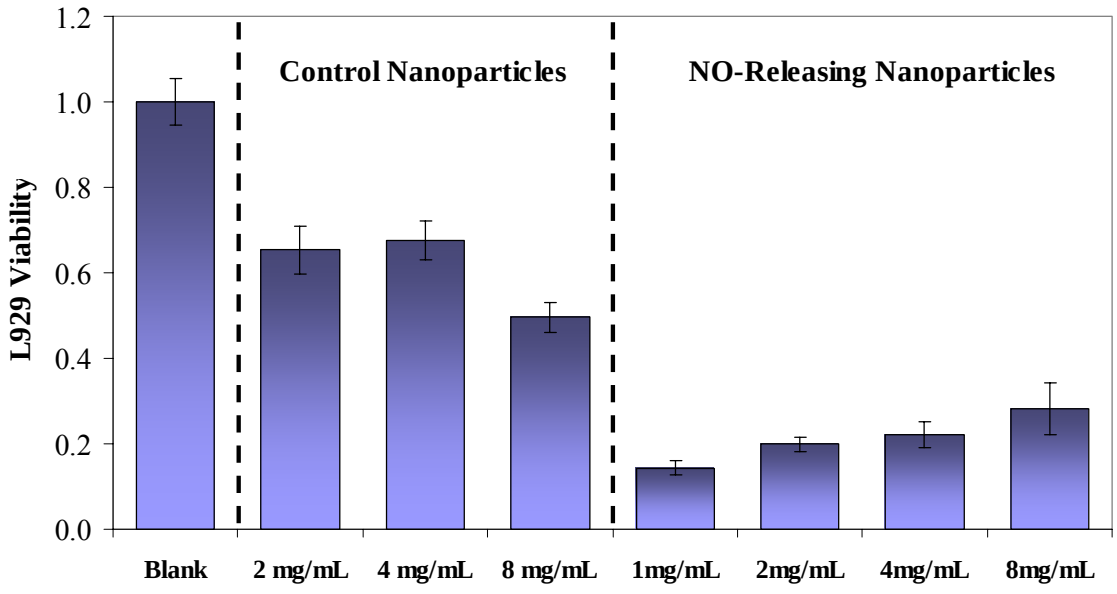

Figure 5.9. Viability of L929 mouse fibroblasts exposed to control and NO-releasing 70 mol% MAP3 silica nanoparticles (balance TEOS) at various concentrations. Viability was measured via MTT reduction by metabolically-active (viable) fibroblast cells and is expressed normalized to untreated fibroblasts.

concentrations of povidone iodine and chlorhexidine to human fibroblasts reduced cell viability by 89 ± 4% and 100 ± 4%, respectively.[79] Despite considerable in vitro toxicity to fibroblasts, clinical application of both povidone iodine and chlorhexidine has been demonstrated to enhance wound healing by killing wound-based microbes.[21] Thus, the in vitro toxicity observed for the NO-releasing silica nanoparticles should not undermine their potential as a treatment for wound-based biofilms.

5.4 Conclusions

Xerogel polymers modified to release NO were shown to reduce surface proliferation of a pathogenic bacterial species (*P. aeruginosa*). A threshold NO flux of ~15 pmol cm^{-2} s^{-1} was identified as necessary to inhibit *P. aeruginosa* proliferation. The 40% AHAP3 xerogel polymers examined herein are capable of maintaining NO fluxes above this threshold for approximately 12 h, well in excess of the 6-h "critical window" necessary for effective tissue integration. Thus, it is expected that applying a NO-releasing coating to an indwelling medical device may prevent bacterial adhesion and surface colonization for periods long enough to allow for effective tissue integration, thus greatly reducing the possibility of device-associated infection. Future work must focus on other biofilm-forming pathogens (e.g., *S. aureus* and *S. epidermidis*) for which different NO-release thresholds may be required to limit proliferation. Indeed, it has been shown that different bacterial/fungal species exhibit varying susceptibilities to NO as an antimicrobial agent. It will become important to design surfaces capable of inhibiting adhesion and proliferation of all pathogens common to device-associated infections as such infections are commonly polymicrobial (i.e., caused by more than one species).

Additionally, NO-releasing silica nanoparticles proved to be effective against gram-negative, gram-positive, and fungal biofilms. When compared to AHAP3 nanoparticles, MAP3 nanoparticles exhibited a 1000-fold improvement in efficacy, suggesting that rapid delivery of NO is more effective at biofilm eradication than slow/prolonged NO delivery. The MAP3 silica nanoparticles demonstrated anti-biofilm activity against a range of pathogens with the greatest efficacy (≥99.999% killing) against the species most problematic for wound infections (i.e., gram-negative bacteria). The toxicity of the nanoparticles to fibroblasts was also examined and found to be comparable to or less than currently-applied antiseptics with proven wound-healing benefits. Experiments are currently underway to examine possible synergistic enhancement of NO treatment with other antibacterial agents, including silver ion and traditional antibiotics. It will become important to understand the role of nanoparticle size on anti-biofilm efficacy. This and other parameters (i.e., surface charge, hydrophobicity, etc.) are easily tuned during synthesis by varying the solvent and/or precursor types and concentrations. Nanoparticle size may also influence cytotoxicity to healthy cells. A primary advantage of nanoparticle-based drug delivery involves the ability to graft different ligands to the nanoparticle surface to target the particles to particular cells. Ligands useful for promoting the antimicrobial efficacy of NO-releasing silica nanoparticles may include antibodies and/or sugars, both of which may promote nanoparticle association with and/or uptake by bacterial cells. Modifications to nanoparticle synthesis to alter the charge of the nanoparticles will also be examined to possibly exploit the difference in electrostatic properties between gram-negative and gram-positive biofilms. In terms of its application to wounds, NO release is expected to exert beneficial secondary effects on the healing process. Nitric oxide has been shown to modulate both inflammation and

angiogenesis, as well as participate in matrix remodeling and re-epithelialization. In general, chronic wounds have been shown to be deficient in NO. Application of NO-releasing silica nanoparticles may speed healing by both killing bacteria and overcoming the general NO deficiency. To understand the dose of NO necessary to promote wound healing and aid the host response to infection, in vivo wound-healing experiments (both with and without bacterial challenge) will be necessary.

5.5 References

(1) Hetrick, E. M.; Schoenfisch, M. H. "Reducing implant-associated infections: Active release strategies." *Chem. Soc. Rev.* **2006,** *9*, 780-789.

(2) Ryan, T. J. "Infection following soft tissue injury: Its role in wound healing." *Curr. Opin. Infect. Dis.* **2007,** *20*, 124-128.

(3) O'Grady, N. P.; Alexander, M.; Dellinger, E. P.; Gerberding, J. L.; Heard, S. O.; Maki, D. G.; Masur, H.; McCormick, R. D.; Mermel, L. A.; Pearson, M. L.; Raad, I. I.; Randolph, A.; Weinstein, R. A. "Guidelines for the prevention of intravascular catheter-related infections." *Morbidity and Mortality Weekly Report* **2002,** *51(RR10)*, 1-26.

(4) Muto, C.; Herbert, C.; Harrison, E.; Edwards, J. R.; Horan, T.; Andrus, M.; Jernigan, J. A.; Kutty, P. K. "Reduction in central line-associated bloodstream infections among patients in intensive care units -- Pennsylvania, April 2001 - March 2005." *Morbidity and Mortality Weekly Report* **2005,** *54*, 1013-1016.

(5) "Burns Fact Sheet." *Mass Cas. Prepared. Respon.* **2006**, U.S. Centers for Disease Control and Prevention, pp 1-5.

(6) DeQueiroz, G. A.; Day, D. F. "Antimicrobial activity and effectiveness of a combination of sodium hypochlorite and hydrogen peroxide in killing and removing *Pseudomonas aeruginosa* biofilms from surfaces." *J. Appl. Microbiol.* **2007,** *103*, 794-802.

(7) Smith, A. W. "Biofilms and antibiotic therapy: Is there a role for combating bacterial resistance by the use of novel drug delivery systems?" *Adv. Drug Delivery Rev.* **2005,** *57*, 1539-1550.

(8) Davis, S. C.; Martinez, L.; Kirsner, R. "The diabetic foot: The importance of biofilms and wound bed preparation." *Curr. Diabet. Rep.* **2006,** *6*, 439-445.

(9) Mah, T.; O'Toole, G. "Mechanisms of biofilm resistance to antimicrobial agents." *Trends Microbiol.* **2001,** *9*, 34-39.

(10) Kingshott, P.; Wei, J.; Bagge-Ravn, D.; Gadegaard, N.; Gram, L. "Covalent attachment of poly(ethylene glycol) to surfaces, critical for reducing bacterial adhesion." *Langmuir* **2003,** *19*, 6912-6921.

(11) Kaper, H. J.; Busscher, H. J.; Norde, W. "Characterization of poly(ethylene oxide) brushes on glass surfaces and adhesion of *Staphylococcus epidermidis*." *J. Biomater. Sci., Polym. Ed.* **2003,** *14*, 313-324.

(12) Nagel, J. A.; Dickinson, R. B.; Cooper, S. L. "Bacterial adhesion to polyurethane surfaces in the presence of pre-adsorbed high molecular weight kininogen." *J. Biomater. Sci., Polym. Ed.* **1996,** *7*, 769-780.

(13) Fu, J.; Ji, J.; Yuan, W.; Shen, J. "Construction of anti-adhesive and antibacterial multilayer films via layer-by-layer assembly of heparin and chitosan." *Biomaterials* **2005,** *26*, 6684-6692.

(14) Broekhuizen, C. A. N.; de Boer, L.; Schipper, K.; Jones, C. D.; Quadir, S.; Feldman, R. G.; Dankert, J.; Vandenbroucke-Grauls, C. M. J. E.; Weening, J. J.; Zaat, S. A. J. "Peri-implant tissue is an important niche for *Staphylococcus epidermidis* in experimental biomaterial-associated infection in mice." *Infect. Immun.* **2007,** *75*, 1129-1136.

(15) Broekhuizen, C. A. N.; de Boer, L.; Schipper, K.; Jones, C. D.; Quadir, S.; Vandenbroucke-Grauls, C. M. J. E.; Zaat, S. A. J. "*Staphylococcus epidermidis* is cleared from biomaterial implants but persists in peri-implant tissue in mice despite rifampicin/vancomycin treatment." *J. Biomed. Mater. Res.* **2008,** *85A*, 498-505.

(16) Singh, V. A.; Barbul, A. "Bacterial biofilms in wounds." *Wound Rep. Reg.* **2008,** *16*, 1.

(17) James, G. A.; Swogger, E.; Wolcott, R.; deLancey Pulcini, E.; Secor, P.; Sestrich, J.; Costerton, J. W.; Stewart, P. S. "Biofilms in chronic wounds." *Wound Rep. Reg.* **2008,** *16*, 37-44.

(18) Davis, S. C.; Ricotti, C.; Cazzaniga, A.; Welsh, E.; Eaglstein, W. H.; Mertz, P. M. "Microscopic and physiologic evidence for biofilm-associated wound colonization in vivo." *Wound Rep. Reg.* **2008,** *16*, 23-29.

(19) Bjarnsholt, T.; Kirketerp-Moller, K.; Jensen, P. O.; Madsen, K. G.; Phipps, R.; Krogfelt, K.; Hoiby, N.; Bivskov, M. "Why chronic wounds will not heal: A novel hypothesis." *Wound Rep. Reg.* **2008,** *16*, 2-10.

(20) Percival, S. L.; Bowler, P.; Woods, E. J. "Assessing the effect of an antimicrobial wound dressing on biofilms." *Wound Rep. Reg.* **2008,** *16*, 52-57.

(21) White, R. J.; Cutting, K.; Kingsley, A. "Topical antimicrobials in the control of wound bioburden." *Ostomy/Wound Management* **2006,** *52*, 26-58.

(22) Bowler, P. G.; Duerden, B. I.; Armstrong, D. G. "Wound microbiology and associated approaches to wound management." *Clin. Microbiol. Rev.* **2001,** *14*, 244-269.

(23) Ebright, J. R. "Microbiology of chronic leg and pressure ulcers: Clinical significance and implications for treatment." *Nurs. Clin. North Am.* **2005,** *40*, 207-216.

(24) Eron, L. J.; Lipsky, B. A.; Low, D. E.; Nathwani, D.; Tice, A. D.; Volturo, G. A. "Managing skin and soft tissue infections: Expert panel recommendations on key decision points." *J. Antimicrob. Chemother.* **2003,** *52*, i3-i17.

(25) Wright, J. B.; Lam, K.; Burrell, R. E. "Wound management in an era of increasing bacterial antibiotic resistance: A role for topical silver treatment." *Am. J. Infect. Control* **1998,** *26*, 572-577.

(26) "Bad bugs, no drugs: As antibiotic discovery stagnates, a public health crisis brews." *Infectious Diseases Society of America* **2004**, 1-35.

(27) Silver, S. "Bacterial silver resistance: Molecular biology and uses and misuses of silver compounds." *FEMS Microbiol. Rev.* **2003,** *27*, 341-353.

(28) Li, X. Z.; Nikaido, H.; Williams, K. E. "Silver-resistant mutants of *Escherichia coli* display active efflux of Ag^{+} and are deficient in porins." *J. Bacteriol.* **1997,** *179*, 6127-6132.

(29) Balin, A. K.; Pratt, L. "Dilute povidone-iodine solutions inhibit human skin fibroblast growth." *Dermatol. Surg.* **2002,** *28*, 210-214.

(30) Rodeheaver, G. "Controversies in topical wound management." *WOUNDS* **1989,** *1*, 19-27.

(31) Lawrence, J. C. "The use of iodine as an antiseptic agent." *J. Wound Care* **1998,** *7*, 421-425.

(32) Lawrence, J. C. "A povidone-iodine medicated dressing." *J. Wound Care* **1998,** *7*, 332-336.

(33) Thomas, C. "Nursing alert - wound healing halted with the use of povidone iodine." *Ostomy/Wound Management* **1988,** *18*, 30-33.

(34) Goldheim, P. D. "An Appraisal of povidone-iodine and wound healing." *Postgrad. Med. J.* **1993,** *69 (Suppl.)*, S97-S105.

(35) Gulliver, G. "Arguments over iodine." *Nurs. Times* **1999,** *95*, 68-70.

(36) Stickler, D.; Hewett, P. "Activity of antiseptics against biofilms of mixed bacterial species growing on silicone surfaces." *Eur. J. Clin. Microbiol. Infect. Dis.* **1991,** *10*, 157-162.

(37) Presterl, E.; Suchomel, M.; Eder, M.; Reichmann, S.; Lassnigg, A.; Graninger, W.; Rotter, M. "Effects of alcohols, povidone-iodine and hydrogen peroxide on biofilms of *Staphylococcus epidermidis*." *J. Antimicrob. Chemother.* **2007,** *60*, 417-420.

(38) Torricelli, R.; Wuthrich, B. "Life-threatening anaphylactic shock due to skin application of chlorhexidine." *Clin. Experiment. Allergy* **1996,** *26*, 112.

(39) Autegarden, J. E.; Pecquet, C.; Huet, S.; Bayrou, O.; Leynadier, F. "Anaphylactic shock after application of chlorhexidine to unbroken skin." *Contact Dermatitis* **1999,** *40*, 215.

(40) Krautheim, A. B.; Jermann, T. H. M.; Bircher, A. J. "Chlorhexidine anaphylaxis: Case report and review of the literature." *Contact Dermatitis* **2004,** *50*, 113-116.

(41) Meiller, T. F.; Kelley, J. I.; Jabra-Rizk, M. A.; DePaola, L. G.; Baqui, A. A. M. A.; Falkler, W. A. "In vitro studies of the efficacy of antimicrobials against fungi." *Oral Surg. Oral. Med. Oral Pathol. Oral Radiol. Endod.* **2001,** *91*, 663-670.

(42) Fang, F. C. "Mechanisms of nitric oxide-related antimicrobial activity." *J. Clin. Invest.* **1997,** *99*, 2818-2825.

(43) Fang, f. C. "Antimicrobial reactive oxygen and nitrogen species: Concepts and controversies." *Nat. Rev. Microbiol.* **2004,** *2*, 820-832.

(44) MacMicking, J.; Xie, Q.; Nathan, C. "Nitric oxide and macrophage function." *Annu. Rev. Immunol.* **1997,** *15*, 323-350.

(45) Raulli, R.; McElhaney-Feser, G.; Hrabie, J. A.; Cihlar, R. L. "Antimicrobial properties of nitric oxide using diazeniumdiolates as the nitric oxide donor." *Rec. Res. Devel. Microbiol.* **2002,** *6*, 177-183.

(46) Ghaffari, A.; Miller, C. C.; McMullin, B.; Ghahary, A. "Potential application of gaseous nitric oxide as a topical antimicrobial agent." *Nitric Oxide* **2006,** *14*, 21-29.

(47) Hetrick, E. M.; Schoenfisch, M. H. "Antibacterial nitric oxide-releasing xerogels: Cell viability and parallel plate flow cell adhesion studies." *Biomaterials* **2007,** *28*, 1948-1956.

(48) Vacheethasanee, K.; Marchant, R. E., *Nonspecific Staphylococcus epidermidis adhesion: Contributions of biomaterial hydrophobicity and charge*. Humana Press: Totowa, NJ, 2000.

(49) Hetrick, E. M.; Shin, J. H.; Stasko, N. A.; Johnson, C. B.; Wespe, D. A.; Holmuhamedov, E.; Schoenfisch, M. H. "Bactericidal efficacy of nitric oxide-releasing silica nanoparticles." *ACS Nano* **2008,** *2*, 235-246.

(50) Lancaster, J. R. "A tutorial on the diffusability and reactivity of free nitric oxide." *Nitric Oxide: Biology and Chemistry* **1997,** *1*, 18-30.

(51) Marxer, S. M.; Rothrock, A. R.; Nablo, B. J.; Robbins, M. E.; Schoenfisch, M. H. "Preparation of nitric oxide (NO)-releasing sol-gels for biomaterial applications." *Chem. Mater.* **2003,** *15*, 4193-4199.

(52) Shin, J. H.; Metzger, S. K.; Schoenfisch, M. H. "Synthesis of nitric oxide-releasing silica nanoparticles." *J. Am. Chem. Soc.* **2007,** *129*, 4612-4619.

(53) Shin, J. H.; Schoenfisch, M. H. "Inorganic/organic hybrid silica nanoparticles as a nitric oxide delivery scaffold." *Chem. Mater.* **2008,** *20*, 239-249.

(54) Beckman, J. S.; Conger, K. A. "Direct measurement of dilute nitric oxide in solution with an ozone chemiluminescent detector." *Methods in Enzymology* **1995,** *7*, 35-39.

(55) Poelstra, K. A.; van der Mei, H. C.; Gottenbos, B.; Grainger, D. W.; van Horn, J. R.; Busscher, H. J. "Pooled human immunoglobulins reduce adhesion of *Pseudomonas aeruginosa* in a parallel plate flow chamber." *J. Biomed. Mater. Res.* **2000,** *51*, 224-232.

(56) Mosmann, T. "Rapid colorimetric assay for cellular growth and survival: Application to proliferation and cytotoxicity assays." *J. Immunol. Methods* **1983,** *65*, 55-63.

(57) Nablo, B. J.; Chen, T. Y.; Schoenfisch, M. H. "Sol-gel derived nitric-oxide releasing materials that reduce bacterial adhesion." *J. Am. Chem. Soc.* **2001,** *123*, 9712-9713.

(58) Nablo, B. J.; Schoenfisch, M. H. "Antibacterial properties of nitric oxide-releasing sol-gels." *J. Biomed. Mater. Res.* **2003,** *67A*, 1276-1283.

(59) Nablo, B. J.; Schoenfisch, M. H. "Poly(vinyl chloride)-coated sol-gels for studying the effects of nitric oxide release on bacterial adhesion." *Biomacromolecules* **2004,** *5*, 2034-2041.

(60) Nablo, B. J.; Rothrock, A. R.; Schoenfisch, M. H. "Nitric oxide-releasing sol-gels as antibacterial coatings for orthopedic implants." *Biomaterials* **2005,** *26*, 917-924.

(61) Hetrick, E. M.; Prichard, H. L.; Klitzman, B.; Schoenfisch, M. H. "Reduced foreign body response at nitric oxide-releasing subcutaneous implants." *Biomaterials* **2007,** *28*, 4571-4580.

(62) Wink, D. A.; Mitchell, J. B. "Chemical biology of nitric oxide: Insights into regulatory, cytotoxic, and cytoprotective mechanisms of nitric oxide." *Free Radical Biol. Med.* **1998,** *25*, 434-456.

(63) Moller, M. N.; Li, Q.; Lancaster, J. R.; Denicola, A. "Acceleration of nitric oxide autoxidation and nitrosation by membranes." *IUBMB Life* **2007,** *59*, 243-248.

(64) Gristina, A. G. "Biomaterial-centered infection: Microbial adhesion vs. tissue integration." *Science* **1987,** *237*, 1588-1595.

(65) Poelstra, K. A.; Barekzi, N. A.; Rediske, A. M.; Felts, A. G.; Slunt, J. B.; Grainger, D. W. "Prophylactic treatment of gram-positive and gram-negative abdominal implant infections using locally-delivered polyclonal antibodies." *J. Biomed. Mater. Res.* **2002,** *60*, 206-215.

(66) Miller, C. C.; Miller, M. K.; Ghaffari, A.; Kunimoto, B. "Treatment of chronic nonhealing leg ulceration with gaseous nitric oxide: A case study." *J. Cutaneous Med. Surg.* **2004,** *8*, 233-238.

(67) Ghaffari, A.; Neil, D. H.; Ardakani, A.; Road, J.; Ghahary, A.; Miller, C. C. "A direct nitric oxide gas delivery system for bacterial and mammalian cell cultures." *Nitric Oxide* **2005,** *12*, 129-140.

(68) Barraud, N.; Hassett, D. J.; Hwang, S. H.; Rice, S. A.; Kjelleberg, S.; Webb, J. S. "Involvement of nitric oxide in biofilm dispersal of *Pseudomonas aeruginosa*." *J. Bacteriol.* **2006,** *188*, 7344-7353.

(69) Ceri, H.; Olson, M.; Morck, D.; Storey, D.; Read, R.; Buret, A.; Olson, B. "The MBEC assay system: Multiple equivalent biofilms for antibiotic and biocide susceptibility testing." *Methods Enzymol.* **2001,** *337*, 377-385.

(70) Shin, J. H.; Stevens, E. V.; Der, C.; Schoenfisch, M. H. "Nitric oxide-releasing silica nanoparticles: Synthesis, characterization, and efficacy against ovarian cancer cells." *PMSE Preprints* **2006,** *95*, 685-686.

(71) Martineau, L.; Dosch, H. M. "Biofilm reduction by a new burn gel that targets nociception." *J. Appl. Microbiol.* **2007,** *103*, 297-304.

(72) Giacometti, A.; Cirioni, O.; Ghiselli, R.; Orlando, F.; Silvestri, C.; Renzone, G.; Testa, I.; Mocchegiani, F.; Vittoria, A. D.; Saba, V.; Scaloni, A.; Scalise, G. "Distinctin improves the efficacies of glycopeptides and betalactams against staphylococcal biofilm in an experimental model of central venous catheter infection." *J. Biomed. Mater. Res.* **2007,** *81A*, 233-239.

(73) Pruitt, B. A.; McManus, A. T.; Kim, S. H.; Goodwin, C. W. "Burn wound infections: Current status." *World J. Surg.* **1998,** *22*, 135-145.

(74) Ruiz, C.; McMurry, L. M.; Levy, S. B. "Role of the multidrug resistance regulator MarA in global regulation of the hdeAB acid resistance operon in *Escherichia coli*." *J. Bacteriol.* **2008,** *190*, 1290-1297.

(75) Lyczak, J. B.; Cannon, C. L.; Pier, G. B. "Establishment of *Pseudomonas aeruginosa* infection: Lessons from a versatile opportunist." *Microb. Infect.* **2000,** *2*, 1051-1060.

(76) Hsueh, P. R.; Teng, L. J.; Yang, P. C.; Chen, Y. C.; Ho, S. W.; Luh, K. T. "Persistence of a multidrug-resistant *Pseudomonas aeruginosa* clone in an invasive care burn unit." *J. Clin. Microbiol.* **1998,** *36*, 1347-1351.

(77) Wong, T.; McGrath, J. A.; Navsaria, H. "The role of fibroblasts in tissue engineering and regeneration." *British J. Dermatol.* **2007,** *156*, 1149-1155.

(78) Werner, S.; Krieg, T.; Smola, H. "Keratinocyte-fibroblast interactions in wound healing." *J. Invest. Dermatol.* **2007,** *127*, 998-1008.

(79) Pyo, H. C.; Kim, Y. K.; Whang, K. U.; Park, Y. L.; Eun, H. C. "A comparative study of cytotoxicity of topical antimicrobials to cultured human keratinocytes and fibroblasts." *Korean J. Dermatol.* **1995,** *33*, 895-906.

Chapter 6:

Summary and Future Research Directions

6.1 Summary

The ability of NO-releasing materials (i.e., xerogel films and silica nanoparticles) to both mitigate the foreign body response and act as antimicrobial surfaces/vehicles has been described. Chapter 2 described both the study of bacterial adhesion to xerogel substrates in a parallel plate flow cell and the viability of bacterial cells adhered to NO-releasing surfaces. The flow cell avoids the passage of an air-liquid interface and allows real-time tracking of bacterial adhesion. At a controlled bacterial suspension flow rate of 0.2 mL/min, the NO-releasing xerogels reduced bacterial adhesion in a flux-dependent fashion with a NO flux of ~21 pmol cm^{-2} s^{-1} reducing *P. aeruginosa* adhesion by ~65% compared to controls. When the flow rate was increased to 0.6 mL/min, the anti-adhesion properties of NO release were diminished, likely due to more rapid removal of interfacial NO. However, a significant decrease in bacterial adhesion was still observed at the higher flow rate compared to control surfaces. Fluorescent staining with SYTO-9 and propidium iodide viability probes indicated that bacterial cells adhered to NO-releasing xerogels were killed within 7 h. Quantitative cell-plating viability studies showed that the extent of bactericidal activity was dependent on the total amount of NO released, with 750 nmol cm^{-2} killing >90% more adhered bacteria than xerogels that released 25 nmol cm^{-2}. Thus, NO-releasing xerogels were shown to both

inhibit *P. aeruginosa* adhesion and kill adhered bacterial cells, two important steps toward designing anti-infective biomaterial coatings.

As discussed in Chapter 3, model silicone elastomer implants were employed to study the foreign body response in a rat model. One-third of the implants were coated with NO-releasing 40% AHAP3/BTMOS xerogel, one-third were coated with control xerogel (not modified to release NO), and one-third were left uncoated to serve as blanks. The implants were surgically inserted into the subcutaneous tissue of adult male Sprague-Dawley rats where they remained for one, three or six weeks. At each time point, implants and surrounding tissue were removed from the rats, fixed in formalin, and stained with either Gomori's trichrome, hematoxylin & eosin (H&E), or CD-31 immunohistochemical stain which is selective for an antigen on endothelial cells. Characteristic measures of the progression of the foreign body response at each type of implant were observed from optical micrographs of the stained tissue samples. Collagen capsule thickness at each type of implant was calculated from trichrome-stained samples. Nitric oxide-releasing samples were characterized by significantly ($p < 0.05$) thinner capsules than those observed at both blank and control implants. Angiogenesis, monitored from the CD-31-stained tissue samples, was significantly enhanced at the site of NO-releasing implants at the 1-week time point. The inflammatory response factor (IRF), monitored from H&E-stained tissue samples, was found to be significantly reduced after both three and six weeks compared to both blank and control implants. Collectively, the data indicate that delivery of NO (a total of ~1.35 μmol cm^{-2} of implant surface area over 3 d) was shown to significantly mitigate the foreign body response.

A study of the antibacterial efficacy of NO-releasing silica nanoparticles was presented in Chapter 4. Nitric oxide-releasing nanoparticles were prepared via co-

condensation of a tetraalkoxysilane (i.e., TEOS) with an aminoalkoxysilane (i.e., AHAP3) modified with diazeniumdiolate NO donors, allowing for the storage of large NO payloads.[1,2] Comparison of the bactericidal efficacy of the NO-releasing nanoparticles to PROLI/NO (i.e., diazeniumdiolate-modified proline), a small molecule NO donor, revealed enhanced bactericidal efficacy for the nanoparticle-derived NO. At bactericidal doses, PROLI/NO demonstrated 100% cytotoxicity to mammalian cells (L929 mouse fibroblasts), while >90% fibroblast viability was maintained in the presence of silica nanoparticles. Confocal microscopy revealed that fluorescently labeled NO-releasing nanoparticles associated with the bacterial cells, providing rationale for the enhanced bactericidal efficacy of the nanoparticles. Employing the NO-sensitive fluorescent probe DAF-2, intracellular NO delivery was observed when the NO was delivered from nanoparticles. In contrast, intracellular NO levels remained below the detection threshold when PROLI/NO was administered. Collectively, these results demonstrate the advantage of delivering NO via nanoparticles for antimicrobial applications.

Studies investigating the anti-biofilm properties of NO were described in Chapter 5. The first aspect of the study aimed at demonstrating the ability of surface-derived NO to prevent bacterial surface colonization, a critical step in the formation biofilms.[3] A second aspect focused on establishing the broad-spectrum anti-biofilm properties of NO-releasing silica nanoparticles. A surface flux of NO from a xerogel coating (40% AHAP3/BTMOS) proved capable of preventing proliferation of *P. aeruginosa* cells adhered to the substrate surface for 12 – 14 h. This period is well in excess of the 6-h "critical window" over which preventing bacterial colonization is most important for ensuring the long-term success of a medical implant.[4] The doubling time of *P. aeruginosa* cells adhered to control and NO-

releasing xerogel surfaces was 94 and 890 min, respectively. The anti-biofilm properties of NO-releasing silica nanoparticles were tested against biofilms of two gram-negative species (*P. aeruginosa* and *E. coli*), two gram-positive species (*S. aureus* and *S. epidermidis*), and a pathogenic fungus (*C. albicans*). At the highest concentration tested (8 mg/mL), the silica nanoparticles were most effective at eradicating gram-negative biofilms (>5 logs of killing) and least effective against gram-positive biofilms (2 logs of killing), with intermediate efficacy against *C. albicans* biofilms (3 logs of killing). Cytotoxicity testing against L929 mouse fibroblasts revealed that roughly 25% of cells remained viable compared to controls when treated with silica nanoparticles at 8 mg/mL. Such viability exceeded that observed when fibroblasts and keratinocytes were treated with clinically-relevant doses of other currently-employed wound antiseptics (e.g., povidone iodine and chlorhexidine).[5, 6]

6.2 Future research directions

The ability of NO-releasing xerogels to reduce bacterial adhesion under flowing conditions was presented in Chapter 2. Future research in this area should focus on testing the antimicrobial properties of NO-releasing xerogels against a broader library of pathogenic organisms. Of note, this process has been initiated by Charville et al., who reported on the ability of NO-releasing xerogels to reduce adhesion of *E. coli*, *S. aureus*, and *S. epidermidis*.[7] In that work, a mediating layer of the plasma protein fibrinogen was first adhered to the xerogel surface to more accurately mimic in vivo conditions. Future work should also seek to expand such protein-mediated bacterial adhesion studies to other plasma proteins known to influence bacterial adhesion in vivo, including fibronectin and vitronectin.[8, 9]

Another avenue of future study should involve new xerogel compositions currently in development. For example, Privett et al. have created a new class of xerogels capable of storing and releasing much greater levels of NO via pre-forming diazeniumdiolates on aminoalkoxysilanes prior to condensation with alkylalkoxysilanes.[10] In addition to bacterial adhesion assays, the efficacy of these new xerogel constructs at killing planktonic microbial cells should also be examined. Such studies would provide useful information about the ability of NO-releasing materials to kill bacteria that are not necessarily adhered to the substrate surface but which may reside in and infect tissue surrounding an implanted material.[11-13] In vivo studies should also be conducted to determine the efficacy of NO-release coatings at killing bacteria that infect the peri-implant tissue, as that region has been found to harbor bacteria when the associated implant becomes infected.[11-13] Finally, a primary advantage of the flow cell apparatus described in Chapter 2 is that it allows access to a range of physiologically-relevant shear forces, such as those present in arterial and venous regions of the cardiovascular system.[14] This attribute, coupled with the ability to introduce both individual plasma proteins and/or whole plasma to the immobilized substrate, makes the flow cell an attractive method for modeling bacterial adhesion at central venous catheters, which suffer from exceedingly high infection rates.[15, 16]

The results presented in Chapter 3 demonstrate the ability of implant-derived NO to mitigate the foreign body response. While these results show promise as a strategy for improving the biocompatibility of subcutaneous implants, other studies are required to more fully elucidate the mechanism of NO's activity as it relates to capsule formation, angiogenesis, and the inflammatory response. The xerogel system employed (40% AHAP3/BTMOS), released ~1.35 μmol of NO per cm^2 of implant surface area over 3 d. It

remains to be determined what threshold "dose" of NO must be released to observe reductions in the foreign body response, or if different kinetics of NO release may further alter the foreign body response. For example, NO release from the AHAP3 xerogel system occurs rapidly, with 50% of the total NO released within the first 5 h after immersion in buffer and >99% of the total NO release complete within 72 h. However, the tissue response at the implants was examined at 1, 3, and 6 weeks – periods after which the NO release had long been exhausted. Future efforts should focus on developing materials with extended NO release durations and determining the influence of NO flux on the foreign body response. Other research related to this work should focus on determining the cytokine profile elicited in tissue adjacent to control and NO-releasing implants. Cytokines important in the foreign body response that are known to be influenced by NO include transforming growth factor-β (TGF-β), vascular endothelial growth factor (VEGF), basic fibroblast growth factor (bFGF), macrophage chemoattractant protein-1 (MCP-1), and interleukin-6 (IL-6).[17-22] Studies to profile the expression of such cytokines may be accomplished by in vivo microdialysis experiments,[23-26] or by profiling whole explanted tissue samples with MALDI-TOF mass spectrometry.[27-29] Alternatively, in vitro experiments such as those developed by Reichert et al. may be conducted to determine the cytokine response of macrophages to NO-releasing xerogel materials.[30] Examination of the cytokine response should also be extended to other cell types, including fibroblasts, keratinocytes, and endothelial cells.

Future studies in the area of NO-releasing silica nanoparticles should focus on the antimicrobial activity of such particles against other species of pathogenic bacteria and fungi, including gram-positive species such as *S. aureus*, *S. epidermidis*, and *Enterococcus faecalis*. In addition to testing the AHAP3/TEOS nanoparticle system against other species of

pathogens, it will become important to determine the planktonic antimicrobial efficacy of different nanoparticle compositions with altered NO release kinetics. One of the main advantages of macromolecular drug delivery includes the ability to multi-functionalize the particle surface with targeting agents.[31, 32] Compounds that may prove useful for targeting NO-releasing nanoparticles to bacterial cells include antibodies (e.g., IgG)[33, 34] and peptides that include the RGD binding motif.[35] Further studies should focus on the antimicrobial efficacy of NO-releasing nanoparticles in combination with other antimicrobial agents such as Ag^+ and conventional antibiotics. Studies by McElhaney-Feser et al. have demonstrated synergy between small molecule NO-donors and azoles against fungal species.[36] Preliminary results from Johnson et al.[37] and Deupree et al.[38] have shown similar synergistic activity between NO and Ag^+ against bacteria. Additionally, the ability of bacteria to develop resistance to antimicrobial NO donors has not yet been determined.[39, 40] Such studies should include exposing bacterial cultures to sub-lethal doses of NO, growing colonies of the surviving cells, repeating the process through several iterations, and testing the susceptibility of the resulting cells to NO treatment.

Chapter 5 detailed the anti-biofilm properties of NO from the standpoint of both preventing biofilm formation and treating established biofilms. In terms of preventing biofilm formation, future studies should focus on understanding the efficacy of surface-derived NO in the presence of a protein mediating layer, which may scavenge a portion of the NO thus reducing the efficacy of the coating. The proliferation of other species of biofilm-forming pathogens should also be investigated in the presence of NO. Although Nablo et al. reported the in vivo anti-infective efficacy of NO-releasing xerogels,[41] further in vivo studies focusing on biofilm formation at implants are warranted. For example, xerogel

coatings can be applied to medical devices ranging from central venous catheters to fracture fixation devices, both of which are susceptible to infection.[42] After removing control and NO-releasing devices from an animal model that had been challenged with biofilm-forming bacteria, imaging the surface with SEM would provide direct evidence of the extent of biofilm formation. In terms of treating established biofilms, it will be important to study the anti-biofilm synergy between NO and other antimicrobial agents, as discussed above. Due to the prevalence of biofilms in chronic wounds,[43] future studies should focus on the ability of NO-releasing nanoparticles to eradicate wound-based biofilms in an animal model. Of note, enhanced wound healing may be observed due to NO's known influence in multiple processes of the wound healing cascade.[44] The influence of certain physicochemical properties of the nanoparticles, such as charge, should be investigated as they relate to anti-biofilm efficacy. For example, the matrix of *P. aeruginosa* biofilms is known to be highly anionic while that of *S. epidermidis* biofilms is cationic,[45] suggesting that the charge of NO-releasing nanoparticles may greatly influence their efficacy against biofilms of different microbial species.

Additionally, the cytotoxicity testing presented in Chapter 5 should be expanded to more fully elucidate the influence of NO on fibroblast cells. More specifically, it should be determined if the reduced proliferation of fibroblasts is due to NO-induced cell killing, or if NO is acting as a signaling molecule that influences the proliferation of fibroblasts without actually killing the cells.[46] It may be possible to distinguish between cell killing and reduced proliferation due to signaling via the use of cytotoxicity tests other than the MTT assay, including either propidium iodide and/or lactate dehydrogenase viability assays.[47, 48] Both the propidium iodide and lactate dehydrogenase assays directly measure cell death due to the

destruction of the cell membrane, as opposed to the MTT assay, which measures cellular metabolism.

6.3 Conclusions

The results presented herein have demonstrated the antimicrobial and wound healing properties of NO-releasing materials. As the physiological roles of NO in vivo become clearer, the demand for NO-based therapies will grow, and will in turn create a demand for strategies to chemically store NO in a manner such that it can be administered in a controlled fashion at the intended site of action. Nitric oxide-releasing xerogel-based materials, from polymeric implant coatings to NO-releasing silica nanoparticles, represent an important step in the field of NO delivery for therapeutic applications. Polymeric NO release was shown to reduce the inflammatory response, limit collagen deposition, and promote angiogenesis at the site of a subcutaneous implant. These finding may prove important in the development of indwelling medical devices, which are constantly plagued by issues associated with poor biocompability and the foreign body response. Equally problematic for indwelling medical devices is the ever-present threat of microbial infection. Polymeric NO release has been shown to confer desirable antimicrobial properties to substrates by reducing bacterial adhesion under both static and flow conditions, killing bacterial cells that adhere to the substrate surface, and preventing bacterial colonization/biofilm formation at the substrate surface. The use of NO-based therapies for antimicrobial applications, such as treating wound-based biofilm infections, will undoubtedly benefit from the positive impact that NO exerts on wound healing and may represent a new paradigm in the search for better antimicrobial treatments.

6.4 References

(1) Shin, J. H.; Metzger, S. K.; Schoenfisch, M. H. "Synthesis of nitric oxide-releasing silica nanoparticles." *J. Am. Chem. Soc.* **2007,** *129*, 4612-4619.

(2) Shin, J. H.; Schoenfisch, M. H. "Inorganic/organic hybrid silica nanoparticles as a nitric oxide delivery scaffold." *Chem. Mater.* **2008,** *20*, 239-249.

(3) Vacheethasanee, K.; Marchant, R. E., "Nonspecific *Staphylococcus epidermidis* adhesion: Contributions of biomaterial hydrophobicity and charge." In *Handbook of Bacterial Adhesion: Principles, Methods, and Applications*, An, Y. H.; Friedman, R. J., Eds. Humana Press: Totowa, NJ, 2000; p 74.

(4) Poelstra, K. A.; van der Mei, H. C.; Gottenbos, B.; Grainger, D. W.; van Horn, J. R.; Busscher, H. J. "Pooled human immunoglobulins reduce adhesion of *Pseudomonas aeruginosa* in a parallel plate flow chamber." *J. Biomed. Mater. Res.* **2000,** *51*, 224-232.

(5) Balin, A. K.; Pratt, L. "Dilute povidone-iodine solutions inhibit human skin fibroblast growth." *Am. Soc. Derm. Surg.* **2002,** *28*, 210-214.

(6) Pyo, H. C.; Kim, Y. K.; Whang, K. U.; Park, Y. L.; Eun, H. C. "A comparative study of cytotoxicity of topical antimicrobials to cultured human keratinocytes and fibroblasts." *Korean J. Dermatol.* **1995,** *33*, 895-906.

(7) Charville, G. C.; Hetrick, E. M.; Geer, C. B.; Schoenfisch, M. H. "Reduction of bacterial adhesion to fibrinogen-coated substrates via nitric oxide release." *submitted* **2008**.

(8) Yu, J. L.; Andersson, R.; Wang, L. Q.; Bengmark, S.; Ljungh, A. "Fibronectin on the surface of biliary drain materials -- a role in bacterial adherence." *J. Surg. Res.* **1995,** *59*, 596-600.

(9) Lundberg, F.; Schliamser, S.; Ljungh, A. "Vitronectin may mediate Staphylococcal adhesion to polymer surfaces in perfusing human cebrospinal fluid." *J. Med. Microbiol.* **1997,** *46*, 285-296.

(10) Privett, B. J.; Storm, W.; Schoenfisch, M. H. "Synthesis of nitric oxide-releasing xerogels via pre-formed diazeniumdiolate-modified aminoalkoxysilanes." **2008,** *in preparation.*

(11) Broekhuizen, C. A. N.; de Boer, L.; Schipper, K.; Jones, C. D.; Quadir, S.; Feldman, R. G.; Dankert, J.; Vandenbroucke-Grauls, C. M. J. E.; Weening, J. J.; Zaat, S. A. J. "Peri-implant tissue is an important niche for *Staphylococcus epidermidis* in experimental biomaterial-associated infection in mice." *Infect. Immun.* **2007,** *75*, 1129-1136.

(12) Boelens, J. J.; Dankert, J.; Murk, J. L.; Weening, J. J.; van der Poll, T.; Dingemans, K. P.; Koole, L.; Laman, J. D.; Zaat, S. A. J. "Biomaterial-associated persistence of *Staphylococcus epidermidis* in pericatheter macrophages." *J. Infect. Dis.* **2000,** *181*, 1337-1349.

(13) Boelens, J. J.; Zaat, S. A. J.; Meeldijk, J.; Dankert, J. "Subcutaneous abscess formation around catheters induced by viable and nonviable *Staphylococcus epidermidis* as well as by small amounts of bacterial cell wall components." *J. Biomed. Mater. Res.* **2000,** *50*, 546-556.

(14) Kroll, M. H.; Hellums, J. D.; McIntire, L. V.; Schafer, A. I.; Moake, J. L. "Platelets and shear stress." *Blood* **1996,** *88*, 1525-1541.

(15) O'Grady, N. P.; Alexander, M.; Dellinger, E. P.; Gerberding, J. L.; Heard, S. O.; Maki, D. G.; Masur, H.; McCormick, R. D.; Mermel, L. A.; Pearson, M. L.; Raad, I. I.; Randolph, A.; Weinstein, R. A. "Guidelines for the prevention of intravascular catheter-related infections." *Morbidity and Mortality Weekly Report* **2002,** *51(RR10)*, 1-26.

(16) Muto, C.; Herbert, C.; Harrison, E.; Edwards, J. R.; Horan, T.; Andrus, M.; Jernigan, J. A.; Kutty, P. K. "Reduction in central line-associated bloodstream infections among patients in intensive care units -- Pennsylvania, April 2001 - March 2005." *Morbidity and Mortality Weekly Report* **2005,** *54*, 1013-1016.

(17) Craven, P. A.; Studer, R. K.; Felder, J.; Phillips, S.; DeRubertis, F. R. "Nitric oxide inhibition of transforming growth factor-B and collagen synthesis in mesangial cells." *Diabetes* **1997,** *46*, 671-681.

(18) Chu, A. J.; Prasad, J. K. "Up-regulation by human recombinant transforming growth factor B-1 of collagen production in cultured dermal fibroblasts is mediated by inhibition of nitric oxide signaling." *J. Am. Coll. Surg.* **1999,** *188*, 271-280.

(19) Schwentker, A.; Vodovotz, Y.; Weller, R.; Billiar, T. R. "Nitric oxide and wound repair: Role of cytokines?" *Nitric Oxide* **2002,** *7*, 1-10.

(20) Olbrich, K. C.; Meade, R.; Bruno, W.; Heller, L.; Klitzman, B.; Levin, L. S. "Halofuginone inhibits collagen deposition in fibrous capsules around implants." *Ann. Plast. Surg.* **2005,** *54*, 293-296.

(21) Dulak, J.; Jozkowicz, A. "Regulation of vascular endothelial growth factor synthesis by nitric oxide: Facts and controversies." *Antioxid. Redox Signal.* **2003,** *5*, 123-132.

(22) Cooke, J. P. "NO and angiogenesis." *Atherosclerosis Suppl.* **2003,** *4*, 53-60.

(23) Ao, X.; Sellati, T. J.; Stenken, J. A. "Enhanced microdialysis relative recovery of inflammatory cytokines using antibody-coated microspheres analyzed by flow cytometry." *Anal. Chem.* **2004,** *76*, 3777-3784.

(24) Ao, X.; Rotundo, R. F.; Loegering, D. J.; Stenken, J. A. "In vivo microdialysis sampling of cytokines produced in mice given bacterial lipopolysaccharide." *J. Microbiol. Meth.* **2005,** *62*, 327-336.

(25) Ao, X.; Stenken, J. A. "Microdialysis sampling of cytokines." *Methods* **2006,** *38*, 331-341.

(26) Wang, X.; Lennartz, M. R.; Loegering, D. J.; Stenken, J. A. "Interleukin-6 collection through long-term implanted microdialysis sampling probes in rat subcutaneous space." *Anal. Chem.* **2007,** *79*, 1816-1824.

(27) Chaurand, P.; Stoeckli, M.; Caprioli, R. M. "Direct profiling of proteins in biological tissue sections by MALDI mass spectrometry." *Anal. Chem.* **1999,** *71*, 5263-5270.

(28) Khatib-Shahidi, S.; Andersson, M.; Herman, J. L.; Gillespie, T. A.; Caprioli, R. M. "Direct molecular analysis of whole-body animal tissue sections by imaging MALDI mass spectrometry." *Anal. Chem.* **2006,** *78*, 6448-6456.

(29) Reyzer, M. L.; Caprioli, R. M. "MALDI mass spectrometry for direct tissue analysis: A new tool for biomarker discovery." *J. Proteome Res.* **2005,** *4*, 1138-1142.

(30) Li, Y.; Schutte, R. J.; Abu-Shakra, A.; Reichert, W. M. "Protein array method for assessing in vitro biomaterial-induced cytokine expression." *Biomaterials* **2005,** *26*, 1081-1085.

(31) Barbe, C.; Bartlett, J.; Kong, L.; Finnie, K.; Lin, H. Q.; Larkin, M.; Calleja, S.; Bush, A.; Calleja, G. "Silica particles: A novel drug-delivery system." *Adv. Mater.* **2004,** *16*, 1959-1966.

(32) Giri, S.; Trewyn, B. G.; Lin, V. S. Y. "Mesoporous silica nanomaterial-based biotechnological and biomedical delivery systems." *Nanomedicine* **2007,** *2*, 99-111.

(33) Ramkumar, A.; Lal, R. In "Silica nanoparticle tags for capacitive affinity sensors," IEEE Engineering in Medicine and Biology 27th Annual Conference, Shanghai, China, September 1-4, 2005; Shanghai, China, **2005**; pp 266-269.

(34) Casadevall, A.; Scharff, M. D. "Return to the past: The case for antibody-based therapies in infectious diseases." *Clin. Infect. Dis.* **1995,** *21*, 150-161.

(35) An, Y. H.; Dickinson, R. B.; Doyle, R. J., "Mechanisms of bacterial adhesion and pathogenesis of implant and tissue infections." In *Handbook of Bacterial Adhesion: Principles, Methods, and Applications*, An, Y. H.; Friedman, R. J., Eds. Humana Press: Totowa, NJ, 2000.

(36) McElhaney-Feser, G. E.; Raulli, R. E.; Cihlar, R. L. "Synergy of nitric oxide and azoles against *Candida* species in vitro." *Antimicrob. Agents Chemother.* **1998,** *42*, 2342-2346.

(37) Johnson, C. B.; Schoenfisch, M. H. "Silver sulfadiazene and nitric oxide as synergistic biocides." **2008,** *in preparation.*

(38) Deupree, S.; White, A.; Schoenfisch, M. H. "Antimicrobial synergy between nitric oxide and other antimicrobial agents." **2008,** *in preparation.*

(39) Richardson, A. R.; Libby, S. J.; Fang, F. C. "A nitric oxide-inducible lactate dehydrogenase enables *Staphylococcus aureus* to resist innate immunity." *Science* **2008,** *319*, 1672-1676.

(40) Carlsson, S.; Weitzberg, E.; Wiklund, P.; Lundberg, J. O. "Intravesical nitric oxide delivery for prevention of catheter-associated urinary tract infections." *Antimicrob. Agents Chemother.* **2005,** *49*, 2352-2355.

(41) Nablo, B. J.; Prichard, H. L.; Butler, R. D.; Klitzman, B.; Schoenfisch, M. H. "Inhibition of implant-associated infections via nitric oxide release." *Biomaterials* **2005,** *26*, 6984-6990.

(42) Darouiche, R. O. "Treatment of infections associated with surgical implants." *N. Engl. J. Med.* **2004,** *350*, 1422-1429.

(43) Ryan, T. J. "Infection following soft tissue injury: Its role in wound healing." *Curr. Opin. Infect. Dis.* **2007,** *20*, 124-128.

(44) Luo, J. D.; Chen, A. F. "Nitric oxide: A newly discovered function on wound healing." *Acta Pharm. Sinica* **2005,** *26*, 259-264.

(45) Sutherland, I. W. "Biofilm exopolysaccharides: A strong and sticky framework." *Microbiology* **2001,** *147*, 3-9.

(46) Gansauge, S.; Gansauge, F.; Nussler, A. K.; Rau, B.; Poch, B.; Schoenberg, M. H.; Berger, H. G. "Exogenous, but not endogenous, nitric oxide increases proliferation rates in senescent human fibroblasts." *FEBS Letters* **1997,** *410*, 160-164.

(47) Tas, J.; Westerneng, G. "Fundamental aspects of the interaction of propidium diiodide with nucleic acids studied in a model system of polyacrylamide films." *J. Histochem. Cytochem.* **1981,** *29*, 929-936.

(48) Puranam, K. L.; Boustany, R. M., "Assessment of cell viability and histochemical methods in apoptosis." In *Apoptosis in Neurobiology*, Hannun, Y. A.; Boustany, R. M., Eds. CRC Press LLC: Boca Raton, FL, 1998; pp 129-152.